UNIVERSITE PARIS IX DAUPHINE U.F.R. MATHEMATIQUES DE LA DECISION

THESE

pour l'obtention du titre de

DOCTEUR EN SCIENCES

spécialité : Mathématiques Appliquées

arrêté du 23 novembre 1988

Sujet :

TRAITEMENT NUMERIQUE D'IMAGES ET DE FILMS :
EQUATIONS AUX DERIVEES PARTIELLES
PRESERVANT FORME ET RELIEF.

Candidat : Lionel MOISAN

Directeur de recherche : Jean-Michel MOREL

Jury :

Président :	Monsieur Yves MEYER
Rapporteur :	Monsieur Guy BARLES
Rapporteur :	Monsieur Vicent CASELLES
Examinateur :	Monsieur Vladimir ARNOLD
Examinateur :	Monsieur Robert AZENCOTT
Examinateur :	Monsieur Jean-Michel MOREL
Examinateur :	Monsieur Leonid YAROSLAVSKY

juin 1997

L'université n'entend donner aucune approbation ni improbation aux opinions émises dans les thèses : ces opinions doivent être considérées comme propres à leurs auteurs.

A mes parents,

à Claire.

Monsieur Yves Meyer a accepté de présider ce jury. Je voudrais lui exprimer ici ma très vive gratitude pour cette attention portée à mon travail et pour l'honneur qu'il me fait ainsi.

Je tiens à remercier particulièrement Monsieur Vicent Caselles pour ses conseils et ses encouragements qui m'ont été extrêmement précieux : nos discussions ont toujours été pour moi une source stimulante de réflexion. Pour avoir rapporté cette thèse et pour toute son aide, qu'il soit assuré de ma très profonde reconnaissance.

A Monsieur Guy Barles, je souhaite également dire ma sincère gratitude, pour avoir accepté aussi la charge de rapporteur, et pour la grande disponibilité dont il a fait preuve à cette occasion.

Monsieur Robert Azencott, qui m'a accueilli comme caïman à l'Ecole Normale Supérieure de Cachan avec Monsieur Jean-Michel Ghidaglia, a accepté de se joindre à ce jury. Qu'il me permette de lui dire ici ma reconnaissance. Mes remerciements vont aussi à Monsieur Yaroslavsky, qui participe à ce jury, et à Monsieur Vladimir Arnold, qui me fait également l'honneur de s'y joindre, malgré un emploi du temps que je sais très chargé.

Pour une collaboration stimulante, je voudrais remercier toute l'équipe de traitement d'images du CEREMADE, et particulièrement Francine Catté, Thierry Cohignac, Françoise Dibos, Jacques Froment, Georges Koepfler et Christian Lopez. Merci également aux membres du CMLA et du département de mathématiques de l'ENS Cachan pour leur accueil sympathique. Pour m'avoir fait découvrir le traitement d'images en milieu industriel, merci à Jean-Paul Boujot et à la CISI, ainsi qu'à Pierre-Louis Lions pour les discussions très enrichissantes que nous avons eues à ces occasions. Je remercie également Thierry Cohignac et le Ministère de la Défense, grâce à qui j'ai pu effectuer mon service militaire dans les meilleures conditions d'un laboratoire de recherche.

Sans Michel Vanbreugel, cette thèse n'aurait pas résisté à la loi de Murphy. Pour avoir su maîtriser un parc informatique toujours grandissant, et pour m'avoir ainsi permis de travailler dans les meilleures conditions, merci à lui. Merci également à Lucette Jean Pierre, Josette Lévy, Magali Marc-Dibildos et Irène Mazzella pour l'aide qu'elles m'ont apportée dans toutes les démarches administratives.

Je souhaite également exprimer ma profonde sympathie à Jean-Pierre d'Alès, Mohamed Bouguecha, Kaouther Boussema, Frédéric Cao, Rafia Elkalay, Orlando Fernandez, Yann Gousseau, Frédéric Guichard, David Khuat Duy, Simon Masnou, Pascal Monasse, Jacques-Olivier Moussafir, Denis Pasquignon et Fatma Trigui, pour des discussions toujours passionnantes, pour leur soutien moral, et pour la bonne humeur et l'atmosphère de recherche motivante qui règnent dans les bureaux du CEREMADE. Merci aussi à mes amis de L'Ecole Normale Supérieure pour le recul et l'ouverture d'esprit qu'ils ont su m'apporter.

Enfin, je ne saurais comment remercier Monsieur Jean-Michel Morel, qui a dirigé cette thèse, m'a guidé et soutenu tout au long de ces années de recherche. Son attention constante à mon travail, les discussions extrêmement stimulantes par lesquelles il m'a fait découvrir le monde passionant de la recherche, ont été pour moi une aide irremplaçable. Pour tout ce qu'il m'a ainsi apporté, je veux lui témoigner ici ma très profonde et sincère reconnaissance.

Résumé

La reconnaissance de formes planes partiellement masquées ne peut se faire que localement en calculant des points caractéristiques (extremas de courbure, points d'inflexions,...), et ce calcul requiert un procédé de lissage des formes. Si l'on veut effectuer cette reconnaissance modulo toutes les déformations affines du plan, alors ce procédé est unique : c'est le *scale space affine*, découvert en 1993, qui peut être décrit par une équation d'évolution. Dans la première partie de cette thèse, nous montrons comment résoudre cette équation numériquement avec précision, en itérant un opérateur continu, géométrique, global et exactement calculable. Des propriétés de consistance forte et de convergence sont établies et validées par de nombreuses expériences numériques. Ce procédé offre des performances bien supérieures aux schémas classiques aux différences finies, qui ne peuvent vérifier rigoureusement l'invariance affine et le principe d'inclusion.

Dans une deuxième partie, nous étudions l'un des problèmes fondamentaux de la robotique, la reconstruction du relief à partir d'une séquence d'images. Il s'avère que lorsque le mouvement de l'observateur peut être déterminé, il n'existe fondamentalement qu'une seule manière de filtrer la séquence d'images tout en préservant le relief sous-jacent. Ce filtrage, obtenu grâce à une démarche axiomatique, se formule par une équation aux dérivées partielles non linéaire du second ordre, parabolique dégénérée, qui présente une singularité très forte inhérente au problème de reconstruction. Nous établissons des résultats d'existence et d'unicité pour cette équation, puis mettons en évidence certaines propriétés mathématiques qui se prêtent facilement à une interprétation physique. Enfin, nous décrivons un schéma numérique adapté, et réalisons des expériences qui montrent que ce filtrage, par la cohérence qu'il induit, ramène le procédé de reconstruction à un calcul élémentaire et fiable.

Abstract

The recognition of partially occluded planar shapes necessarily involves a local computation of characteristic points (curvature extrema, inflexion points,...), and this computation requires a shape smoothing process. If the recognition is considered up to all affine transformations of the plane, then this process is unique : this is the *affine scale space*, discovered in 1993, which can be described by an evolution equation. In the first part of this study, we show how this equation can be solved numerically with a high accuracy, by iterating a continuous, geometric and global operator which can be exactly computed. Full consistency and convergence results are provided, as well as conclusive numerical experiments. This method goes beyond classical finite differences schemes that never manage to satisfy rigorously the affine invariance and the inclusion principle.

In a second part, we study a fundamental problem of robotics : the depth recovery from a sequence of images. We prove that when the camera motion can be controlled, there fundamentally exists only one way to process the image sequence and preserve the underlying depth in the same time. This process, obtained from an axiomatic formulation, can be described by a non-linear second-order degenerate parabolic partial differential equation, which presents a strong singularity inherent to the depth recovery problem. We establish existence and uniqueness results for this equation, and we highlight several properties which can be easily interpreted from a physical point of view. Last, we describe a numerical scheme, and show on experiments how the filtering process, thanks to the coherence it induces, brings back the depth recovery to an elementary and robust computation.

Contents

Chapter 1

Introduction

Le traitement d'images a fait son apparition dans les années 1970, lorsque le développement des ordinateurs a rendu possibles les premiers calculs numériques sur des images digitales. Pendant longtemps, il fut un domaine presque exclusivement réservé à des équipes d'ingénieurs motivés par des applications immédiates ; ce n'est que depuis quelques années qu'il a fait l'objet d'une étude mathématique plus rigoureuse, qui a permis de classifier bon nombre de techniques antérieures, et d'en expliquer le succès ou l'échec.

1.1 Problèmes et Enjeux du traitement d'images

Aujourd'hui encore, le traitement d'images (et de films) pose essentiellement trois grands problèmes : celui de **l'analyse** (comment obtenir des informations concernant les "objets" présents sur une image donnée ?), celui de **la restauration** (comment améliorer la qualité d'une image, la rendre plus nette ?) et celui de **la compression** (comment coder une image sous la forme la plus compacte possible ?). Nous ne parlerons pas ici de la synthèse d'images, qui ne relève pas à proprement parler du traitement d'images, même si elle lui est souvent complémentaire. L'analyse d'images est un maillon essentiel de la robotique, puisqu'elle doit définir les mécanismes de perception visuelle des robots. Elle a aussi beaucoup d'autres applications : reconnaissance de formes, cartographie aérienne, contrôle de qualité sur une chaîne de production, etc... La restauration d'images, quant à elle, est un outil très appréciable pour corriger des défauts qui apparaissent lors de la production d'une image : flou de focalisation ou flou de bougé, présence de "bruit", etc... Enfin, la compression d'images est un domaine relativement nouveau, devenu indispensable avec le développement massif des moyens de communication ; le débit de transmission d'un canal (hertzien ou filaire) étant toujours limité par des contraintes physiques, la compression apparaît comme un moyen simple d'augmenter le débit d'information. Malgré les apparences, ces trois problèmes ne sont pas indépendants : par exemple, le débruitage (suppression d'artefacts créés lors de l'acquisition) est une forme de restauration quasiment indispensable pour l'analyse. De même, le processus de simplification induit par l'analyse d'une image est une

étape préliminaire à certains algorithmes de compression. Enfin, certains algorithmes de compression avec perte d'information (cas de la norme JPEG par exemple) justifient une étape de restauration visant à corriger les défauts induits par la boucle compression-décompression. Dans toute cette étude, notre point de vue sera celui de l'analyse des images, même si nous aurons l'occasion d'illustrer quelques applications de ces procédés à la restauration.

1.2 Analyse des images : la notion de *scale space*

Quelles informations peut-on extraire d'une image donnée ? Cette question très générale est le point de départ de l'analyse d'images, qui précède souvent une phase d'interprétation. Par exemple, le fait que deux objets se déplacent à des vitesses différentes dans une séquence d'images est une information objective ; mais si l'on sait que ces deux objets sont en réalité fixes et que leur mouvement apparent est dû au déplacement de la caméra, on peut alors en déduire que l'objet qui se déplace le plus vite est plus proche de la caméra que l'autre, et même quantifier la distance de chaque objet au plan focal de la caméra.

Historique. Dans les années 1970, Bela Julesz mit en évidence l'existence de mécanismes réflexes dans la vision humaine. Il montra notamment que cette vision "bas niveau", opérée dans les premières millisecondes du processus de vision, permet à l'homme de percevoir le relief et de discriminer des textures. Ses conclusions amenèrent les scientifiques à conjecturer l'existence d'un modèle mathématique simple de la vision préattentive. C'est ainsi que David Marr [53] formula quelques années plus tard le concept de "raw primal sketch", ou pyramide visuelle. Selon lui, l'analyse visuelle résulte d'une représentation de l'image à des échelles différentes, allant d'une description très fine à l'échelle 0 vers une description de plus en plus globale et simplifiée à mesure que l'échelle augmente. Ainsi, une image brute est en réalité "vue" comme une collection d'images indexées par un paramètre d'échelle correspondant au degré de simplification opéré par rapport à l'image brute (échelle 0). Ce paramètre d'échelle peut d'ailleurs être identifié au temps d'analyse dans le système visuel humain. Cette représentation multiéchelle d'une image, qui fait donc intervenir une variable d'espace et une variable d'échelle, est appelée *scale space* [80] : son adéquation à modéliser la vision humaine préattentive a été bien vérifiée depuis, tant d'un point de vue psychophysique que biologique.

Le premier exemple de scale space, basé sur un filtrage linéaire, a rapidement montré ses limites. En effet, alors que la structure des appareils d'acquisition d'images rend, par la présence de filtres passe-bas, les théories linéaires bien adaptées à la compression (cf. la compression par ondelettes : [56], [28]), voire à la restauration (pour le déflouage par exemple), en revanche la nature "occlusive" des images à des échelles supérieures rend ces théories peu adaptées à l'analyse. En fait, le processus de formation d'une image naturelle[1] (un paysage, une scène

[1] c'est-à-dire issue d'un processus de vision, par opposition a une image scientifique utilisée pour représenter des données abstraites.

urbaine, ...) résulte d'un principe d'occlusion : lorsqu'un objet (non transparent) en cache un autre, seul le premier est visible, et l'on n'observe pas une espèce de superposition des images des deux objets. Cette constatation condamne immédiatement la généralisation hâtive des techniques linéaires employées en traitement du signal, pour l'analyse de la parole notamment, où il est clair que la nature même des ondes sonores implique un principe de superposition.

Le principe morphologique. Une alternative aux scale spaces linéaires apparut lors du développement de la Morphologie Mathématique ([70], [54]). Poussé à l'extrême, le principe morphologique s'énonce de la manière suivante : *"Dans une image, seul compte le fait qu'un point est plus clair ou plus foncé qu'un autre ; la valeur absolue de l'intensité n'est pas une information en soi."* Cette hypothèse est d'ailleurs légitimée par l'exemple de la vision humaine : on ne voit pas différemment à travers une vitre teintée ! Concrètement, si l'on représente une image par une fonction $u : \mathbb{R}^2 \to \mathbb{R}$ qui mesure en chaque point du plan l'intensité lumineuse reçue (le niveau de gris), ce principe dit que l'analyse de l'image u et d'une image de type $g(u)$ (avec $g : \mathbb{R} \to \mathbb{R}$ monotone) doit être la même. De tels changements de contraste g, qui opèrent une redistribution des niveaux de gris, sont de toute façon présents dans la chaîne d'acquisition. En pratique, le principe morphologique implique que le scale space opère indépendamment sur les lignes de niveau $u = cte$: l'analyse d'images se ramène donc à une analyse purement géométrique.

Une classification axiomatique. Peu à peu, de nouveaux modèles morphologiques sont apparus, et c'est en 1993 qu'une démarche axiomatique rigoureuse (cf. [4]) a permis de classifier complètement les théories existantes. Dans cette approche, chaque scale space est caractérisé en fonction de ses propriétés :

- Comment le scale space opère-t-il sur les niveaux de gris d'une image : est-il linéaire, morphologique, ... ?
- Avec quel groupe de transformations du plan le scale space commute-t-il : translations, rotations, symétries, affinités ?

D'autres propriétés, notamment le principe de comparaison (ou principe du maximum) qui assure qu'un scale space est un processus de simplification, avaient déjà été identifiées comme des propriétés fondamentales. De cette classification axiomatique, qui permit de regrouper au sein d'un même formalisme de nombreuses théories existantes, a alors émergé un nouveau modèle, baptisé *Affine Morphological Scale Space*. Ce scale space morphologique possède le groupe d'invariance le plus gros (en l'occurence le groupe affine) que l'on puisse obtenir pour simplifier des images. La démarche axiomatique a aussi été appliquée en dimension supérieure, par exemple pour obtenir le premier scale space de films ([40]).

1.3 Plan de l'exposé.

Cette thèse est divisée en deux parties indépendantes. La première est consacrée à la reconnaissance de formes : nous élaborons et étudions un algorithme géométrique permettant de calculer avec précision le scale space affine d'une courbe plane. Dans la deuxième partie, nous rappelons comment, à partir d'un film, il est possible — en théorie — de retrouver le relief des objets apparaissant sur chaque image. Nous montrons ensuite comment le film doit être analysé pour qu'une telle opération soit effectivement réalisable.

La reconnaissance de formes. Le problème de la reconnaissance de formes peut être posé comme suit : *"Etant donné une base de formes de référence, comment reconnaître une nouvelle forme (ou la rejeter si elle n'est pas référencée dans la base), sachant qu'elle peut avoir été déformée et altérée ?"* Dans ce qui suit, nous entendrons par forme une région du plan délimitée par un nombre fini de courbes de Jordan. D'un point de vue pratique, l'approche morphologique permet d'extraire naturellement des formes d'une image en considérant simplement ses ensembles de niveau

$$\chi_\lambda(u) = \{\boldsymbol{x} \in \mathbb{R}^2,\ u(\boldsymbol{x}) \geqslant \lambda\}.$$

Grâce à cette décomposition, il devient alors équivalent de traiter une forme (c'est-à-dire un ensemble de courbes) et une image. Nous devons bien sûr préciser sous quelles conditions nous considérons deux formes comme semblables : par exemple, il semble naturel que la reconnaissance d'une forme ne dépende pas de sa position dans l'image. Mathématiquement, cela se traduit par l'identification d'un groupe de transformations du plan (contenant les translations d'après ce que nous venons de voir) qui induira une classe d'équivalence sur les formes.

Lorsque la reconnaissance est globale, un processus de normalisation peut être effectué : on choisit un représentant canonique dans la classe d'équivalence de chaque forme connue, et la reconnaissance se ramène alors à une comparaison entre deux représentants. Mais si l'on suppose que des masquages partiels peuvent intervenir, c'est à dire que les formes à reconnaître ne sont pas nécessairement "entières", une telle normalisation devient impossible, à cause de la perte d'information induite par le masquage. Il faut alors tenter une reconnaissance locale, généralement basée sur un calcul de points caractéristiques (extremas de courbure, points d'inflexion, cf. [26]). Ces points caractéristiques, définis localement, impliquent souvent l'estimation de dérivées le long de la courbe, ce qui n'a en général pas de sens sur une courbe brute, dont le contour peut avoit été rendu très irrégulier par la présence de bruit dans l'image originale. Ainsi, un lissage préalable est nécessaire, et s'exprime naturellement sous la forme d'un scale space géométrique. Pour qu'un scale space géométrique soit effectivement un procédé de simplification, il faut qu'il satisfasse ce que l'on appelle le *principe d'inclusion locale* (cf. figure 1.1) : *"Si une forme est localement contenue dans une autre, alors cette inclusion doit persister localement pour une échelle d'analyse suffisamment petite."* Ce principe est fondamental : il garantit notamment la

stabilité des algorithmes qui le vérifient. Formulé en termes d'images, il est alors équivalent au principe du maximum.

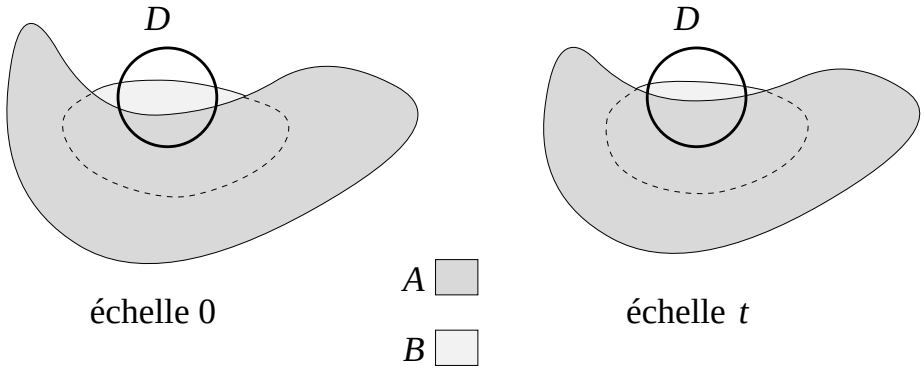

Figure 1.1: Illustration du principe d'inclusion locale.

Une analyse multiéchelle vérifie le principe d'inclusion locale lorsque la condition suivante est vérifiée : "si une forme A est localement contenue dans une forme B (i.e $A \cap D \subset B \cap D$ pour un certain voisinage D), alors cette propriété reste vraie pour les formes analysées à une échelle suffisamment petite". Ce principe garantit qu'une telle analyse multiéchelle est un processus de simplification, et assure la stabilité des algorithmes qui le vérifient.

Moyennant une hypothèse supplémentaire de régularité relevant plus d'un artifice mathématique que d'une hypothèse physique, on obtient alors un unique modèle de scale space "maximal", c'est à dire commutant avec le plus gros groupe possible de transformations du plan, en l'occurence le groupe affine, engendré par les translations et les applications linéaires inversibles. Ce scale space affine, que nous avons évoqué précedemment, fut découvert simultanément deux équipes de chercheurs : L.Alvarez, F.Guichard, P.-L.Lions et J.-M.Morel [4] en termes d'analyse d'images, et par G.Sapiro et A.Tannenbaum dans sa version géométrique. Pour l'analyse de courbes, c'est cette dernière formulation qui est la plus adaptée : une courbe initiale $s \mapsto \boldsymbol{C}(s,0)$ évolue selon l'équation

$$\frac{\partial \boldsymbol{C}}{\partial t}(s,t) = \gamma(s,t)^{\frac{1}{3}}\, \boldsymbol{N}(s,t), \tag{1.1}$$

où $\gamma(s,t)$ et $\boldsymbol{N}(s,t)$ représentent respectivement la courbure et la normale au point $\boldsymbol{C}(s,t)$ à la courbe $s \mapsto \boldsymbol{C}(s,t)$. La variable t représente le paramètre d'échelle que nous avons évoqué précédemment. Ainsi, la reconnaissance locale et affine-invariante de formes peut être effectuée de la manière suivante : on calcule le scale space affine à différentes échelles de la forme à reconnaître, puis on calcule des points caractéristiques sur la courbe obtenue à partir d'invariants affines locaux (la courbure affine par exemple) ou semi-locaux (cf. [26]). Enfin, on compare ces points caractéristiques avec ceux des formes de référence, ceci d'une manière affine invariante.

D'un point de vue numérique, la difficulté majeure qui intervient dans ce procédé est le calcul du scale space affine de la forme initiale. En effet, il n'existait jusqu'à présent qu'une manière raisonnable de calculer le scale space affine d'une forme, la méthode étant due à S.Osher et

J.A.Sethian. L'idée était de considérer l'image "fonction-distance" associée à la forme $S \subset \mathbb{R}^2$:

$$u(\boldsymbol{x},0) = \begin{cases} -\mathrm{dist}(\boldsymbol{x},\partial S) & \text{si} \quad \boldsymbol{x} \in S, \\ +\mathrm{dist}(\boldsymbol{x},\partial S) & \text{si} \quad \boldsymbol{x} \notin S, \end{cases}$$

et de lui appliquer un schéma aux différences finies pour calculer son scale space morphologique affine $(u(\cdot,t))_{t\geqslant 0}$. Grâce au principe morphologique, l'analyse de la forme S à l'échelle t était alors donnée par $\{\boldsymbol{x} \in \mathbb{R}^2,\ u(\boldsymbol{x},t) \leqslant 0\}$.

Pourquoi le seul schéma "raisonnable" de scale space affine semblait-il nécessiter une formulation en termes d'images ? Simplement parce qu'*un schéma géométrique aux différences finies basé sur une évolution de points est condamné à échouer* : un tel schéma ne peut pas vérifier le principle d'inclusion, pourtant crucial pour assurer la stabilité de l'algorithme et sa consistance avec le scale space affine. En termes d'évolution d'images, le principe correspondant au principe d'inclusion (principe de comparaison, ou principe du maximum) est beaucoup plus facile à garantir numériquement, ce qui explique l'intérêt de la méthode d'Osher-Sethian. En revanche, l'invariance affine devient quelque peu illusoire, ne serait-ce qu'à cause de la grille fixe sur laquelle se placent les pixels de l'image. De plus, outre une certaine lourdeur, ce procédé est limité dans la précision de ses résultats à cause du pas de la grille sous-jacente.

Dans la première partie de cette thèse, nous proposons une alternative géométrique à la méthode d'Osher-Sethian pour calculer numériquement le scale space affine d'une courbe. Le schéma que nous décrivons est basé sur l'itération d'un opérateur **géométrique** et **non-local** (cf. figure 1.2), qui vérifie le principe d'inclusion et l'invariance affine, et qui peut être calculé facilement pour des courbes polygonales. L'algorithme obtenu est rapide, stable et très précis, comme l'illustrent les nombreuses expériences que nous effectuons.

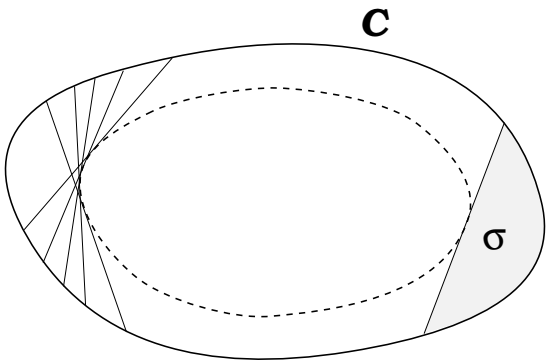

Figure 1.2: "Erosion affine" d'une courbe convexe.

Représentée en pointillés, l'érosion affine de paramètre σ de la courbe convexe $\mathcal{C}$ est obtenue en éliminant de l'intérieur de $\mathcal{C}$ toutes les régions d'aire σ délimitées par un arc de courbe et une corde de $\mathcal{C}$. Cela revient en général à considérer l'enveloppe (ou encore les milieux) de telles cordes. En itérant un tel opérateur, on obtient alors une approximation fine et numériquement stable du scale space affine de $\mathcal{C}$.

La détermination du relief. Comme nous l'avons évoqué auparavant, l'un des enjeux majeurs de la robotique est de résoudre le problème de la perception. Lorsqu'un robot se déplace dans un environnement connu ou inconnu, il lui est nécessaire de pouvoir se repérer, voire d'établir une carte tridimensionnelle du monde qui l'entoure. Ce genre d'opération est effectué en permanence par le système visuel humain, qui utilise conjointement differents types d'informations. Par exemple, la quantité de lumière réfléchie en chaque point d'une surface donne en général une information sur la direction de la normale à cette surface : c'est le *shape from shading*. L'utilisation de la stéréovision, basée sur l'analyse des petites différences entre les images reçues par chaque oeil, permet aussi de déterminer le relief. Mais même lorsque l'on ferme un oeil, notre système visuel reconstruit sans problème le relief observé pour peu que l'on se déplace un peu : le mouvement apparent des objets nous renseigne sur leur distance effective, les objets les plus près étant animés d'un mouvement apparent plus rapide, alors que les objets très éloignés restent quasiment fixes. D'autres informations, relevant de connaissances a priori, sont aussi couramment utilisées par le système visuel humain : connaissant la taille approximative d'une voiture, nous pouvons facilement déduire de sa taille apparente la distance à laquelle elle se trouve. Ce type de perception du relief est cependant beaucoup plus complexe, et ne résulte pas d'un processus de vision préattentive, contrairement à la stéréovision par exemple.

Les premiers essais de reconstruction automatique du relief furent basés en toute logique sur le procédé de stéréovision. A partir de deux images obtenues grâce à deux caméras légèrement décalées, il semblait possible de reconstruire entièrement le relief de la scène observée. Bien que correcte d'un point de vue théorique, cette méthode se heurta assez rapidement à deux problèmes majeurs. Le premier, structurel, fut mis en évidence par un calcul simple montrant l'impossibilité d'obtenir à la fois un algorithme robuste (la comparaison des deux images est d'autant plus facile que les deux caméras sont proches) et une bonne estimation du relief (cet estimation est d'autant plus précise que les deux caméras sont éloignées). Le deuxième problème majeur survint à cause des techniques développées pour comparer les deux images : généralement basée sur l'extraction de contours rectilignes fortement contrastés, la comparaison n'est vraiment efficace que pour des scènes artificielles (bâtiments, routes, machines, ...), et ses performances chutent complètement dans le cas de scènes naturelles où des textures apparaissent plutôt que des arêtes vives (champs, herbe, feuillage, ...).

Ainsi, il était naturel de se tourner vers un procédé plus robuste, le *shape from motion*. L'idée est de considérer non plus deux images mais une séquence de plusieurs dizaines d'images, et d'analyser le déplacement apparent des objets entre chaque couple d'images successives, sous l'hypothèse que les objets sont en réalité fixes et que leur mouvement apparent n'est dû qu'au déplacement de la caméra. Une telle approche est en quelque sorte une généralisation du principe de stéréovision, et l'on devine que la redondance de l'information disponible (théoriquement, chaque couple d'images de la séquence produit une interprétation du relief d'après le principe de stéréovision) doit permettre de vaincre les problèmes de robustesse et de précision inhérents

au procédé de stéréovision. Si une telle approche semble en effet beaucoup plus fiable, de nouveaux problèmes apparaissent néanmoins. Dans l'approche continue généralement adoptée pour représenter la séquence d'images obtenue, la reconstruction du relief implique le calcul d'un rapport de dérivées, qui s'avère être très instable à cause de l'irrégularité spatiale des images et de leur trop rapide évolution temporelle tout au long de la séquence. D'autre part, la redondance de l'information contenue dans la séquence ne peut être pleinement exploitée que par une analyse globale de la séquence, et non par le calcul de dérivées à un instant donné.

Dans la deuxième partie de cette thèse, nous montrons comment, sous l'hypothèse que le mouvement de la caméra est donné, le problème de l'analyse du relief peut être résolu à l'aide d'un filtrage adéquat de la séquence d'images, qui permet d'induire une cohérence temporelle globale entre toutes les images de la séquence, ramenant ainsi l'analyse globale du relief à un calcul local. Ce processus de filtrage — un scale space faisant intervenir le temps, l'espace et l'échelle — est même unique, caractérisé par un ensemble de propriétés imposées par la géométrie du problème de la détermination du relief. Si le mouvement est donné par la variable spatiale x, l'analyse d'un film $u(x, y, \theta, 0)$ (θ représentant le temps et la dernière coordonnée l'échelle t) est décrit par l'équation d'évolution[2]

$$u_t = u_{\theta\theta} - 2\frac{u_\theta}{u_x}u_{\theta x} + \left(\frac{u_\theta}{u_x}\right)^2 u_{xx}. \tag{1.2}$$

Cette équation aux dérivées partielles non linéaire du second ordre, parabolique dégénérée, présente une singularité très forte lorsque la dérivée u_x s'annule, ce qui l'empêche de relever de la théorie classique des solutions de viscosité (cf. [27]), seule théorie de solutions faibles a priori adaptée à ce type d'équation. Néanmoins, nous établissons des résultats d'existence et d'unicité pour (1.2), et mettons en évidence certaines de ses propriétés qui se prêtent facilement à une interprétation physique. En particulier, il apparaît que ce scale space est vraiment compatible avec la reconstruction du relief, puisqu'il préserve tout film idéal, c'est-à-dire possédant déjà une interprétation cohérente en termes de relief observé et de mouvement de la caméra. Nous décrivons ensuite un schéma numérique pour résoudre (1.2), basé sur l'itération d'opérateurs morphologiques de type inf-sup. Enfin, par quelques expériences, nous confirmons numériquement les effets de cet équation : l'établissement d'une cohérence globale entre toutes les images du film qui ramène le calcul du relief à un processus simple et fiable.

[2]Selon la convention habituelle, les indices désignent des dérivées partielles.

Part I

A strongly consistent geometrical scheme for the Affine Scale Space

Chapter 2

The Affine Scale Space

2.1 Image analysis and scale spaces

When devising an algorithm to analyze images, a major question must be raised : what kind of information are we looking for, and how can we extract it from the image ? In particular, it is clear that what we can see on an image depends on the focalization of the look we take at it : we cannot at the same time examine small details and recognize large structures. Hence, there is a natural *scale* parameter that cannot be eluded in the analysis process. This suggests that an image should be represented in a multiscale way, the smallest details being described at small scales and the largest ones at large scales. Such a multiscale representation of an image is called a **scale-space** : to a raw image u_0 we associate a continuous collection of images $(u(t))_{t>0}$ that are obtained from u_0 by a simplification process which "eliminates" details as the scale increases. The collection of operators (T_t) that define $u(t)$ from u_0 is called a **multiscale analysis** of images.

From a mathematical point of view, an image shall be regarded in the following as a map $u_0 : \mathbb{R}^2 \to \mathbb{R}$, the value $u(\boldsymbol{x})$ corresponding to the grey-level[1] (the luminance) at point $\boldsymbol{x} = (x, y)$ of the plane[2]. Then, a scale space is represented by a map $u : \mathbb{R}^2 \times [0, +\infty[\to \mathbb{R}$, the third coordinate being the scale t. A simple example of a linear scale space can be defined by the heat equation

$$\begin{cases} \dfrac{\partial u}{\partial t} = \Delta u \\ \\ u(\cdot, 0) = u_0(\cdot), \end{cases} \tag{2.1}$$

where $\Delta = \frac{\partial^2}{\partial x^2} + \frac{\partial^2}{\partial y^2}$ is the two-dimensional Laplacian operator. The simplification process induced by Equation 2.1 is an isotropic diffusion that can also be described by the convolution of u_0 with a two-dimensional Gaussian kernel. Although Equation 2.1 satisfies the required properties to define an interesting scale space, as we shall see later, it is not well adapted to

[1] We do not consider the case of color images.

[2] In practice, a grey-level image is represented by computers as a finite two-dimensional array of integer values.

image analysis due to its linear nature. The main reason is that the image formation process results from a superimposition of objects rather than from a linear combination of them.

2.2 Definition

The affine scale space has been discovered a few years ago in its image and geometrical formulation (see [4] and [68]).

2.2.1 Image formulation

Let us first express it in terms of image processing. The affine morphological scale space (shortly written AMSS) is defined by the degenerated parabolic evolution equation

$$\begin{cases} \dfrac{\partial u}{\partial t} = |Du|\mathrm{curv}(u)^{\frac{1}{3}} \\ \\ u(\cdot,0) = u_0(\cdot). \end{cases} \tag{2.2}$$

The term $Du = (u_x, u_y)$ represents the spatial gradient of u, u_x and u_y being short notations for the partial derivatives $\frac{\partial u}{\partial x}$ and $\frac{\partial u}{\partial y}$. The second order operator

$$\mathrm{curv}(u) = \mathrm{div}\left(\frac{Du}{|Du|}\right) = \frac{(u_x)^2 u_{yy} - 2u_x u_y u_{xy} + (u_y)^2 u_{xx}}{|Du|^3}$$

can be viewed as the curvature at point $\boldsymbol{x}$ of the level line[3] of u going through $\boldsymbol{x}$. In the following, we take the convention that $r^{\frac{1}{3}}$ means $-|r|^{\frac{1}{3}}$ when r is negative. When $Du = 0$, $\mathrm{curv}(u)$ is not defined, but

$$|Du|\mathrm{curv}(u)^{\frac{1}{3}} = \left[(u_x)^2 u_{yy} - 2u_x u_y u_{xy} + (u_y)^2 u_{xx}\right]^{\frac{1}{3}}$$

is naturally equal to zero, so that Equation 2.2 remains defined. Hence, from now on we assume that $|Du|\mathrm{curv}(u)^{\frac{1}{3}}$ is defined and equal to 0 when $Du = 0$.

In fact, Equation 2.2 is a parabolic PDE of the kind

$$\frac{\partial u}{\partial t} = F(D^2 u, Du),$$

where $F : \mathcal{S}(\mathbb{R}^2) \times \mathbb{R}^2 \to \mathbb{R}$ is a continuous function, nondecreasing with respect to its first argument (for the usual order defined on $\mathcal{S}(\mathbb{R}^2)$, the set of symmetric 2×2 real matrices). For this kind of evolution equations, weak solutions —only continuous— have been defined, and are called for historical reasons *viscosity solutions*. We shall be more precise in Chapter 5, but one may refer to [10] or [27] for further details. The reason why Equation 2.2 is called Affine Morphological Scale Space comes from important properties of the associated multiscale analysis $(T_t)_{t \geqslant 0}$, defined by

$$(T_t\, u_0)\,(\boldsymbol{x}) = u(\boldsymbol{x}, t).$$

[3] Of course, this makes sense only at points where the equation $u = cte$ defines locally a smooth curve.

First, the nature of Equation 2.2 concedes a semi-group structure to this family of operators, inasmuch as

$$T_{t+s} = T_t \circ T_s.$$

Secondly, these operators are morphological, that is, they satisfy the property

[**Morphological Invariance**] : For any nondecreasing (or nonincreasing) continuous function $g : \mathbb{R} \to \mathbb{R}$,

$$\forall u, \forall t, \qquad T_t(g \circ u) = g \circ T_t(u).$$

The fact that T_t commutes with any contrast change g implies that it operates on the level lines of u ; we shall give a geometric interpretation of this later. The word "affine" comes from an interesting geometrical invariance :

[**Affine invariance**] : For any bijective affine map ϕ,

$$\forall t, \exists t', \forall u, \qquad T_t(u \circ \phi) = T_{t'}(u) \circ \phi.$$

By affine map, we mean any linear operator on $\mathbb{R}^2$. If ϕ belongs to the special linear group — i.e. $\det \phi = 1$ —, we have $T_t(u \circ \phi) = T_t(u) \circ \phi$. Another relevant property of the semi-group (T_t) is the maximum principle, which gives sense to viscosity solutions for (2.2). This principle can be expressed by

[**Comparison Principle**] : $\forall u, v, \quad u \leqslant v \quad \Rightarrow \quad \forall t > 0, \ T_t u \leqslant T_t v.$

A local version of this principle (called Local Comparison Principle) is also satisfied (see Chapter 5). These principles are very important, and they guarantee that Equation 2.2 "simplifies" the initial image u_0 as the scale t increases. They also ensure numerical stability to associated algorithms.

We shall come back to these fundamental properties, but it is interesting to mention that the AMSS is the only regular multiscale analysis which satisfies them. This was proved by L.Alvarez, F.Guichard, P.-L.Lions and J.-M.Morel in [4]. As regards the linear scale space we defined in introduction by Equation 2.1, it also satisfies the semi-group property and the comparison principle, but it is neither affine invariant nor morphological. Figure 2.1 compares this scale space with the AMSS for an image of a cheetah.

Figure 2.1: Two scale spaces of a cheetah image.

The two images of first column are the same original image of a cheetah head. This image is analyzed with two different scale spaces : the affine morphological scale space (row 1) and the linear scale space (row 2). Column 2 corresponds to a medium scale of analysis and column 3 to a larger scale. Notice how the affine morphological scale space preserves geometrical structures, whereas the linear scale space performs mainly a global blur.

2.2.2 Geometric formulation

We now come to the geometric formulation of the affine scale space. Because of the morphological invariance, the evolution of u_0 according to Equation 2.2 is formally equivalent to the evolution of its level curves. This curve evolution was discovered by G.Sapiro and A.Tannenbaum : it is the affine analog of the Euclidean shortening flow studied by M.Gage and R.S.Hamilton in [36] and M.A.Grayson in [39]. An initial curve $p \mapsto \boldsymbol{C}_0(p) = \boldsymbol{C}(p,0)$ evolves according to the equation

$$\frac{\partial \boldsymbol{C}}{\partial t}(p,t) = \gamma(p,t)^{\frac{1}{3}} \boldsymbol{N}(p,t), \tag{2.3}$$

where $\gamma(p,t)$ and $\boldsymbol{N}(p,t)$ are respectively the curvature and the normal vector of the curve $\boldsymbol{C}(\cdot,t)$ in $\boldsymbol{C}(p,t)$. Replacing p with an affine arclength parameter s satisfying the constant determinant relation

$$\left[\frac{\partial \boldsymbol{C}}{\partial s}, \frac{\partial^2 \boldsymbol{C}}{\partial s^2}\right] = 1,$$

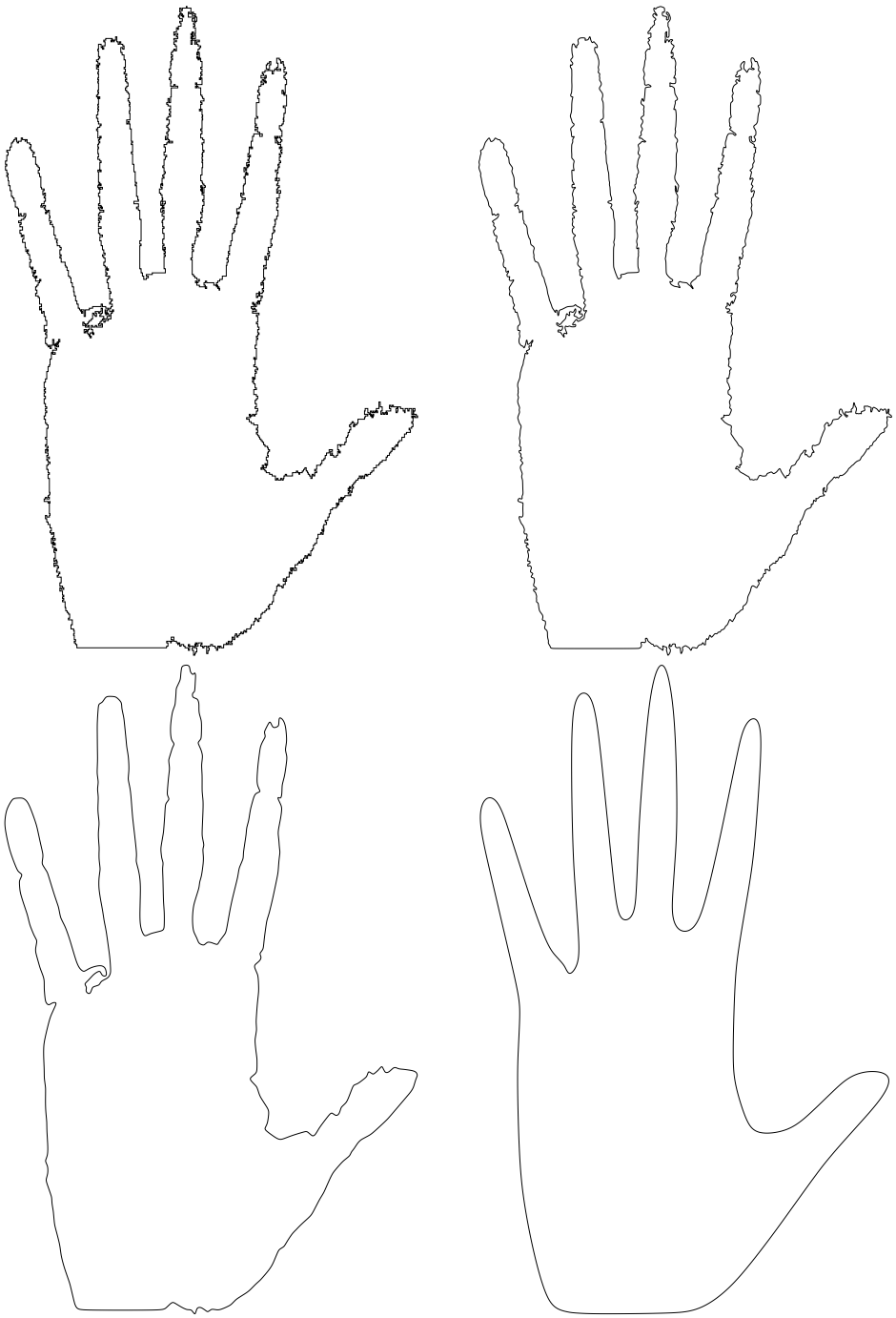

Figure 2.2: Affine Scale Space of a "hand" curve.

The scale of analysis is, from left to right, and then top to bottom : 0 (original curve), 1, 8, 200. It is clear that the original curve (top-left) cannot be directly analyzed by a shape recognition device due to its very noisy aspect. This is the reason why we need to simplify it in the most natural possible way, which has been theoretically proven to be the affine scale space. To ensure good performances of the shape recognition process, a high accuracy is needed in the computation of the scale space, even for large scales.

Equation 2.3 reduces to a nonlinear intrinsic heat equation

$$\frac{\partial \boldsymbol{C}}{\partial t} = \frac{\partial^2 \boldsymbol{C}}{\partial s^2}.$$

As for the image formulation, the collection of curves $(\boldsymbol{C}(\cdot,t))_{t\geqslant 0}$ is called Affine Scale Space.

We must mention the fact that the existence and uniqueness of a solution of (2.3) for an initial non-convex curve has not been proved so far (whereas it has been proved in [36], [39] in the Euclidean case). Hence, although the image and the geometrical formulations of the affine scale space are formally equivalent, we shall rather use the first one to establish precise results.

Figure 2.2 shows the geometrical affine scale space of a "real-world" curve that was obtained from the photograph of a hand.

2.2.3 Applications

By now, the main application of the affine scale space is probably shape analysis. It was used by T.Cohignac in [26] to perform an affine invariant shape recognition algorithm for partially occluded shapes. In this case, classical methods based on a global affine normalization cannot be used anymore, and one needs to characterize a shape locally by affine invariant descriptors. This was done by T.Cohignac by means of a technique which is directly related to the affine scale space (see Figure 2.3). To perform an efficient shape recognition, an accurate implementation of the affine scale space is required, both for small and for large scales.

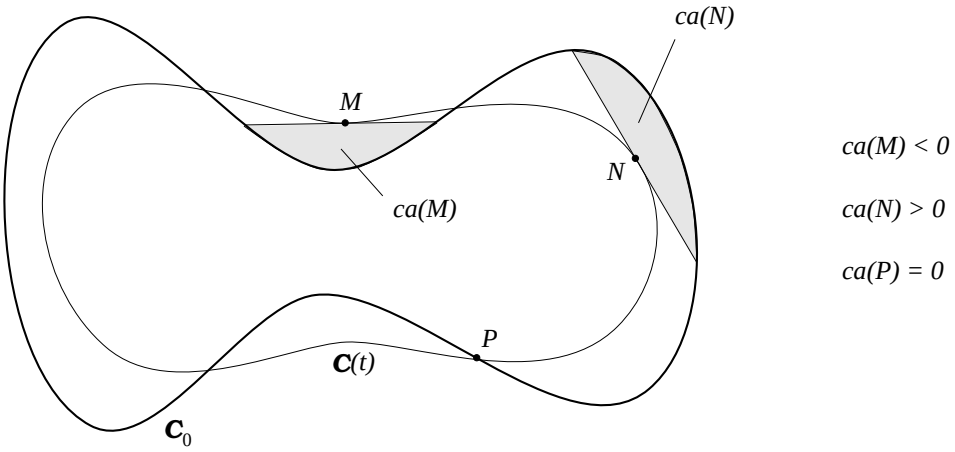

Figure 2.3: Characteristic area as defined by T.Cohignac.

The original curve $\boldsymbol{C}_0$ is smoothed by the affine scale space at scale t into a new curve $\boldsymbol{C}(t)$. Then, to each point M of $\boldsymbol{C}(t)$ we associate the (algebraic) area $ca(M)$ of the domain bounded by $\boldsymbol{C}_0$ and the tangent to $\boldsymbol{C}(t)$ in M. The characteristic points are defined on $\boldsymbol{C}(t)$ as the points M where the characteristic area $ca(M)$ attains an extremum. A local affine invariant shape recognition device is obtained by identifying these characteristic points in all intrinsic affine bases (see [26] for more details).

The AMSS model can also be viewed, when applied at small scales, as an affine invariant denoising process, very efficient —like the median filter— in the case of non-additive noises (impulse noise[4] for example). This property is illustrated on Figure 2.4.

Figure 2.4: Denoising effects of scale spaces.

Top-Left	:	*original Lena image,*
Top-Right	:	*Lena image corrupted with 30% impulse noise ,*
Bottom-Left	:	*Top-Right image smoothed by the linear scale space,*
Bottom-Right	:	*Top-Right image smoothed by the AMSS*

Due to its morphological nature, the Affine Morphological Scale Space *(AMSS) performs a much better noise removal than any linear process, especially in the case of a non-additive noise.*

[4]Corrupting an image with a 10% impulse noise means that random, independent and uniformly distributed values are attributed to a uncorrelated random 10% amount of the image pixels.

2.3 Numerical schemes for the Affine Scale Space

2.3.1 Definitions

Consider a numerical scheme for the AMSS, described by the iteration of an operator T depending on a scale step Δt and a space step $\Delta \boldsymbol{x}$. As in [40], we shall say that T is **consistent** with the AMSS if

$$\frac{Tu - u}{\Delta t} \to |Du|\mathrm{curv}(u)^{\frac{1}{3}}$$

when the steps $\Delta \boldsymbol{x}$ and Δt tend to 0 in a suitable way. The scheme is **convergent** if the iterated filter $T^n = T \circ T \circ \ldots T$ converges[5] towards the AMSS at scale t when Δt and $\Delta \boldsymbol{x}$ tend to 0 in a suitable way, and $n\Delta t \to t$.

2.3.2 The Osher-Sethian's method

Since the image formulation of the affine scale space (Equation 2.2) and the geometrical formulation (Equation 2.3) are equivalent, a numerical scheme for a formulation can be transposed into a numerical scheme for the other one. S.Osher and J.A.Sethian successfully used an image formulation to compute the affine scale space of a planar set (see [65], [71]). They also applied to several other evolution equations the general idea of viewing a hypersurface as the level set of a scalar function. The great advantage of this method is that the topological changes on the evolving set (e.g. loss of connectedness) are automatically handled by the function ; this approach permits complicated curve evolutions, but it inherits the drawbacks of the numerical scheme used for the associated scalar function. Moreover, it is likely — though not proven by now — that no topological change can occur in the special case of the planar affine scale space (that is, a Jordan curve remains a Jordan curve), so that such an image formulation is not absolutely required to compute the affine scale space of a curve.

2.3.3 State of the art

The Bence-Merriman-Osher Algorithm for Mean Curvature Motion

In [12], J.Bence, B.Merriman and S.Osher proposed a very simple algorithm for computing the mean curvature flow. The mean curvature scale space is defined by

$$\begin{cases} \dfrac{\partial u}{\partial t} = |Du|\mathrm{curv}(u) \\ \\ u(\cdot, 0) = u_0(\cdot). \end{cases} \tag{2.4}$$

It is quite similar to the AMSS, except that it is not affine invariant. The Bence-Merriman-Osher scheme seems difficult to extend to the affine case, but we would still like to mention it. The idea is to compute the evolution of a set by applying the heat equation to its characteristic

[5] We shall be more precise later about the kind of convergence we mean (simple, uniform, ...).

function, the result being thresholded after each iteration. In other words, the evolution of a set S_0 is obtained by iterating the kernel

$$\mathcal{H}(t) = Q \circ G_t \circ \chi,$$

where

$$Q(u) = \{\boldsymbol{x} \in \mathbb{R}^n,\ u(\boldsymbol{x},t) \geqslant \frac{1}{2}\}, \qquad \chi(S)(x) = \begin{cases} 1 \text{ if } \boldsymbol{x} \in S, \\ 0 \text{ otherwise,} \end{cases}$$

and G_t is the Gaussian convolution kernel solving the heat equation

$$\frac{\partial u}{\partial t} = \Delta u.$$

As $n \to \infty$, $\mathcal{H}(t/m)^m S_0$ tends towards the mean curvature flow of S_0 at scale t, at least in the viscosity sense for the associated characteristic function. This convergence property has been proved by G.Barles and C.Georgelin in [9], and by L.C.Evans in [30]. H.Ishii also proposed a generalization in [45]. However, such a scheme does not remain consistent in its discrete implementation, as F.Guichard remarked in [40].

A quasilinear scheme

An efficient quasilinear finite difference scheme was proposed in 1993 by L.Alvarez and F.Guichard (see [40] for example). The idea is to iterate the discrete evolution

$$u_{n+1}(\boldsymbol{x}) = u_n(\boldsymbol{x}) + \Delta t \cdot A(u_n)(\boldsymbol{x}),$$

where $A(u)(\boldsymbol{x})$ is a discrete approximation at point $\boldsymbol{x}$ of $|Du|\text{curv}(u)^{\frac{1}{3}}$ using the 9 values of u on a 3x3 neighborhood of $\boldsymbol{x}$. They proved that one can choose $A(u)$ in order that the approximation $A(u) \simeq |Du|\text{curv}(u)^{\frac{1}{3}}$ is exact for any polynomial u of degree 3. The resulting scheme is neither morphological nor monotone, but is experimentally stable. Of course, such a local scheme cannot be really affine invariant, because the neighborhood size is fixed in advance.

Inf-Sup operators

In [41], F.Guichard and J.-M.Morel showed that appropriate iterated inf-sup operators converge towards the affine morphological scale space. We shall describe these operators more precisely in Chapter 5. The Euclidean case had been treated before by F. Catté and F. Dibos in [22]. However, because of the spatial quantization and the morphological invariance (no new grey-level is created on the image), the discrete alternate iterated inf-sup operator gets "stuck" after several iterations (that is, no evolution occurs any longer). Indeed, on a spatial grid, a level curve is constrained to move at entire speeds : at each step, either it does not move, or it jumps over one pixel at least (see [26]).

A multiscale spline representation

In [17], G.Sapiro, A.Cohen and A.M.Bruckstein described a multiscale representation of planar shapes using B-splines. This representation is affine invariant, but it cannot be described by an evolution equation, and in particular it does not satisfy the inclusion principle (analog for sets to the comparison principle for images) :

$$A \subset B \quad \Rightarrow \quad \forall t \geqslant 0, \;\; T_t(A) \subset T_t(B). \tag{2.5}$$

For that reason, it is not well adapted to image analysis and has little to do with the affine morphological scale space.

The Osher-Sethian algorithm

As we described in Introduction, one can apply a numerical scheme for the AMSS to a set S by considering its signed distance image $u(x) = \varepsilon(x)\text{dist}(x, S)$, where $\varepsilon(x) = -1$ if $x \in S$, 1 otherwise. With this method, S.Osher and J.A.Sethian transposed the difficult problem of a geometric curve evolution into the implementation of the AMSS. However, the major drawback is that the full affine invariance is impossible to obtain with such a method, since no image representation can be affine invariant. In addition, the large image size required to achieve a reasonable precision in the curve evolution makes the process rather slow.

2.3.4 Point evolution schemes

For the affine scale space of curves, all geometrical schemes that have been proposed so far suffer from the space quantization of the curves (see [40]), which prevents the inclusion principle (2.5) from being satisfied. The main difficulty comes from the fact that there is no a priori relation between the number of vertices of a polygon and the number of the vertices needed to represent its affine shortening[6] (this number increases drastically for a triangle, but decreases as much for a very irregular curve). Thus, any algorithm based on a point-by-point evolution cannot implement the affine scale space successfully.

However, it is likely that the most accurate implementation of the Affine Scale Space is a curve evolution one, because it seems impossible to achieve precise evolutions and to guarantee a full affine invariance in any image evolution algorithm.

2.4 A fully consistent scheme

How can we implement the affine scale space with a geometrical algorithm ? Since no point evolution scheme can be efficient, we have to consider the problem globally, that is, to find an

[6] i.e. its affine scale space at a given scale.

operator T acting on curves and consistent with the affine scale space : this way, we can hope to build a numerical scheme for the affine scale space by iterating T. Moreover, we would like this operator to be affine invariant, monotone (i.e. preserving global inclusion), and easy to compute on a general kind of discrete curves (on polygons for example).

We shall propose such an operator and call it *affine erosion*. It is more or less a continuous generalization of a discrete operator briefly described in [40]. It is also somewhat related to the notion of characteristic area introduced by T.Cohignac (see [26]) : indeed, the following study proves that as the scale t tends towards 0, the characteristic area of all non-inflexion points of the curve is equivalent to $\pm c.t^{\alpha}$, c and α being universal constants. This can suggest our definition of the affine erosion.

In Chapter 3, we define precisely the affine erosion for a certain kind of curves and sets. We investigate some properties of this operator, and point out an important characterization for convex curves. We also prove that the number of inflexion points (in a generalized sense) cannot increase when this operator is applied to a non-convex curve. Last, we establish the geometrical consistency of the affine erosion with respect to the geometrical affine scale space.

In Chapter 4, we compare the Affine Scale Space and the affine erosion on a few examples, namely conics. We compute explicitly the action of these operators, and show that the affine erosion remains a good approximation of the affine scale space not only for small scales. This suggests that the affine erosion can be iterated using rather large scale steps to approximate the affine scale space efficiently.

We extend the affine erosion to grey-level images in Chapter 5, by applying the geometrical affine erosion to the level sets of an image. The resulting operator is fully consistent, inasmuch as it satisfies the most important properties of the affine scale space (the affine and morphological invariances and the comparison principle), except —naturally— the semi-group property (this is why we need to iterate the affine erosion). We also make a comparison with the inf-sup operators studied in [41], and in particular we prove that for C^1 curves, a classical affine invariant inf-sup operator acts exactly like the affine erosion for small scales. Then, we establish precise consistency and convergence properties for the alternated iterated scheme associated with the affine erosion. We link these results with Matheron's Theorem and techniques used in [41].

Chapter 6 is devoted to the numerical scheme. We prove that the affine erosion of a polygon is made of the concatenation of hyperbola pieces and segments. We present an algorithm to compute exactly the affine erosion of a polygon, and show that the resulting curve can be quantized in an affine invariant way. We compare the space and scale discretizations, and show that our algorithm has little to do with classical finite element methods. Then we present an approximate algorithm, which is very close to the first one, much faster, and which also gives accurate results.

Last, we present in Chapter 7 several experiments. Affine erosions and scale spaces are computed for simple polygons and more complicated curves, including "real-world" curves given by level curves of digitized photographs.

We conclude in Chapter 8 on the possible application of such a global technique to other evolution equations, and we indicate further axes of development.

Chapter 3

Affine erosion of curves and sets

3.1 Preliminaries

In order to define what we shall call the affine erosion of a curve or a set, we first need to make clear what kind of curves and sets we are going to consider, since it is impossible to dissociate the relation between a set and its boundary in the definition. We first restrain our study to sets whose boundaries can be described by piecewise convex curves, for which the definition and the basic properties of the affine erosion are natural. In a further chapter, we shall extend the affine erosion to any set of the plane and to grey-level images.

Let us begin with some notations and definitions. We write $\mathrm{dist}(A,B)$ for the Euclidean distance between two points A and B of the plane, AB for the vector $B-A$, $|AB| = \mathrm{dist}(A,B)$ for the Euclidean norm of AB and $[AB]$ (resp. $]AB[$) for the closed (resp. open) segment with endpoints A and B. The determinant of two vectors $\boldsymbol{v}_1$ and $\boldsymbol{v}_2$ will be noted $[\boldsymbol{v}_1, \boldsymbol{v}_2]$, and if they are both nonzero we note $\angle(\boldsymbol{v}_1, \boldsymbol{v}_2) \in S^1 = \mathbb{R}/_{2\pi\mathbb{Z}}$ the angle from $\boldsymbol{v}_1$ to $\boldsymbol{v}_2$.

When s and t belong to the circle S^1, $[s,t]$ means the class of the interval $[s',t']$ where s' and t' are real number such that $s' = s$ and $t' = t$ modulo 2π and $s' \leqslant t' < s' + 2\pi$. As well, the inequality $a_1 \leqslant a_2 \leqslant ... \leqslant a_n$ on S^1 means that we can find some real numbers $a'_1, a'_2, ...a'_n$ equal to $a_1, a_2, ...a_n$ modulo 2π such that $a'_1 \leqslant a'_2 \leqslant ... \leqslant a'_n < a'_1 + 2\pi$ (which makes sense for $n \geqslant 3$).

We choose to call a **simple curve** any subset of $\mathbb{R}^2$ homeomorphic to the circle S^1 (**closed curve**) or $\mathbb{R}$ (**non closed curve**). We shall often refer to a simple curve using the notation $C(I)$, which means implicitly that $C : I \to C(I)$ is a parameterization of the curve ; unless additional specification is given, we shall suppose in general that $I = \mathbb{R}$ or $I = S^1$. Among all possible parameterizations of a curve, two classes can be distinguished according to the set $\{C([s,t[);\ s,t \in I\}$. Choosing a class of parameterization defines an orientation of the curve. As usual, a curve $\mathcal{C}$ is of class C^1 if it admits a parameterization $C : I \to \mathcal{C}$ of class C^1 such that C' never vanishes (such a parameterization is called **regular**). A curve is of class C^n $(n > 1)$ if it admits a regular parameterization of class C^n.

We define a **semi-closed curve** as an oriented simple curve $\mathcal{C}$ such that $\mathbb{R}^2 - \mathcal{C}$ has exactly two connected components, called the inside part and the outside part of $\mathcal{C}$ according to the orientation of $\mathcal{C}$ (with the classical convention that the inside part of $\mathcal{C}$, noted $\mathcal{I}(\mathcal{C})$, is "on the left" when one runs positively on $\mathcal{C}$). A semi-closed curve can also be viewed as a simple oriented closed curve defined on the Alexandroff compactification of the plane $\mathbb{R}^2 \cup \{\infty\}$; in particular, a closed curve is semi-closed.

Let $C(I)$ be a simple curve. Then, $(s,t) \in I^2$ is a **chord** of C if and only if the piece of curve $C(]s,t[)$ and the open segment $]C(s)C(t)[$ are disjoint or equal. The connected closed set enclosed by $C(]s,t[)$ and the chord segment $]C(s)C(t)[$ is a **chord set** of C, written $C_{s,t}$ (see Figure 3.1). If area $(C_{s,t}) = \sigma$, then (s,t) is called a σ-chord and $C_{s,t}$ a σ-chord set of C.

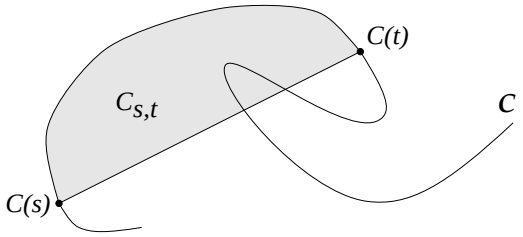

Figure 3.1: A chord set of a simple curve.
Notice that the chord segment $[C(s)C(t)]$ can intersect $\mathcal{C} \setminus C([s,t])$.

Following this idea, if $C(]a,b[)$ is a semi-closed curve ($\{a,b\} \subset \overline{\mathbb{R}}$), we say that (s,b) is an **infinite σ-chord** of C if there exists a half line D with start-point $C(s)$ such that $C(]s,b))\cap D = \emptyset$ and the chord set $C_{s,b}$ enclosed by D and $C(]s,b[)$ is of finite area σ. The case of the infinite chord (a,s) is symmetric. Last, (a,b) is an infinite σ-chord of C if there exists a line D such that $C(]a,b[) \cap D = \emptyset$ and the chord set $C_{a,b}$ enclosed by D and $C(]s,b[)$ is of finite area σ. For example, if we consider the curve $C(\mathbb{R})$ defined by $C(x) = (x, e^{-x^2})$ in an orthonormal basis of the plane, then the line $\{y = 0\}$ is an infinite chord segment associated to the $\sqrt{\pi}$-chord set $C_{-\infty,+\infty}$ (from now on, we assume that a "chord segment" can be finite or infinite, i.e. either a true segment, a half line, or a line).

If $\mathcal{C}$ is oriented and area $(C_{s,t}) \neq 0$, the orientation induced by C on the boundary of $C_{s,t}$ tells whether (s,t) is a positive or a negative chord. We take the convention that a 0-chord set is both positive and negative. The collection of all positive (resp. negative) σ-chord sets of C will be written $\mathcal{K}^+_\sigma(C)$ (resp. $\mathcal{K}^-_\sigma(C)$). Since the previous definition of a chord set does not depend on the parameterization of the curve, it makes sense to write $\mathcal{K}^+_\sigma(\mathcal{C})$ (resp. $\mathcal{K}^-_\sigma(\mathcal{C})$) for the collection of all positive (resp. negative) σ-chord sets of an oriented curve $\mathcal{C}$.

Now we give a definition of convex curves which makes also sense in the case of non semi-closed curves.

Definition 1 *An oriented simple curve $C(I)$ is*

- ***locally convex*** *in $C(s)$ if for $\varepsilon > 0$ small enough,*

$$[C(s-\varepsilon)C(s), C(s)C(s+\varepsilon)] \geqslant 0.$$

- ***locally concave*** *in $C(s)$ if for $\varepsilon > 0$ small enough,*

$$[C(s-\varepsilon)C(s), C(s)C(s+\varepsilon)] \leqslant 0.$$

- ***convex*** *(resp.* ***concave****) if it is locally convex (resp. concave) everywhere.*

A (non oriented) simple curve is convex if it is convex for a certain orientation.

We may use the term "strictly convex" (resp. strictly concave) for an oriented curve which is convex and nowhere locally concave (resp. concave and nowhere locally convex). In other words, a curve is strictly convex if it is convex and does not contain any segment of nonzero length.

For a convex curve, it is not true in general that any chord set is convex (see Figure 3.2). However, if the curve is convex and semi-closed, then its inside part is convex and any couple $(s,t) \in I^2$ (with $s \leqslant t$ if $I \subset \mathbb{R}$) defines a convex chord set. Conversely, any convex subset of the plane is the inside part of a semi-closed convex curve.

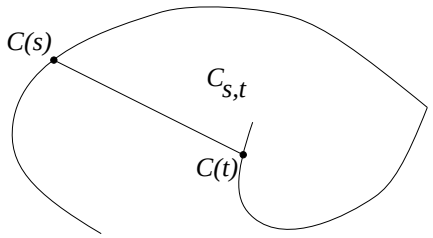

Figure 3.2: A non convex chord-set of a convex curve.

We recall that if $\mathcal{C}$ is a convex curve, one can find a regular parameterization C admitting everywhere a non-vanishing left and right derivative C'_- and C'_+ (which can differ at most on a countable number of points). Given a point A of an oriented convex curve $\mathcal{C}$, we note $\boldsymbol{T}_A^-$ (resp. $\boldsymbol{T}_A^+$) the unitary left-tangent (resp. right-tangent) of $\mathcal{C}$ in A. Thus, if $\mathcal{C} = C(I)$ and $A = C(s)$, we have $C'_+(s) = |C'_+(s)|\ \boldsymbol{T}_A^+$ and $C'_-(s) = |C'_-(s)|\ \boldsymbol{T}_A^-$.

Definition 2 *A* ***piecewise convex curve*** *is a simple curve $C(I)$ for which there exists a finite subdivision $(s_1, s_2, \ldots s_n)$ of I such that each sub-curve $C(]s_i, s_{i+1}[)$ is convex.*

In general, we shall suppose that the subdivision (s_i) is optimal, i.e. that n is minimal. However, even with this constraint the decomposition is not necessarily unique (consider the case of a polygonal curve for example). We shall see later that there exists a canonical decomposition.

Definition 3 *An open subset S of the plane $\mathbb{R}^2$ is a* ***C-set*** *if*

(i) it has a finite number of connected components

(ii) the boundary of any connected component is a finite disjoint union of semi-closed piecewise convex curves.

These oriented curves enclosing the connected components of S are called the ***components of*** *∂S.*

Remark : One should be careful not to mix up the connected components of a C-set S with the components of ∂S. In particular, the components of ∂S are not necessarily disjoint : if S is the inside of a "8", the boundary of S is connected but has two components. On Figure 3.3 for example, the initial C-set S has 3 connected components and ∂S has 4 components.

The previous definition of a C-set is a compromise between regularity (the boundary of a C-set admits a tangent almost everywhere) and generality (any finite union of convex sets is a C-set, as well as the inside part of any polygon).

Definition 4 *A C-set is simple if its boundary has only one component.*

A simple C-set S shall often be written $\mathcal{I}(\mathcal{C})$, which means that $\mathcal{C}$ is a semi-closed piecewise convex curve whose inside part is S. Notice that a C-set S can always be written

$$S = \bigsqcup_i \left(S_i \setminus \overline{\bigsqcup_j T_{i,j}} \right),$$

where the S_i and $T_{i,j}$ are finite collections of simple C-sets and the symbols $\sqcup$ and $\overline{A}$ mean respectively a disjoint union of sets and the topological closure of a set A.

3.2 Affine erosion of sets

In this section, we define the affine erosion of a C-set, and we establish some basic properties of this operator.

3.2.1 Definition

Definition 5 *The* ***σ-affine erosion*** *of a C-set S is the set of the points of S which cannot be enclosed in any positive chord set with area less than σ of a component of ∂S.*

$$E_\sigma(S) = S \quad \setminus \bigcup_{\substack{\sigma' \leqslant \sigma \\ K \in \mathcal{K}^+_{\sigma'}(\partial S)}} K.$$

Here, $\mathcal{K}^+_{\sigma'}(\partial S)$ means all the σ'-chord sets of all components of ∂S. Figure 3.3 represents an intricate C-set and its affine erosion (only the oriented boundaries of the sets have been drawn for a better understanding).

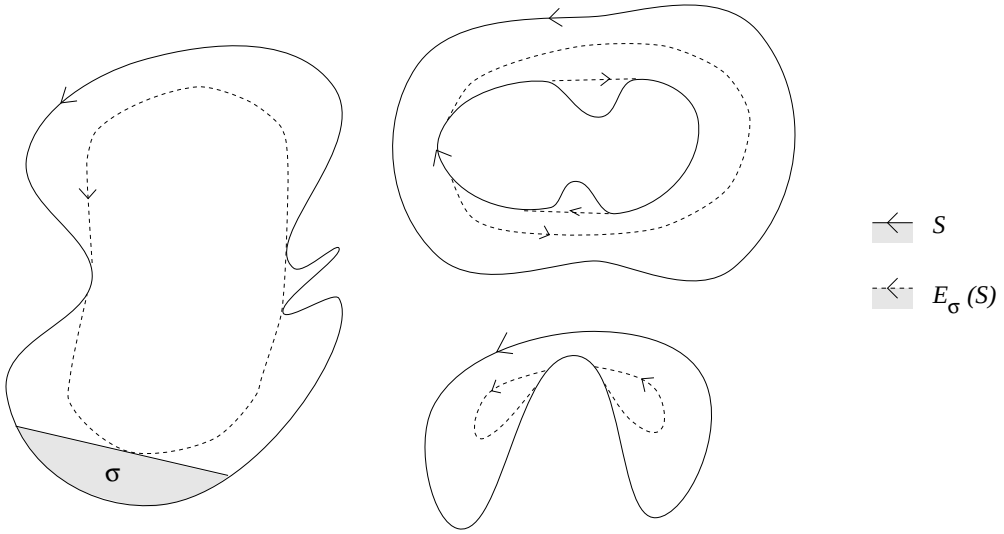

Figure 3.3: Affine erosion of an intricate C-set

3.2.2 Example

Before we go further, let us compute explicitly the affine erosion of a "corner". This computation has strong consequences on the numerical scheme we present later. Other exact computations can be found in the next chapter.

Proposition 1 *The σ-affine erosion of the "corner"*

$$W = \{O + x\,\boldsymbol{v}_1 + y\,\boldsymbol{v}_2;\ x > 0, y > 0\}$$

is the inside (convex) part of a hyperbola, given in the affine basis $(O, \boldsymbol{v}_1, \boldsymbol{v}_2)$ by the equation

$$x.y > \frac{\sigma}{2\,[\boldsymbol{v}_1, \boldsymbol{v}_2]}, \quad x > 0, y > 0. \tag{3.1}$$

*In what follows, σ will be called the **apparent area** of the hyperbola defined by Equation 3.1.*

Proof :

First, we notice that only the positive chord sets with area σ are significant to define the affine erosion of W because W is convex (a positive chord set with area less than σ can always be enclosed in a positive σ-chord set).

Now, any positive σ-chord segment of W is supported by a line with equation $x/a + y/b = 1$ (see Figure 3.4) submitted to the area constraint $2\sigma = ab\,[\boldsymbol{v}_1, \boldsymbol{v}_2]$. Consequently, the boundary

of $E_\sigma(W)$ is obtained by the envelope of these lines, given by the system

$$\begin{cases} D_a : \dfrac{x}{a} + \dfrac{a\,[\boldsymbol{v}_1, \boldsymbol{v}_2]\,y}{2\sigma} = 1 \\ D'_a : \dfrac{-x}{a^2} + \dfrac{[\boldsymbol{v}_1, \boldsymbol{v}_2]\,y}{2\sigma} = 0. \end{cases}$$

Then, eliminating a yields

$$xy = \frac{\sigma}{2\,[\boldsymbol{v}_1, \boldsymbol{v}_2]}.$$

□

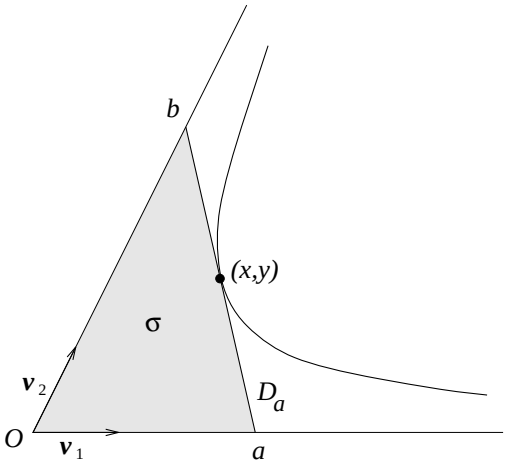

Figure 3.4: Affine erosion of a "corner"

3.2.3 Topological structure

We now establish a useful property of the affine erosion : if S is a C-set, each point of the boundary of $E_\sigma(S)$ lies on a chord segment of S.

Definition 6 *Let S be a C-set and $C(I)$ a component of ∂S, then a σ'-chord (s,t) of C is* ***σ-limit chord*** *if $\sigma' \leqslant \sigma$ and C has no chord (s',t') of area lower than σ including strictly (s,t) (i.e. such that $s' < s \leqslant t \leqslant t'$ or $s' \leqslant s \leqslant t < t'$ in $\overline{I}$).*

Lemma 1 *For any C-set S, the boundary of $E_\sigma(S)$ is included in the union of the positive σ-limit chord segments of S.*

Proof :

1. First, we prove that any $M \in \partial E_\sigma(S)$ belongs to a positive σ'-chord segment of a component of ∂S, where $\sigma' \leqslant \sigma$.

$M \in \partial E_\sigma(S)$ means that we can find a sequence (A_n, B_n) of finite and positive chords with area less than σ and such that $\mathrm{dist}(M, [A_n B_n]) \to 0$ as $n \to \infty$. Since S has a finite number of

components, necessarily one component $\mathcal{C}$ of ∂S contains a infinite number of chords (A_n, B_n). Thus, we can extract from the sequence (A_n, B_n) a subsequence $(A_{\varphi(n)}, B_{\varphi(n)})$ of σ_n chords of $\mathcal{C}$, and we can suppose that $\sigma_n \to \sigma' \leqslant \sigma$ either (up to another subsequence extraction).

1.a. If $(A_{\varphi(n)})$ and $(B_{\varphi(n)})$ are bounded, we can extract from $(A_{\varphi(n)}, B_{\varphi(n)})$ a convergent subsequence in $\mathcal{C}^2$. The limit (A, B) satisfies $d(M, [AB]) = 0$, which means that $M \in [AB]$, and a part of $[AB]$ — or $[AB]$ itself — defines a σ'-chord segment of S containing M (with $\sigma' \leqslant \sigma$).

1.b. If $(A_{\varphi(n)})$ is bounded and $(B_{\varphi(n)})$ is not, we can extract from $(A_{\varphi(n)})$ a subsequence that converges towards $A \in \mathcal{C}$. If $A = M$, then M belongs to the chord $[A, A]$ of $\mathcal{C}$ and we have finished. If $A \neq M$, then a part of the half line $[AM)$ defines a positive chord segment of $\mathcal{C}$ (finite or infinite) containing M. The case $(B_{\varphi(n)})$ bounded and $(A_{\varphi(n)})$ not bounded is symmetric.

1.c. If both $(A_{\varphi(n)})$ and $(B_{\varphi(n)})$ are not bounded, then up to a subsequence extraction we can find a nonzero vector $\boldsymbol{v}$ such that $\angle(\boldsymbol{v}, A_{\varphi(n)}B_{\varphi(n)})$ is defined and converges towards zero. Then, the line $(M, \boldsymbol{v})$ defines a σ'-chord segment of S (finite or infinite) containing M (with $\sigma' \leqslant \sigma$).

2. Last, we note that only the σ-limits chord sets are significant to define $E_\sigma(S)$, because if a chord (A, B) is not σ-limit we can find a σ-limit chord set which contains strictly the chord set associated to (A, B). □

Corollary 1 *The affine erosion of a C-set is an open subset of the plane.*

Proof :

From Lemma 1 we know that if S is a C-set, the boundary of $E_\sigma(S)$ is part of

$$A = \bigcup_{\substack{\sigma' \leqslant \sigma \\ K \in \mathcal{K}^+_{\sigma'}(\partial S)}} K.$$

Therefore, ${}^cE_\sigma(S) = A \cup {}^cS$ is closed (because it contains its boundary) and $E_\sigma(S)$ is open (${}^cS$ denotes the complementary set of S, i.e. ${}^cS = \mathbb{R}^2 \setminus S$). □

Remark : Lemma 1 highlights the necessity of considering infinite chords for non-bounded curves. Look at the previous example of the C-set S defined in an orthonormal basis of the plane by the equation $y < e^{-x^2}$: if we had not allowed infinite chords in the affine erosion of S, then the σ-affine erosion of S would have been the *closed* half plane $\{y \leqslant 0\}$ for any $\sigma \geqslant \sqrt{\pi}$ (instead of the open half plane $\{y < 0\}$), and Corollary 1 would not have been satisfied any more.

However, infinite chord are rather rare, because :

- a bounded C-set has no infinite chord,
- if a non-bounded C-set S admits an infinite chord, then it contains a half line which is an asymptote to a component of ∂S.

We could have restrained our definition of the affine erosion to less general sets (to bounded sets, for example) in order to avoid the case of infinite chords ; however, in the next chapter we shall be interested in non-bounded conics like hyperbolae and parabolae. Moreover, it is more satisfactory to define the affine erosion of any convex set (bounded or not).

3.2.4 Affine dilation

We can define in two equivalent ways the dual operator to affine erosion, that we shall call affine dilation. The first one is to reverse the orientation of the curves, the second one is to consider the open complementary of each set (for which the orientation of the boundary is reversed).

Definition 7 *The* σ***-affine dilation*** *of a C-set* S *is defined by*

$$D_\sigma(S) = E_\sigma({}^c\overline{S}).$$

Proposition 2 *The closure of the* σ*-affine dilation of a C-set* S *is the union of* S *and all negative chord-sets with area less than* σ *of the components of* ∂S*.*

$$\overline{D_\sigma(S)} = S \quad \cup \bigcup_{\substack{\sigma' \leqslant \sigma \\ K \in \mathcal{K}^-_{\sigma'}(\partial S)}} K.$$

Proof :

This is a simple consequence of the identity $\mathcal{K}^-_\sigma(S) = \mathcal{K}^+_\sigma({}^c\overline{S})$.

3.2.5 Basic properties of the affine erosion

Lemma 2 $E_\sigma(S)$ *is nonincreasing with respect to* σ*, i.e.*

$$\sigma_1 \leqslant \sigma_2 \quad \Rightarrow \quad E_{\sigma_2}(S) \subset E_{\sigma_1}(S).$$

Proof :

We just need to notice that if $\sigma_1 \leqslant \sigma_2$ then

$$\bigcup_{\substack{\sigma' \leqslant \sigma_1 \\ K \in \mathcal{K}^+_{\sigma'}(\partial S)}} K \quad \subset \quad \bigcup_{\substack{\sigma' \leqslant \sigma_2 \\ K \in \mathcal{K}^+_{\sigma'}(\partial S)}} K,$$

and consequently $E_{\sigma_2}(S) \subset E_{\sigma_1}(S)$. □

Definition 8 *We call* ***extinction scale*** *of a C-set S and we note $\sigma_e(S)$ the lower bound of the scales σ for which $E_\sigma(S) = \emptyset$.*

Proposition 3 *If S is a simple bounded C-set, then $\sigma_e(S) \leqslant \frac{1}{2}\,\text{area}\,(S)$.*

Proof :

Let us prove that for any simple bounded C-set S of area 2σ, $E_\sigma(S) = \emptyset$. Consider M a point of S : there exist two points A and B lying on ∂S such that the open segment $]AB[$ is included in S and contains M. This segment defines two positive chord-sets of S of area σ_1 and σ_2 such that $\sigma_1 + \sigma_2 = \text{area}\,(S)$. Necessarily, $\sigma_1 \leqslant \sigma$ or $\sigma_2 \leqslant \sigma$, which means that M belongs to a positive chord set of area not larger than σ, i.e. $M \notin E_\sigma(S)$. □

One could think that the extinction scale of a simple bounded C-set is exactly half of its area. Although this is true for convex C-sets symmetric with respect to a point, this result is generally false for other simple C-sets, even convex. In the next chapter, we show that the extinction area of a triangle is $\frac{4}{9}$ of its area.

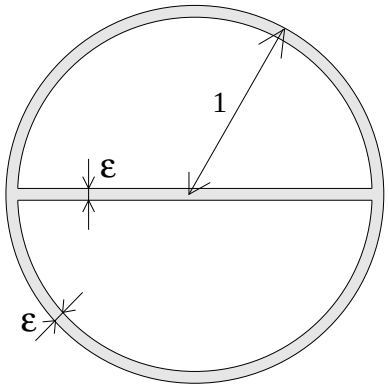

Figure 3.5: A C-set with small area and large extinction area

Proposition 3 is not true for a non simple bounded C-set. In fact, it is possible to build a C-set of area as small as we want comparatively to its extinction area. The shaded part of Figure 3.5 defines a C-set of area less than $2\varepsilon(\pi + 1)$, whereas its extinction scale is exactly $\pi/2$, i.e. half of the area of the enclosing disk. Indeed, we can deduce from Proposition 3 that the extinction area of any bounded C-set is less than half the external area of its largest connected component (the external area of a connected C-set is the area enclosed by its external boundary, i.e. including the area of its "holes").

Proposition 4 *$E_\sigma(S)$ is nondecreasing with respect to S, i.e.*

$$S_1 \subset S_2 \quad \Rightarrow \quad E_\sigma(S_1) \subset E_\sigma(S_2).$$

Proof :

Let S_1 and S_2 be two C-sets such that $S_1 \subset S_2$, and consider M a point of S_2. If M does not belong to $E_\sigma(S_2)$, there exists a positive σ'-chord segment D (finite or infinite) of a component of ∂S_2 such that $\sigma' \leqslant \sigma$ and M belongs to the associated chord set.

1. If $M \notin S_1$, then $E_\sigma(S_1) \subset S_1$ yields $M \notin E_\sigma(S_1)$.

2. If $M \in S_1$, consider the connected component A of S_1 containing M.

2.a. If $A \cap D = \emptyset$, then the external boundary of A encloses a subset of area less than σ', so that from Proposition 3 we get $M \notin E_\sigma(S_1)$.

2.b. If $A \cap D \neq \emptyset$, then $A \cap D$ is a disjoint union of chord segments of S_1 (finite or infinite), and one of these chord segments defines a σ''-chord set of S_1 containing M (see Figure 3.6). But since $S_1 \subset S_2$, we have $\sigma'' \leqslant \sigma'$, so that $M \notin E_\sigma(S_1)$.

Thus, $M \notin E_\sigma(S_2) \Rightarrow M \notin E_\sigma(S_1)$, which means that $E_\sigma(S_1) \subset E_\sigma(S_2)$. □

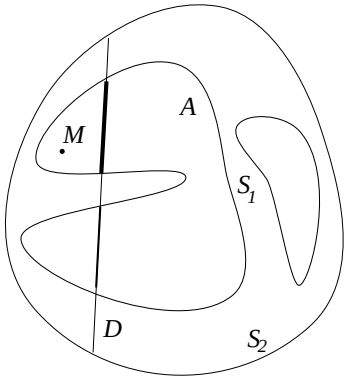

Figure 3.6: E_σ is monotone

Proposition 5 *The affine erosion is covariant with respect to the affine transformations of the plane, i.e for any affine map ϕ,*

$$\phi\left(E_\sigma(S)\right) = E_{\sigma\cdot|\det\phi|}\left(\phi(S)\right),$$

$\det\phi$ *being the determinant of the linear part of ϕ, i.e.* $\det\phi = \det A$ *where $\phi(M) = AM + B$ and $(A, B) \in L(\mathbb{R}^2) \times \mathbb{R}^2$.*

Proof :

This elementary result simply arises from the fact that for a C-set S, we have

$$\phi\left[\mathcal{K}^+_\sigma(\partial S)\right] = \{\phi(K);\ K \in \mathcal{K}^+_\sigma(\partial S)\} = \mathcal{K}^+_{\sigma\cdot|\det\phi|}(\partial\phi(S)).$$

□

3.3 Affine erosion of convex curves

Let us first consider two particular kinds of convex C-sets : half planes, and strips (i.e. sets enclosed by two parallel straight lines). These C-sets (to which we shall refer as *trivial* C-sets) are invariant under affine erosion, because they only have 0-chord sets. One easily checks that they are the only simple C-sets which satisfy this property. So, since they would not satisfy most of the statements which follow, we shall exclude them most of the time. Another reason is that any nontrivial convex C-set is simple.

3.3.1 Basic statements

Proposition 6 *The affine erosion of a convex C-set is a convex C-set.*

Proof :

If S is a convex C-set, then $S - K$ is also convex for any positive σ-chord set K of ∂S. It follows that

$$E_\sigma(S) = \bigcap_{\substack{\sigma' \leqslant \sigma \\ K \in \mathcal{K}_{\sigma}^{+}(S)}} (S - K)$$

is convex as an intersection of convex sets. □

A consequence of this proposition is that we can define the affine erosion for convex curves. According to the previous remark, we call *trivial* any convex semi-closed curve made of a straight line. From now on, we also suppose that a convex semi-closed curve is naturally oriented in such a way that its inside is convex. Hence, nontrivial convex semi-closed curves and nontrivial convex C-sets are equivalent since the map $\mathcal{C} \mapsto \mathcal{I}(\mathcal{C})$ establishes a bijective correspondence between them. Notice incidentally that any chord set of a convex set is positive and finite (i.e. bounded).

Definition 9 *The σ-affine erosion of a convex semi-closed curve $\mathcal{C}$ is the convex semi-closed curve*

$$E_\sigma(\mathcal{C}) = \partial E_\sigma(\mathcal{I}(\mathcal{C})).$$

Of course, the notation $E_\sigma(\mathcal{C})$ is abusive, but more simple. We shall always avoid any possibility of confusion between the affine erosion of a set and the affine erosion of a curve anyway.

Proposition 7 *If S is a non-trivial convex C-set, then for any $\sigma \leqslant \sigma_e(S)$, only the σ-chord sets matter in the definition of the σ-affine erosion of S, i.e.*

$$E_\sigma(S) = S - \bigcup_{K \in \mathcal{K}_{\sigma}^{+}(\partial S)} K.$$

Proof :

Let $C(I)$ be the boundary of S : since S is convex, any couple $(s,t) \in I^2$ is a chord of C, and the map $t \mapsto$ area $(C_{s,t})$ is continuous and increasing from 0 towards area (S) (which may be infinite) unless S is trivial, which is not the case here. Consequently, if (s,t) is a σ'-chord of S with $\sigma' < \sigma \leqslant \sigma_e(S) \leqslant$ area (S), then $(s,t+\varepsilon)$ is a σ-chord of S for a judicious choice of ε, and $C_{s,t} \subset C_{s,t+\varepsilon}$, which means that (s,t) is not a σ-limit chord of C. In other words, all σ-limit chords of S are σ-chords of S and Lemma 1 achieves the proof. □

3.3.2 The middle point property

We now establish an interesting property of convex semi-closed curves : their σ-affine erosion is always included in the set of the middle points of their σ-chord segments, and the equality holds beyond a limit scale of erosion (which is nonzero for most of the curves). The reason is roughly explained on Figure 3.7 : given a curve $\mathcal{C} = C(I)$ and σ-chord segment $[C(s)C(t)]$, another σ-chord segment of $\mathcal{C}$ intersects $[C(s)C(t)]$ in $I(\theta)$, and as $\theta \to 0$, the area equality forces

$$\frac{1}{2} r_1^2(\theta) \cdot \theta = \frac{1}{2} r_2^2(\theta) \cdot \theta + o(\theta),$$

so that $r_1(\theta) - r_2(\theta) \to 0$ and $I(\theta)$ converges towards the middle of $[C(s)C(t)]$. This means that the envelope of the σ-chord segments of $\mathcal{C}$ is made of the middle points of these segments. Under additional conditions, we shall prove that this envelope is exactly the σ-affine erosion of $\mathcal{C}$.

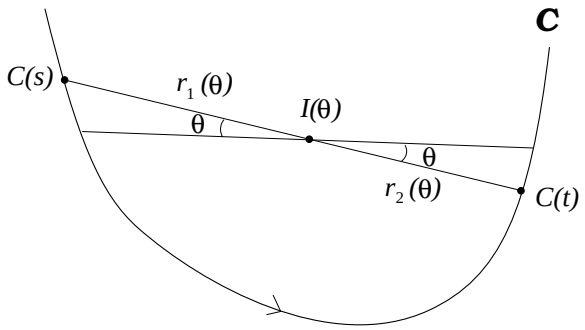

Figure 3.7: The middle point property

We begin with a useful geometric lemma.

Lemma 3 *Consider A,B,A',B' four distinct points of the plane such that*

$$[AB] \cap [A'B'] = \{M\}$$

and

$$\text{area}\,(MAA') = \text{area}\,(MBB').$$

Then,

$$\frac{\text{dist}(A,B)}{\text{dist}(A,M)} = 2 - \frac{[AA', BB']}{[AB, BB']}.$$

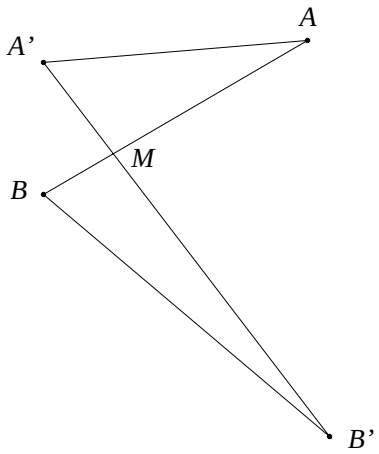

Figure 3.8: 4 points Lemma

Proof :

Let us first define λ with $AM = \lambda AB$, which implies $MB = (1-\lambda)AB$. Since the area of the triangles MAA' and MBB' are equal, we have

$$[AA', AM] = [BB', BM],$$

which gives

$$\lambda\,[AA', AB] = (1-\lambda)\,[AB, BB']. \tag{3.2}$$

Moreover, as M also lies on the segment $[A'B']$, we can write

$$[MA', MB'] = 0 = [MA + AA', MB + BB'] = [-\lambda AB + AA', (1-\lambda)AB + BB'],$$

so that

$$-\lambda\,[AB, BB'] + (1-\lambda)\,[AA', AB] + [AA', BB'] = 0. \tag{3.3}$$

Now, multiplying Equation 3.3 by λ and replacing the second term from Equation 3.2, we obtain

$$-\lambda^2\,[AB, BB'] + (1-\lambda)^2\,[AB, BB'] + \lambda\,[AA', BB'] = 0,$$

and the terms in λ^2 cancel so that

$$\lambda\,(2\,[AB, BB'] - [AA', BB']) = [AB, BB'].$$

Finally, we obtain as announced

$$\frac{1}{\lambda} = \frac{\text{dist}(A,B)}{\text{dist}(A,M)} = 2 - \frac{[AA', BB']}{[AB, BB']}.$$

□

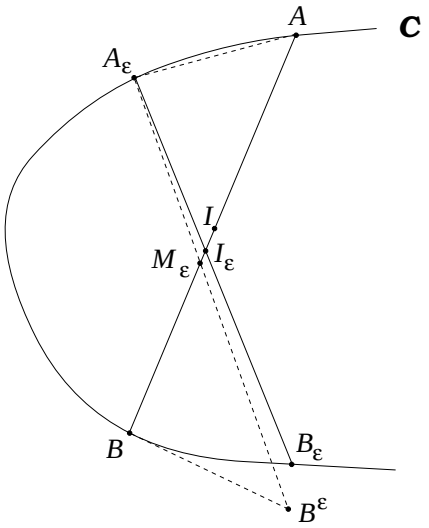

Figure 3.9: The middle point property (1)

Proposition 8 *If $\mathcal{C}$ is a non-trivial convex semi-closed curve, then for any scale σ, $E_\sigma(\mathcal{C})$ is included in the set of the middle points of the σ-chord segments of $\mathcal{C}$.*

Proof :

First recall that since $\mathcal{C}$ is convex, we can choose a regular parameterization C of $\mathcal{C}$ (i.e. such that its left and right derivative C'_- and C'_+ never vanish). Let I be a point of $E_\sigma(\mathcal{C})$. Lemma 1 states that we can find a σ-chord (s,t) of C such that $[AB] = [C(s)C(t)]$ contains I. Defining λ by $I = (1-\lambda)A + \lambda B$, we shall prove that both $\lambda \leqslant \frac{1}{2}$ and $\lambda \geqslant \frac{1}{2}$, or, in other words, that I is the middle of $[AB]$.

1. First consider $\varepsilon > 0$ such that $s + \varepsilon < t$. Since the map $x \mapsto \text{area}\,(C(s+\varepsilon, t+x))$ is increasing, there exists a unique ε', depending on s, t and ε, such that $(s+\varepsilon, t+\varepsilon')$ is another σ-chord of C. Necessarily, $[AB]$ and $[A_\varepsilon B_\varepsilon] = [C(s+\varepsilon)C(t+\varepsilon')]$ have a common point I_ε, and the areas of the curved triangles $I_\varepsilon A A_\varepsilon$ and $I_\varepsilon B B_\varepsilon$ are equal.

2. It is clear that there exists a unique real $k(\varepsilon)$ such that A, B, A_ε and $B^\varepsilon = B + k(\varepsilon)C'_+(t)$ are four points satisfying the hypotheses of Lemma 3. Moreover, the convexity of C forces the related intersection point $M_\varepsilon = [AB] \cap [A_\varepsilon B^\varepsilon]$ to belong to the segment $[BI_\varepsilon]$ (cf. Figure 3.9). Since every point of $[BI_\varepsilon]$ belongs to the chord set $C_{s+\varepsilon, t+\varepsilon'}$, necessarily $I \notin [BM_\varepsilon]$, which means that $\lambda \leqslant \lambda_\varepsilon$ where λ_ε is defined by $I_\varepsilon = (1-\lambda_\varepsilon)A + \lambda_\varepsilon B$.

3. From Lemma 3, we know that

$$\frac{1}{\lambda_\varepsilon} = 2 - \frac{[AA_\varepsilon, BB^\varepsilon]}{[AB, BB^\varepsilon]} = 2 - \frac{[AA_\varepsilon, C'_+(t)]}{[AB, C'_+(t)]},$$

and since $AA_\varepsilon \to 0$ as $\varepsilon \to 0$, we get

$$\frac{1}{\lambda_\varepsilon} \to 2 \quad \text{as} \quad \varepsilon \to 0,$$

which proves that $\lambda \leqslant \frac{1}{2}$ according to Step 2.

4. A symmetrical reasoning proves that $\lambda \geqslant \frac{1}{2}$ as well, and consequently $\lambda = \frac{1}{2}$, i.e. I is the middle of the segment associated to the σ-chord (s,t). □

From this result, it is natural to wonder whether there is an exact correspondence between the σ-affine erosion of a non-trivial convex semi-closed curve and the set of the middle points of its σ-chord segments. We are going to prove that the answer is positive for a large class of curves, including C^1 curves and many polygons, provided that σ is small enough. For that purpose, we introduce the following definitions of regular chord and regular scale.

Definition 10 *Let $\mathcal{C}$ be a convex semi-closed curve, then a chord (A,B) of $\mathcal{C}$ is* ***regular*** *if* $\angle(\boldsymbol{T}_A^-, \boldsymbol{T}_B^+) \in [0,\pi[$.

Definition 11 *Let $\mathcal{C}$ be a non-trivial convex semi-closed curve. A real $\sigma \geqslant 0$ is a* ***regular scale*** *for C if any σ-chord of $\mathcal{C}$ is regular. We note $\sigma_r(\mathcal{C})$ the upper bound of the regular scales of $\mathcal{C}$.*

Theorem 1 (middle point property) *Let $\mathcal{C}$ be a non-trivial convex semi-closed curve, and σ a regular scale of $\mathcal{C}$. Then $E_\sigma(\mathcal{C})$ is exactly the set of the middle points of the σ-chord segments of $\mathcal{C}$, and there is a natural homeomorphism between $\mathcal{C}$ and $E_\sigma(\mathcal{C})$.*

Proof :

According to Proposition 8, we only have to prove that the middle point of any σ-chord belongs to $E_\sigma(\mathcal{C})$. Consider C a regular parameterization of $\mathcal{C}$, let (s,t) be a σ-chord of C, and define α the smallest positive number x such that $(s-x,s)$ is a σ-chord of C. Finally, let $\mathcal{D}^+ =]-\alpha, 0[$ and $\mathcal{D}^- =]0, t-s[$ (if $\mathcal{C}$ is closed, then these intervals must be considered in S^1). For any $a \in \mathcal{D}^- \cup \mathcal{D}^+$, we call $I(a)$ the intersection between $[C(s)C(t)]$ and the chord segment associated to the σ-chord of origin $s+a$, and define $\lambda(a)$ by $C(s)I(a) = \lambda(a)\, C(s)C(t)$.

Notice that if a σ-chord of C intersects $]C(s)C(t)[$ then its origin can be taken in $\mathcal{D}^- \cup \{0\} \cup \mathcal{D}^+$. Hence, to prove that no σ-chord set of C contains I, the middle of $[C(s)C(t)]$, it is sufficient to prove that $\lambda > \frac{1}{2}$ on $\mathcal{D}^+$ as well as $\lambda < \frac{1}{2}$ on $\mathcal{D}^-$.

1. We first establish that for $\varepsilon > 0$ small enough, $\lambda(-\varepsilon) < \frac{1}{2} < \lambda(\varepsilon)$.

Consider $\varepsilon, \varepsilon'$ such that $s < s+\varepsilon < t < t+\varepsilon'$ and $(s+\varepsilon, t+\varepsilon')$ is another σ-chord of $\mathcal{C}$ (implicitly, ε' depends on s,t and ε). Now define $k(\varepsilon)$ such that $C(t), C(t+\varepsilon'), C(s)$ and $A^\varepsilon = C(s) + k(\varepsilon)C'_+(s)$ are four points satisfying the equi-area hypothesis of Lemma 3. Necessarily, $M_\varepsilon = [C(t)C(s)] \cap [C(t+\varepsilon')A^\varepsilon]$ belongs to $[I(\varepsilon)C(s)]$, so that $\lambda(\varepsilon) \geqslant \lambda'(\varepsilon)$ where $\lambda'(\varepsilon)$ is defined by $C(s)M_\varepsilon = \lambda'(\varepsilon)C(s)C(t)$. Moreover, from Lemma 3 we get

$$\begin{aligned} \frac{1}{1-\lambda'(\varepsilon)} &= 2 - \frac{[C(t)C(t+\varepsilon'), k(\varepsilon)C'_+(s)]}{[C(t)C(s), k(\varepsilon)C'_+(s)]} \\ &= 2 + \frac{[C'_+(s), C(t)C(t+\varepsilon')]}{[C'_+(s), C(s)C(t)]}. \end{aligned}$$

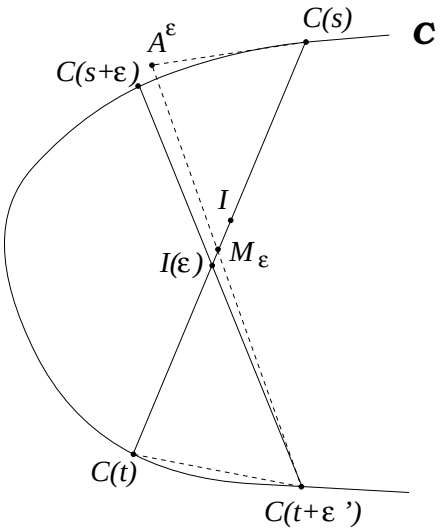

Figure 3.10: The middle point property (2)

Since $\mathcal{C}$ is convex, $[C'_+(s), C(s)C(t)] > 0$, and as (s,t) is a regular chord of C, we have as well, for $\varepsilon > 0$ small enough, $[C'_+(s), C(t)C(t+\varepsilon')] > 0$. Consequently, $\lambda(\varepsilon) \geqslant \lambda'(\varepsilon) > \frac{1}{2}$ for $\varepsilon > 0$ small enough, and a symmetric proof would establish $\lambda(-\varepsilon) < \frac{1}{2}$ for $\varepsilon > 0$ small enough.

2. Let us check that λ is continuous. Given $a \in \mathcal{D}^- \cup \mathcal{D}^+$, there exists a unique $b(a)$ such that $(s+a, t+b(a))$ is a σ-chord of $\mathcal{C}$. Since the map $(s,t) \mapsto \text{area}\,(C_{s,t})$ is continuous, so is the map $a \mapsto b(a)$. Now, as $I(a) = [C(s)C(t)] \cap [C(s+a(C(t+b(a))]$, a simple computation gives

$$\lambda(a) = \frac{[C(s+a)C(t+b(a)), C(s)C(t+b(a))]}{[C(s+a)C(t+b(a)), C(s)C(t)]},$$

and the non-vanishing denominator ensures that λ is continuous on $\mathcal{D}^+ \cup \mathcal{D}^-$. Last, we know from Proposition 8 that λ can be continuously extended to 0 by taking $\lambda(0) = \frac{1}{2}$.

3. Now we prove that λ has no local maximum on $\mathcal{D}^+$, and no local minimum on $\mathcal{D}^-$.

If λ has a local maximum in $a \in \mathcal{D}^+$, then for ε small enough, $I(a+\varepsilon)$ and $I(a-\varepsilon)$ belong to the segment $[I(a)C(s)]$ (see Figure 3.11). Then, due to the position of $C(s+a+\varepsilon)$ and $C(s+a-\varepsilon)$ relatively to $C(s+a)$, it is clear that the intersection of the σ-chords of origin $s+a$ and $s+a+\varepsilon$ lies on $[C(s+a)I(a)]$, whereas the intersection of the σ-chords of origin $s+a$ and $s+a-\varepsilon$ cannot lie on $[C(s+a)I(a)[$. But this is a contradiction with Step 1 applied to the σ-chord of origin $s+a$, since we would have $\lambda'(-\varepsilon) \geqslant \lambda'(\varepsilon)$ for the corresponding λ'. As a conclusion, λ has no local maximum on $\mathcal{D}^+$, and a symmetric proof establishes that λ has no local minimum on $\mathcal{D}^-$ either.

4. From Step 2 and 3 we deduce that λ is monotone on $\mathcal{D}^+$ (resp. on $\mathcal{D}^-$), and the only possibility according to Step 1 (and to the fact that $\lambda(\varepsilon) \to \frac{1}{2}$ as $\varepsilon \to 0$) is that λ is nondecreasing on $\mathcal{D}^+$ (resp. on $\mathcal{D}^+$) and remains strictly larger than $\frac{1}{2}$ on $\mathcal{D}^+$ (resp. strictly lower than $\frac{1}{2}$ on $\mathcal{D}^-$). Consequently, I does belong to $E_\sigma(\mathcal{C})$.

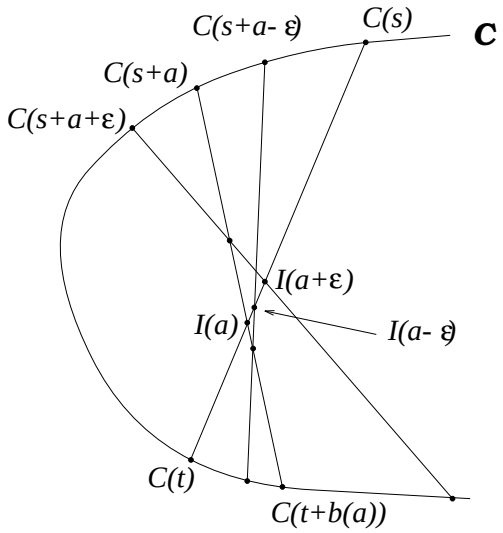

Figure 3.11: The middle property (3)

5. Now we can build a bijective and continuous correspondence between $\mathcal{C}$ and $E_\sigma(\mathcal{C})$ as follows : given $C(s) \in \mathcal{C}$, there exists a unique $\delta(s,\sigma)$ such that $(s-\delta, s+\delta)$ is a σ-chord of C. According to Theorem 1,

$$C_\sigma(s) = \frac{1}{2}(C(s-\delta) + C(s+\delta))$$

belongs to $E_\sigma(\mathcal{C})$, and the correspondence $C(s) \mapsto C_\sigma(s)$ is one to one and clearly bicontinuous. □

Notice that the natural correspondence between $\mathcal{C}$ and its affine erosion gives sense to $E_\sigma(C)$, meaning the parameterization induced by C on the σ-affine erosion of the curve $C(I)$.

Corollary 2 *If $\mathcal{C}$ is a non-trivial convex semi-closed curve and σ a regular scale of $\mathcal{C}$, then $E_\sigma(\mathcal{C})$ is of class C^1.*

Proof :

If this is not the case, then we can find a $M \in E_\sigma(\mathcal{C})$ such that $\boldsymbol{T}_M^+ \neq \boldsymbol{T}_M^-$. But necessarily these semi-tangents arise from two distinct σ-chord segment containing M, which is impossible according to Theorem 1. □

We shall estimate the regularity of $E_\sigma(\mathcal{C})$ more precisely later . Now, let us compute again the affine erosion of the "corner" of Proposition 1 using Theorem 1. First, it is clear that the boundary of the "corner"

$$\{O + x\boldsymbol{v}_1 + y\boldsymbol{v}_2;\ x > 0, y > 0\}$$

is a semi-closed curve $\mathcal{C}$ with $\sigma_r(\mathcal{C}) = +\infty$ (any scale is regular) : thus, we know from Theorem 1 that its σ-affine erosion is exactly given by the middle of its σ-chords.

The chord set $(O, \boldsymbol{v}_1, \boldsymbol{v}_2)$ of $\mathcal{C}$ delimited by the points $O + 2x\,\boldsymbol{v}_1$ and $O + 2y\,\boldsymbol{v}_1$ has an area equal to $2\,xy.[\boldsymbol{v}_1, \boldsymbol{v}_2]$ (cf. figure 3.12). Consequently, the σ-affine erosion of $\mathcal{C}$ is the set of the middle points $O + x\,\boldsymbol{v}_1 + y\,\boldsymbol{v}_2$ constrained by the area equality $2\,xy.[\boldsymbol{v}_1, \boldsymbol{v}_2] = \sigma$, which corresponds to the hyperbola defined in Equation 3.1.

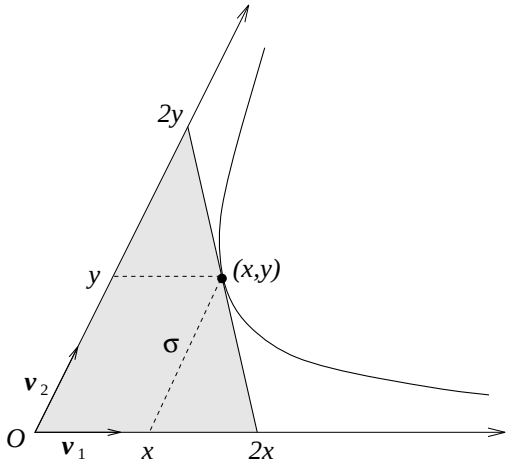

Figure 3.12: Affine erosion of a "corner" (2)

3.3.3 Regular scales

In this section, we characterize the regular scales of a non-trivial convex semi-closed curve.

Proposition 9 *Let $\mathcal{C}$ be a non-trivial convex semi-closed curve. The set of the regular scales of $\mathcal{C}$ is $[0, \sigma_r(\mathcal{C})[$.*

Proof :

Suppose that $\sigma_r(\mathcal{C}) < +\infty$ (otherwise there is nothing to prove), and consider $C : I \to \mathbb{R}^2$ a regular parameterization of $\mathcal{C}$. In what follows, we consider $\boldsymbol{v}_0$ an arbitrary nonzero vector of the plane, and the angle function $\alpha_+ : I \to S^1$ (respectively $\alpha_- : I \to S^1$) defined by $\alpha_+(s) = \angle(\boldsymbol{v}_0, C'_+(s))$ ($\alpha_-(s) = \angle(\boldsymbol{v}_0, C'_-(s))$ respectively).

1. First we show that if σ is a regular scale of $\mathcal{C}$ and $0 \leqslant \sigma' \leqslant \sigma$, then σ' is also a regular scale of $\mathcal{C}$. Suppose that it is not the case, i.e. that we can find a non-regular σ'-chord (s, t) of C. We can choose $\varepsilon > 0$ in such a manner that $(s, t+\varepsilon)$ is a σ-chord of C. Since $\alpha_+(t) \leqslant \alpha_+(t+\varepsilon) \leqslant \alpha_-(s)$ and $\alpha_+(t) - \alpha_-(s) \in [\pi, 2\pi[$, we have $\alpha_+(t+\varepsilon) - \alpha_-(s) \in [\pi, 2\pi[$ which means that $(s, t+\varepsilon)$ is a non-regular σ-chord of C. This contradiction proves that σ' is a regular scale of $\mathcal{C}$. Hence, the set of regular scales of $\mathcal{C}$ is $[0, \sigma_r(\mathcal{C})[$ or $[0, \sigma_r(\mathcal{C})]$.

2. Now we prove that $\sigma_r(\mathcal{C})$ is not a regular scale of $\mathcal{C}$.

2.a. If C is closed, then $I = S^1$, and there exist two sequences (s_n) and (t_n) such that (s_n, t_n) is a non-regular σ_n-chord of C with $\sigma_n \to \sigma_r(\mathcal{C})$ as $n \to +\infty$. Since S^1 is compact, we can find

an increasing map $\varphi : \mathbb{N} \to \mathbb{N}$ such that

$$\lim_{n\to\infty} (s_{\varphi(n)}, t_{\varphi(n)}) = (a, b) \in I \times I.$$

Now, because area $(C_{s,t})$ is continuous with respect to s and t, we have

$$\text{area}\,(C_{a,b}) = \sigma_r(\mathcal{C}).$$

If we define $a_n = \min(a, s_{\varphi(n)})$ and $b_n = \max(b, t_{\varphi(n)})$, we have, in S^1 and for n large enough,

$$\alpha_+(b_n) - \alpha_-(a_n) \in [\pi, 2\pi[. \tag{3.4}$$

Now remark that α_- is left-continuous and α_+ is right-continuous and deduce from (3.4) that modulo 2π,

$$\alpha_+(b) - \alpha_-(a) \in [\pi, 2\pi],$$

and since $\alpha_+(b) - \alpha_-(a) = 2\pi$ is impossible, (a, b) is a non-regular chord of C.

2.b. If $\mathcal{C}$ is not closed, then we can suppose that $I = \mathbb{R}$ and as $\mathcal{C}$ is a semi-closed curve,

$$\lim_{+\infty} \alpha^+ - \lim_{-\infty} \alpha^- \in [0, \pi],$$

so that if (a, b) is a non-regular σ-chord, necessarily $\alpha_+(b) - \alpha_-(a) = \pi$ and $C(]-\infty, a[)$ and $C([b, +\infty[)$ must be two parallel half lines. Now define $a' = \sup\{x;\ \alpha_-(x) = \alpha_-(a)\}$ and $b' = \inf\{x;\ \alpha_+(x) = \alpha_+(b)\}$: (a', b') is a non-regular chord of C and clearly area $(C_{a'b'}) = \sigma_r(\mathcal{C})$. □

Corollary 3 *Let $\mathcal{C}$ be a non-trivial convex semi-closed curve, then $\sigma_r(\mathcal{C}) > 0$ if and only if no part of C is a segment $[AB]$ such that $\angle(\boldsymbol{T}_A^-, \boldsymbol{T}_B^+) \in [\pi, 2\pi[$.*

Proof :

1. If $[AB]$ is a piece of $\mathcal{C}$ such that $\angle(\boldsymbol{T}_A^-, \boldsymbol{T}_B^+) \in [\pi, 2\pi[$, then (A, B) is a non-regular 0-chord of $\mathcal{C}$, and consequently $\sigma_r(\mathcal{C}) = 0$.

2. Conversely, let us suppose now that $\sigma_r(\mathcal{C}) = 0$. From Proposition 9 we know that we can find a non-regular 0-chord of $\mathcal{C}$, i.e. a part of $\mathcal{C}$ which is a segment $[AB]$ such that $\angle(\boldsymbol{T}_A^-, \boldsymbol{T}_B^+) \in [\pi, 2\pi[$. □

This result allows us to check that the characteristic constant σ_r is non zero for a large class of convex semi-closed curves, including C^1 ones and all polygons such that the sum of two successive angle steps remains strictly below π.

Corollary 4 *If $\mathcal{C}$ is a convex semi-closed curve of class C^1, then $\sigma_r(\mathcal{C}) > 0$.*

Proof :

Suppose that $\mathcal{C}$ is a convex semi-closed curve of class C^1 for which $\sigma_r(\mathcal{C}) = 0$, from Corollary 3 a part of $\mathcal{C}$ should be a segment $[AB]$ such that $\boldsymbol{T}_A^- \neq \boldsymbol{T}_B^+$, which is impossible since $\boldsymbol{T}_A^+ = \boldsymbol{T}_B^-$ and the regularity of $\mathcal{C}$ forces $\boldsymbol{T}_B^+ = \boldsymbol{T}_B^-$ and $\boldsymbol{T}_A^+ = \boldsymbol{T}_A^-$. □

Corollary 5 *If $\mathcal{C} = A_0A_1...A_n$ is a convex polygon, then $\sigma_r(\mathcal{C}) > 0$ iff for all i modulo n,*

$$[A_iA_{i+1}, A_{i+2}A_{i+3}] > 0.$$

Proof :

This is a simple consequence of Corollary 3, and if $[A_iA_{i+1}, A_{i+2}A_{i+3}] > 0$ for all i we even know that

$$\sigma_r(A_1A_2...A_n) \geqslant \min_i \text{area}\,(A_iA_{i+1}A_{i+2}).$$

□

What happens for a non-regular chord ? Considering the proof of Theorem 1, we can see that if $\angle(\boldsymbol{T}_A^-, \boldsymbol{T}_B^+) \in]\pi, 2\pi[$ we have both $\lambda > \frac{1}{2}$ and $\lambda < \frac{1}{2}$, i.e. no point of the σ-chord segment $[AB]$ belongs to $E_\sigma(\mathcal{C})$. In other words, the curve described by the middle points of the σ-chord segments has "ghost parts" which must be removed to obtain the desired affine erosion. For instance, these "ghost parts" appear at any scale of erosion for a triangle, for which $\sigma_r = 0$ (see Figure 3.13).

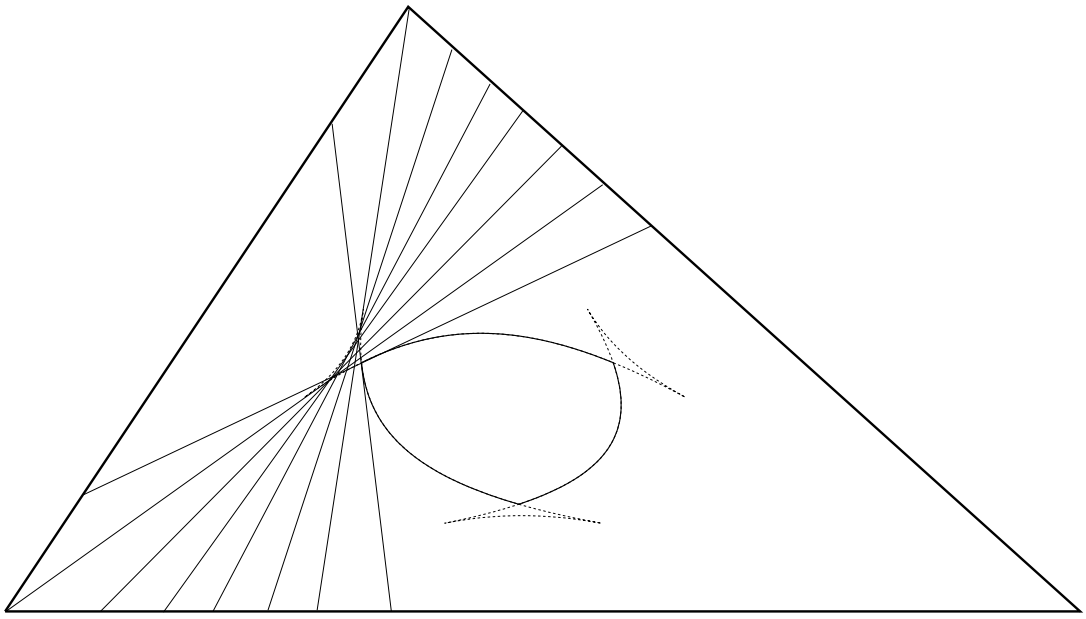

Figure 3.13: "ghost parts" always appear in the affine erosion of a triangle

The need to remove these ghost parts is in some way related to the Huygen's principle construction used for the propagation of fronts. Behind this construction hides an entropy

condition : if the propagating front is viewed as a burning flame, then *once a particle is burnt it stays burnt and cannot burn any more* (see [65]), so that such "ghost parts" of fronts have no physical meaning.

If $\angle(\boldsymbol{T}_A^-, \boldsymbol{T}_B^+) = \pi$ (i.e. $\boldsymbol{T}_A^- = -\boldsymbol{T}_B^+$), Definition 10 makes the chord (A, B) non regular despite the fact that the middle point of the associated chord segment does belong to $E_\sigma(\mathcal{C})$. The reason why we did not allow this configuration in our definition of a regular chord is that we want not only the reverse inclusion between the middle points and the affine erosion, but also a bijective correspondence. The case of a square highlights this phenomenon : at any scale, four points of the affine erosion are the middle points of an infinite number of σ-chord segments, which produces singularities (discontinuity of the tangent) at these points (see Figure 3.14).

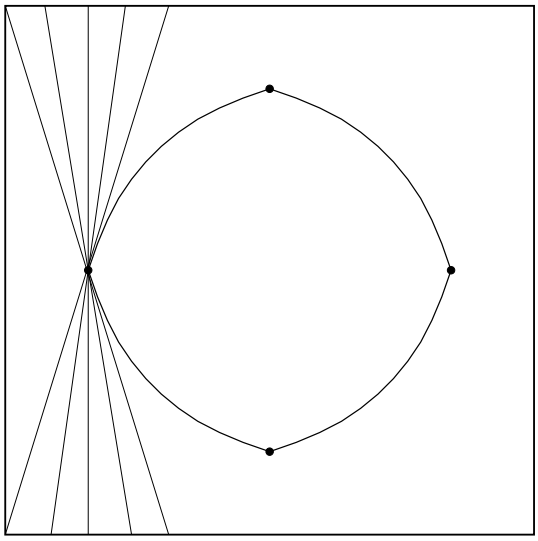

Figure 3.14: Four singularities appear in the affine erosion of a square

3.3.4 Consistency

Theorem 2 *Let $\mathcal{C} = C(I)$ be a semi-closed convex curve of class C^n with $n \geqslant 1$. Then for any $\sigma < \sigma_r(\mathcal{C})$, $E_\sigma(\mathcal{C})$ is a semi-closed convex curve of class C^n. If $n \geqslant 2$, the infinitesimal evolution as $\sigma \to 0$ of a point $C(s) \in \mathcal{C}$ is given by*

$$C_\sigma(s) = C(s) + \omega.\sigma^{\frac{2}{3}} \cdot \gamma(s)^{\frac{1}{3}}\, \boldsymbol{N}(s) + o(\sigma^{\frac{2}{3}}) \quad \text{with} \quad \omega = \frac{1}{2}\left(\frac{3}{2}\right)^{\frac{2}{3}},$$

where $\gamma(s)$ and $\boldsymbol{N}(s)$ are respectively the curvature of $\mathcal{C}$ and the normal vector to $\mathcal{C}$ at point $C(s)$. Moreover, if $n \geqslant 3$, the remaining part is $O(\sigma^{\frac{4}{3}})$ at any point where the curvature $\gamma(s)$ is nonzero.

Proof :

1. Consider $s \mapsto C(s)$ an Euclidean length parameterization of $\mathcal{C}$ (i.e. $|C'(s)| = 1$ everywhere). Since $\mathcal{C}$ is convex, we know from Theorem 1 that $E_\sigma(\mathcal{C})$ is exactly made of the middle of the σ-chords of $\mathcal{C}$ as soon as $0 < \sigma < \sigma_r(\mathcal{C})$ (which makes sense because we know from Corollary 4 that $\sigma_r(\mathcal{C}) > 0$). Let $(s-\delta, s+\delta)$ be a σ-chord of C and $C_\sigma(s)$ the middle of the associated segment (see Figure 3.15).

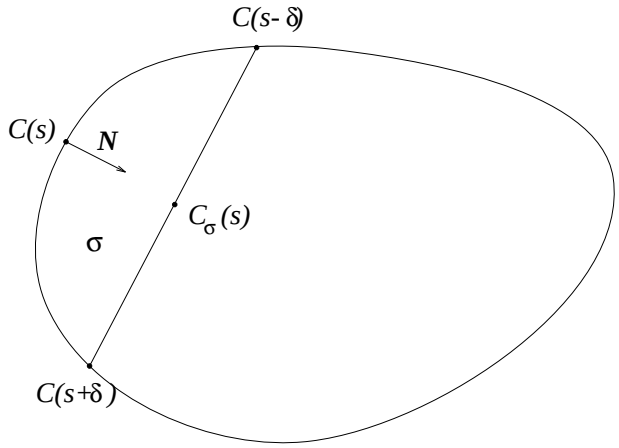

Figure 3.15: Affine erosion of a convex semi-closed curve

Since C is of class C^1, we can use the Green formula to compute the area

$$\sigma = \frac{1}{2} F(s, \delta(s,\sigma)), \quad \text{where}$$

$$F(s,t) = \int_{s-t}^{s+t} [C(h), C'(h)]\, dh \; + \; [C(s+t), C(s-t) - C(s+t)]\,.$$

A simple computation gives

$$\frac{\partial F}{\partial t}(s,t) = [C(s+t) - C(s-t), C'(s+t) - C'(s-t)]$$

$$\text{and} \quad \frac{\partial F}{\partial s}(s,t) = [C(s+t) - C(s-t), C'(s+t) + C'(s-t)]\,.$$

C being convex, we have, for any distinct points $C(a)$ and $C(b)$ of C, the inequality

$$[C'(a), C(b) - C(a)] \geqslant 0,$$

and the equality holds if and only if the piece of curve $C([a,b])$ is a segment. Hence, the numbers $[C(s+t) - C(s-t), C'(s+t)]$ and $[C(s+t) - C(s-t), -C'(s-t)]$ are positive and their sum cannot be zero unless $\sigma = 0$, which is not the case, or unless $C(s+t) = C(s-t)$, which is impossible as soon as $0 < t \leqslant \delta$. As a consequence,

$$\frac{\partial F}{\partial t}(s,\delta) > 0$$

(which simply means that the area σ of the chord-set $C_{s-\delta,s+\delta}$ increases with δ), and the global inversion theorem allows us to claim that the map $s \mapsto \delta(s,\sigma)$ is of class C^n as well as the map $(s,t) \mapsto F(s,t)$.

We just proved that the function

$$s \mapsto C_\sigma(s) = \frac{1}{2}\left(C(s-\delta(s,\sigma)) + C(s+\delta(s,\sigma))\right)$$

is of class C^n. Moreover, since the vectors $C'(s-\delta(s,\sigma))$ and $C'(s+\delta(s,\sigma))$ cannot be colinear for $\sigma < \sigma_r(\mathcal{C})$, the derivative

$$2\frac{\partial}{\partial s}C_\sigma(s) = (1-\frac{\partial\delta}{\partial s})C'(s-\delta) + (1+\frac{\partial\delta}{\partial s})C'(s+\delta) \tag{3.5}$$

never vanishes. As a consequence, the curve C_σ is of class C^n in the geometric sense (that is C_σ is a regular parameterization).

Incidentally, remark that it can easily check from Equation 3.5 that $\frac{\partial}{\partial s}C_\sigma$ and $C(s+\delta) - C(s-\delta)$ are colinear, i.e. that the σ-chord segments of $\mathcal{C}$ are the tangents to $E_\sigma(\mathcal{C})$ as expected.

2.a. If C is of class C^2, the curvature at point $C(s)$ is defined by $\gamma(s) = [C'(s), C''(s)]$. A simple expansion near $t = 0$ gives

$$\frac{\partial F}{\partial t}(s,t) = [2tC'(s) + o(t), 2tC''(s) + o(t)] = 4t^2\gamma(s) + o(t^2), \tag{3.6}$$

which can be integrated to obtain

$$2\sigma = \frac{4}{3}\delta^3\gamma(s) + o(\delta^3).$$

Thus, whenever $\gamma(s) \neq 0$ we have

$$\delta(s,\sigma) = \left(\frac{3\sigma}{2\gamma(s)}\right)^{\frac{1}{3}} + o(\sigma^{\frac{1}{3}}),$$

and finally

$$\begin{aligned} C_\sigma(s) &= \frac{1}{2}\left[C(s-\delta) + C(s+\delta)\right] \\ &= C(s) + \frac{\delta^2}{2}C''(s) + o(\delta^2) \\ &= C(s) + \frac{1}{2}\left(\frac{3}{2}\right)^{\frac{2}{3}}\sigma^{\frac{2}{3}}\cdot\gamma^{\frac{1}{3}}(s)\,\boldsymbol{N}(s) + o(\sigma^{\frac{2}{3}}), \end{aligned}$$

where $\boldsymbol{N}(s)$ is the normal vector to C in $C(s)$.

2.b. If $\gamma = 0$ we use a geometric argument. Given $\varepsilon > 0$, let $R = \varepsilon^{-3}$. Since $\gamma(s) = 0$, the disk D_R with center $C(s) + R\boldsymbol{N}(s)$ and radius R is locally contained in $\mathcal{I}(\mathcal{C})$ near $C(s)$ (see Figure 3.16). In particular, there exists $\sigma_0 > 0$ such that

$$\forall\,\sigma < \sigma_0, \quad C(s) + R\boldsymbol{N}(s) \notin C_{s-\delta,s+\delta} \quad \text{and} \quad D_R \cap C_{s-\delta,s+\delta} \subset \mathcal{I}(\mathcal{C})$$

(once again, δ depends on s and σ). Now, calling H the orthogonal projection of $C(s)$ on the chord segment $[C(s-\delta), C(s+\delta)]$ and writing $d = \mathrm{dist}(C(s), H)$, we claim that

$$\sigma \geqslant d\sqrt{R^2 - (R-d)^2}.$$

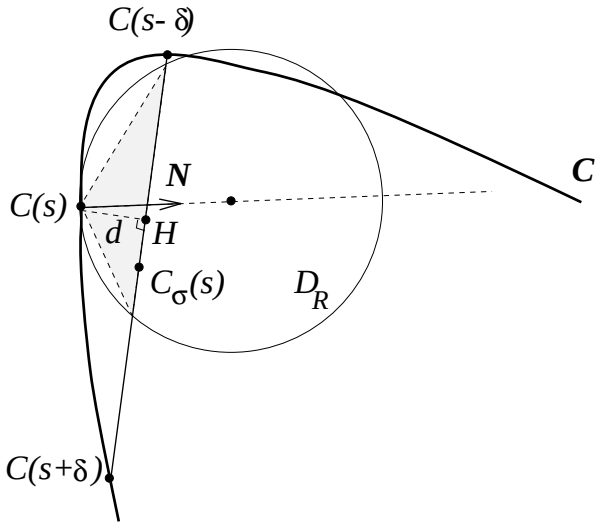

Figure 3.16: Case $\gamma = 0$

The reason for this last inequality is that σ is larger than the shaded zone of Figure 3.16, which is itself larger than $d\sqrt{R^2-(R-d)^2}$ (the equality happens when the chord is orthogonal to $\boldsymbol{N}$). Hence,

$$\sigma \geqslant d\sqrt{2Rd-d^2}$$

and

$$d^{\frac{3}{2}} \leqslant \frac{\sigma}{\sqrt{2R-d}} \leqslant \frac{\sigma}{\sqrt{R}}$$

since $d \leqslant R$ due to the fact that $C(s)+R\boldsymbol{N}(s) \notin C_{s-\delta,s+\delta}$. Consequently,

$$d \leqslant \frac{\sigma^{\frac{2}{3}}}{R^{\frac{1}{3}}} \leqslant \varepsilon\sigma^{\frac{2}{3}},$$

which means that

$$d = o(\sigma^{\frac{2}{3}}). \tag{3.7}$$

Now, we constrain σ to be small enough in order to ensure that $\angle(C'(s-\delta), C'(s))$ and $\angle(C'(s), C'(s+\delta))$ belong to $[0, \pi/2]$. Recalling that the pieces of curve $C([s-\delta, s])$ and $C([s, s+\delta])$ have length δ, we deduce that both $\mathrm{dist}(C(s-\delta), H)$ and $\mathrm{dist}(H, C(s+\delta))$ belong to $[\delta-d, \delta]$, so that

$$\mathrm{dist}(H, C_\sigma(s)) \leqslant \frac{d}{2}.$$

Then, Equation 3.7 implies that

$$\mathrm{dist}(C(s), C_\sigma(s)) = o(\sigma^{\frac{2}{3}})$$

as announced.

3. If $n \geqslant 3$, the expansion of Equation 3.6 can be improved into

$$\frac{\partial F}{\partial t}(s,t) = 4t^2\gamma(s) + O(t^3),$$

and following the same computation as in Step 2.a, on can establish that

$$C_\sigma(s) = C(s) + \omega \cdot \sigma^{\frac{2}{3}} \cdot \gamma^{\frac{1}{3}}(s)\, \boldsymbol{N}(s) + O(\sigma^{\frac{4}{3}}).$$

□

Remark : If the curvature vanishes, we can be more precise. Suppose that C is locally C^5 near s where $\gamma(s) = 0$ and $\gamma''(s) \neq 0$. At point s, we have, writing $\boldsymbol{T} = C'(s)$,

$$\begin{aligned} C'' &= \gamma \boldsymbol{N} = \boldsymbol{0} \\ C''' &= -\gamma^2 \boldsymbol{T} + \gamma' \boldsymbol{N} = \gamma' \boldsymbol{N} \\ C^{(4)} &= -3\gamma\gamma' \boldsymbol{T} + (\gamma'' - \gamma^3)\boldsymbol{N} = \gamma'' \boldsymbol{N} \end{aligned}$$

Consequently,

$$\frac{\partial F}{\partial t}(s,t) = \left[2tC'(s) + O(t^3), \frac{t^3}{3}C^{(4)}(s) + O(t^5)\right] = 2\frac{t^4}{3}\gamma''(s) + O(t^6),$$

and an integration yields

$$2\sigma = \frac{2}{15}\delta^5\gamma''(s) + O(\delta^7),$$

or equivalently

$$\delta(s,\sigma) = \left(\frac{15\sigma}{\gamma''(s)}\right)^{\frac{1}{5}} + O(\sigma^{\frac{3}{5}}).$$

Therefore, the point $C(s)$ is mapped onto

$$\begin{aligned} C_\sigma(s) &= \frac{1}{2}\left[C(s-\delta) + C(s+\delta)\right] \\ &= C(s) + \frac{\delta^4}{24}C^{(4)}(s) + O(\delta^6) \\ &= C(s) + \frac{15^{\frac{1}{5}}}{24}\sigma^{\frac{4}{5}} \cdot (\gamma''(s))^{\frac{1}{5}}\, \boldsymbol{N}(s) + O(\sigma^{\frac{6}{5}}). \end{aligned}$$

Incidentally, we check that

$$C_\sigma(s) = C(s) + o(\sigma^{\frac{2}{3}}),$$

but we can see that the expansion

$$C_\sigma(s) = C(s) + O(\sigma^{\frac{4}{3}})$$

is not generally true when $\gamma(s) = 0$ (and is false as soon as $\gamma''(s) \neq 0$). □

Remark : Theorem 2 proves that the affine erosion preserves the regularity of a convex curve. Unfortunately, it does not regularize a convex curve of class C^n into a convex curve of class C^m with $m > n$. One can check this on the C^1 curve $\mathcal{C}$ made of the half line $\{y = 0, x \leqslant 0\}$ and the half parabola $\{y = x^2, x > 0\}$: for any $\sigma > 0$, $E_\sigma(\mathcal{C})$ is not C^2.

3.4 Affine erosion of non convex curves

3.4.1 Structure

Lemma 4 *If S is a simple C-set and $M \in \partial E_\sigma(S) - \partial S$, then $\partial E_\sigma(S)$ is locally a convex curve near M.*

Proof :

Let M belong to $\partial E_\sigma(S) - \partial S$. We know from Lemma 1 that M belongs to a (possibly infinite) chord segment of a component of ∂S. As S is open and $M \in S$, for $\varepsilon > 0$ small enough, the open disk $D(M, \varepsilon)$ is included in S (see Figure 3.17). But since the complementary set to any chord set of S in $D(M, \varepsilon)$ is convex, necessarily $E_\sigma(S) \cap D(M, \varepsilon)$ is convex (it is the intersection of convex subsets of $D(M, \varepsilon)$). Consequently, $\partial E_\sigma(S)$ is near M a convex curve, because it is locally the boundary of a convex set. □

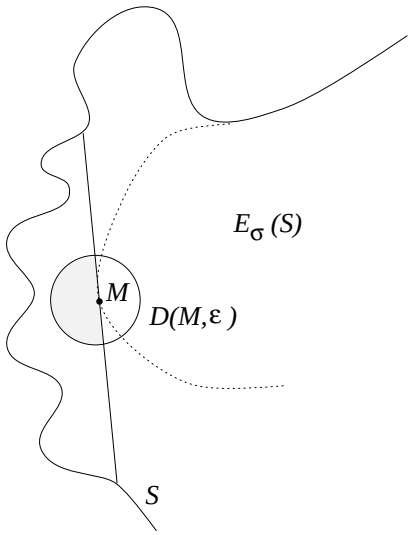

Figure 3.17: local convexity in $M \in \partial E_\sigma(S) - S$

Lemma 5 *If S is a simple C-set and $M \in \partial E_\sigma(S) \cap \partial S$ with $\sigma > 0$, then ∂S is not locally concave near M.*

Proof :

Suppose that $M \in \partial E_\sigma(S) \cap \partial S$ and ∂S is not locally concave near M. Using a parameterization C of ∂S near $M = C(s)$, we have for $\varepsilon > 0$ small enough,

$$[C(s-\varepsilon)C(s), C(s)C(s+\varepsilon)] > 0.$$

Thus, M belongs to the topological opening of a σ-chord set $C_{s-\varepsilon,s+\varepsilon}$ for $\varepsilon > 0$ small enough, which is in contradiction with $M \in \partial E_\sigma(S)$. □

According to Lemma 4 and Lemma 5, the boundary of the affine erosion of a simple C-set is everywhere locally concave or locally convex. Thus, it is a collection of curves. Hence, we can give sense to the affine erosion of a piecewise convex semi-closed curve as a collection of semi-closed curves (and we shall prove later that these curves are also piecewise convex).

Definition 12 *The σ-affine erosion of a piecewise convex semi-closed curve $\mathcal{C}$ is the collection of semi-closed curves*

$$E_\sigma(\mathcal{C}) = \partial E_\sigma(\mathcal{I}(\mathcal{C})).$$

Proposition 10 *The affine erosion of a piecewise convex semi-closed curve $\mathcal{C}$ is, up to a finite number of points, the disjoint union of a finite union of concave curves $(\mathcal{C}_i)$ and convex curves $(\mathcal{D}_j)$, with*

- $\forall i,\ \mathcal{C}_i \subset \mathcal{C}$, *and no concave sub-curve of $\mathcal{C}$ contains more than one $\mathcal{C}_i$.*
- $\forall j,\ \mathcal{D}_j \cap \mathcal{C} = \emptyset$.

Proof :

Let us define the curves $\mathcal{C}_\rangle$ as the connected components of $E_\sigma(\mathcal{C}) \cap \mathcal{C}$ (minus their extremal points if any). According to Lemma 5, these curves are concave, and if $\mathcal{C}_i$ and $\mathcal{C}_{i'}$ belong to the same concave component of $\mathcal{C}$, necessarily $i = i'$ (a nonnegative chord segment of $\mathcal{C}$ cannot have both its endpoints on the same concave component of $\mathcal{C}$). Hence, there is a finite number of curves $\mathcal{C}_i$. Now, call $\mathcal{D}_j$ the connected components of

$$E_\sigma(\mathcal{C}) \setminus \bigcup_i \overline{\mathcal{C}}_i.$$

We have to prove that there is a finite number of such curves.

First, there can be only a finite number of non semi-closed $\mathcal{D}_j$, because these $\mathcal{D}_j$ are connected to some $\mathcal{C}_i$ according to Lemma 5. Second, let us choose an arbitrary direction $\boldsymbol{v}$ of the plane, and consider the multivalued map φ which associate, to any line D directed by $\boldsymbol{v}$, all area values of all chord sets of $\mathcal{C}$ defined from a piece of D. Because $\mathcal{C}$ has a finite number of components, φ can be described by a finite set of continuously increasing single-valued maps (φ_k) (only a finite number of accidents happen to φ when D sweeps the plane). Then, to each map φ_k is associated at most one closed $\mathcal{D}_j$, so that the number of closed $\mathcal{D}_j$'s is finite. Last, as for the semi-closed but nonclosed $\mathcal{D}_j$'s, there is at most two of them. □

Corollary 6 *The affine erosion of a piecewise convex semi-closed curve is a collection of piecewise convex semi-closed curves. Equivalently, the affine erosion of a C-set is a C-set.*

Proof :

The first part is a direct consequence of Proposition 10. As for a C-set S, it is sufficient to notice that the boundary of $E_\sigma(S)$ is included in the affine erosion of the components of ∂S. □

3.4.2 Inflexion points

We would like to prove that the number of inflexion points (in a generalized sense) cannot increase when we compute the affine erosion of a piecewise convex closed curve. This is another stability property of the affine erosion, complementary to the inclusion principle.

Let $\mathcal{C} = C(I)$ be a piecewise convex curve. We define a canonical decomposition of $\mathcal{C}$ into convex curves. We say that a point M of $\mathcal{C}$ is

- convex if $\mathcal{C}$ is locally convex near M,
- concave if $\mathcal{C}$ is locally concave near M,

We consider the sub-curves $\mathcal{C}_i^+$ of $\mathcal{C}$ defined as the open connected components of the set of all convex points of $\mathcal{C}$, and the concave sub-curves $\mathcal{C}_j^-$ symmetrically defined. If a convex curve $\mathcal{C}_i^+$ and a concave curve $\mathcal{C}_j^-$ overlap, either they are equal to the same segment, or, if not, they have each a segment in common at one of their endpoints. In that case, we remove from $\mathcal{C}_i^+$ and $\mathcal{C}_j^-$ half of this segment. This way, we obtain a canonical (and minimal) decomposition of $\mathcal{C}$ into convex and concave parts. A junction between some $\mathcal{C}_i^+$ and some $\mathcal{C}_j^-$ is called a **simple junction**, while a junction between two $\mathcal{C}_i^+$'s or two $\mathcal{C}_j^-$'s is called a **double junction** (see Figure 3.18).

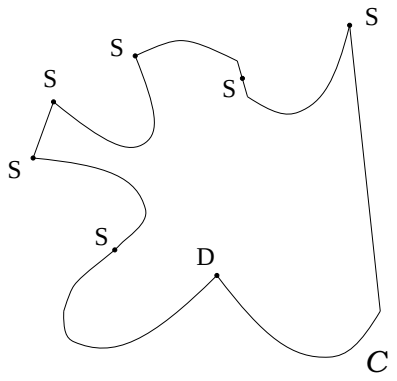

Figure 3.18: Simple (S) and double (D) junctions of a closed curve $\mathcal{C}$.

We define $\#\mathcal{J}(\mathcal{C})$, the **number of junctions** of $\mathcal{C}$ as the number of simple junctions of $\mathcal{C}$ plus twice the number of double junctions of $\mathcal{C}$. If $\mathcal{C}$ is a C^2 closed curve whose curvature vanishes at a finite number of points, the junctions of C are all simple and correspond to the inflexion points of $\mathcal{C}$. A polygon has no double junction either.

Proposition 11 *If $\mathcal{C}$ is a piecewise convex closed curve and $\sigma > 0$, then $E_\sigma(\mathcal{C})$ has no double junction and*

$$\#\mathcal{J}(E_\sigma(\mathcal{C})) \leqslant \#\mathcal{J}(\mathcal{C}).$$

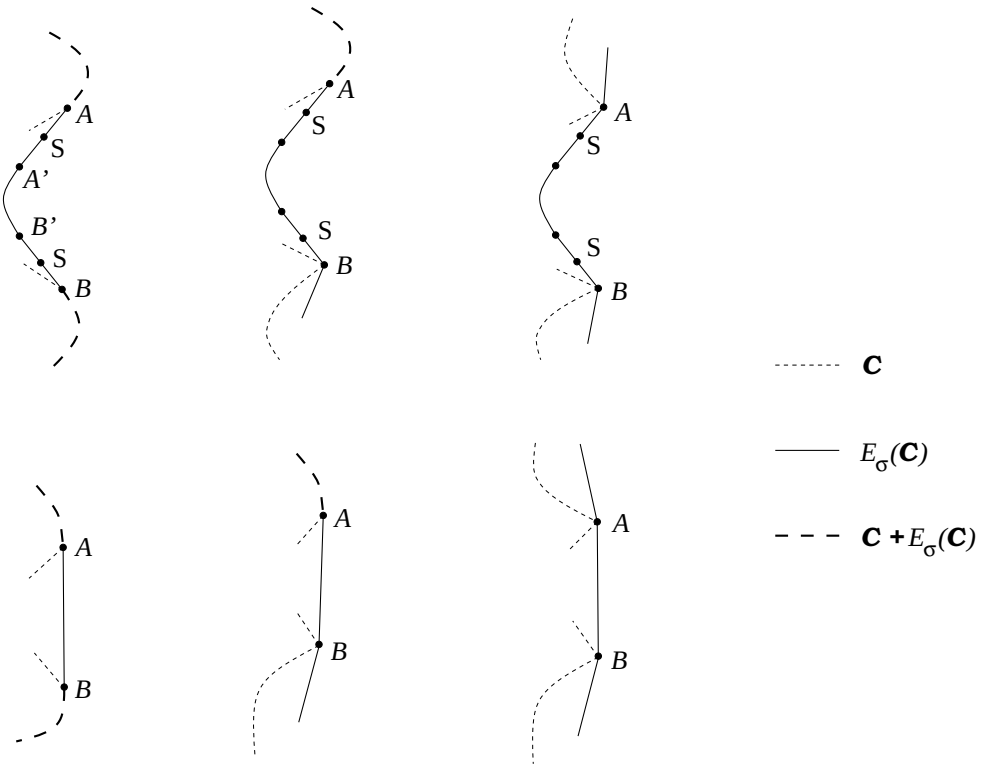

Figure 3.19: Simple junctions of $E_\sigma(\mathcal{C})$.

Proof :

1. Suppose that a component $D(J)$ of $E_\sigma(\mathcal{C})$ has a double junction $M = D(s)$. Since $D(I)$ is not locally convex near M, necessarily M belongs to $\mathcal{C} = C(I)$ and $\mathcal{C}$ is locally concave near M. Hence, near M, $\mathcal{C} \cap D(J) = \{M\}$. This means that $D(]s-\varepsilon, s[)$ and $D(]t, t+\varepsilon[)$ are segments for $\varepsilon > 0$ small enough. Thus, M cannot be a double junction of $D(J)$, which is a contradiction. We deduce that $E_\sigma(\mathcal{C})$ has no double junction as soon as $\sigma > 0$.

2. We prove that

$$\#\mathcal{J}(E_\sigma(\mathcal{C})) \leqslant \#\mathcal{J}(\mathcal{C}).$$

2.a. Let us consider $\mathcal{D}_j$ a maximum convex piece of $E_\sigma(\mathcal{C})$, i.e. such that $E_\sigma(\mathcal{C})$ is not locally convex at the extremal points A and B of $\mathcal{D}_j$. From Lemma 4 we know that A and B must belong to $\mathcal{C}$.

If $\mathcal{D}_j \subset \mathcal{C}$, it is a segment and neither $\mathcal{C}$ nor $E_\sigma(\mathcal{C})$ can have any junction on $\overline{\mathcal{D}_j}$. If $\mathcal{D}_j \not\subset \mathcal{C}$ but $\mathcal{D}_j$ is a segment, then $E_\sigma(\mathcal{C})$ has no junction between A and B (see Figure 3.19). Last, if $\mathcal{D}_j$ is not a segment, then $E_\sigma(\mathcal{C})$ has exactly two simple junctions between A and B (see Figure 3.19). But since the piece of $\mathcal{C}$ between A and B cannot be concave (it has a nonzero positive chord), the number of junctions of $\mathcal{C}$ between A and B included is at least 2 (with the convention that a double junction in A (or in B) is counted once for each of the two D_j it belongs to). Hence, in all cases, between A and B (included), $E_\sigma(\mathcal{C})$ has not more junctions than $\mathcal{C}$.

2.b. We claim that $E_\sigma(\mathcal{C})$ cannot have any junction outside a piece of curve $\overline{\mathcal{D}_j}$ of the previous kind. The reason is that on these remaining parts, $E_\sigma(\mathcal{C})$ is strictly concave (i.e. nowhere locally convex), so that any junction between these remaining parts should be a double junction, which is impossible according to Step 1. Hence, we have

$$\#\mathcal{J}(E_\sigma(\mathcal{C})) \leqslant \#\mathcal{J}(\mathcal{C})$$

as announced. □

3.4.3 Consistency

Theorem 3 *If $\mathcal{C}$ is a piecewise convex semi-closed curve of class piecewise C^n, then $E_\sigma(\mathcal{C})$ is a collection of piecewise convex semi-closed curves of class piecewise C^n. If $n \geqslant 2$, each point M of $\mathcal{C}$ can be associated to a point M_σ of $E_\sigma(\mathcal{C})$ such that*

$$M_\sigma = M + \omega \cdot \sigma^{\frac{2}{3}} \cdot (\gamma^+)^{\frac{1}{3}} \boldsymbol{N} + o(\sigma^{\frac{2}{3}}),$$

where γ and $\boldsymbol{N}$ are respectively the curvature of $\mathcal{C}$ and the normal vector[1] to $\mathcal{C}$ at point M. As usual, we set $\omega = \frac{1}{2}\left(\frac{3}{2}\right)^{\frac{2}{3}}$ and $\gamma^+ = \max(0, \gamma)$.

Proof :

1. From Proposition 10, we know that $E_\sigma(\mathcal{C})$ is made of a finite number of curves of three kinds : pieces of $\mathcal{C}$, which are C^n, segments, which are C^∞, and new convex pieces, which can be proved to be C^n using the arguments of Theorem 2. Hence, $E_\sigma(\mathcal{C})$ is piecewise C^n.

2. Consider M a point of $\mathcal{C}$, and call γ the curvature of $\mathcal{C}$ in M.

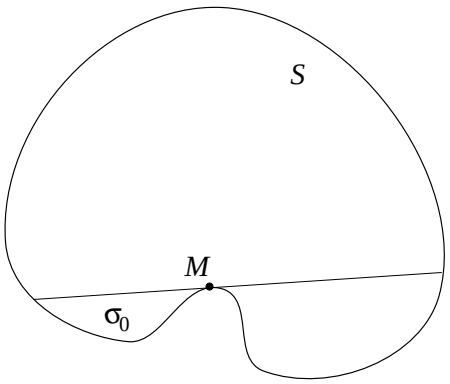

Figure 3.20: Case $\gamma < 0$

2.a. If $\gamma < 0$, call $\boldsymbol{T}$ the tangent to $\mathcal{C}$ in M, and let σ_0 be the nonzero area of the C-set delimited by a segment of the kind $]M - a\boldsymbol{T}, M + b\boldsymbol{T}[$, where both a and b are positive. Any

[1] If $\gamma = 0$, $\boldsymbol{N}$ is not uiquely defined but any choice is convenient since $(\gamma^+)^{\frac{1}{3}}\boldsymbol{N} = \boldsymbol{0}$.

chord-set of $\mathcal{C}$ containing M contains the previous chord set (see Figure 3.20), and consequently its area must be larger than σ_0. In other words, for any $\sigma < \sigma_0$, M belongs to $E_\sigma(\mathcal{C})$ and taking $M_\sigma = M$ closes the case.

2.b. If $\gamma > 0$, call $\mathcal{C}_i$ the largest convex component of $\mathcal{C}$ containing M. For σ small enough, any σ-chord set of $\mathcal{C}$ containing M is defined by two points of $\mathcal{C}_i$, so that the "evolution" of M is given by Theorem 2 and the proof is complete.

2.c. If $\gamma = 0$, the geometric argument used in the proof of Theorem 2 still applies. □

3.4.4 Other possible definitions of the affine erosion

The affine erosion of a convex set S is obtained in a simple way, by removing from S any part of S with area σ of the kind $H \cap S$, where H is a half plane. This may be the simplest way to obtain a global affine invariant set-shortening process tangent to the affine scale space. Now, if one wants to generalize this definition to non-convex sets, one must be careful, and the natural generalization (removing from S any connected component of $H \cap S$ with area σ) is not that good : this definition does not ensure a very important property, the global inclusion principle (see Figure 3.21), which states that $E_\sigma(S_1) \subset E_\sigma(S_2)$ when $S_1 \subset S_2$. This principle has strong consequences for the iterated operator, and guarantees numerical stability.

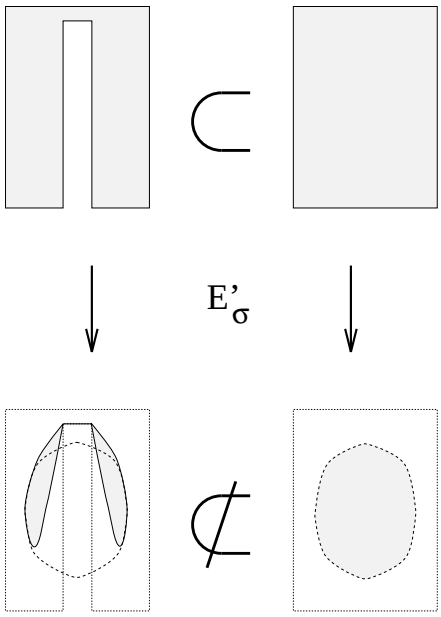

Figure 3.21: Inclusion principle is lost for the alternative definition of the affine erosion

With our definition of the affine erosion, the global inclusion principle is satisfied, but the connectedness is not preserved (whereas it is preserved for the former definition). Notice, however, that these two definitions yield the same infinitesimal evolution (for scales small enough).

Chapter 4

Comparison between affine erosion and scale space

In this chapter, we compute exactly the affine erosion and the affine scale space of conics. We show that for these curves the affine erosion remains a good approximation of its tangent operator not only for infinitesimal areas : this suggests that we can build a fast scheme for the affine scale space by iterating the affine erosion with rather large scale steps.

4.1 Affine scale space of curves

From now on, we note $t \mapsto ASS_t(\mathcal{C})$ the affine scale space of a curve $\mathcal{C}$, when it exists. In other words, if we can find a function $(s,t) \mapsto C(s,t)$ such that $s \mapsto C(s,0)$ is a parameterization of $\mathcal{C}$, we say that $s \mapsto C(s,t)$ is a parameterization of $ASS_t(\mathcal{C})$ if we have for all s and $t \geqslant 0$,

$$\frac{\partial C}{\partial t}(s,t) = \gamma(s,t)^{\frac{1}{3}}\, \boldsymbol{N}(s,t), \tag{4.1}$$

where $\gamma(s,t)$ and $\boldsymbol{N}(s,t)$ represent the curvature and the unit normal vector of the curve $C(\cdot,t)$ at point $C(s,t)$. As before, we take the convention that if r is a negative number, $r^{1/3} = -|r|^{1/3}$. At an inflexion point, $\boldsymbol{N}$ is not defined but since we have $\gamma = 0$, the right hand term of Equation 4.1 is naturally equal to zero. Notice that Equation 4.1 assumes that C is derivable with respect to t and twice derivable with respect to s.

If the curves $(ASS_t(\mathcal{C}))_{t>0}$ can be represented by functions of the kind $x \mapsto (x, y(x,t))$ in an orthonormal basis, then Equation 4.1 is equivalent to

$$\frac{\partial y}{\partial t} = \left(\frac{\partial^2 y}{\partial x^2}\right)^{\frac{1}{3}}. \tag{4.2}$$

Indeed, let us denote by y' and y'' the first and second order derivatives of y with respect to x. For such a Cartesian parameterization we have

$$\gamma(x,t) = \frac{y''}{(1+y'^2)^{\frac{3}{2}}},$$

and in the associated orthonormal basis, the unit tangent and normal vectors to the curve are respectively

$$\boldsymbol{T}(x,t) = \frac{1}{\sqrt{1+y'^2}}\,(1,y')$$

and

$$\boldsymbol{N}(x,t) = \frac{1}{\sqrt{1+y'^2}}\,(-y',1).$$

Thus, we have in the same basis,

$$(0,1) = \frac{1}{\sqrt{1+y'^2}}\,(\boldsymbol{N} + y'\,\boldsymbol{T}),$$

so that Equation 4.2 is equivalent to

$$\frac{\partial C}{\partial t} = (y'')^{\frac{1}{3}} \cdot (0,1) = \gamma^{\frac{1}{3}}\,\boldsymbol{N} + \frac{y''^{1/3}\,y'}{\sqrt{1+y'^2}}\,\boldsymbol{T}. \tag{4.3}$$

It has been proven (see [68],[29]) that the tangential component is of no influence on the whole curve evolution since it corresponds to a renormalization of the space parameter s (i.e. a movement of each point $C(s,t)$ along the curve $C(\cdot,t)$). Therefore, Equation 4.3 is equivalent to Equation 4.1.

Theorem 2 states that for regular convex curves the operator $E_{h^{3/2}}$ is tangent to the the operator $ASS_{\omega.h}$ when $h \to 0$, provided we set

$$\omega = \frac{1}{2}\left(\frac{3}{2}\right)^{\frac{2}{3}}.$$

In this chapter, we compute explicitly the affine scale space and the affine erosion for several convex curves, and we check that these operators are very close for small scales. In fact, for conics (ellipses, hyperbolae, parabolae, and "corners" as degenerated hyperbolae), both the affine erosion and the affine scale space can be exactly computed.

4.2 Affine erosion and scale space of an ellipse

4.2.1 Affine erosion

Proposition 12 *The σ-affine erosion of an ellipse with area A_0 is an ellipse with same axes and excentricity and with area*

$$A(\sigma) = A_0\,\cos^2\frac{\theta(\sigma)}{2},$$

where $\theta(\sigma)$ is defined by

$$\theta(\sigma) - \sin\theta(\sigma) = \frac{2\pi\sigma}{A_0}.$$

In particular, for an infinitesimal erosion, we have the following canonical expansion

$$A^{\frac{2}{3}}(t^{\frac{3}{2}}) = A_0^{\frac{2}{3}} - \sqrt[3]{\frac{2\pi^2}{3}} \cdot t + O(t^2). \tag{4.4}$$

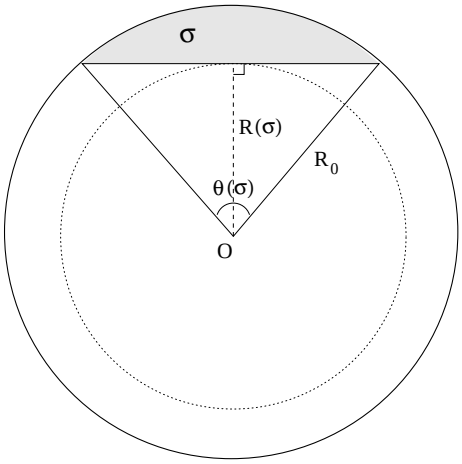

Figure 4.1: Affine erosion of a circle

Proof :

1. Consider the parameterization of the ellipse

$$M(t) = \sqrt{\frac{A_0}{\pi}}(\cos t\, \boldsymbol{v}_1 + \sin t\, \boldsymbol{v}_2)$$

satisfying $[\boldsymbol{v}_1, \boldsymbol{v}_2] = 1$. We can find a linear map ϕ with determinant 1 which transforms the affine basis $(\boldsymbol{v}_1, \boldsymbol{v}_2)$ into an orthogonal basis, in which $\phi(M(t))$ describes a circle enclosing the same area A_0. Then, because the affine erosion commutes with the rotations, the affine erosion of a circle with radius R_0 cannot be anything but a circle with same center and with radius $R(\sigma) < R_0$. On Figure 4.1 we can see that

$$\begin{aligned} R(\sigma) &= R_0 \cos\frac{\theta(\sigma)}{2} \\ \text{and} \quad \sigma &= R_0^2\left(\frac{\theta}{2} - \frac{\sin\theta}{2}\right). \end{aligned}$$

Hence, as ϕ commutes with the affine erosion and with the homothetic transformations, we deduce that on the ellipse as well as on the circle, the affine erosion acts as a homothetic transformation with ratio $\cos\frac{\theta(\sigma)}{2}$, which proves the first result of Proposition 12.

2. Let us evaluate now $A(\sigma) = A_0 \cos^2\frac{\theta(\sigma)}{2}$ when σ tends towards 0. From

$$\theta - \sin\theta = \frac{2\pi\sigma}{A_0}$$

we see that $\theta(\sigma) \to 0$ as $\sigma \to 0$, and

$$\frac{\theta^3(\sigma)}{6}\left(1 + O(\theta^2(\sigma))\right) = \frac{2\pi\sigma}{A_0},$$

which gives $\theta(\sigma) = O(\sigma^{\frac{1}{3}})$ and

$$\theta(\sigma) = \left(\frac{12\pi\sigma}{A_0}\right)^{\frac{1}{3}} + O(\sigma).$$

In this way, we obtain

$$A(\sigma) = A_0\left(1-\sin^2\frac{\theta(\sigma)}{2}\right) = A_0 - \frac{A_0}{4}\left(\frac{12\pi\sigma}{A_0}\right)^{\frac{2}{3}} + O(\sigma^{\frac{4}{3}}) = A_0 - A_0^{\frac{1}{3}}\left(\frac{3\pi\sigma}{2}\right)^{\frac{2}{3}} + O(\sigma^{\frac{4}{3}}).$$

The "canonical" expansion of $A(\sigma)$ is

$$A^{\frac{2}{3}}(t^{\frac{3}{2}}) = A_0^{\frac{2}{3}} - \omega\cdot t + O(t^2),$$

with

$$\omega = \frac{2}{3}\left(\frac{3\pi}{2}\right)^{\frac{2}{3}} = \sqrt[3]{\frac{2\pi^2}{3}}.$$

We remark incidentally that as σ goes near its critical value $\sigma_e = \frac{A_0}{2}$ corresponding to the ellipse extinction, we have

$$\theta(\sigma_e + h) = \pi - \frac{2\pi}{A_0}h + o(h)$$

and consequently

$$\cos\frac{\theta(\sigma_e+h)}{2} = -\frac{\pi}{4}\cdot\frac{2h}{A_0} + o(h).$$

It follows that the ratio $\sqrt{\frac{A(\sigma)}{A_0}} = \cos\frac{\theta(\sigma)}{2}$ admits a linear expansion near its extinction value.

Figure 4.2 shows the value of the normalized area $\frac{A}{A_0}$ and the ratio $\sqrt{\frac{A}{A_0}}$ depending on the normalized erosion parameter $\frac{\sigma}{\sigma_e}$.

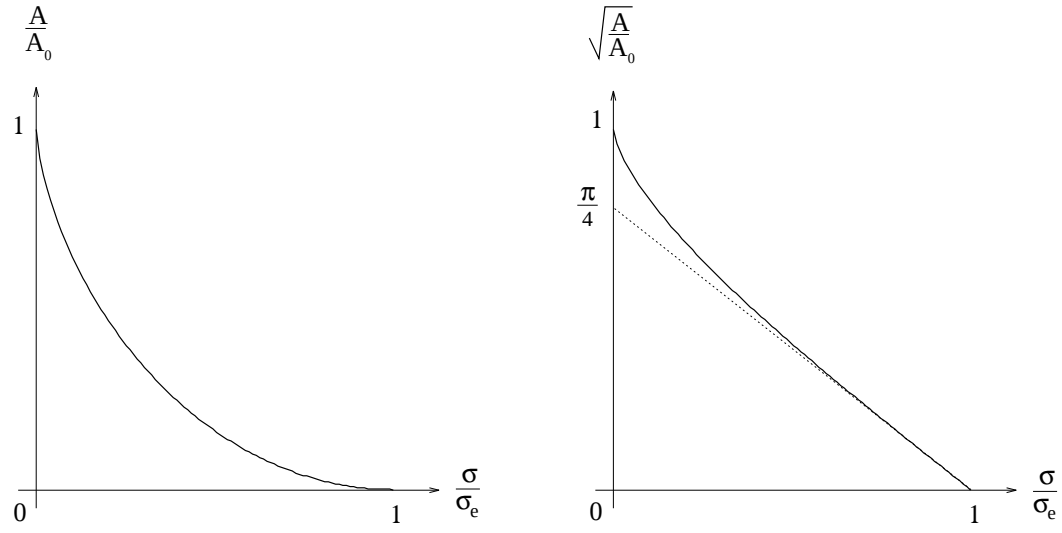

Figure 4.2: Area for the affine erosion of an ellipse

4.2.2 Affine scale space

Proposition 13 *The affine scale space at scale t of an ellipse with area A_0 is an ellipse with same axes and excentricity, whose area $A(t)$ satisfies*

$$A^{\frac{2}{3}}(t) = A_0^{\frac{2}{3}} - \frac{4}{3}\pi^{\frac{2}{3}}t. \tag{4.5}$$

Proof :

As for the affine erosion, the affine invariance of the affine scale space reduces the problem to the computation of the affine scale space of a circle. Because of the rotation invariance, the ASS of a circle is a a family of circles $(\mathcal{C}_t)_{t>0}$ with same center O and radius $R(t)$. A trigonometric parameterization of the circles $\mathcal{C}_t$ satisfies Equation 4.1 as soon as we have for any $t \geqslant 0$,

$$R'(t) = -\left(\frac{1}{R}\right)^{\frac{1}{3}}.$$

The solution of this ordinary differential equation is given by

$$R^{\frac{4}{3}}(t) = R^{\frac{4}{3}}(0) - \frac{4}{3}t,$$

and Equation 4.5 simply arises from the equality $A(t) = \pi R^2(t)$. □

If we compare Equations 4.5 and 4.4, we can check that the operator $ASS_{\omega.h}$ is tangent to $E_{h^{3/2}}$, simply because

$$\frac{4}{3}\pi^{\frac{2}{3}} \cdot \omega = \sqrt[3]{\frac{2\pi^2}{3}}.$$

This property is illustrated on Figure 4.3. The normalized area $(A(\cdot)/A_0)^{\frac{2}{3}}$ is represented both for the affine erosion E_σ and for the normalized affine scale space ASS_t (with $t = \omega \cdot \sigma^{\frac{2}{3}}$ for the reason we explained before).

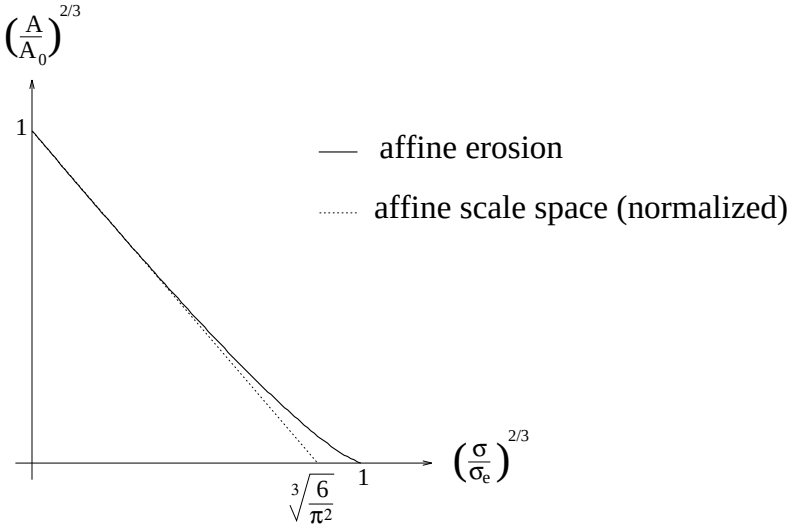

Figure 4.3: Comparison between the affine erosion and scale space of an ellipse

As we can see, the action of the affine erosion on ellipses is very close to the one of its tangent operator, the ASS, even for large scales. This suggests that we can build a fast scheme for the ASS by iterating the affine erosion with rather large scale steps.

4.3 Affine erosion and scale space of a hyperbola

4.3.1 Affine erosion

Proposition 14 *The σ-affine erosion of a hyperbola with apparent area A_0 is a hyperbola with same axes and with apparent area*

$$A(\sigma) = A_0 \operatorname{ch}^2 \frac{\theta(\sigma)}{2}, \tag{4.6}$$

where $\theta(\sigma)$ is defined by

$$\theta(\sigma) - \operatorname{sh} \theta(\sigma) = \frac{2\sigma}{A_0}.$$

In particular, for an infinitesimal erosion, we have the canonical expansion

$$A^{\frac{2}{3}}(t^{\frac{3}{2}}) = A^{\frac{2}{3}}(0) + \sqrt[3]{\frac{2}{3}} \cdot t + O(t^2).$$

Proof :

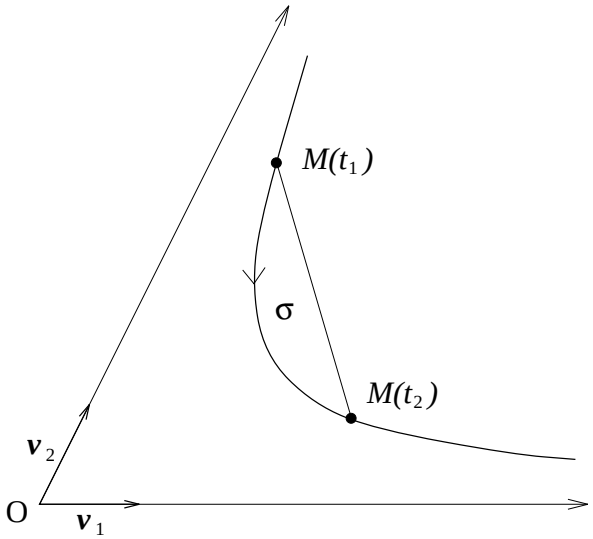

Figure 4.4: Affine erosion of a hyperbola

Let $(O, \boldsymbol{v}_1, \boldsymbol{v}_2)$ be an affine basis with same axes as the hyperbola $\mathcal{C}$. In this basis, a parametric equation of $\mathcal{C}$ is given by

$$M(t) = (X(t), Y(t)) = a(e^t, e^{-t}), \quad \text{with} \quad a^2 = \frac{A_0}{2\,[\boldsymbol{v}_1, \boldsymbol{v}_2]}.$$

Let us now consider two points $M(t_1)$ and $M(t_2)$ of $\mathcal{C}$ with $t_1 = t - \frac{\theta}{2}$ and $t_2 = t + \frac{\theta}{2}$ (see Figure 4.4) . In order that the chord set (t_1, t_2) of $\mathcal{C}$ has area σ, we should have

$$\frac{\sigma}{[\boldsymbol{v}_1, \boldsymbol{v}_2]} \;=\; \frac{1}{2}\int_{t_1}^{t_2} [M'(t), M(t)]\; dt \;+\; \frac{1}{2}\,[M(t_1) - M(t_2), M(t_2)]$$

$$\begin{aligned} &= \frac{1}{2}\int_{t_1}^{t_2} Y\frac{dX}{dt} - X\frac{dY}{dt}\,dt \;+\; \frac{1}{2}\left(X(t_1)Y(t_2) - Y(t_1)X(t_2)\right) \\ &= \frac{a^2}{2}\int_{t_1}^{t_2} e^{-t}e^{t} + e^{t}e^{-t}\,dt \;+\; \frac{a^2}{2}(e^{-\theta} - e^{\theta}) \\ &= a^2(\theta - \operatorname{sh}\theta). \end{aligned}$$

Since $\sigma_r(\mathcal{C}) = +\infty$, Theorem 1 ensures that the affine erosion of $\mathcal{C}$ is the set of the middle points of such σ-chord segments, i.e.

$$P(t) = \frac{a}{2}\cdot\left(e^{t-\frac{\theta}{2}} + e^{t+\frac{\theta}{2}}, e^{-t+\frac{\theta}{2}} + e^{-t-\frac{\theta}{2}}\right) = a\,\operatorname{ch}\frac{\theta}{2}\cdot(e^{t}, e^{-t}).$$

As θ does not depend on t, this proves that the affine erosion acts on $\mathcal{C}$ as a homothetic transformation with center O and ratio $\operatorname{ch}\frac{\theta}{2}$, and

$$\theta - \operatorname{sh}\theta = \frac{\sigma}{a^2\,[\boldsymbol{v}_1, \boldsymbol{v}_2]} = \frac{2\sigma}{A_0}.$$

As regards the canonical expansion of $A(t)$ near $t = 0$, the computation is the same as for the ellipse, except that the constant π disappears, so that the coefficient $\sqrt[3]{\frac{2\pi^2}{3}}$ becomes $\sqrt[3]{\frac{2}{3}}$. □

Remark : One can be surprised that θ does not depend on t. It can be simply explained by the fact that the parametric representation of the hyperbola we used is, up to a multiplicative factor, the affine abscissa representation, and since the affine curvature of a hyperbola is constant, the area of a σ-chord set $(t, t+x)$ only depends on x.

Let us now evaluate $A(\sigma)$ when σ tends to infinity. We have

$$\frac{e^{\theta(\sigma)}}{2} + O(e^{-\theta(\sigma)}) = \frac{2\sigma}{A_0},$$

which gives

$$e^{\theta(\sigma)} = \frac{4\sigma}{A_0} + O(\frac{1}{\sigma}).$$

Replacing this expression in Equation 4.6 yields

$$\begin{aligned} A(\sigma) &= \frac{A_0}{4}\left(e^{\theta(\sigma)} + 2 + O(e^{-\theta(\sigma)})\right) \\ &= \sigma + \frac{A_0}{2} + O(\frac{1}{\sigma}). \end{aligned}$$

Hence, $A(\sigma)$ admits an asymptotic linear expansion at infinity. Figure 4.5 represents the normalized apparent area $\frac{A}{A_0}$ depending on the normalized erosion parameter $\frac{\sigma}{A_0}$, for the affine erosion of a hyperbola.

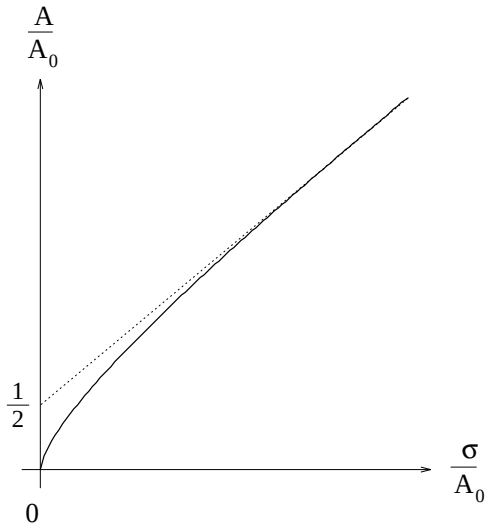

Figure 4.5: Area evolution for the affine erosion of a hyperbola

4.3.2 Affine scale space

The affine scale space of a hyperbola has been computed by Alvarez and Morales in [5]. Here we use a different parameterization.

Proposition 15 *The affine scale space at scale t of a hyperbola with apparent area A_0 is a hyperbola with same axes and whose apparent area satisfies*

$$A^{\frac{2}{3}}(t) = A_0^{\frac{2}{3}} + \frac{4}{3}\,t. \tag{4.7}$$

Proof :

Let H_0 be a hyperbola with apparent area A_0 and $\mathcal{R} = (O, \boldsymbol{v}_1, \boldsymbol{v}_2)$ an orthonormal basis of the plane, we can find an affine map with determinant 1 which transforms the axes of H_0 into $(O, \boldsymbol{v}_1)$ and $(O, \boldsymbol{v}_2)$, so that $\tilde{H}_0 = \phi(H_0)$ can be represented in $\mathcal{R}$ by the function

$$y(x) = \frac{A_0}{2x}.$$

Now, let us consider a family of hyperbolae $\tilde{H}_t = M(\cdot, t)$ of apparent area $A(t) > 0$ defined by

$$y(x,t) = \frac{A(t)}{2x}.$$

On one hand,

$$\frac{\partial y}{\partial t} = \frac{A'(t)}{2x},$$

and on the other hand,

$$\left(\frac{\partial^2 y}{\partial x^2}\right)^{\frac{1}{3}} = \frac{A^{\frac{1}{3}}(t)}{x}.$$

Consequently, the family $\tilde{H}_t$ is the scale space of $\tilde{H}_0$ as soon as Equation 4.2 is satisfied, i.e. as soon as $A(t)$ is solution of the differential equation

$$A'(t) = 2A^{\frac{1}{3}}(t).$$

Solving this equation yields

$$A^{\frac{2}{3}}(t) = A_0^{\frac{2}{3}} + \frac{4}{3}t. \tag{4.8}$$

Hence, the scale space of H_0, given by $\phi^{-1}(\tilde{H}_t)$, is the one announced in Proposition 15, and since the apparent area is invariant under ϕ^{-1}, Equation 4.8 remains true. □

Figure 4.6 represents the compared apparent areas obtained on a hyperbola with the affine erosion E_σ and with the normalized affine scale space ASS_t ($t = \omega\sigma^{\frac{2}{3}}$). As for ellipses, notice how close the affine scale space and the affine erosion behave.

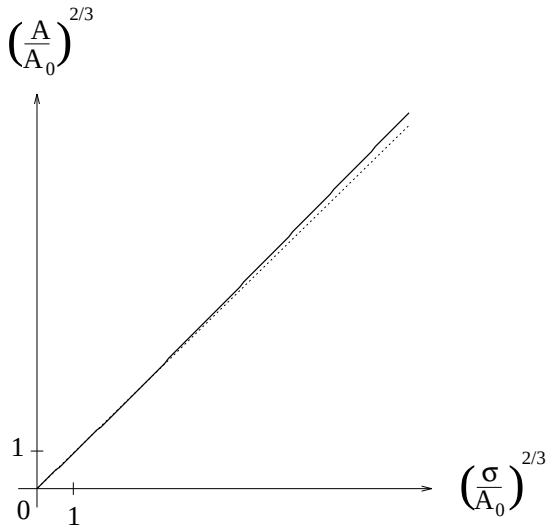

Figure 4.6: Canonical area evolution for the affine erosion of a hyperbola

4.4 Affine erosion and scale space of a parabola

Proposition 16 *The σ-affine erosion of the parabola of equation $y = px^2$ in an orthonormal basis is the translated parabola of equation*

$$y = px^2 + p^{\frac{1}{3}}\sigma^{\frac{2}{3}}\left(\frac{3}{4}\right)^{\frac{2}{3}} \tag{4.9}$$

in the same basis. In particular, $E_{h^{3/2}}$ acts as a semi-group operator upon the family of parabolae $P_\lambda : y = px^2 + \lambda$ since

$$E_{(h_1)^{3/2}} \circ E_{(h_2)^{3/2}}(P_\lambda) = E_{(h_1+h_2)^{3/2}}(P_\lambda).$$

A consequence is the exact equality

$$ASS_{\omega \cdot h}(P_\lambda) = E_{h^{3/2}}(P_\lambda),$$

where as usual

$$\omega = \frac{1}{2}\left(\frac{3}{2}\right)^{\frac{2}{3}}.$$

Proof :

Since a parabola is a semi-closed convex curve with $\sigma_r = +\infty$, we know from Theorem 1 that its σ-affine erosion is given by the set of the middle points of its σ-chord segments. Consider a σ-chord $(x-\delta, x+\delta)$ of the parabola $y = px^2$, the resulting middle point is $(x, y_\sigma(x))$ where

$$y_\sigma(x) = p\frac{(x-\delta)^2 + (x+\delta)^2}{2} = p(x^2+\delta^2).$$

Besides, a simple computation yields

$$\begin{aligned}\sigma &= \delta p[(x-\delta)^2 + (x+\delta)^2] - \int_{x-\delta}^{x+\delta} ps^2 ds \\ &= 2\delta p(x^2+\delta^2) - \frac{p}{3}[(x+\delta)^3 - (x-\delta)^3] \\ &= \frac{4}{3}\delta^3,\end{aligned}$$

and finally,

$$y_\sigma(x) = px^2 + p\left(\frac{3\sigma}{4}\right)^{\frac{2}{3}} = px^2 + p^{\frac{1}{3}}\sigma^{\frac{2}{3}}\left(\frac{3}{4}\right)^{\frac{2}{3}}.$$

Consequently, $E_{h^{3/2}}(P_\lambda) = P_{\lambda+\alpha h}$ where $\alpha = p^{\frac{1}{3}}\left(\frac{3}{4}\right)^{\frac{2}{3}}$, which establishes the announced semi-group property. But since $ASS_{\omega \cdot h}$ is the tangent operator to $E_{h^{3/2}}$, we have (as we shall prove later)

$$ASS_{\omega \cdot h}(P_\lambda) = \lim_{n\to\infty}\left[E_{(h/n)^{3/2}}\right]^n (P_\lambda) = E_{h^{3/2}}(P_\lambda).$$

We can also check this result directly by using Equation 4.2. Taking the second order derivative with respect to x in Equation 4.9 yields

$$\frac{\partial^2 y}{\partial x^2} = 2p,$$

so that $x \mapsto y(x,t)$ represents the affine scale space of P_0 as soon as

$$\frac{\partial y}{\partial t} = (2p)^{\frac{1}{3}}.$$

Consequently, $ASS_{\omega \cdot h}(P_0)$ is the curve given by

$$y(x,t) = px^2 + (2p)^{\frac{1}{3}} \cdot \omega h = px^2 + p^{\frac{1}{3}} h\left(\frac{3}{4}\right)^{\frac{2}{3}}.$$

□

4.5 Affine erosion of a triangle

The complete description of the affine erosion of a polygon will be given further. Here we just deal with the simplest case, namely the triangle. This case is interesting because all triangles are equivalents in Affine Geometry. One may refer to Chapter 6 (numerical scheme) for the precise description on the affine erosion of a general polygon.

Proposition 17 *The affine erosion of a triangle is a "hyperbolic triangle", i.e. the concatenation of three hyperbola pieces, each one given in barycentric coordinates by the equation*

$$(e^t, e^{-t}, \frac{2}{\sqrt{\sigma}} - e^t - e^{-t}), \quad |t| \leqslant \ln\left(\frac{1}{\sqrt{\sigma}} - \sqrt{\frac{1}{\sigma} - 2}\right)$$

In particular, the extinction scale of a unit area triangle is

$$\sigma_e = \frac{4}{9} = 0,444...$$

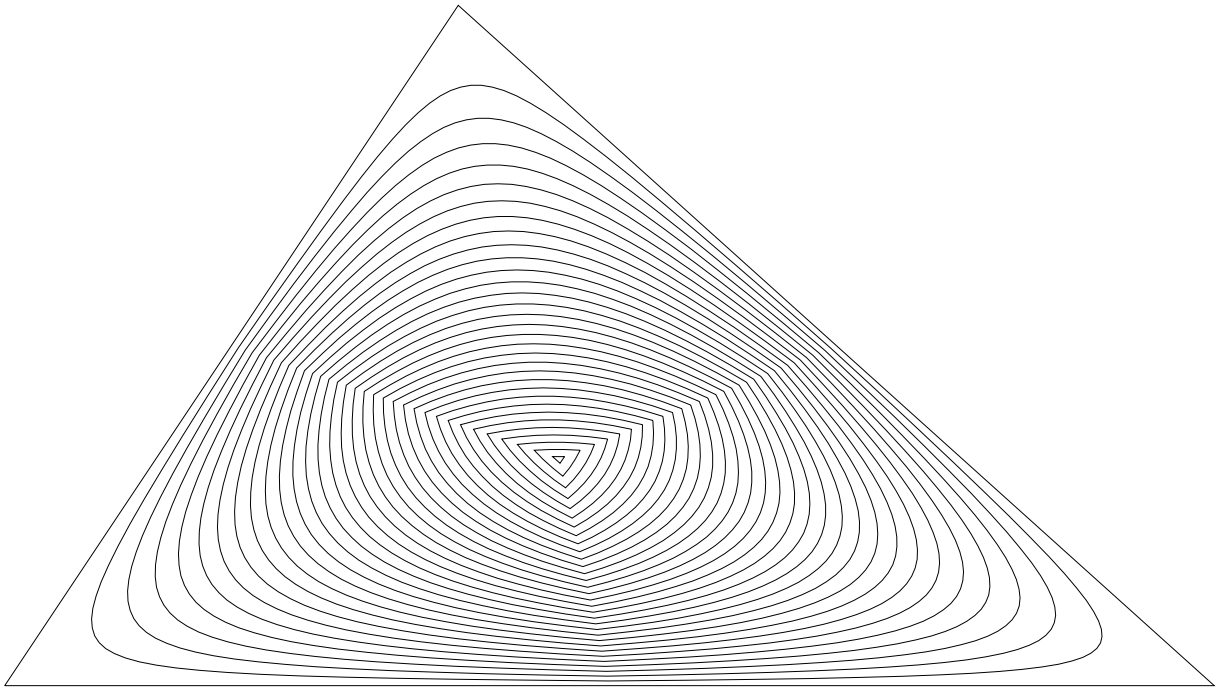

Figure 4.7: Affine erosions of a triangle for different scales
Notice that this is NOT the scale space spanned by the iteration of the affine erosion ! Each curve represents the action of the affine erosion on the initial triangle, for different values of the erosion area.

Proof :

1. First, notice that we can find an affine map which transforms a given triangle into a unit area equilateral triangle. Thus, it is sufficient to establish the proof for such a triangle thanks to the affine invariance of the affine erosion (see Proposition 5). By symmetry, it is clear that the

extinction point of an equilateral triangle is its center. As a consequence, the extinction point of any triangle must be the barycenter of its vertices (notice that this property is false for other polygons in general). One can check easily that the chord set of minimum area which contains the barycenter of a unit area equilateral triangle has area $\frac{4}{9}$ (see Figure 4.8). Consequently, the extinction scale of any triangle is $\frac{4}{9}$ of its area.

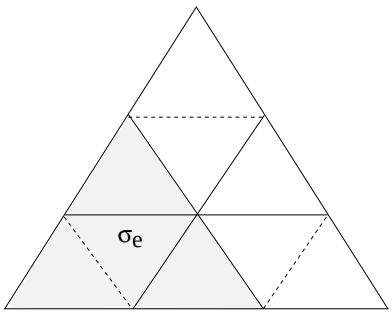

Figure 4.8: Extinction area of a triangle

2. Consider the σ-chords segments of the triangle whose endpoints lie on two fixed edges of the triangle. The middle points of these σ-chord segments span a piece of hyperbola, simply because the affine erosion of a "corner" is, as we saw previously in Proposition 1, a piece of hyperbola. Consequently, Proposition 8 ensures that the affine erosion of a triangle is the concatenation of three pieces of hyperbola (there are exactly three different pairs of edges for a triangle).

3. The previous hyperbolae can be described in barycentric coordinates by an equation of the kind

$$(e^t, e^{-t}, K(\sigma) - e^t - e^{-t}), \quad t_1 \leqslant t \leqslant t_2. \tag{4.10}$$

(we recall that (a, b, c) are barycentric coordinates of M in the affine basis (A, B, C) if and only if $(a + b + c)\,OM = a\,OA + b\,OB + c\,OC$ for any point O if the plane). Let us compute $K(\sigma)$. Remember that if $\boldsymbol{v}_1, \boldsymbol{v}_2, \boldsymbol{v}_3$ are three vectors of $\mathbb{R}^2$, one has

$$[\boldsymbol{v}_1, \boldsymbol{v}_2]\,\boldsymbol{v}_3 + [\boldsymbol{v}_2, \boldsymbol{v}_3]\,\boldsymbol{v}_1 + [\boldsymbol{v}_3, \boldsymbol{v}_1]\,\boldsymbol{v}_2 = \boldsymbol{0}.$$

Applying this to MA, MB and MB where ABC is a triangle with unit area, we get

$$M = \frac{1}{2}\,[MA, MB]\,C + \frac{1}{2}\,[MB, MC]\,A + \frac{1}{2}\,[MC, MA]\,B.$$

In other words, a system of barycentric coordinates of M in the basis (A, B, C) is given by the areas of the triangles MBC, MCA and MAB. Now, if we make $t = 0$ in Equation 4.10, we obtain the point M of Figure 4.9, which, according to the previous remark, can be represented in the basis (A, B, C) by $(\frac{1-S}{2}, \frac{1-S}{2}, S)$. Moreover, one can see easily that $S = \frac{C'M}{CM}$ and $\sigma = \left(\frac{CM}{CC'}\right)^2$. Now, identifying the previous coordinates (up to a multiplicative factor) with $(1, 1, K(\sigma) - 2)$, we get

$$\frac{1 - S}{2}(K(\sigma) - 2) = S,$$

so that

$$K(\sigma) = \frac{2}{1-S} = \frac{2}{\sqrt{\sigma}}.$$

Now, a simple computation resulting from the permutation of the affine bases gives the bound value

$$|t| \leqslant \ln\left(\frac{1}{\sqrt{\sigma}} - \sqrt{\frac{1}{\sigma} - 2}\right).$$

Then, by solving the equation

$$\frac{1}{\sqrt{\sigma}} - \sqrt{\frac{1}{\sigma} - 2} = 1,$$

we find again the extinction scale $\sigma = \frac{4}{9}$. □

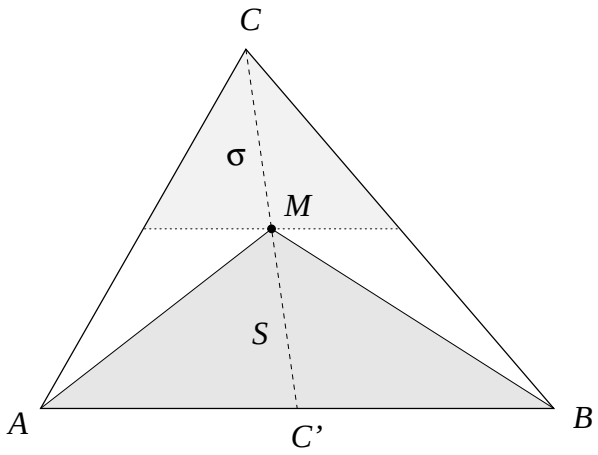

Figure 4.9: Computing $K(\sigma)$

Remark : As announced in the previous chapter, the triangle is an example of a simple convex C-set whose extinction area is less than half of its area.

As far as we know, the affine scale space of a triangle has not been computed exactly, and it is uncertain that there exists a simple analytic expression for it. However, we can observe that for the reasons previously explained, the affine invariance constrains the extinction point of a triangle to be its barycenter. Numerical simulations give for the normalized extinction area of the affine scale space of a triangle the value $\sigma'_e \simeq 0,42$ (it means that a unit area triangle and an ellipse of area $2\sigma'_e$ disappear simultaneously).

Chapter 5

Affine erosion of grey-level images

In this chapter, we first extend the affine erosion to any set of the plane and to lower semi-continuous grey level images. Then, we study its asymptotic behaviour and prove the convergence of the iterated affine erosion+dilation towards the affine morphological scale space. We also compare the affine erosion to classical affine inf-sup operators, and we establish the link with Matheron's Theorem (characterization of morphological operators).

5.1 Morphological principles

Suppose that we want to analyze an image u, given as a map $u : \mathbb{R}^2 \to \mathbb{R}$. The first question we should answer is : what relevant informations does contain u, physically speaking ? A important remark is that our interpretation of an image does not depend on its absolute contrast, but rather on the fact that some objects are brighter than others (we can check this each time we put on sunglasses). Hence, we should consider that a given image u (i.e. a map $u : \mathbb{R}^2 \to \mathbb{R}$) carries the same information as any image of the kind $g(u)$, where g is an arbitrary contrast change, that is to say an increasing and continuous scalar function. This point of view has been successfully adopted by Mathematical Morphology (in the case of flat grey-scale kernels) to design efficient operators for image analysis. Formally, we are led to consider equivalence classes of the relation

$$u \sim v \quad \Leftrightarrow \quad \exists\, g,\ v = g(u).$$

According to this equivalence, an image u reduces to the decreasing collection of its level sets[1]

$$\chi_\lambda(u) = \{\boldsymbol{x} \in \mathbb{R}^2;\ u(\boldsymbol{x}) > \lambda\}.$$

Conversely, any image u can be recovered from the family of its level sets by the relation

$$u(\boldsymbol{x}) = \sup\{\lambda;\ \boldsymbol{x} \in U_\lambda\},$$

[1]For our study, it is more convenient to consider the open level sets rather than the closed ones defined by

$$\chi_\lambda(u) = \{\boldsymbol{x} \in \mathbb{R}^2;\ u(\boldsymbol{x}) \geqslant \lambda\}.$$

and two images having the same collection of level sets are equivalent (see [41]).

From this point of view, it is natural to say that an operator T acting on images is **a morphological operator** if it satisfy the morphological invariance described in Chapter 2 :

[Morphological Invariance] : For any increasing continuous function g,

$$T(g \circ u) = g \circ T(u).$$

Although this idea is directly inspired from Mathematical Morphology, we must mention that the previous definition of a morphological operator is different from what Serra calls a morphological filter[2]. As well, the affine erosion we defined in Chapter 3 is not an erosion on a lattice in Serra's sense (see [70]). The reason is that the relation

$$E_\sigma(A \cap B) = E_\sigma(A) \cap E_\sigma(B)$$

is false in general (whereas it is true for the Euclidean erosion).

5.2 From sets to images

Let us consider an operator T acting on sets : we would like to define a corresponding operator $\tilde{T}$ on an image u by applying T to the level sets of u. In other words, we ask the following question : is there an operator $\tilde{T}$ which satisfies $\chi_\lambda(\tilde{T}(u)) = T(\chi_\lambda(u))$ for any λ and a certain class of images u ? Obviously, T must satisfy some hypotheses because the level sets of an image u satisfy the inclusion

$$\lambda \geqslant \mu \quad \Rightarrow \quad \chi_\lambda(u) \subset \chi_\mu(u)$$

and

$$\chi_{\lambda+\varepsilon}(u) \nearrow \chi_\lambda(u) \quad \text{as} \quad \varepsilon \searrow 0.$$

This last relation means that $\varepsilon \mapsto \chi_{\lambda+\varepsilon}(u)$ is nonincreasing and that

$$\forall \lambda, \quad \chi_\lambda(u) = \bigcup_{\varepsilon>0} \chi_{\lambda+\varepsilon}(u);$$

it is equivalent to say that

$$\forall \boldsymbol{x}, \quad u(\boldsymbol{x}) = \sup\{\lambda;\ \boldsymbol{x} \in \chi_\lambda(u)\}. \tag{5.1}$$

From now on, $\mathcal{O}$ denotes the set of the open sets of $\mathbb{R}^2$, and $LSC(\mathbb{R}^2)$ the set of the lower semi-continuous functions defined on $\mathbb{R}^2$. We recall that $u : \mathbb{R}^2 \to \mathbb{R}$ is lower semi-continuous (l.s.c.) if and only if each level set of u is open.

Definition 13 *An operator T acting on sets is nondecreasing if*

$$\forall X, Y, \quad X \subset Y \ \Rightarrow \ T(X) \subset T(Y).$$

[2] in [70], an operator ψ is a morphological filter if it is both nondecreasing ($u \leqslant v \ \Rightarrow \ \psi(u) \leqslant \psi(v)$) and idempotent ($\psi \circ \psi = \psi$).

Definition 14 *A nondecreasing operator $T : \mathcal{O} \mapsto \mathcal{O}$ is $\nearrow$-continuous if*

$$\forall (X_n) \in \mathcal{O}^{\mathbb{N}}, \qquad X_n \nearrow_n X \;\Rightarrow\; T(X_n) \nearrow_n T(X).$$

For a nondecreasing operator $T : \mathcal{O} \mapsto \mathcal{O}$, it equivalent to say that T is $\nearrow$-continuous or that it is lower-semi-continuous for the so-called "hit and miss" topology[3] (see [69]).

Proposition 18 *If $T : \mathcal{O} \mapsto \mathcal{O}$ is a nondecreasing $\nearrow$-continuous operator, then the relation*

$$\chi_\lambda(\tilde{T}(u)) = T(\chi_\lambda(u)) \tag{5.2}$$

defines a unique operator $\tilde{T} : LSC(\mathbb{R}^2) \to LSC(\mathbb{R}^2)$. Moreover, $\tilde{T}$ is a nondecreasing, morphological and 1-Lipschitz operator.

Proof :

1. If $\tilde{T}$ exists, then it is unique. The reason is that Equation 5.1 rewritten for $\tilde{T}(u)$ yields

$$\forall \boldsymbol{x}, \quad \tilde{T}(u)(\boldsymbol{x}) = \sup\{\lambda;\ \boldsymbol{x} \in \chi_\lambda(\tilde{T}(u))\},$$

and if $\tilde{T}$ satisfies Equation 5.2, it is completely defined from T by

$$\tilde{T}(u)(\boldsymbol{x}) = \sup\{\lambda;\ \boldsymbol{x} \in T(\chi_\lambda(u))\}. \tag{5.3}$$

2. Let us now consider the operator defined by Equation 5.3, and prove that it satisfies Equation 5.2. On one hand,

$$\begin{aligned} \boldsymbol{x} \in \chi_\lambda(\tilde{T}(u)) \quad &\Rightarrow \quad \tilde{T}(u)(\boldsymbol{x}) > \lambda \\ &\Rightarrow \quad \exists \lambda_0 > \lambda,\ \ \boldsymbol{x} \in T(\chi_{\lambda_0}(u)) \\ &\Rightarrow \quad \boldsymbol{x} \in T(\chi_\lambda(u)), \end{aligned}$$

the last inference arising from the monotonicity of T, because

$$\lambda < \lambda_0 \;\Rightarrow\; \chi_{\lambda_0}(u) \subset \chi_\lambda(u) \;\Rightarrow\; T(\chi_{\lambda_0}(u)) \subset T(\chi_\lambda(u)).$$

On the other hand, remember that

$$\chi_{\lambda+\varepsilon}(u) \nearrow \chi_\lambda(u) \quad \text{as} \quad \varepsilon \searrow 0,$$

and since T is lower semi-continuous we have

$$T(\chi_{\lambda+\varepsilon}(u)) \nearrow T(\chi_\lambda(u)) \quad \text{as} \quad \varepsilon \searrow 0$$

[3] This topology on open sets of the plane is spanned by the sets

$$\mathcal{O}^K_{G_1,G_2,\ldots G_p} = \{O \in \mathcal{O},\ K \subset O \text{ and } \forall i,\ G_i \not\subset O\},$$

where K is a compact set and each G_i is an open set.

and in particular

$$\bigcup_{\varepsilon>0} T(\chi_{\lambda+\varepsilon}(u)) = T(\chi_\lambda(u)) = T(\bigcup_{\varepsilon>0} \chi_{\lambda+\varepsilon}(u)).$$

Hence,

$$\begin{aligned}
\boldsymbol{x} \in T(\chi_\lambda(u)) \quad &\Rightarrow \quad \boldsymbol{x} \in \bigcup_{\varepsilon>0} T(\chi_{\lambda+\varepsilon}(u)) \\
&\Rightarrow \quad \exists \varepsilon > 0, \quad \boldsymbol{x} \in T(\chi_{\lambda+\varepsilon}(u)) \\
&\Rightarrow \quad \exists \varepsilon > 0, \quad \tilde{T}(u)(\boldsymbol{x}) \geqslant \lambda + \varepsilon \\
&\Rightarrow \quad \tilde{T}(u)(\boldsymbol{x}) > \lambda \\
&\Rightarrow \quad \boldsymbol{x} \in \chi_\lambda(\tilde{T}(u)).
\end{aligned}$$

As a consequence, $\tilde{T}$ defined in Equation 5.3 satisfies Equation 5.2.

3. Let us check the announced properties of $\tilde{T}$.

3.a. T is nondecreasing, and $\tilde{T}$ inherits this property because of Equation 5.3. Indeed, if u_1 and u_2 are two l.s.c. images such that $u_1 \leqslant u_2$, then we have for any λ, $\chi_\lambda(u_1) \subset \chi_\lambda(u_2)$, and consequently $\tilde{T}(u_1) \leqslant \tilde{T}(u_2)$ because of Equation 5.3.

3.b. $\tilde{T}$ is morphological because if g is a contrast change, i.e. an increasing continuous scalar function, we have

$$\chi_\lambda(u) = \chi_{g(\lambda)}(g(u)),$$

and Equation 5.3 ensures that

$$\tilde{T}(g(u)) = g(\tilde{T}(u)).$$

3.c. Let us prove that $\tilde{T}$ is 1-Lipschitz. Let u and v be two l.s.c. images such that for any $\boldsymbol{x}$, $|u(\boldsymbol{x}) - v(\boldsymbol{x})| \leqslant k$. The monotonicity of $\tilde{T}$ yields

$$\forall \boldsymbol{x}, \quad \tilde{T}(u-k)(\boldsymbol{x}) \leqslant \tilde{T}(v)(\boldsymbol{x}) \leqslant \tilde{T}(u+k)(\boldsymbol{x}),$$

and since $\tilde{T}(u+k) = \tilde{T}(u) + k$, we have for any $\boldsymbol{x}$,

$$|\tilde{T}(u)(\boldsymbol{x}) - \tilde{T}(v)(\boldsymbol{x})| \leqslant k.$$

Hence, we proved that $\tilde{T}$ is 1-Lipschitz, i.e.

$$\|\tilde{T}(u) - \tilde{T}(v)\|_\infty \leqslant \|u - v\|_\infty.$$

A consequence is that $\tilde{T}$ restricted to L^∞ is uniformly continuous. □

5.3 Affine erosion of grey level images

We would like to extend the affine erosion to grey-level images through the morphological level set decomposition. For that purpose, we first need to define the affine erosion of any subset

of the plane (or, at least, of any open set). But the geometrical definition of the affine erosion (Definition 5) does not make sense for any subset of the plane, since in general its boundary is not a curve in a reasonable sense.

We could use the following result due to E. Giusti [38] : if u is of bounded variation, then its λ-level sets are Caccioppoli sets for almost any λ. This result could be of great interest for our purpose since up to a negligeable set of points, the essential boundary of a Caccioppoli set is made of a countable number of closed curves, for we have

$$||u||_{BV} = \int \text{length}(\partial\chi_\lambda(u))\, d\lambda.$$

We prefer, however, to define the affine erosion of an image in a more simple way, using the inclusion property.

Definition 15 *The σ-affine erosion of a set $U \subset \mathbb{R}^2$ is the set*

$$E_\sigma(U) = \bigcup_{S \text{ C}-\text{set},\ S\subset U} E_\sigma(S).$$

This definition makes sense because if U is a C-set, we know that for any C-set S subset of U we have $E_\sigma(S) \subset E_\sigma(U)$. Moreover, the extended operator E_σ is clearly nondecreasing because if $U \subset V$, any C-set subset of U is also subset of V, that is

$$\{S \text{ C} - \text{set};\ S \subset U\} \ \subset\ \{S \text{ C} - \text{set};\ S \subset V\}$$

and consequently

$$\bigcup_{S \text{ C}-\text{set},\ S\subset U} E_\sigma(S) \quad \subset \quad \bigcup_{S \text{ C}-\text{set},\ S\subset V} E_\sigma(S).$$

Lemma 6 *For any set $U \subset \mathbb{R}^2$, $E_\sigma(U)$ is open.*

Proof :

By Corollary 1 we know that for any C-set S, $E_\sigma(S)$ is open, and consequently

$$E_\sigma(U) = \bigcup_{S \text{ C}-\text{set},\ S\subset U} E_\sigma(S)$$

is open as a reunion of open sets. □

Lemma 7 *For any set $U \subset \mathbb{R}^2$, we have*

$$E_\sigma(U) = \bigcup_{S \text{ bounded C}-\text{set},\ \overline{S}\subset U} E_\sigma(S).$$

Proof :

Since

$$E_\sigma(U) = \bigcup_{S \text{ C-set},\, S \subset U} S,$$

we only need to prove Lemma 7 when U is a C-set.

1. We claim that there exists a nondecreasing sequence S_n of bounded C-sets such that $U = \cup_n S_n$ and $\overline{S_n} \subset U$ for all n. Let us define

$$A^n_{i,j} = [\frac{i}{2^n}, \frac{i+1}{2^n}] \times [\frac{j}{2^n}, \frac{j+1}{2^n}], \quad (i,j) \in \mathbb{Z}^2,$$

and consider K_n an increasing sequence of compact sets such that $\mathbb{R}^2 = \cup_n K_n$. The increasing sequence S_n, defined as the topological opening of the union of the $A^n_{i,j}$ for which $\overline{A^n_{i,j}} \subset U \cap K_n$, satisfies the previous constraints.

2. Let $M \in E_\sigma(U)$, and suppose that $M \notin \cup_n E_\sigma(S_n)$ (we are going to prove that this is not possible). If we define D_α as the line going through M and oriented by $\alpha \in S^1$, then for any n we can find $\alpha_n \in S^1$ and a σ_n-chord segment of S_n included in D_{α_n} (and with the same orientation), such that $\sigma_n \leqslant \sigma$. Now, up to a subsequence extraction, we can suppose that the sequence (α_n, σ_n) converges towards $(\tilde{\alpha}, \tilde{\sigma}) \in S^1 \times [0, \sigma]$.

Since $E_\sigma(U)$ is open and $M \in E_\sigma(U)$ we can find a closed disk $\overline{D}(M, \varepsilon)$ with center M and radius $\varepsilon > 0$ such that $\overline{D}(M, \varepsilon) \subset E_\sigma(U)$. Consider N the intersection between $\partial D(M, \varepsilon)$ and $D_{\tilde{\alpha}+\pi/2}$ (see Figure 5.1). The line going through N and oriented by $\tilde{\alpha}$ defines on U a bounded chord set K containing N, and for n large enough we have $D_{\alpha_n} \cap K = \emptyset$, so that $\sigma_n \geqslant \text{area}\,(K)$, and letting n tend to infinity yields $\text{area}\,(K) \leqslant \tilde{\sigma} \leqslant \sigma$, which is in contradiction with $N \in E_\sigma(U)$. □

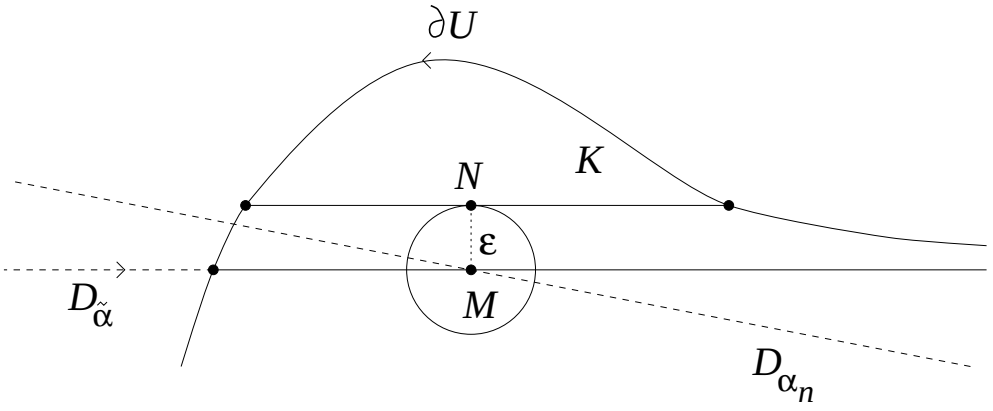

Figure 5.1: For n large enough, $D_{\alpha_n} \cap K = \emptyset$.

Proposition 19 *The restriction $E_\sigma : \mathcal{O} \to \mathcal{O}$ is $\nearrow$-continuous.*

Proof :

Since E_σ is nondecreasing, we have to prove that for any nondecreasing sequence (X_n) of open sets,

$$\bigcup_{n\in\mathbb{N}} E_\sigma(X_n) \supset E_\sigma(\bigcup_{n\in\mathbb{N}} X_n).$$

Let $X = \cup_n X_n$, consider a bounded C-set S such that $\overline{S} \subset \cup X_n$, and suppose that for any n we can find $x_n \in S \setminus X$. Since $\overline{S}$ is compact, we can extract from (x_n) a subsequence which converges towards $x \in \overline{S}$. But for any n, $\overline{S} \setminus X_n$ is closed, and as $x_k \in \overline{S} \setminus X_n$ for any $k \geqslant n$, we have $x \in \overline{S} \setminus X_n$ for all n. This means $x \in \overline{S} \setminus X$, which is impossible, this set being empty since $\overline{S} \subset X$.

Consequently, there exists $n_0 \in \mathbb{N}$ such that $S \subset X_{n_0}$, which proves that

$$E_\sigma(S) \subset E_\sigma(X_{n_0}) \subset \bigcup_{n\in\mathbb{N}} E_\sigma(X_n).$$

The last inclusion being true for any bounded C-set S such that $\overline{S} \subset X$, we deduce from Lemma 7 that

$$E_\sigma(X) = \bigcup_{S \text{ bounded C}-\text{set}, \overline{S}\subset X} E_\sigma(S) \subset \bigcup_{n\in\mathbb{N}} E_\sigma(X_n).$$

□

Now, since $E_\sigma : \mathcal{O} \to \mathcal{O}$ is nondecreasing and $\nearrow$-continuous, we can define the affine erosion of a lower semi-continuous image according to Proposition 18.

Definition 16 *The σ-affine erosion of a l.s.c. image $u : \mathbb{R}^2 \to \mathbb{R}$ is the image*

$$E_\sigma(u) : \boldsymbol{x} \mapsto \sup\{\lambda \in \mathbb{R};\ \boldsymbol{x} \in E_\sigma(\chi_\lambda(u))\},$$

where $\chi_\lambda(u) = \{\boldsymbol{x};\ u(\boldsymbol{x}) > \lambda\}$ is the λ-level set of u.

Once again, we use the same notation for the affine erosion of an image, without risk of confusion.

Lemma 8 *$E_\sigma : LSC(\mathbb{R}^2) \to LSC(\mathbb{R}^2)$ is a nondecreasing, morphological, 1-Lipschitz and affine invariant operator.*

Proof :

The first three properties are a consequence of Proposition 18. As regards the affine invariance, we have to prove that for any affine map ϕ,

$$E_{\sigma\cdot|\det\phi|}(u) \circ \phi = E_\sigma(u \circ \phi).$$

This is a consequence of Proposition 5, since $\chi_\lambda(u \circ \phi) = \phi(\chi_\lambda(u))$. □

Lemma 9 *For any image u, $E_\sigma(u)$ is nonincreasing with respect to σ, i.e.*

$$\sigma_1 \leqslant \sigma_2 \quad \Rightarrow \quad E_{\sigma_1}(u) \geqslant E_{\sigma_2}(u).$$

Proof :

This is a consequence of Lemma 2. □

Lemma 10 *If u is k-Lipschitz, so is $E_\sigma(u)$.*

Proof :

The map u being k-Lipschitz, we have

$$u(\boldsymbol{x}) - k\|y\| \leqslant u(\boldsymbol{x}+y) \leqslant u(\boldsymbol{x}) + k\|y\|.$$

Considering this last inequality as the comparison between three functions of $\boldsymbol{x}$ (i.e. with y fixed), the monotonicity and the translation invariance of E_σ yield

$$E_\sigma(u)(\boldsymbol{x}) - k\|y\| \leqslant E_\sigma(u)(\boldsymbol{x}+y) \leqslant E_\sigma(u)(\boldsymbol{x}) + k\|y\|,$$

which proves that $E_\sigma(u)$ is k-Lipschitz. □

We just saw that the affine erosion satisfies three main axioms of the affine morphological scale space, namely

[Global Comparison Principle] : $u \leqslant v \quad \Rightarrow \quad E_\sigma(u) \leqslant E_\sigma(v)$.

[Morphology] : For every increasing continuous function g, $E_\sigma(g \circ u) = g \circ E_\sigma(u)$.

[Affine invariance] : For every affine map ϕ, $E_{\sigma\cdot|\det\phi|}(u) \circ \phi = E_\sigma(u \circ \phi)$.

We shall prove later that the **[Local Comparison Principle]** is also satisfied by the affine erosion. Thus, the major differences between the affine erosion and the AMSS are :

- The axiom **[Contrast reversal]** : $T_t(-u) = -T_t(u)$, which is satisfied by the AMSS but not by the affine erosion. This leads us to define the dual operator to the affine erosion, called affine dilation and satisfying

  $$D_\sigma(u) = -E_\sigma(-u)$$

  for any continuous image u. The relation

  $$E_\sigma \circ D_\sigma(-u) = -D_\sigma \circ E_\sigma$$

  ensures that the **[Contrast reversal]** axiom is asymptotically satisfied when the operator $D_\sigma \circ E_\sigma$ (or, equivalently, $E_\sigma \circ D_\sigma$) is iterated.

- The semi-group property

$$T_{t+t'} = T_t \circ T_{t'},$$

which is not satisfied by the affine erosion, even for any scale normalization of the kind $T_t = E_{f(t)}$. This is the reason why we need to iterate the affine erosion (or, to be precise, an associated alternate operator) in order to build a good approximation of the AMSS.

5.4 Comparison with the inf-sup operators

In this section, we compare the action of E_σ with the one of the inf-sup operator associated to the basis $\mathcal{B}_c$ made of all closed convex sets with area 1 and symmetrical with respect to $\boldsymbol{0}$. We define

$$SI_\sigma(u)(\boldsymbol{x}) = \sup_{B\in\mathcal{B}_c} \inf_{\boldsymbol{y}\in B} u(\boldsymbol{x}+\sqrt{\sigma}.\boldsymbol{y}), \quad \text{and}$$

$$IS_\sigma(u)(\boldsymbol{x}) = \inf_{B\in\mathcal{B}_c} \sup_{\boldsymbol{y}\in B} u(\boldsymbol{x}+\sqrt{\sigma}.\boldsymbol{y}).$$

We know from [41] that if we iterate n times on a continuous periodic image u_0 the alternated operator $SI_\sigma \circ IS_\sigma$, then as $n \to +\infty$, $\sigma \to 0$ with $n\sigma^{\frac{2}{3}} \to t$, we obtain the flow of images $u(.,t)$ which is a viscosity solution of the equation

$$\frac{\partial u}{\partial t} = c\,|Du|\,curv(u)^{\frac{1}{3}}$$

with initial condition $u(\cdot,0) = u_0$, c being a positive constant. Notice that these morphological operators on images can be simply extended to sets via Equation 5.2. For any subset U of the plane, we define

$$SI_\sigma(U) = \{\boldsymbol{x} \in \mathbb{R}^2,\ \ SI_\sigma(1_U(\boldsymbol{x})) = 1\},$$

which is equivalent to

$$SI_\sigma(U) = \{\boldsymbol{x} \in U,\ \ \exists B \in \mathcal{B},\ \boldsymbol{x} + \sqrt{\sigma}\cdot B \subset U\}.$$

Proposition 20 *For any open set U and any scale σ,*

$$SI_{2\sigma}(U) \subset E_\sigma(U) \subset U.$$

Equivalently, for any lower semi-continuous image u,

$$SI_{2\sigma}(u) \leqslant E_\sigma(u) \leqslant u.$$

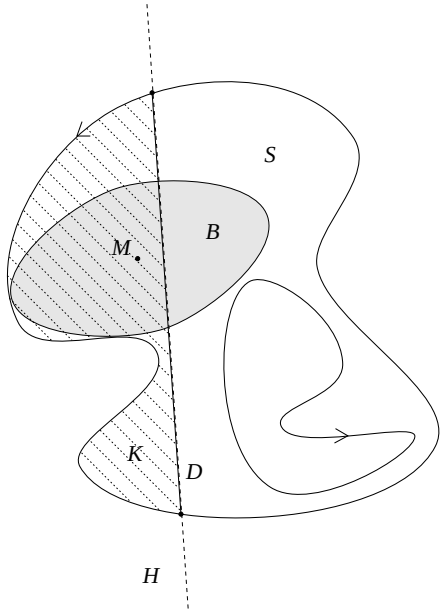

Figure 5.2: $SI_{2\sigma}(S) \subset E_\sigma(S)$.

This result simply means that E_σ "erodes" a shape less than $SI_{2\sigma}$ does.

Proof :

1. We first establish the proof for a C-set S. If M belongs to $SI_{2\sigma}(S)$, then there exists a convex closed set B of area 2σ, symmetrical with respect to M, and contained in S. Now, if D is a positive chord segment of S such that the associated chord set K contains M, let H be the half plane containing K and delimited by the line supporting D (cf. Figure 5.2). Then, $B \cap H$ is connected (as the intersection of two convex sets) and contains M, so that it is contained in K. Consequently, the symmetry of B yields

$$\text{area}\,(K) > \frac{1}{2}\text{area}\,(B) = \sigma$$

(the inequality is strict because B is closed and S is open), which means that M belongs to $E_\sigma(S)$. Hence, for any C-set S we have $SI_{2\sigma}(S) \subset E_\sigma(S)$.

2. If U is an open subset of the plane we have

$$\bigcup_{S\ \mathrm{C-set},\ S\subset U} SI_{2\sigma}(S) \quad \subset \quad \bigcup_{S\ \mathrm{C-set},\ S\subset U} E_\sigma(S) = E_\sigma(U) \subset U. \tag{5.4}$$

Now, if $\boldsymbol{x} \in SI_{2\sigma}(U)$, we can find $B \in \mathcal{B}_c$ such that $\boldsymbol{x}+\sqrt{2\sigma}B \ \subset \ U$. Let $S_\varepsilon = \boldsymbol{x}+(\sqrt{2\sigma}+\varepsilon)\ \mathring{B}$, where $\mathring{B}$ is the topological opening of B. Since B is compact and ${}^cU$ is closed, the distance between these disjoint sets is nonzero and consequently $S_\varepsilon \subset U$ for a certain $\varepsilon > 0$ small enough. Thus, S_ε is a C-set included in U and such that $\boldsymbol{x} \in SI_{2\sigma}(S_\varepsilon)$, and we get

$$\boldsymbol{x} \in \bigcup_{S\ \mathrm{C-set},\ S\subset U} SI_{2\sigma}(S).$$

We just proved the inclusion

$$SI_{2\sigma}(U) \subset \bigcup_{S \text{ C}-\text{set},\ S \subset U} SI_{2\sigma}(S). \tag{5.5}$$

Finally, Equations (5.4) and (5.5) imply as required

$$SI_{2\sigma}(U) \subset E_\sigma(U) \subset U \tag{5.6}$$

for any open set U.

3. If u_1 and u_2 are two images such that

$$\forall \lambda,\ \ \chi_\lambda(u_1) \subset \chi_\lambda(u_2),$$

then $\forall \boldsymbol{x},\ \ u_1(\boldsymbol{x}) \leqslant u_2(\boldsymbol{x})$. Now, if u is a lower semi-continuous image, we can apply Equation 5.6 to $\chi_\lambda(u)$ to obtain

$$\forall \lambda,\ \ SI_{2\sigma}(\chi_\lambda(u)) \subset E_\sigma(\chi_\lambda(u)) \subset \chi_\lambda(u),$$

and since Equation 5.2 defines $E_\sigma(u)$ and $SI_{2\sigma}(u)$, we have

$$\forall \lambda,\ \ \chi_\lambda(SI_{2\sigma}(u)) \subset \chi_\lambda(E_\sigma(u)) \subset \chi_\lambda(u),$$

which proves that

$$\forall \boldsymbol{x},\ \ SI_{2\sigma}(u)(\boldsymbol{x}) \leqslant E_\sigma(u)(\boldsymbol{x}) \leqslant u(\boldsymbol{x}).$$

□

Remark : The preceeding result is not true for a closed set in general : for a closed disk D, $SI_{2\sigma}(D)$ is the closure of the open disk $E_\sigma(D)$. One may also wonder if the reverse inclusion $E_\sigma(U) \subset SI_{2\sigma}(U)$ happens. For a triangle T with unit area, we have $SI_{2\sigma}(T) = \emptyset \ \Leftrightarrow\ \sigma \geqslant \frac{1}{3}$ (see Figure 5.3), whereas the corresponding extinction scale for E_σ is $\frac{4}{9}$. More precisely, one can prove that $E_\sigma(T) \neq SI_{2\sigma}(T)$ for any scale $0 < \sigma < \frac{4}{9}$. However, for regular convex sets and small scales, this reverse inclusion happens.

Proposition 21 *If S is a closed convex set whose boundary is C^1, then there is a limit scale $\sigma_l(S) > 0$ such that $SI_{2\sigma}(S) = E_\sigma(S)$ for all $\sigma < \sigma_l(S)$.*

Proof :

1. Let S be a closed convex set whose boundary $\mathcal{C}$ is defined by a regular parameterization $C : I \to \mathcal{C}$ of class C^1. We first prove that for $\sigma > 0$ small enough and for any σ-chord set $C_{s,t}$, the set symmetrical to $C_{s,t}$ with respect to the middle point of $[C(s)C(t)]$ is included in $\overline{S}$.

1.a. Define $\sigma_1 = \text{area}\,(S)/2$. For any $s \in I$ and $0 \leqslant \sigma \leqslant \sigma_1$, consider the unique σ-chord segment $[C(s)C(t)]$ (where t depends on s and σ) and $I(s)$ the intersection between $\mathcal{C}$

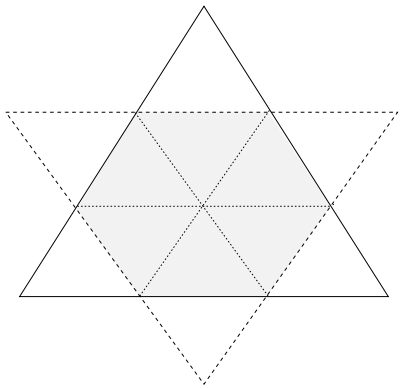

Figure 5.3: The largest symmetric convex set contained in a unit area triangle has area 2/3.

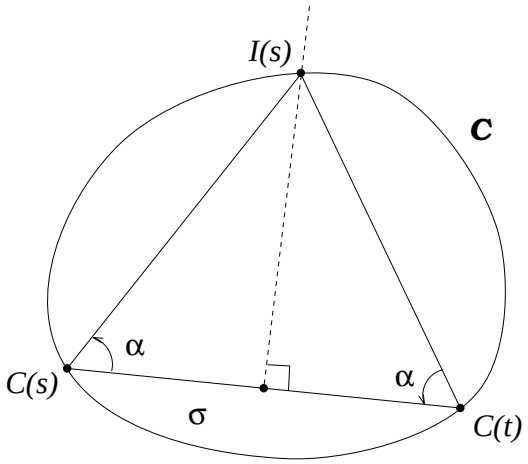

Figure 5.4: Definition of $\alpha(s,\sigma)$

and the midperpendicular of $(C(s),C(t))$ (see Figure 5.4). If $\sigma = 0$, $C(s) = C(t)$ and this midperpendicular is the line which goes through $C(s)$ and which is orthogonal to the tangent to $\mathcal{C}$ in $C(s)$. We call $\alpha(s,\sigma)$ the measure in $]0,\frac{\pi}{2}[$ of the angle between $C(s)C(t)$ and $C(s)I(s)$. Since $(s,\sigma) \mapsto \alpha(s,\sigma)$ is continuous on the compact set $I \times [0,\sigma_1]$, necessarily

$$\alpha_0 = \inf_{(s,\sigma)\in I\times[0,\sigma_1]} \alpha(s,\sigma)$$

is nonzero and for any $\sigma \leqslant \sigma_1$ and $s \in I$, we have $\alpha(s,\sigma) \geqslant \alpha_0$.

1.b. For any $s \in I$, consider $\sigma(s)$ the area of the largest C-set $C_{s,t}$ such that

$$\angle(C'(s),C'(t)) = \frac{1}{2}\alpha_0$$

(such a C-set exists because the map $t \mapsto \angle(C'(s),C'(t))$ increases continuously from 0 towards 2π). Notice that if we had $\sigma(s) = 0$ for some s, then $C([s,t])$ would be a segment, which is impossible since $\angle(C'(s),C'(t)) \neq 0$. Hence, $\sigma(s) = 0$ is nonzero for all $s \in I$, and since $s \mapsto \sigma(s)$ is continuous on the compact set I, we have

$$\sigma_2 = \inf_{s\in I} \sigma(s) > 0.$$

1.c. Now we claim that for any $\sigma \leqslant \min(\sigma_1, \sigma_2)$ and for any σ-chord set $C_{s,t}$, the set $\tilde{C}_{s,t}$ symmetric to $C_{s,t}$ with respect to the middle point of $[C(s)C(t)]$ is included in $\overline{S}$. Define Ω the intersection between the tangents to $\mathcal{C}$ in $C(s)$ and $C(t)$, and $\tilde{\Omega}$ the point symmetric to Ω with respect to the middle point of $[C(s)C(t)]$. Since $\sigma \leqslant \sigma_2$, we have

$$\beta = \angle(C'(s), C'(t)) \in]0, \alpha_0],$$

and as $\sigma \leqslant \sigma_1$ we know that the triangle $C(s)C(t)J$ is included in $\overline{S}$, J being defined by

$$\angle(C(s)C(t), C(s)J) = \angle(C(t)J, C(t)C(s)) = \alpha_0$$

(see Figure 5.5). Now, as $\tilde{C}_{s,t}$ is included in the triangle $C(s)C(t)\tilde{\Omega}$, it is sufficient to prove that $\tilde{\Omega}$ belongs to the triangle $C(s)C(t)J$. But this is a simple consequence of $\beta \leqslant \alpha_0$, because

$$0 \leqslant \angle(C(s)C(t), C(s)\tilde{\Omega}) \leqslant \beta$$

as well as

$$0 \leqslant \angle(C(t)\tilde{\Omega}, C(t)C(s)) \leqslant \beta.$$

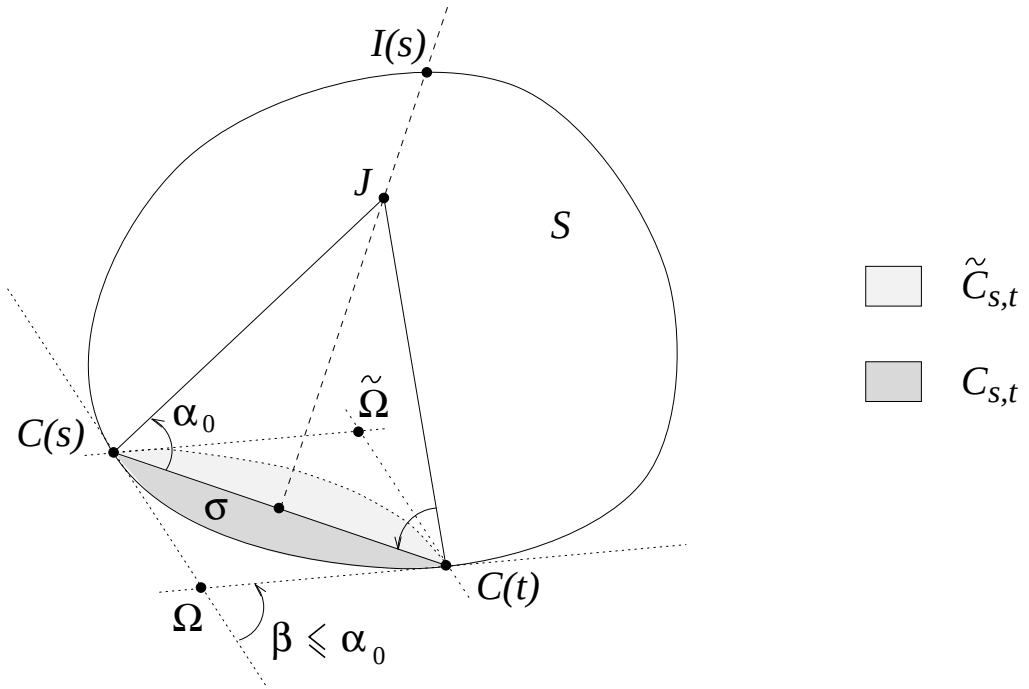

Figure 5.5: $\tilde{C}_{s,t}$ is included in S

2. In order to prove Proposition 21, according to Proposition 20 it is sufficient to check that for $\sigma' \leqslant \min(\sigma_1, \sigma_2)$, $E_{\sigma'}(S) \subset SI_{2\sigma'}(S)$. Consider a point $M \in E_{\sigma'}(S)$: necessarily, any σ-chord segment of S whose middle point is M is such that $\sigma > \sigma'$ (and since S is convex, there exists at least one such chord segment). But in this case, we proved on Step 1.c that we can find a convex closed set B with area 2σ (made from the symmetrization of a chord-set, see

Figure 5.5), symmetrical with respect to M and contained in $\overline{S}$. Applying on B a homothetic transformation with center M and ratio $\sqrt{\sigma'/\sigma} < 1$, we obtain a convex closed set B' with area $2\sigma'$, symmetrical with respect to M and contained in S. Consequently, $M \in SI_{2\sigma'}(S)$, and the proof is complete. □

5.5 Asymptotic behaviour of the affine erosion

In the previous chapter, we investigated the asymptotic behaviour of the geometrical affine erosion, and we proved that it was consistent with the affine scale space of curves. Hence, we can expect the affine erosion of images to be consistent with the affine morphological scale space (AMSS).

In [41], F.Guichard and J.-M.Morel proved that SI_σ is (semi-)consistent with the AMSS. We prove the same result for the affine erosion, i.e. that

$$E_\sigma(u) = u + \omega \cdot \sigma^{\frac{2}{3}}.|Du| \left[\text{curv}^-(u)\right]^{\frac{1}{3}} + O(\sigma^{\frac{3}{4}}).$$

Here, r^- means $\min(r, 0)$ and we keep the convention that if $r < 0$, $r^{\frac{1}{3}} = -|r|^{\frac{1}{3}}$. Using the dual operator to affine erosion, the affine dilation (defined by $D_\sigma(u) = -E_\sigma(-u)$ as we saw previously), we shall obtain the exact consistency with AMSS (i.e. $\text{curv}(u)$ instead of $\text{curv}^-(u)$) by considering the alternate operator $D_\sigma \circ E_\sigma$ (or $E_\sigma \circ D_\sigma$).

The classical way (see [41]) to estimate the asymptotic behaviour of such operators is to reduce the problem to quadratic forms by using a local comparison principle.

5.5.1 A local comparison principle

First, we need to define the concept of C-images (which are to images what C-sets are to sets) and establish an approximation lemma.

Definition 17 *An image u is a **C-image** if all of its non trivial level sets are C-sets.*

By trivial set, we mean either the empty set or the whole plane.

Lemma 11 *Consider a Lipschitz image u. Then, for any compact subset K of the plane and any $\varepsilon > 0$, there exists a C-image u_ε such that $|u - u_\varepsilon| \leqslant \varepsilon$ on K.*

Proof :

u being k-Lipschitz on the compact set K, we first define the family of squares

$$A_{i,j} = [a_i, a_{i+1}] \times [a_j, a_{j+1}], \quad (i,j) \in \mathbb{Z}^2, \quad \text{where} \quad a_n = \frac{n\varepsilon}{k \cdot \sqrt{2}}.$$

Now, we can let

$$u_\varepsilon(\boldsymbol{x}) = \inf\{u(\boldsymbol{y})1_K(\boldsymbol{y});\ \exists(i,j),\ (\boldsymbol{x},\boldsymbol{y}) \in A_{i,j}^2\},$$

where 1_K is the characteristic function of K (i.e. which equals 1 on K and 0 outside). This definition ensures that all non trivial level sets of u_ε are C-sets (their boundaries are made of polygons), and moreover we have

$$\forall \boldsymbol{x}, \quad 0 \leqslant u(\boldsymbol{x})\, 1_K(\boldsymbol{x}) - u_\varepsilon(\boldsymbol{x}) \leqslant k.\mathrm{diam}\,(A_{i,j}) = \varepsilon.$$

Hence, u_ε satisfies $|u - u_\varepsilon| \leqslant \varepsilon$ on K. □

Proposition 22 (Local Comparison Principle) *Let u and v be two k-Lipschitz images such that $u \geqslant v$ on the disk with center $\boldsymbol{x}_0$ and radius r. Then we have, for any $\sigma \geqslant 0$,*

$$E_\sigma(u)(\boldsymbol{x}_0) \geqslant E_\sigma(v)(\boldsymbol{x}_0) - \frac{k\sigma}{r}.$$

Proof :

Given $\varepsilon > 0$, by Lemma 11 we can find a C-image w such that $|w - u| \leqslant \varepsilon$ on the open disk $D(\boldsymbol{x}_0, r)$. Besides, we define w^+ (respectively w^-) as the C-image equal to w on $D(\boldsymbol{x}_0, r)$ and equal to $+\infty$ outside (resp. equal to w on $\overline{D}(\boldsymbol{x}_0, r)$ and to $-\infty$ outside). Notice that infinite values are convenient here, but we could use finite (and large enough) values as well. We are going to prove that

$$E_\sigma(w^-)(\boldsymbol{x}_0) \geqslant E_\sigma(w^+)(\boldsymbol{x}_0) - \frac{k\sigma}{r} + O(\varepsilon) \tag{5.7}$$

as $\varepsilon \to 0$. For that purpose, we consider α, β such that

$$E_\sigma(w^-)(\boldsymbol{x}_0) < \alpha < \beta < E_\sigma(w^+)(\boldsymbol{x}_0)$$

(if $E_\sigma(w^-)(\boldsymbol{x}_0) = E_\sigma(w^+)(\boldsymbol{x}_0)$, this is not possible, but we are done since Equation 5.7 is clearly satisfied).

The definition of E_σ states the existence of a chord (A, B) of the level set $\chi_\beta(w^+)$ such that $\boldsymbol{x}_0 \in [AB]$ and the associated chord set K has an area not larger than σ (see Figure 5.6). The construction of w^+ ensures that K is bounded. Besides, no piece of $[AB]$ can define a chord set of $\chi_\alpha(w^-)$ contained in K because since this chord set would have an area not larger than σ, it would be a contradiction to the fact that $\alpha > E_\sigma(w^-)(\boldsymbol{x}_0)$. As a consequence, the set $\mathcal{C} = \partial\chi_\alpha(w^-) \cap K \cap D(\boldsymbol{x}_0, r)$ "attains" the boundary of the circle $\partial D(\boldsymbol{x}_0, r)$. If we define as well $\mathcal{C}' = \partial\chi_\beta(w^+) \cap K \cap D(\boldsymbol{x}_0, r)$ and

$$d = \inf\{|\boldsymbol{x} - \boldsymbol{x}'|;\ (\boldsymbol{x}, \boldsymbol{x}') \in \mathcal{C} \times \mathcal{C}'\},$$

on the one side we have

$$\beta - \alpha \leqslant 2\varepsilon + kd, \tag{5.8}$$

because u is k-Lipschitz and $|w - u| \leqslant \varepsilon$ on $D(\boldsymbol{x}_0, r)$. On the other side, one can easily inscribe in K a triangle with basis r and height d, which proves that area $(K) \geqslant rd$, and consequently

$$\sigma \geqslant rd. \tag{5.9}$$

Finally, Equations 5.8 and 5.9 give

$$\beta - \alpha \leqslant \frac{k\sigma}{r} + 2\varepsilon,$$

and considering the limits $\alpha \to E_\sigma(w^-)(\boldsymbol{x}_0)$ and $\beta \to E_\sigma(w^+)(\boldsymbol{x}_0)$, we obtain the desired Equation 5.7.

Last, as we have both $u \geqslant w^- - \varepsilon$ and $v \leqslant w^+ + \varepsilon$ on $\mathbb{R}^2$, we can apply twice the monotonicity of E_σ to deduce from Equation 5.7 that

$$E_\sigma(u)(\boldsymbol{x}_0) \geqslant E_\sigma(v)(\boldsymbol{x}_0) - \frac{k\sigma}{r} + O(\varepsilon),$$

and letting $\varepsilon \to 0$ achieves the proof. □

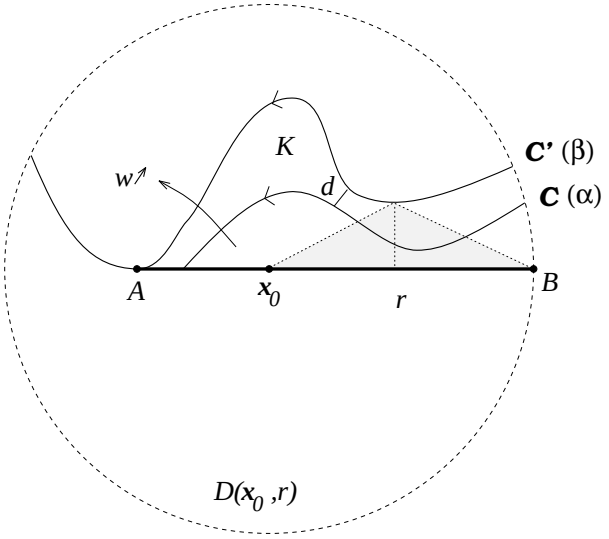

Figure 5.6: A local comparison principle

Corollary 7 (Uniform Local Comparison Principle) *Let u and v be two k-Lipschitz images such that $u \geqslant v$ on $D(\boldsymbol{x}_0, r)$. Then,*

$$\forall \boldsymbol{x} \in D(\boldsymbol{x}_0, \frac{r}{2}), \quad E_\sigma(u)(\boldsymbol{x}) \geqslant E_\sigma(v)(\boldsymbol{x}) - \frac{2k\sigma}{r}.$$

Proof :

For any $\boldsymbol{x} \in D(\boldsymbol{x}_0, \frac{r}{2})$ we can apply Proposition 22 since $u \geqslant v$ on $D(\boldsymbol{x}, \frac{r}{2})$ and we obtain the desired inequality. □

5.5.2 Consistency

Lemma 12 (Locality) *Let u and v be two k-Lipschitz images such that*

$$u(\boldsymbol{x}) - v(\boldsymbol{x}) = O(|\boldsymbol{x} - \boldsymbol{x}_0|^3) \quad \text{as} \quad \boldsymbol{x} \to \boldsymbol{x}_0.$$

Then,

$$E_\sigma(u)(\boldsymbol{x}_0) - E_\sigma(v)(\boldsymbol{x}_0) = O(\sigma^{\frac{3}{4}}) \quad \text{as} \quad \sigma \to 0.$$

Proof :

We borrow the proof from [41]. Since $u(\boldsymbol{x}) - v(\boldsymbol{x}) = O(|\boldsymbol{x} - \boldsymbol{x}_0|^3)$, we can find two positive numbers R and C such that

$$\forall r < R,\ \forall \boldsymbol{x} \in D(\boldsymbol{x}_0, r), \quad v(\boldsymbol{x}) - Cr^3 \leqslant u(\boldsymbol{x}) \leqslant v(\boldsymbol{x}) + Cr^3.$$

These three functions are k-Lipschitz, so we can apply the local comparison principle (Proposition 22) to obtain, for any σ,

$$E_\sigma(v)(\boldsymbol{x}_0) - Cr^3 - \frac{2k\sigma}{r} \leqslant E_\sigma(u)(\boldsymbol{x}_0) \leqslant E_\sigma(v)(\boldsymbol{x}_0) + Cr^3 + \frac{2k\sigma}{r}.$$

Choosing $\sigma = r^4$, we get as announced

$$E_\sigma(u)(\boldsymbol{x}_0) - E_\sigma(v)(\boldsymbol{x}_0) = O(\sigma^{\frac{3}{4}}) \quad \text{as} \quad \sigma \to 0.$$

□

Remark : Lemma 12 remains true if we write "uniformly with respect to $\boldsymbol{x}_0$" for the hypothesis and the conclusion.

Lemma 13 *If u is a polynomial whose degree is at most 2, then for any $\boldsymbol{x}_0 \in \mathbb{R}^2$,*

$$E_\sigma(u)(\boldsymbol{x}_0) = u(\boldsymbol{x}_0) + \omega \cdot \sigma^{\frac{2}{3}} \cdot |Du|(\boldsymbol{x}_0)\, [\gamma^-(u)(\boldsymbol{x}_0)]^{\frac{1}{3}} + O(\sigma^{\frac{3}{4}}). \tag{5.10}$$

Proof :

If the degree of u is strictly less than 2, then $E_\sigma(u) = u$, and Equation 5.10 is clearly satisfied. Otherwise, according to the morphological invariance of E_σ, we can assume that $u(\boldsymbol{x}_0) = 0$. Moreover, we can chose a (positively oriented) system of coordinates such that $\boldsymbol{x}_0 = (x_0, y_0)^T$ and either

$$u((x, y)^T) = ax^2 + by^2$$

or

$$u((x,y)^T) = ax^2 + by,$$

where $(a,b) \in \mathbb{R} \times \{-1,1\}$. If $u((x,y)^T)$ does not depend on x, the level lines of u are straight lines and Equation 5.10 is clearly satisfied. Hence, we suppose $a \neq 0$ in the following.

1. Case $u((x,y)^T) = ax^2 + by$.

We deal with the case $b = 1$, the case $b = -1$ being similar. The level lines of u are parabolae, so that we can use Proposition 16 to compute

$$\begin{aligned} E_\sigma(u)(\boldsymbol{x}_0) = \lambda \quad &\Rightarrow \quad \boldsymbol{x}_0 \in E_\sigma(\{y = -ax^2 + \lambda\}) \\ &\Rightarrow \quad \boldsymbol{x}_0 \in \{y = -ax^2 + \omega((-2a)^+)^{\frac{1}{3}}\sigma^{\frac{2}{3}} + b\lambda\}), \end{aligned}$$

so that

$$E_\sigma(u)(\boldsymbol{x}_0) = u(\boldsymbol{x}_0) + \omega((2a)^-)^{\frac{1}{3}}\sigma^{\frac{2}{3}}.$$

On the other hand,

$$\mathcal{A}(u)(\boldsymbol{x}_0) = \left[\left((u_x)^2 u_{yy} - 2u_x u_y u_{xy} + (u_y)^2 u_{xx}\right)^-\right]^{\frac{1}{3}}(\boldsymbol{x}_0) = (2a^-)^{\frac{1}{3}},$$

so that u satisfies Equation 5.10 (with no remainder).

2. Case $u((x,y)^T) = ax^2 + by^2$, $ab > 0$.

The case $b = 1$ is obvious since $E_\sigma(u) = u$ and $\mathcal{A}(u) = 0$. Thus we suppose that $b = -1$ and $a < 0$. The level line $\{u(\boldsymbol{x}) = \lambda\}$ is empty if $\lambda > 0$, and it is an ellipse with area $\pi|\lambda||a|^{-1/2}$ otherwise. Hence, we can apply Proposition 12 and a simple computation based on the asymptotic expansion (4.4) yields

$$E_\sigma(u)(\boldsymbol{x}_0) = u(\boldsymbol{x}_0) + \omega(8au(\boldsymbol{x}_0))^{\frac{1}{3}}\sigma^{\frac{2}{3}} + O(\sigma^{\frac{4}{3}}),$$

and

$$\mathcal{A}(u)(\boldsymbol{x}_0) = (8a(ax_0^2 - y_0^2))^{\frac{1}{3}}$$

as expected.

3. Case $u((x,y)^T) = ax^2 + by^2$, $ab < 0$.

The level lines of u are hyperbolae, and the reasoning is similar to Step 2 using Proposition 14. □

Proposition 23 (Consistency) *Let u be a k-Lipschitz image of class C^3 near $\boldsymbol{x}_0$, then as $\sigma \to 0$,*

$$\begin{aligned} E_\sigma(u)(\boldsymbol{x}_0) &= u(\boldsymbol{x}_0) + \omega \cdot \sigma^{\frac{2}{3}} \cdot |Du|(\boldsymbol{x}_0)\,[\gamma^-(u)(\boldsymbol{x}_0)]^{\frac{1}{3}} + O(\sigma^{\frac{3}{4}}), \\ D_\sigma(u)(\boldsymbol{x}_0) &= u(\boldsymbol{x}_0) + \omega \cdot \sigma^{\frac{2}{3}} \cdot |Du|(\boldsymbol{x}_0)\,[\gamma^+(u)(\boldsymbol{x}_0)]^{\frac{1}{3}} + O(\sigma^{\frac{3}{4}}), \end{aligned}$$

Proof :

u being a C^3 near $\boldsymbol{x}_0$, we can consider $\tilde{u}$, its Taylor expansion at order 2 near $\boldsymbol{x}_0$. Thus,

$$u(\boldsymbol{x}) = \tilde{u}(\boldsymbol{x}) + O(|\boldsymbol{x} - \boldsymbol{x}_0|^3)$$

as $\boldsymbol{x} \to \boldsymbol{x}_0$. From Lemma 12, we deduce that as $\sigma \to 0$,

$$E_\sigma(u)(\boldsymbol{x}_0) - E_\sigma(\tilde{u})(\boldsymbol{x}_0) = O(\sigma^{\frac{3}{4}}),$$

and using Lemma 13 we get as expected

$$E_\sigma(u)(\boldsymbol{x}_0) = u(\boldsymbol{x}_0) + \omega \cdot \sigma^{\frac{2}{3}} \cdot |Du|(\boldsymbol{x}_0)\,[\gamma^-(u)(\boldsymbol{x}_0)]^{\frac{1}{3}} + O(\sigma^{\frac{3}{4}}).$$

The consistency for D_σ follows immediatly since $D_\sigma(u) = -E_\sigma(-u)$. □

Remark : In fact, the consistency is uniform in a neighborhood of $\boldsymbol{x}_0$.

Next, we extend this consistency property to the alternate operators $D_\sigma \circ E_\sigma$ and $E_\sigma \circ D_\sigma$. We first prove that they satisfy a Local Comparison Principle.

Lemma 14 *Let u and v be two k-Lipschitz images such that $u \geqslant v$ on $D(\boldsymbol{x}_0, r)$. Then,*

$$\forall \boldsymbol{x} \in D(\boldsymbol{x}_0, \frac{r}{4}), \quad D_\sigma \circ E_\sigma(u)(\boldsymbol{x}) \geqslant D_\sigma \circ E_\sigma(v)(\boldsymbol{x}) - \frac{6k\sigma}{r},$$

and the same inequality holds for $E_\sigma \circ D_\sigma$.

Proof :

The proof is a direct consequence of Lemma 7. We know that for $\boldsymbol{x} \in D(\boldsymbol{x}_0, \frac{r}{2})$, we have

$$E_\sigma(u)(\boldsymbol{x}) \geqslant E_\sigma(v)(\boldsymbol{x}) - \frac{2k\sigma}{r},$$

which we rewrite

$$-E_\sigma(v)(\boldsymbol{x}) \geqslant -E_\sigma(u)(\boldsymbol{x}) - \frac{2k\sigma}{r}.$$

Now, from Lemma 10, $-E_\sigma(u)$ is also k-Lipschitz, as well as $-E_\sigma(v) - \frac{2k\sigma}{r}$. Hence, we can apply the Uniform Local Comparison Principle once again to obtain

$$\forall \boldsymbol{x} \in D(\boldsymbol{x}_0, \frac{r}{4}), \quad E_\sigma\left[-E_\sigma(v)(\boldsymbol{x})\right] \geqslant E_\sigma\left[-E_\sigma(u)(\boldsymbol{x}) - \frac{2k\sigma}{r}\right] - \frac{4k\sigma}{r},$$

which yields

$$D_\sigma \circ E_\sigma(u)(\boldsymbol{x}) \geqslant D_\sigma \circ E_\sigma(v)(\boldsymbol{x}) - \frac{6k\sigma}{r}$$

as announced. □

Theorem 4 (Consistency) *Let u be a k-Lipschitz image of class C^3 near $\boldsymbol{x}_0$, then as $\sigma \to 0$,*

$$T_\sigma(u)(\boldsymbol{x}_0) = u(\boldsymbol{x}_0) + \omega \cdot \sigma^{\frac{2}{3}} \cdot |Du|(\boldsymbol{x}_0)\,[\gamma(u)(\boldsymbol{x}_0)]^{\frac{1}{3}} + O(\sigma^{\frac{3}{4}}),$$

for both $T_\sigma = D_\sigma \circ E_\sigma$ and $T_\sigma = E_\sigma \circ D_\sigma$.

Proof :

We check that the proof of Proposition 23 can be applied here. First, the consistency of the alternate operators for second order polynomials is straightforward since for such polynomials $E_\sigma \circ D_\sigma(u)$ and $D_\sigma \circ E_\sigma(u)$ are both equal to either $E_\sigma(u)$ or $D_\sigma(u)$. Last, the locality property of Lemma 12 for $D_\sigma \circ E_\sigma$ and $E_\sigma \circ D_\sigma$ is a direct consequence of Lemma 14. □

Remark : As for E_σ, one easily proves that the consistency property of Theorem 23 is uniform near $\boldsymbol{x}_0$.

5.6 Using Matheron's Theorem

There is another way to establish the consistency of the operator E_σ : it is based on Matheron's characterization of monotone morphological operators and on a consistency Theorem due to F.Guichard and J.-M.Morel (see [41]).

Theorem 5 (Matheron) *Let T be a translation invariant monotone[4] morphological[5] operator on a set of functions $\mathcal{F}$ containing the characteristic functions of all the level sets of the elements of $\mathcal{F}$. Then, one can find a family $\mathcal{B}$ of subsets of $\mathbb{R}^2$ such that*

$$\forall u \in \mathcal{F},\ \ T(u)(\boldsymbol{x}) = \sup_{B \in \mathcal{B}} \inf_{\boldsymbol{y} \in B} u(\boldsymbol{x} + \boldsymbol{y}).$$

Indeed, the operator E_σ being translation invariant, nondecreasing and morphological, the Matheron's characterization applies and we can write, for any l.s.c. image u,

$$E_\sigma(u)(\boldsymbol{x}) = \sup_{B \in \mathcal{B}_e} \inf_{\boldsymbol{y} \in B} u(\boldsymbol{x} + \sqrt{\sigma} \cdot \boldsymbol{y}).$$

We should take

$$\mathcal{B}_e = \{X \subset \mathbb{R}^2;\ 0 \in E_1(X)\},$$

but from Lemma 7 we know that it is sufficient to take

$$\mathcal{B}_e = \{X \text{ bounded C} - \text{set};\ 0 \in E_1(X)\}.$$

Thus, E_σ belongs to the class of affine invariant inf-sup operators which have been studied in [41]. In particular, we can expect to use the following consistency theorem :

[4] i.e. nondecreasing
[5] i.e. satisfying **[Morphological Invariance]**.

Theorem 6 (F.Guichard, J.-M.Morel) *Let $\mathcal{B}$ be a localizable set of plane closed nonempty bounded sets which is invariant by the special linear group $SL(\mathbb{R}^2)$. Then, there exists two constants c^+ and c^- depending on $\mathcal{B}$ such that, for any image u C^3 in a neighbourhood of $\boldsymbol{x}_0$,*

$$\inf_{B\in\mathcal{B}_e}\sup_{\boldsymbol{y}\in B} u(\boldsymbol{x}+\sqrt{s}\cdot\boldsymbol{y}) = u(\boldsymbol{x}_0) + s^{2/3}\,|Du(\boldsymbol{x}_0)|\,g\,(\mathrm{curv}(u)(\boldsymbol{x}_0)) + o(s^{2/3}),$$

$$\begin{aligned} \text{where}\quad g(r) &= c^+\, r^{\frac{1}{3}} \text{ if } r \geqslant 0 \\ &= c^-\,(-r)^{\frac{1}{3}} \text{ if } r < 0. \end{aligned}$$

To apply Theorem 6 to the affine erosion, the only requirement we have to check is that the basis $\mathcal{B}_e$ is localizable in the following sense (see [41]).

Proposition 24 (Localizability) *The basis $\mathcal{B}_e$ associated with the affine erosion operator is localizable, i.e. there exists a constant $c > 0$ such that*

$$\forall r \geqslant \sqrt{c},\ \forall B \in \mathcal{B}_e,\ \exists B' \in \mathcal{B}_e,\quad B' \subset D(0,r) \quad\text{and}\quad \delta(B',B) \leqslant \frac{c}{r}.$$

Here, the notation $D(0,r)$ represents the open disk of radius r centered at the origin, and $\delta(B',B)$ means the Hausdorff semi-distance between B' and B, given by

$$\delta(B',B) = \sup_{\boldsymbol{x}'\in B'} d(\boldsymbol{x}',B) = \sup_{\boldsymbol{x}'\in B'}\inf_{\boldsymbol{x}\in B} |\boldsymbol{x}-\boldsymbol{x}'|.$$

Proof :

The proof is similar to the proof of the Local Comparison Principle (Proposition 22), which is not surprising.

1. Given $r \geqslant 1$ and a set B element of $\mathcal{B}_e$, we have $0 \in E_1(B)$ and by Definition of $E_1(B)$ we can find a C-set A included in B such that $0 \in E_1(A)$ (i.e. $A \in \mathcal{B}_e$). We consider the $\frac{1}{r}$-Euclidean dilation of A restrained to the disk $D(0,r)$, i.e.

$$B' = \{\boldsymbol{x} \in D(0,r);\ d(\boldsymbol{x},A) \leqslant \frac{1}{r}\}.$$

B' is a C-set containing $A \cap D(0,r)$, contained in $D(0,r)$, and

$$\delta(B',B) \leqslant \delta(B',A) + \delta(A,B) \leqslant \frac{1}{r} + 0.$$

Now we are going to prove that $B' \in \mathcal{B}_e$, that is to say that $0 \in E_1(B')$.

Suppose that 0 belongs to D, a chord segment of B' associated to a chord set K of area σ (see Figure 5.7). Two cases can be distinguished.

1.a. If $A \cap K \subset D(0,r)$, then a subset of K defines a chord set of A containing 0 and of area no more than σ. But since $A \in \mathcal{B}_e$, we necessarily have $\sigma > 1$.

1.b. If $A \cap K$ is not a subset of $D(0,r)$, which means that $K \cap \partial D(0,r)$ is not empty, then we can easily inscribe in K a triangle of base larger than r and height $\frac{1}{r}$ (see Figure 5.7), so that we get $\sigma = \text{area}\,(K) > 1$.

In both cases, 0 belongs to no 1-chord set of B', so that $B' \in \mathcal{B}_e$. Consequently, we proved that

$$\forall r \geqslant \sqrt{c},\ \forall B \in \mathcal{B}_e,\ \exists B' \in \mathcal{B}_e\ (\text{C}-\text{set}), \quad B' \subset D(0,r) \quad \text{and} \quad \delta(B', B) \leqslant \frac{1}{r},$$

which ensures that $\mathcal{B}_e$ is localizable with a constant $c = 1$. □

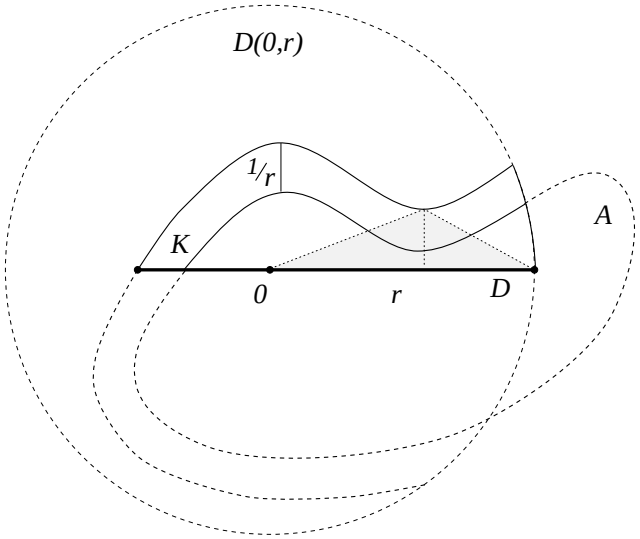

Figure 5.7: Area of K is greater than 1

Hence, Theorem 6 applies to $\mathcal{B}_e$ and we have, for any image C^3 near $\boldsymbol{x}_0$,

$$E_\sigma(u)(\boldsymbol{x}_0) = \sup_{B \in \mathcal{B}_e} \inf_{\boldsymbol{y} \in B} u(\boldsymbol{x}_0 + \sqrt{\sigma} \cdot \boldsymbol{y}) = u(\boldsymbol{x}_0) + |Du(\boldsymbol{x}_0)| g\,(\text{curv}(u)(\boldsymbol{x}_0))\ \sigma^{\frac{2}{3}} + o(\sigma^{\frac{2}{3}}), \quad (5.11)$$

$$\begin{aligned} \text{where} \quad g(r) &= c^+ r^{\frac{1}{3}} \ \text{ if } r \geqslant 0 \\ &= c^- (-r)^{\frac{1}{3}} \ \text{ if } r < 0. \end{aligned}$$

At this stage, one easily checks that $c^+ = 0$ and $c^- = \omega = \frac{1}{2}\left(\frac{3}{2}\right)^{2/3}$.

In [41], the consistency of the alternate operators is proved only when $\mathcal{B}$ is made of all unit area convex sets symmetrical with respect to $\boldsymbol{0}$, and the proof is based on a more precise estimation of the inf-sup and sup-inf operators in this case.

However, it seems that the method we used in the previous section still works for any localizable basis of structuring elements invariant by $SL(\mathbb{R}^2)$ (and in particular for $\mathcal{B}_e$). Since

the consistency mainly requires a local comparison principle, we only need to check that the alternate operators $IS_s \circ SI_s$ and $SI_s \circ IS_s$ satisfy the following local comparison principle. The proof is more or less the same as for Lemma 14.

Lemma 15 *If $\mathcal{B}$ is localizable and invariant by $SL(\mathbb{R}^2)$, and if u and v are two k-Lipschitz functions in $D(\boldsymbol{x}_0, r)$ satisfying $u \leqslant v$ in $D(\boldsymbol{x}_0, r)$, then for any $s \leqslant c^{-1}r^2$,*

$$IS_s \circ SI_s(u)(\boldsymbol{x}_0) \leqslant IS_s \circ SI_s(v)(\boldsymbol{x}_0) + kc\frac{s}{r}, \tag{5.12}$$

where c depends only on $\mathcal{B}$. The same property holds for $IS_s \circ SI_s$.

Proof :

First, we know from [41] that (5.12) is satisfied for both SI_s and IS_s, taking $c = c_{\mathcal{B}}$. But since $c^{-1}r^2$ does not depend on $\boldsymbol{x}_0$, (5.12) is satisfied for SI_s and IS_s in the whole disk $D(\boldsymbol{x}_0, \frac{r}{2})$ as soon as $s \leqslant 2c^{-1}r^2/4$, provided that we take $c = 2c_{\mathcal{B}}$. Hence, we can apply once again the Local Comparison Principle to deduce that for any $s \leqslant c^{-1}r^2$, (5.12) is satisfied for $IS_s \circ SI_s$ and $SI_s \circ IS_s$, with $c = 4c_{\mathcal{B}}$. □

Hence, we can generalize the consistency property of [41] for the alternate operators $IS_s \circ SI_s$ and $SI_s \circ IS_s$ for any localizable and affine-invariant basis of structuring elements.

5.7 Convergence

As we know that the affine erosion of images is consistent with the AMSS, it is natural to wonder whether the iterated infinitesimal affine erosion spans exactly the affine morphological scale space. The answer is yes, and the proof is classical (see [9], [22], [41] and [20]). The only refinement we bring is that we allow non uniform subdivisions.

Definition 18 *A subdivision of an interval $[a, b]$ is a finite sequence $s = (s_0, s_1, \ldots s_n)$ such that $a = s_0 \leqslant s_1 \leqslant \ldots \leqslant s_n = b$. The step of s is*

$$|s| = \sup_{1 \leqslant i \leqslant n} (s_i - s_{i-1}).$$

In the following definition, $\mathcal{S}(\mathbb{R}^2)$ is the set of 2×2 symmetric real matrices.

Definition 19 *A function $F : \mathcal{S}(\mathbb{R}^2) \times \mathbb{R}^2 \to \mathbb{R}^2$ is **elliptic** if*

$$\forall\, (p, X, Y) \in \mathbb{R}^2 \times \mathcal{S}(\mathbb{R}^2) \times \mathcal{S}(\mathbb{R}^2), \quad X \leqslant Y \;\Rightarrow F(X, p) \geqslant F(Y, p).$$

Theorem 7 *Let F be a continuous elliptic function, and T_h an operator on Lipschitz images (the Lipschitz constant being preserved). Suppose that T_h commutes with additions of constants, contrast changes and translations, and that for any u C^3 near $\boldsymbol{x}_0$,*

$$T_h(u)(\boldsymbol{x}_0) = u(\boldsymbol{x}_0) + h\, F(D^2u(\boldsymbol{x}_0), Du(\boldsymbol{x}_0)) + o(h). \tag{5.13}$$

Given a Lipschitz image u_0, we define, for any subdivision s of $[0,t]$,

$$u_s(\boldsymbol{x},0) = u_0(\boldsymbol{x}) \quad \text{and}$$

$$u_s(\boldsymbol{x},s_{i+1}) = T_{s_{i+1}-s_i}\, u_s(\boldsymbol{x},s_i).$$

Then, as $|s| \to 0$, $u_s(.,t)$ converges uniformly on every compact subset of the plane towards a function $\boldsymbol{x} \mapsto u(\boldsymbol{x},t)$, the unique viscosity solution of

$$\begin{cases} \dfrac{\partial u}{\partial t} = F(D^2u, Du) \\ \\ u(\boldsymbol{x},0) = u_0(\boldsymbol{x}). \end{cases}$$

The proof can be found in [41] for example.

Corollary 8 *Let u_0 be a Lipschitz image, and $u_s(\cdot,s_i)$ the filtered images obtained as in theorem 7. Then, as $|s| \to 0$, $u_s(.,t)$ converges uniformly on every compact subset of the plane to the unique viscosity solution of the AMSS partial differential equation*

$$\frac{\partial u}{\partial t} = \omega \cdot |Du| g(\mathrm{curv}(u)),$$

subject to initial condition $u(\boldsymbol{x},0) = u_0(\boldsymbol{x})$, where

$$\begin{aligned} g(c) &= (c^+)^{\frac{1}{3}} \quad \text{if } T_h = E_{h^{3/2}}, \\ &= (c^-)^{\frac{1}{3}} \quad \text{if } T_h = D_{h^{3/2}}, \\ &= c^{\frac{1}{3}} \quad \text{if } T_h = E_{h^{3/2}} \circ D_{h^{3/2}} \quad \text{or} \quad T_h = D_{h^{3/2}} \circ E_{h^{3/2}}. \end{aligned}$$

with as usual $\omega = \frac{1}{2}\left(\frac{3}{2}\right)^{\frac{2}{3}}$.

Proof :

We apply the previous theorem to the operators $E_{h^{3/2}}, D_{h^{3/2}}, \ldots$ and their associated continuous elliptic function

$$F(D^2u, Du) = \omega \cdot |Du| g(\mathrm{curv}(u)).$$

The required consistency property (Equation 5.13) is a direct consequence of Theorem 4. □

Remark : Following [22], we could also use the mean

$$M_h = \frac{1}{2}(E_{h^{3/2}} + D_{h^{3/2}})$$

instead of the alternate operators $E_{h^{3/2}} \circ D_{h^{3/2}}$ and $D_{h^{3/2}} \circ E_{h^{3/2}}$. The consistency follows immediatly from the consistency of $E_{h^{3/2}}$ and $D_{h^{3/2}}$, and the convergence theorem still applies. This "mean" operator has one advantage : it is symmetric, so that the resulting scheme is fully invariant under a contrast reversal (whereas the alternate scheme is only *asymptoticly* invariant under a contrast reversal). However, M_h does not satisfy the morphological invariance axiom, and it creates new grey levels on images.

Chapter 6

Numerical scheme

Numerically, a curve is nothing but a finite set of numbers which are interpreted as coordinates or parameters to produce a continuous curve. The simplest way to represent a curve numerically is to define it as a polygon, but some higher order representations, e.g. splines, have appeared to be more efficient for some applications.

Many reasons lead to choose the polygonal representation to implement the affine erosion on curves. The polygonal representation is very simple, affine invariant, and the level lines of a grey-level discrete image are naturally defined as polygons if we consider the pixels as squares. But the major advantage of this representation in our case is, as we shall see further, that we can compute *exactly* the affine erosion of a polygon. The lack of regularity of polygons (not C^1 everywhere) shall not be a problem, since most of the previous analyses apply to piecewise C^1 curves.

Obviously, neither the affine erosion nor the AMSS of a polygon is a polygon. But since no simple dense set of parameterized curves satisfies this property (as far as we know), an approximation is always required to iterate the affine erosion. The main advantage of being able to compute exactly the affine erosion of a polygon is that *we can fully dissociate the two approximate operations required to compute the AMSS : the scale quantization step* (we have to iterate the affine erosion several times) *and the space quantization step*, which is necessary to work on discrete data. By processing these two steps successively and independently, we avoid a classical trap which prevents geometrical algorithms from satisfying the **[Inclusion Principle]** and **[Affine Invariance]** properties. In particular, our method sets no *a priori* relation between the number of vertices of a polygon and the number of vertices of the polygon resulting on the approximation of its affine scale space at any scale : this number can drastically increase (case of a triangle) or decrease as well (case of a very "noisy" curve). In other words, our algorithm processes a polygon *as a curve* and not as a set of points, and for that reason it is not a point evolution scheme.

In this chapter, we describe exactly the affine erosion of a polygon, convex or not. Then we give a simple numerical algorithm to compute the affine erosion of convex polygons, as well

as an exact algorithm in the general case. We also present briefly a simplified algorithm which runs faster, and produces similar results.

6.1 Affine erosion of a polygon

6.1.1 Regular convex case

Proposition 25 *Let $\mathcal{P} = P_1P_2...P_n$ be a convex polygon, and $0 < \sigma < \sigma_r(\mathcal{P})$. The σ-affine erosion of $\mathcal{P}$ is a C^1 curve made of the concatenation of the pieces of hyperbolae $H_{i,k}$ defined by Equations 6.2 to 6.7, the couples (i,k) satisfying Equation 6.1 and being sorted in lexical order.*

Proof :

If $\mathcal{P} = P_1P_2...P_n$ is a (positively oriented) convex polygon and $0 < \sigma < \sigma_r(\mathcal{P})$, we know from Theorem 1 that $E_\sigma(\mathcal{P})$ is made exactly of the middle points of the σ-chord segments of $\mathcal{P}$. Consider two non-parallel edges $[P_{i-1}P_i]$ and $[P_kP_{k+1}]$, then there exists σ-chords whose endpoints lie on $[P_{i-1}P_i]$ and $[P_kP_{k+1}]$ if and only if

$$\frac{1}{2}\left[IP_k, IP_i\right] \leqslant \sigma + \sigma_{i,k} \leqslant \frac{1}{2}\left[IP_{k+1}, IP_{i-1}\right], \tag{6.1}$$

where I is defined as

$$I := (P_{i-1}P_i) \cap (P_kP_{k+1}). \tag{6.2}$$

and

$$\sigma_{i,k} := \text{area}\left(IP_i...P_k\right) \tag{6.3}$$

(see Figure 6.1). In this case, we know from Proposition 1 that the middles of the σ-chord segments whose endpoints lie on $[P_{i-1}P_i]$ and $[P_kP_{k+1}]$ span a piece of hyperbola

$$H_{i,k}: \quad M(t) = I + \lambda(e^t IP_k + e^{-t} IP_i), \quad t_1 \leqslant t \leqslant t_2 \tag{6.4}$$

whose apparent area is

$$\sigma + \sigma_{i,k} = 2\lambda^2\left[IP_k, IP_i\right],$$

so that

$$\lambda = \sqrt{\frac{\sigma + \sigma_{i,k}}{2\left[IP_k, IP_i\right]}}. \tag{6.5}$$

We need to compute the endpoints of $H_{i,k}$, i.e. the value of t_1 and t_2. Two cases happen for t_1 : if area $(IP_{i-1}P_k) > \sigma + \sigma_{i,k}$, there exists a σ-chord segment $[P_{i-1}J]$ where $J \in [P_kP_{k+1}]$ (see Figure 6.1), otherwise there exists a σ-chord $[JP_k]$ where $J \in [P_{i-1}P_i]$. In the first case, we have

$$I + 2\lambda \cdot e^{-t_1} IP_i = P_{i-1},$$

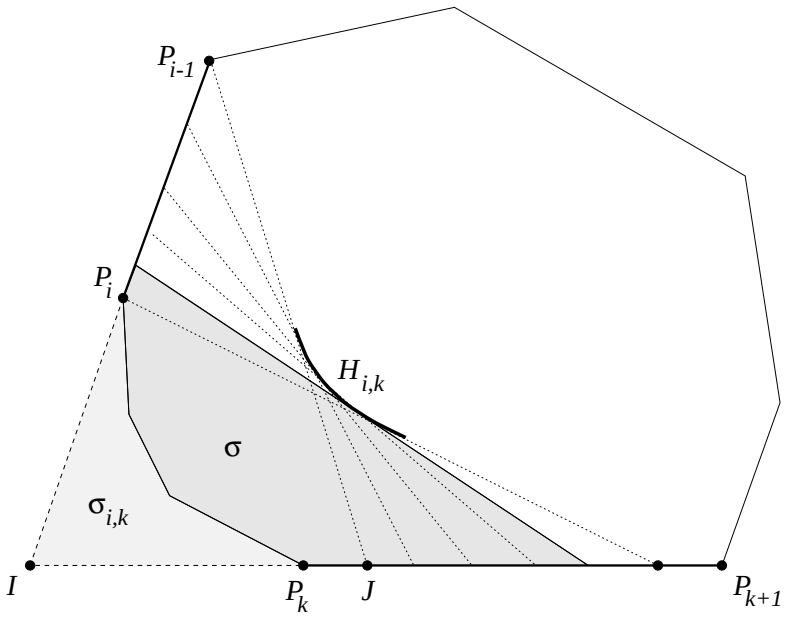

Figure 6.1: Piece of hyperbola resulting from two edges.

whereas

$$I + 2\lambda \cdot e^{t_1} IP_k = P_k$$

for the alternative case. Symmetrically, one easily checks that if area $(IP_iP_{k+1}) > \sigma + \sigma_{i,k}$ we have

$$I + 2\lambda \cdot e^{t_2} IP_k = P_{k+1},$$

and

$$I + 2\lambda \cdot e^{-t_2} IP_i = P_i \quad \text{otherwise.}$$

In other words,

$$t_1 = -\ln \frac{\operatorname{dist}(I, P_{i-1})}{2\lambda \cdot \operatorname{dist}(I, P_i)} \quad \text{if} \quad \text{area}\,(IP_{i-1}P_k) > \sigma + \sigma_{i,k}, \quad t_1 = -\ln(2\lambda) \quad \text{otherwise,} \tag{6.6}$$

$$t_2 = \ln \frac{\operatorname{dist}(I, P_{k+1})}{2\lambda \cdot \operatorname{dist}(I, P_k)} \quad \text{if} \quad \text{area}\,(IP_iP_{k+1}) > \sigma + \sigma_{i,k}, \quad t_2 = \ln(2\lambda) \quad \text{otherwise.} \tag{6.7}$$

The admissible hyperbolae $H_{i,k}$ are encountered on $E_\sigma(\mathcal{P})$ in lexical order, that is $H_{i,k} < H_{i',k'}$ means either "$i < i'$" or "$i = i'$ and $k - i < k' - i < k - i + n$ modulo n". The reason is very simple : as we know that $E_\sigma(\mathcal{P})$ is convex, we must consider the σ-chords segments of $\mathcal{P}$ in such an order that the angles of their directions increase continuously on S^1. Thus, the previous assertion simply results from the inequality

$$i \leqslant j \leqslant k \;\Rightarrow\; \alpha(P_iP_j) \leqslant \alpha(P_iP_k) \leqslant \alpha(P_jP_k) < \alpha(P_iP_j) + 2\pi,$$

where $\alpha(\boldsymbol{v})$ measures on S^1 the angle between a fixed vector and the vector $\boldsymbol{v}$. □

6.1.2 Non regular convex case (removing ghosts parts)

When $\mathcal{P}$ is a convex polygon and $\sigma \geqslant \sigma_r(\mathcal{P})$, we noticed in Chapter 3 (see Figure 3.13 for example) that "ghosts parts" can appear in the curve made of the middle points of the σ-chord segments of $\mathcal{P}$. We cannot avoid this situation since $\sigma_r(\mathcal{P}) = 0$ for some polygons. Moreover, we saw in Chapter 4 that we could hope to iterate the affine erosion with rather large scale steps ; to this aim, we must be able to compute the affine erosion of any polygon with arbitrary large scales, and not only when $\sigma < \sigma_r(\mathcal{P})$.

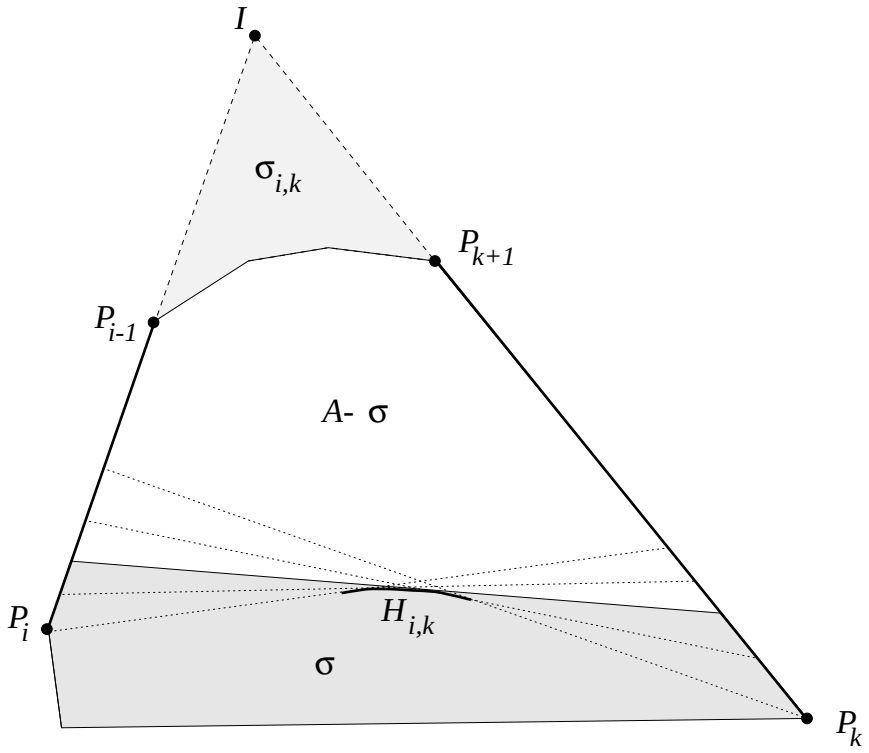

Figure 6.2: Non regular chords span "ghost" hyperbolae.

We can see on Figure 6.2 that non-regular chords span "ghost parts", which do not take part of the affine erosion of $\mathcal{P}$. By the way, these "ghost parts" are also hyperbolae, and their apparent area is equal to $A - \sigma + \sigma_{i,k}$, A being the area of $\mathcal{P}$. Thus, we can forget these ghost hyperbolae, and $E_\sigma(\mathcal{P})$ is included in the collection of hyperbolae defined in Proposition 25, with the restriction

$$[P_{i-1}P_i, P_kP_{k+1}] > 0.$$

Now, in order to compute exactly the affine erosion of $\mathcal{P}$, we have to compute hyperbolae intersections in order to remove the remaining "ghost parts". In general, computing the intersection between two hyperbolae reduces to an algebraic equation of degree 4, but in the situation we are facing, one can see that when two pieces of hyperbola have a common intersection, they must have a common axis, so that the problem reduces to a second degree equation which can be

solved exactly. Hence, *it is quite simple to compute the exact affine erosion of a convex polygon for arbitrary large scales.* In the next section, we investigate the general (and more complicated) case of non-convex polygons.

6.1.3 General case (non convex polygons)

Proposition 26 *The affine erosion of a (possibly non convex) polygon is one or several generalized "hyperbolic polygon", resulting from the concatenation of segments and convex pieces of hyperbolae.*

The proof is straightforward from Proposition 10, because the affine erosion can only "create" segments and hyperbolae pieces. If $\mathcal{P} = P_1P_2 \dots P_n$ is a polygon, we can write

$$E_\sigma(\mathcal{P}) = \mathcal{I}(\mathcal{P}) - \bigcup_{1 \leqslant i,k \leqslant n} C_\sigma(P_i \dots P_k),$$

where $C_\sigma(P_i \dots P_k)$ is the union of the chord sets of $\mathcal{P}$, with area smaller than σ, and resulting from chord segments whose endpoints lie on the edges $[P_iP_{i+1}]$ and $[P_{k-1}P_k]$ (with the circular conventions $P_0 = P_n$, $P_{n+1} = P_1$ and when $k < i$, $P_i \dots P_k = P_iP_{i+1} \dots P_nP_1 \dots P_{k-1}P_k$).

Let $P_i \dots P_k$ be a polygonal curve, and consider two points $(A, B) \in [P_iP_{i+1}] \times [P_{k-1}P_k]$. We shall say that the segment $[AB]$ is **occluded** if it is not a chord segment of $\mathcal{P} = P_i \dots P_k$, i.e. if for some $j \in \{i+1, \dots, k-2\}$,

$$[AB] \cap [P_jP_{j+1}] \neq \emptyset.$$

Now, we shall say that the polygonal curve $\mathcal{P} = P_i \dots P_k$ is

- **partially occluded** if for at least one $(A, B) \in [P_i, P_{i+1}[\times]P_{k-1}, P_k]$, the segment $[AB]$ is occluded,
- **totally occluded** if all segments $[AB]$, $(A, B) \in [P_i, P_{i+1}] \times [P_{k-1}, P_k]$ are occluded.

If $P_i \dots P_k$ is totally occluded, it is clear that $C_\sigma(P_i \dots P_k) = \emptyset$. It is equivalent to say that (P_iP_k) is not a chord of $\mathcal{P}$.

Lemma 16 *Suppose that $P_i \dots P_k$ is partially (but not totally) occluded, and $[P_iP_{i+1}, P_{k-1}P_k] > 0$. Then one can find $(A, B) \in [P_iP_{i+1}] \times [P_{k-1}P_k]$ such that $P_iAP_{i+1} \dots P_{k-1}BP_k$ is not occluded and*

$$C_\sigma(P_i \dots P_k) = C_\sigma(P_iAP_{i+1} \dots P_{k-1}BP_k).$$

Proof :

More than a proof, we give an effective construction of A and B. The first remark is that if $C_\sigma(P_i \dots P_k) = \emptyset$, we can choose $A = P_i$ and $B = P_k$. Hence, we suppose that $C_\sigma(P_i \dots P_k) \neq \emptyset$ in the following.

Since $[P_iP_{i+1}, P_{k-1}P_k] > 0$, we can find an affine map ϕ such such that $\det\phi = 1$ and $\phi(P_j) = (x_j, y_j)$ in an orthonormal basis, with $x_i = x_{i+1} = y_{k-1} = y_k = 0$, $x_k > 0$, $y_i > 0$, $x_{k-1} < x_k$ and $y_{i+1} < y_i$ (see Figure 6.3).

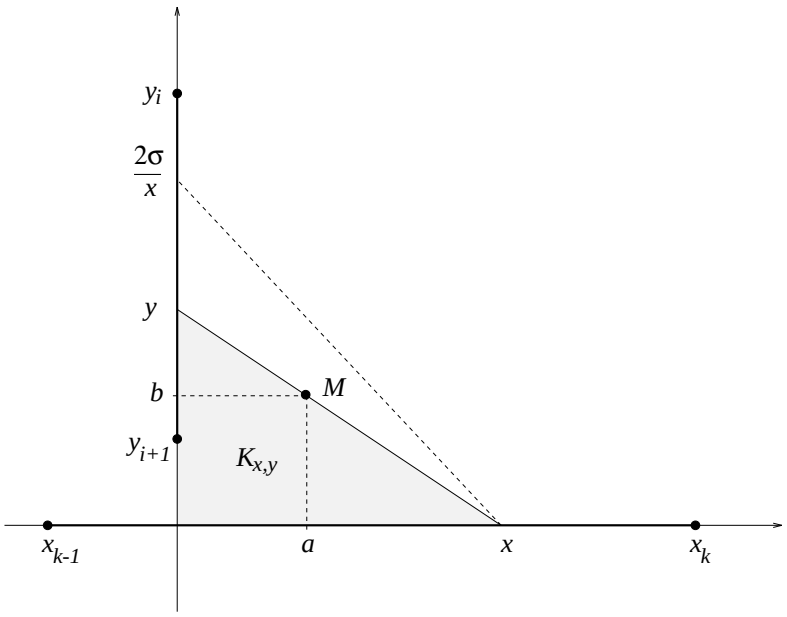

Figure 6.3: Solving partial occlusions.

Now, consider four positive real numbers a, b, x, y and look at Figure 6.3. The point $M(a, b)$ belongs to the boundary of the chord set $K_{x,y}$ of the corner $C = \mathbb{R}_+ \times \mathbb{R}_+$ if and only if

$$\frac{a}{x} + \frac{b}{y} = 1.$$

In this case, we have

$$\text{area}\,(K_{x,y}) = ab + \frac{b(x-a)}{2} + \frac{a(y-b)}{2} = ab + \frac{b(x-a)}{2} + \frac{ab^2}{2(x-a)},$$

and we can deduce that the σ-chord set of $\mathcal{C}$ defined from the segment $[(x,0), (0, \frac{2\sigma}{x}]$ contains M if and only if x belongs to the interval

$$I_\sigma(a,b) = \left\{ x,\ ab + \frac{b(x-a)}{2} + \frac{ab^2}{2(x-a)} \leqslant \sigma \right\}.$$

An explicit computation gives

$$I_\sigma(a,b) = \left[\frac{\sigma}{b}\left(1 - \sqrt{1 - \frac{2ab}{\sigma}}\right), \frac{\sigma}{b}\left(1 + \sqrt{1 - \frac{2ab}{\sigma}}\right) \right],$$

with the conventions $I_\sigma(a,b) = \emptyset$ if the square root is not defined, and $I_\sigma(a,b) = \mathbb{R}$ if one of a, b is not positive.

Let us now define

$$J_1 = \bigcap_{i+2 \leqslant j \leqslant k-2} I_\sigma(x_j, y_j)$$

(with the convention $J_1 = \mathbb{R}$ if $i+2 > k-2$), and

$$J_2 = [\max(0, x_{k-1}), x_k] \cap \left[\frac{2\sigma}{y_i}, \frac{2\sigma}{\max(0, y_{i+1})}\right]$$

(with the convention $1/0 = +\infty$). Since we supposed $C_\sigma(P_i \dots P_k) \neq \emptyset$, $J_1 \cap J_2$ is not empty and we can write $J_1 \cap J_2 = [z_1, z_2]$. Then, one checks easily that the two points

$$A = \phi^{-1}\left((0, \frac{2\sigma}{z_2})\right) \qquad \text{and} \qquad B = \phi^{-1}\left((z_1, 0)\right)$$

satisfy the conclusion of the Lemma. □

We investigate the possible "shapes" of $C_\sigma(P_i \dots P_k)$. According to the previous Lemma, we can suppose without loss of generality that no occlusions appear. In the following, area $(P_i \dots P_k)$ means the algebraic area of the polygon $P_i P_{i+1} \dots P_k$, defined for example by

$$\text{area}\,(P_i \dots P_k) = \frac{1}{2} \sum_{i<j<k} [P_i P_j, P_i P_{j+1}]\,.$$

If area $(P_{i+1} \dots P_{k-1}) > \sigma$, any chord segment whose endpoints lie on $[P_i P_{i+1}]$ and $[P_{k-1} P_k]$ defines a chord set of area greater than σ, so that $C_\sigma(P_i \dots P_k) = \emptyset$. Hence, we shall suppose that area $(P_{i+1} \dots P_{k-1}) \leqslant \sigma$ in the three following cases which remain.

• **case 1 (regular case)** : If area $(P_i \dots P_k) > \sigma$ and $[P_i P_{i+1}, P_{k-1} P_k] > 0$, the inside boundary of $C_\sigma(P_i \dots P_k)$ is made of a piece of hyperbola, completed with two half-chord segments at its endpoints (see Figure 6.4).

• **case 2 (reverse case)** : If area $(P_i \dots P_k) > \sigma$ and $[P_i P_{i+1}, P_{k-1} P_k] \leqslant 0$ the inside boundary of $C_\sigma(P_i \dots P_k)$ is a polygonal curve of the kind $A\Omega B$, where $(A, B) \in [P_i P_{i+1}] \times [P_{k-1} P_k]$. The point Ω is obtained as the intersection between the two σ-chord segments defined from A and B. Remember that as in the convex case, either $A = P_i$ or (A, P_{k-1}) is a σ-chord (and a symmetrical alternative holds for B). As we noticed previously, the ghost hyperbola spanned by the σ-chord segments is strictly contained in $C_\sigma(P_i \dots P_j)$ and does not contribute to its boundary (see Figure 6.5).

• **case 3 (sub-area case)** : If area $(P_i \dots P_j) \leqslant \sigma$, the inside boundary of $C_\sigma(P_i \dots P_j)$ is simply the segment $P_i P_{j+1}$.

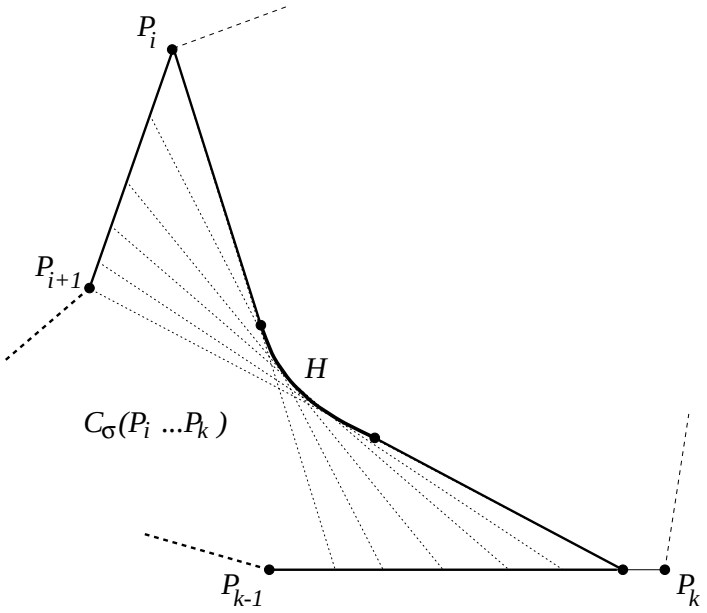

Figure 6.4: Regular case.

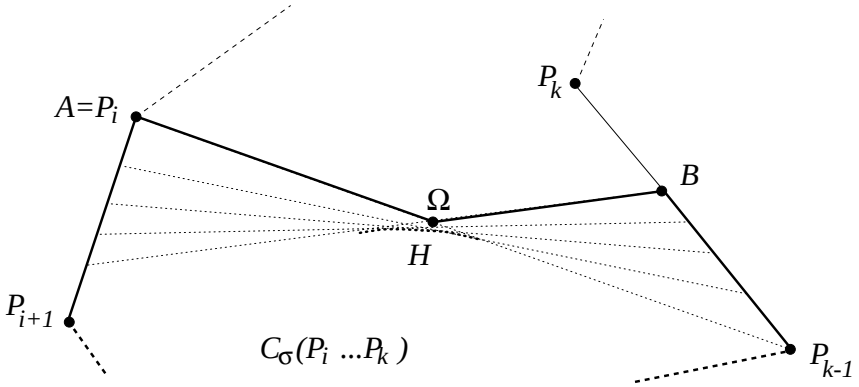

Figure 6.5: Reverse case.

6.2 Algorithm

Now are now in position to describe an *exact* algorithm to compute the affine erosion of any polygon. It consists of three steps.

Step A : We collect all the pieces of curves which can possibly be part of $E_\sigma(\mathcal{P})$. As we noticed previously, these pieces are of three kinds (see Figure 6.6).

1. The valid pieces of hyperbola $H_{i,k}$ described previously, completed with their two half chord segments at their endpoints. As we noticed before, the interval $[t_1, t_2]$ defining each piece of hyperbola (Equation 6.4) may have to be shortened in case of partial occlusions (see Lemma 16).
2. The two "limit" σ-chord segments of each ghost piece of hyperbola resulting from non-regular chords.
3. The σ'-chord segments ($0 \leqslant \sigma' \leqslant \sigma$) defined by two vertices in the sub-area case.

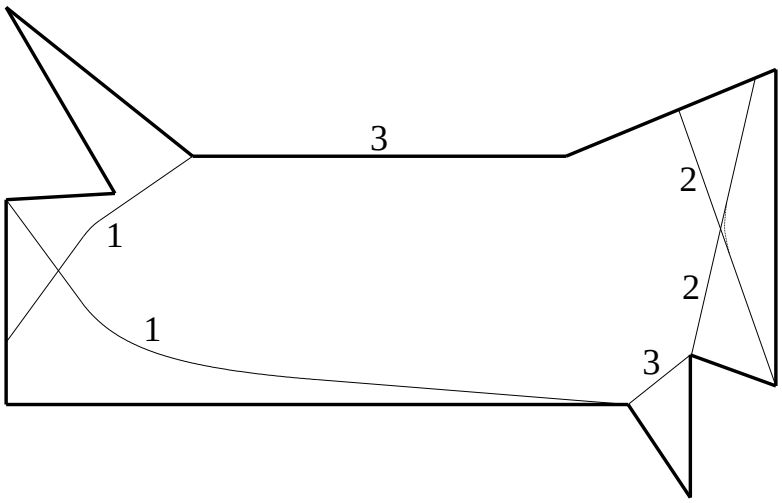

Figure 6.6: The three kinds of curves encountered in the affine erosion of a polygon

Step B : We remove the useless pieces of curves according to their position. More precisely, with each piece of curve $\mathcal{C}$ obtained in step A we associate two numbers $a(\mathcal{C}), b(\mathcal{C})$ representing the starting point of the first chord segment spanning $\mathcal{C}$ and the endpoint of the last chord segment spanning $\mathcal{C}$: since these points belong to the polygon $\mathcal{P}$, we can represent them as numbers $i+\alpha$, meaning the point $(1-\alpha)P_i+\alpha P_{i+1}$. The key point of this representation is that two pieces of curves $\mathcal{C}_1$ and $\mathcal{C}_2$ obtained in Step A have a common intersection if and only if the intervals $[a_1, b_1]$ and $[a_2, b_2]$ are not disjoint. Therefore, if $a_1 < a_2 < b_2 < b_1$, the piece of curve $\mathcal{C}_2$ is useless and can be removed.

Step C : We compute the intersections between the remaining pieces of curves (sorted with respect with their starting number a). At this stage, we may have to compute intersections between

two segments, between a segment and an hyperbola, or between two hyperbolae. The two first cases reduce to equations of degree 1 and 2 respectively. The last case (intersection of two hyperbolae) can be more difficult. If the two hyperbolae have a common axis, then the intersection equation is of degree 2 and can be solved easily. However, in more general cases (which happen), we can have two solve an algebraic equation of degree 4 ; if so, we compute the intersection by using Newton's algorithm, which converges in a few iterations.

Now, for each intersection, we remove from each of the two curves the parts which are "on the right" of the other one, according to the definition of the affine erosion. We have to maintain — at least, formally— two data structures to process this step correctly : one is the original set of curves obtained from step B, the other is a copy of these curves, updated iteratively as we just explained.

We must mention that many intersections simply result from two successive hyperbolae as in the convex case ; to process these intersections, no computation is required : one only needs to remove the two corresponding half-chord segments.

Finally, we obtain the affine erosion of the polygon as the concatenation (in the natural order) of the pieces of curves obtained from step C. This algorithm is a bit heavy (about 1600 lines of C source code), but not too slow for reasonable polygons (1 second or so for a polygon with 100 vertices). One must be careful when computing the intersections, because of the finite numerical precision of the computer (this can be done by considering point equalities modulo a relative error, for instance).

Figures 6.7, 6.8 and 6.9 are an example of the results we obtain after steps A, B and C.

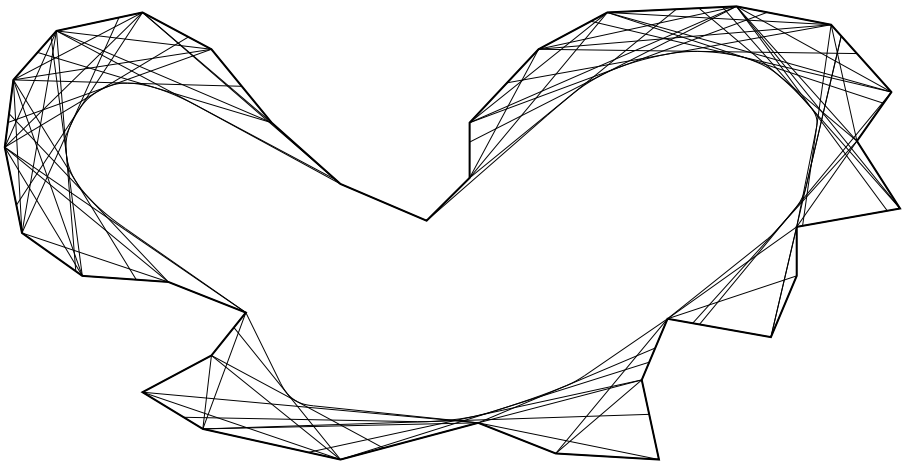

Figure 6.7: curves obtained ater step A

In this algorithm, we did not mention the problem of topological changes that occurs when the initial polygon breaks into non connected parts (remember that the affine erosion does not always preserve the connectedness). This problem is not very difficult to handle, but requires a

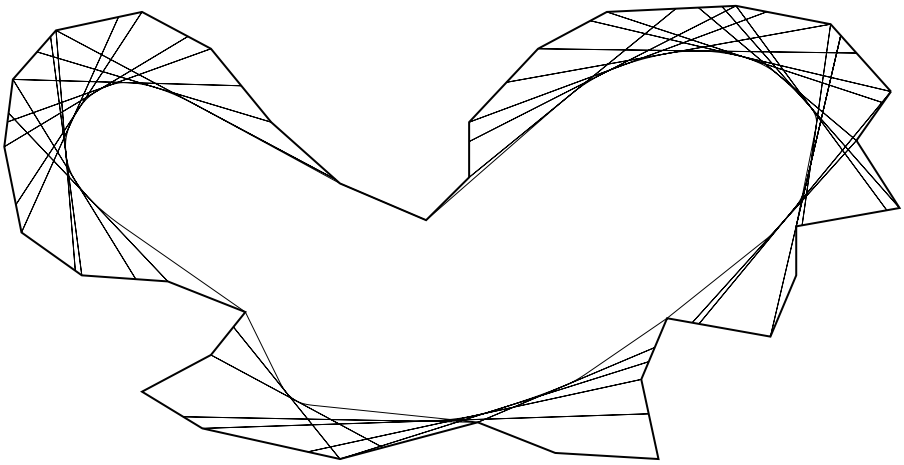

Figure 6.8: curves obtained ater step B

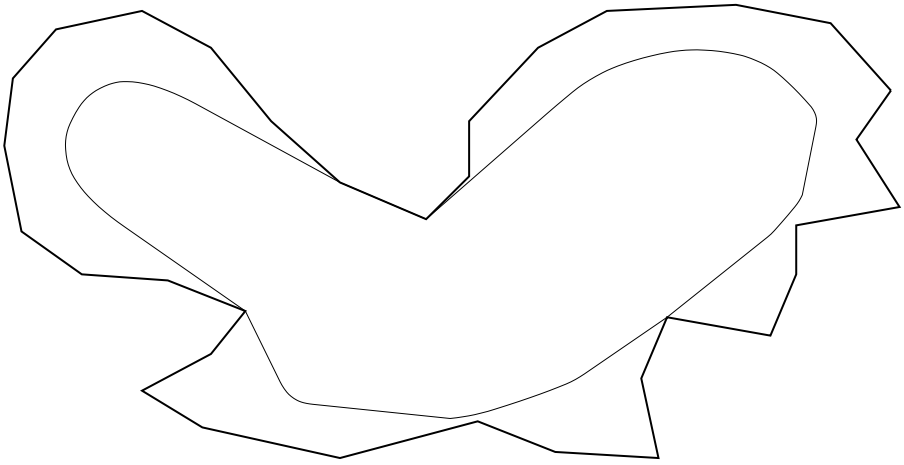

Figure 6.9: curve obtained ater step C

high computation cost : each time an hyperbola or a segment is computed, one must look for a possible intersection with an edge of the polygon, and break the resulting curve into several parts when the case happens. Fortunately, such external occlusions are seldom.

6.3 Affine subsampling and iteration

So far, we know how to compute exactly the affine erosion of a polygon. To iterate this process, we need to quantize the resulting curve (which is, as we shown, a concatenation of hyperbola pieces and segments) in order to get a new polygon. Fortunately, there is a simple way to sample a piece of hyperbola in an affine-invariant way. Consider the parameterization

$$H \ : \ M(t) = \lambda(e^t \boldsymbol{v}_1 + e^{-t}\boldsymbol{v}_2), \qquad t_1 \leqslant t \leqslant t_2 \ :$$

then $(t, t+x)$ is an ε-chord set of H if and only if $\varepsilon = \lambda^2(\mathrm{sh}\, x - x)$, where sh denotes the hyperbolic sine (see the proof of Proposition 14). Hence, the polygon $P_0P_1...P_n$ defined by

$$P_k = M\left((1-\frac{k}{n})t_1 + \frac{k}{n}t_2\right)$$

is a discrete affine invariant quantization of H with "area step"

$$\varepsilon(n) = \lambda^2(\mathrm{sh}\,\frac{1}{n} - \frac{1}{n}).$$

Given $\varepsilon > 0$, we can quantize the affine erosion of a polygon up to the area step ε by choosing, for each piece of hyperbola, the minimum entire value of n such that $\varepsilon(n) \leqslant \varepsilon$. This can be done, for instance, by tabling the inverse function $n(\varepsilon/\lambda^2)$ for the small values and using, for the large ones, the expansion

$$n \simeq \left(\frac{\lambda^2}{6\varepsilon}\right)^{\frac{1}{3}}.$$

Not surprisingly, this quantization step is a kind of discrete affine erosion of scale ε. Thus, as we want to minimize its influence on the affine erosion, we must choose $\varepsilon \ll \sigma$, where σ is the scale of the computed affine erosion. This condition forces the second iteration of E_σ to be **non-local** in the sense that the σ-chord sets of the resulting approximate polygon contain many edges (i.e. $k - i \gg 1$ for the valid $H_{i,k}$, see Figure 6.10). In that sense, our algorithm is quite different from a local point evolution scheme, for which the scale quantization step must be small compared to the space quantization step in order to ensure a minimum of stability. *Here, the inverse phenomenon happens* : the scale quantization step (σ) is much larger than the space quantization step (ε). An important consequence is that we can effectively iterate only a few times (i.e. with large scale steps) the affine erosion to compute the affine scale space. Indeed, we do not loose accuracy since ε can remain small and the affine erosion remains near its tangent operator (the Affine Scale Space) even for rather large scales, as we noticed in Section 2.4.

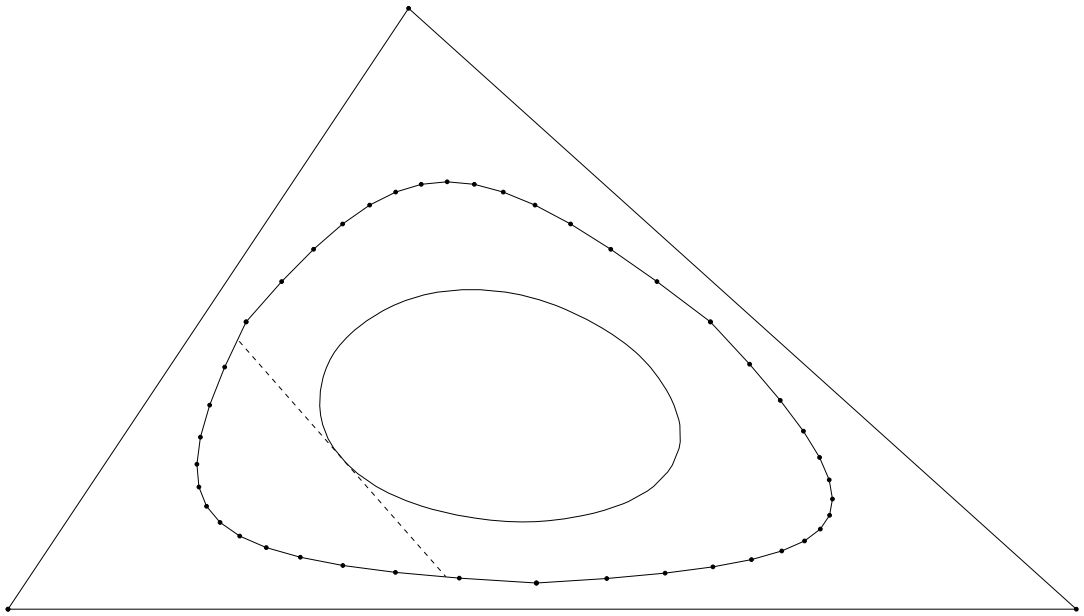

Figure 6.10: Two iterations of the affine erosion on a triangle. The second iteration is non-local with respect to the quantization, since each piece of the second iteration curve depends on many points of the first iteration one.

6.4 A simplified algorithm

Another way to implement the affine scale space is to iterate a pseudo affine erosion, written E'_σ, which processes separately the convex components of a given piecewise convex closed curve.

6.4.1 Pseudo affine erosion

If we want to define a kind of affine erosion for a non semi-closed curve c — that is, a curve with two endpoints —, we must choose a boundary condition. Our approach will be to fix these endpoints : in practice, these endpoints will correspond to inflexion points of a larger curve, and we know that these points do not move at order 1 since the curvature of the curve vanishes at them. How can we define the affine erosion of c ? We shall not investigate the problem in general, but one can see easily that for small scales, no external occlusions appear and c itself is included in the boundary of

$$c_\sigma = \bigcup_{S \in K_\sigma(c)} S,$$

so that it makes sense to define $E_\sigma(c)$ by

$$\partial c_\sigma = c \bigsqcup E_\sigma(c),$$

the symbol $\sqcup$ meaning a disjoint union (see Figure 6.11).

Let us call $\sigma_m(c)$ the maximum scale for which we can compute the affine erosion of c as described previously. If no external occlusion appear at any scale (i.e. it the two endpoints of c

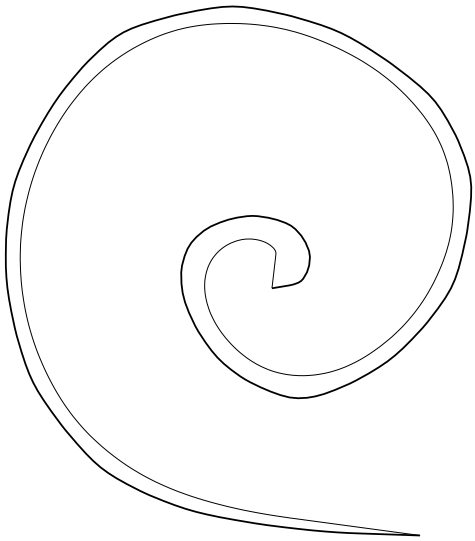

Figure 6.11: Affine erosion of a non semi-closed curve

are a non-zero chord of c), we restrain $\sigma_m(c)$ to the area of c (defined as the area of the chord set associated to the extremal points of c).

Given a piecewise convex closed curve $\mathcal{C}$, we consider the canonical decomposition $\mathcal{C} = c_1 c_2 \ldots c_n$, the curves c_i being defined as the convex (or concave) curves extracted from $\mathcal{C}$ between two successive junctions (see Chapter 3 and Figure 6.12). For any $\sigma < \sigma_m(\mathcal{C}) = \min_i \sigma_m(c_i)$, we can define the pseudo affine erosion of c by

$$E'_\sigma(\mathcal{C}) = E_\sigma(c_1)\, E_\sigma(c_2) \ldots E_\sigma(c_n).$$

As for the affine erosion, one can prove that the pseudo affine erosion of a curve cannot have any double junction.

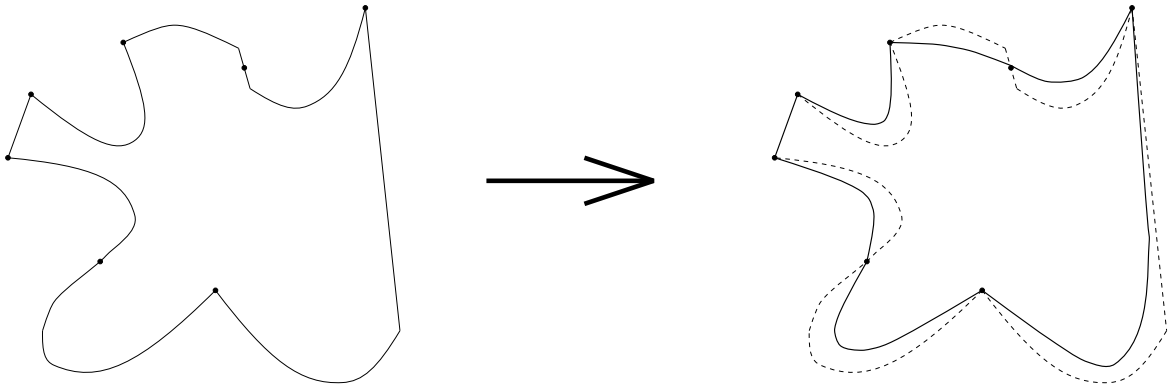

Figure 6.12: Pseudo affine erosion of a closed curve

6.4.2 Algorithm

The algorithm to compute $E'_\sigma(\mathcal{C})$ when $\mathcal{C}$ is a polygon is easy to devise. First, we remark that a polygon has no double junctions, and that its simple junctions are the middle of "inflexion" edges. Then, the algorithm to compute the affine erosion of each convex component of $\mathcal{C}$ is exactly the one we described previously for convex polygons. Hence, computing $E'_\sigma(\mathcal{C})$ is simpler and faster than computing $D_\sigma \circ E_\sigma(\mathcal{C})$, since it does not require to compute intersections in general (unless non-regular chords happen, which is very rare for small scales).

It is clear that E'_σ is consistent with the affine scale space. However, the inclusion property is only satisfied for small scales, because if $\mathcal{C}$ and $\mathcal{C}'$ are two piecewise convex closed curves, we only have

$$\mathcal{I}(\mathcal{C}) \subset \mathcal{I}(\mathcal{C}') \;\Rightarrow\; \forall \sigma \leqslant \min(\sigma_m(\mathcal{C}), \sigma_m(\mathcal{C}')),\;\; \mathcal{I}\left(E'_\sigma(\mathcal{C})\right) \subset \mathcal{I}\left(E'_\sigma(\mathcal{C}')\right).$$

Another drawback of this simplified algorithm is that if the curve $\mathcal{C}$ is very irregular, $\sigma_m(\mathcal{C})$ may be very small and a lot of iterations are required to compute the affine scale space of $\mathcal{C}$ at a large scale. This happens because only a few inflexion points disappear at each iteration.

In practice, the simplified algorithm based on the pseudo affine erosion is faster and simpler. We checked on experiments (see next chapter) that it produces similar results compared to the exact three-steps algorithm we described previously, *provided that the scale steps are chosen small enough*.

Chapter 7

Experiments

In this chapter, we present several experiments obtained with the algorithms described in the previous chapter. We first compute the affine erosion of some polygonal curves for different values of the area parameter, and check the affine invariance of the algorithm. We also show the effects of the affine discretization of the computed curves. Then, we compute the affine scale space of these curves by iterating the affine erosion (plus dilation) on them. We compare the results obtained with the exact algorithm to those obtained with the simplified algorithm based on the pseudo affine erosion.

7.1 Affine erosions

On the following experiments (Figure 7.1 to 7.6), the affine erosion $E_\sigma(\mathcal{C})$ of an initial curve $\mathcal{C}$ is represented for different values of the area parameter σ, actually taken in arithmetic progression. We begin with simple polygons and end with more complicated polygonal curves. It is important to notice that this representation is NOT the affine scale space of the initial curve $\mathcal{C}$, since the affine erosion operator is not iterated but simply computed for the same initial curve and increasing values of the area parameter. We shall compute later the corresponding affine scale spaces.

These figures can also be viewed as the level sets of an "affine distance" function $\boldsymbol{x} \mapsto d(\boldsymbol{x},\mathcal{C})$. For any point $\boldsymbol{x}$ lying inside a closed curve $\mathcal{C}$, $d(\boldsymbol{x},\mathcal{C})$ can be defined as the smallest area of a positive chord set of $\mathcal{C}$ enclosing $\boldsymbol{x}$, i.e.

$$d(\boldsymbol{x},\mathcal{C}) = \inf_{K \in \mathcal{K}^+(\mathcal{C}),\ \boldsymbol{x} \in K} \text{area}\,(K).$$

In particular, we have $d(\boldsymbol{x},\mathcal{C}) = 0$ if and only if $\boldsymbol{x} \in \mathcal{C}$, and

$$E_\sigma(\mathcal{C}) = \{\boldsymbol{x} \in \mathcal{I}(\mathcal{C}),\ d(\boldsymbol{x},\mathcal{C}) = \sigma\}.$$

To give an example, computing the 67 iterations of Figure 7.2 takes 0.3 second (CPU time) on a HP 735/125 station.

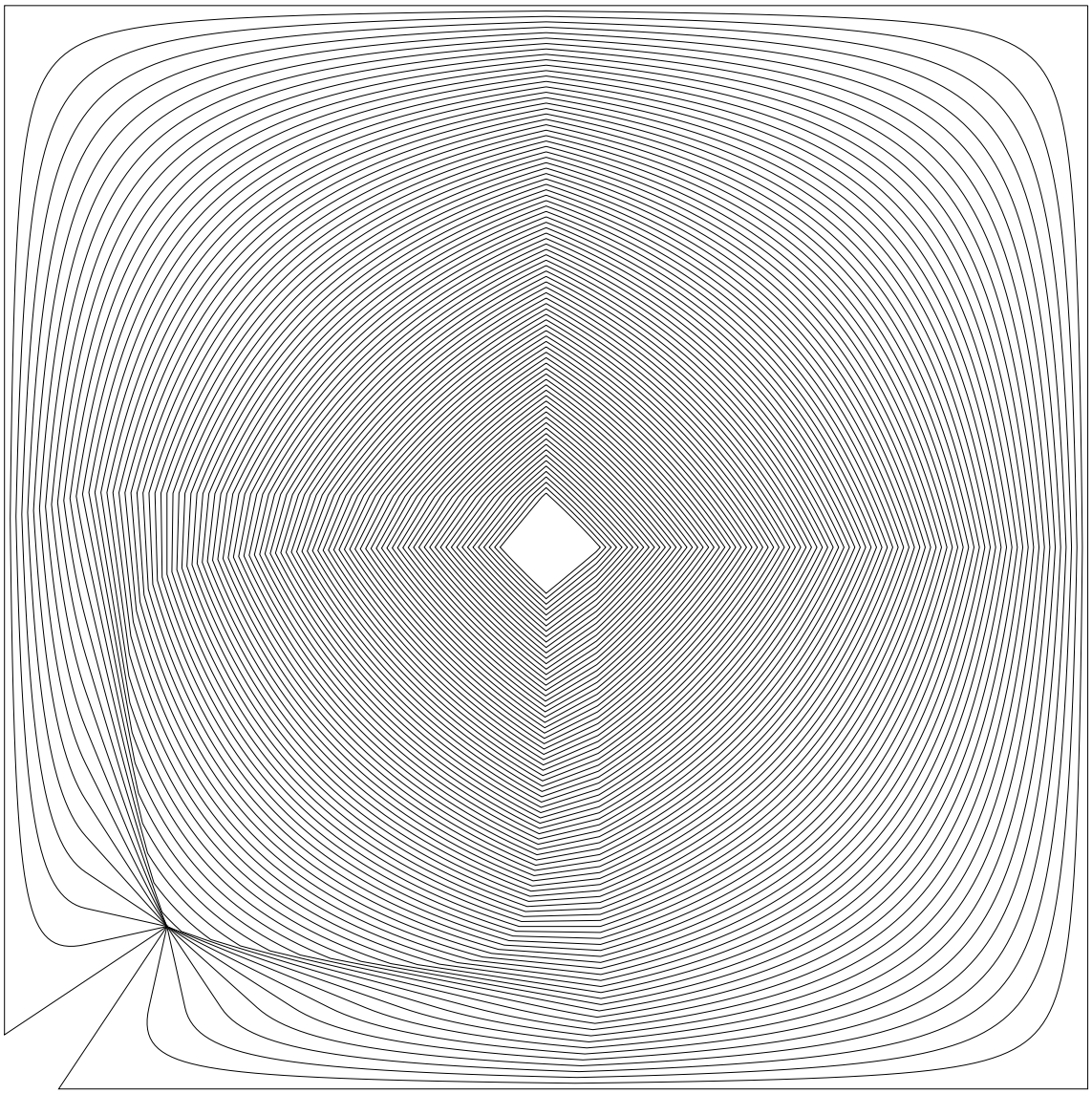

Figure 7.1: Affine erosions (modified square)

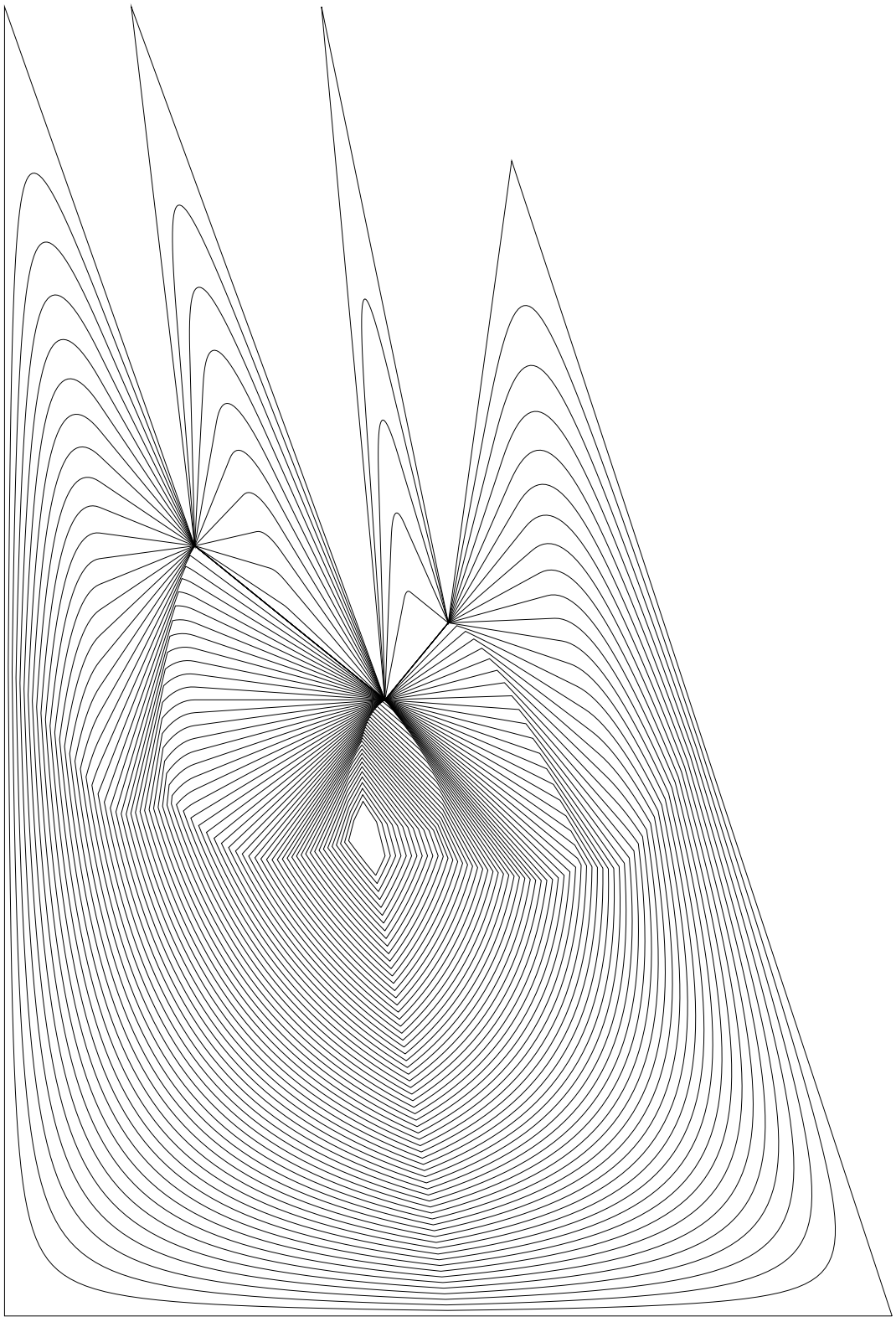

Figure 7.2: Affine erosions (teeth polygon)

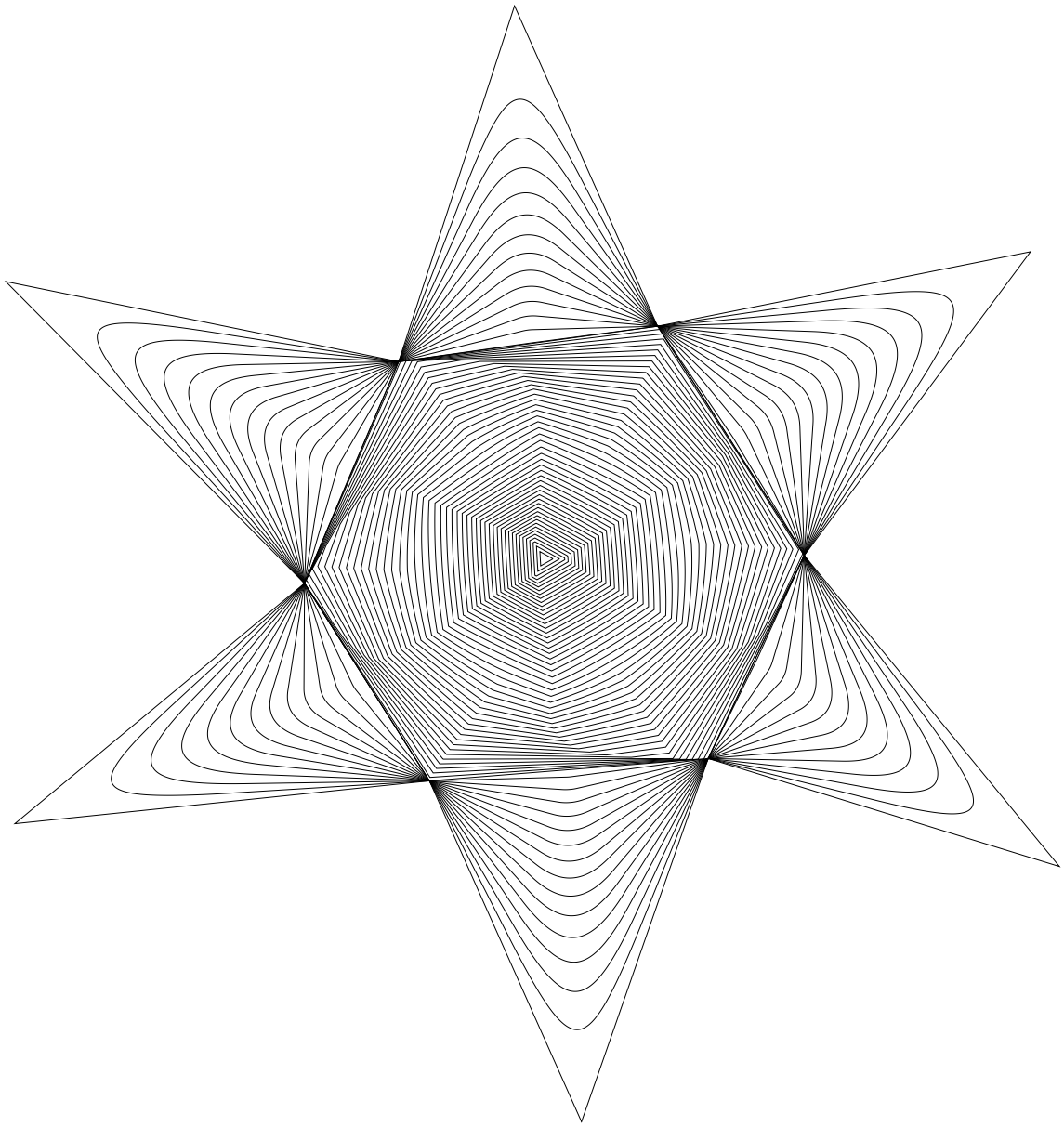

Figure 7.3: Affine erosions (non-symmetric star)

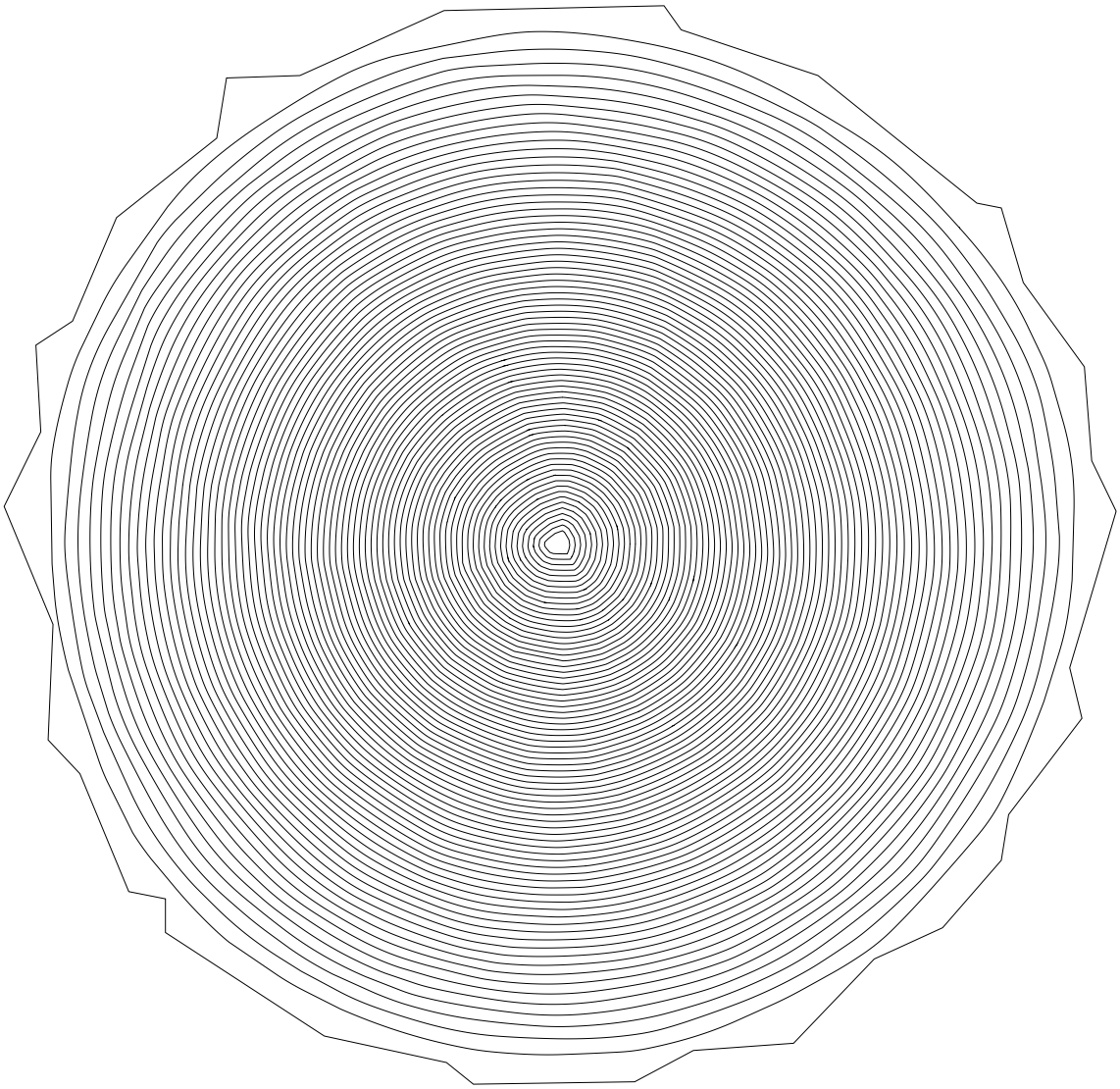

Figure 7.4: Affine erosions (rough circle)

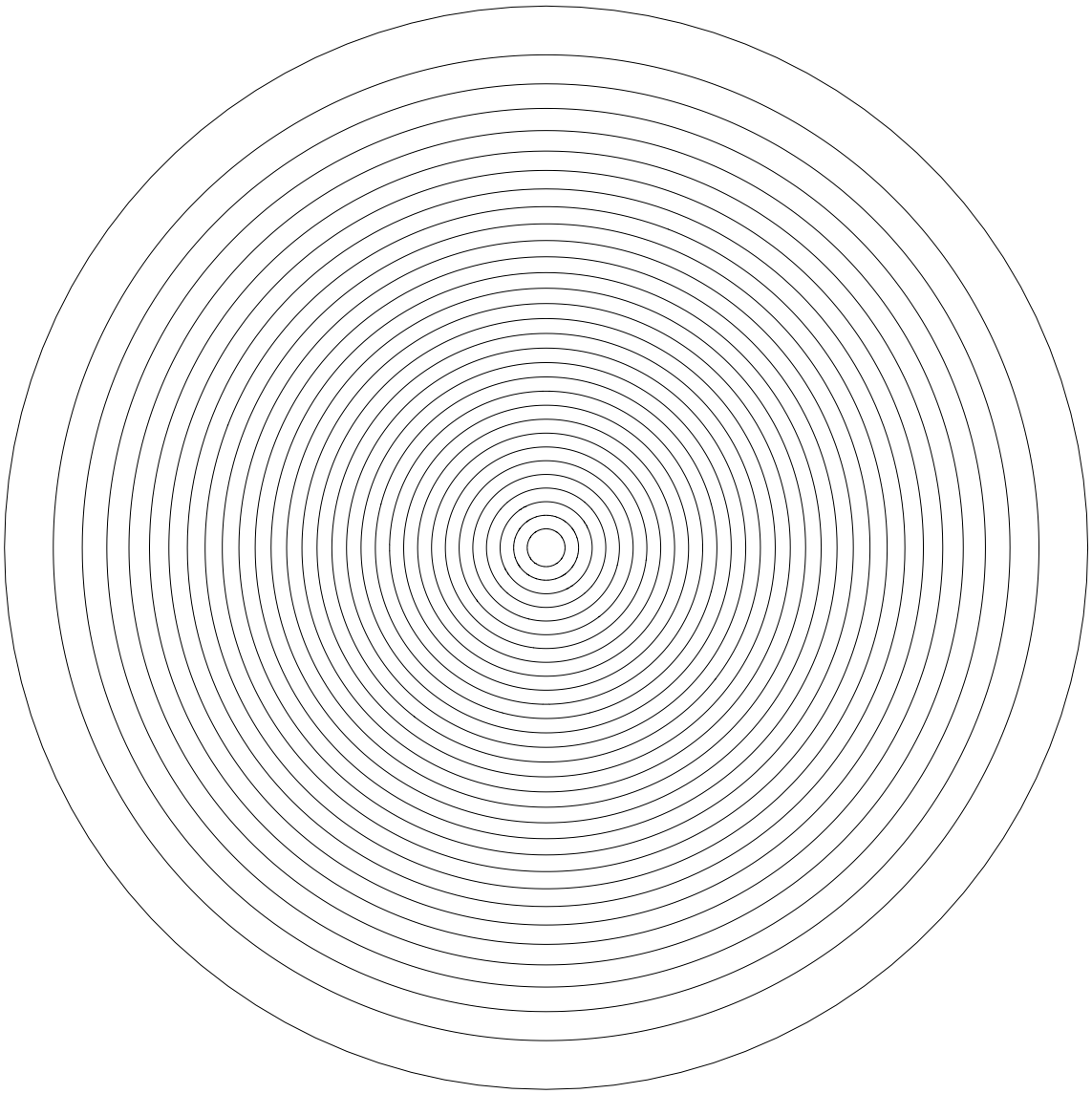

Figure 7.5: Affine erosions (exact circle)

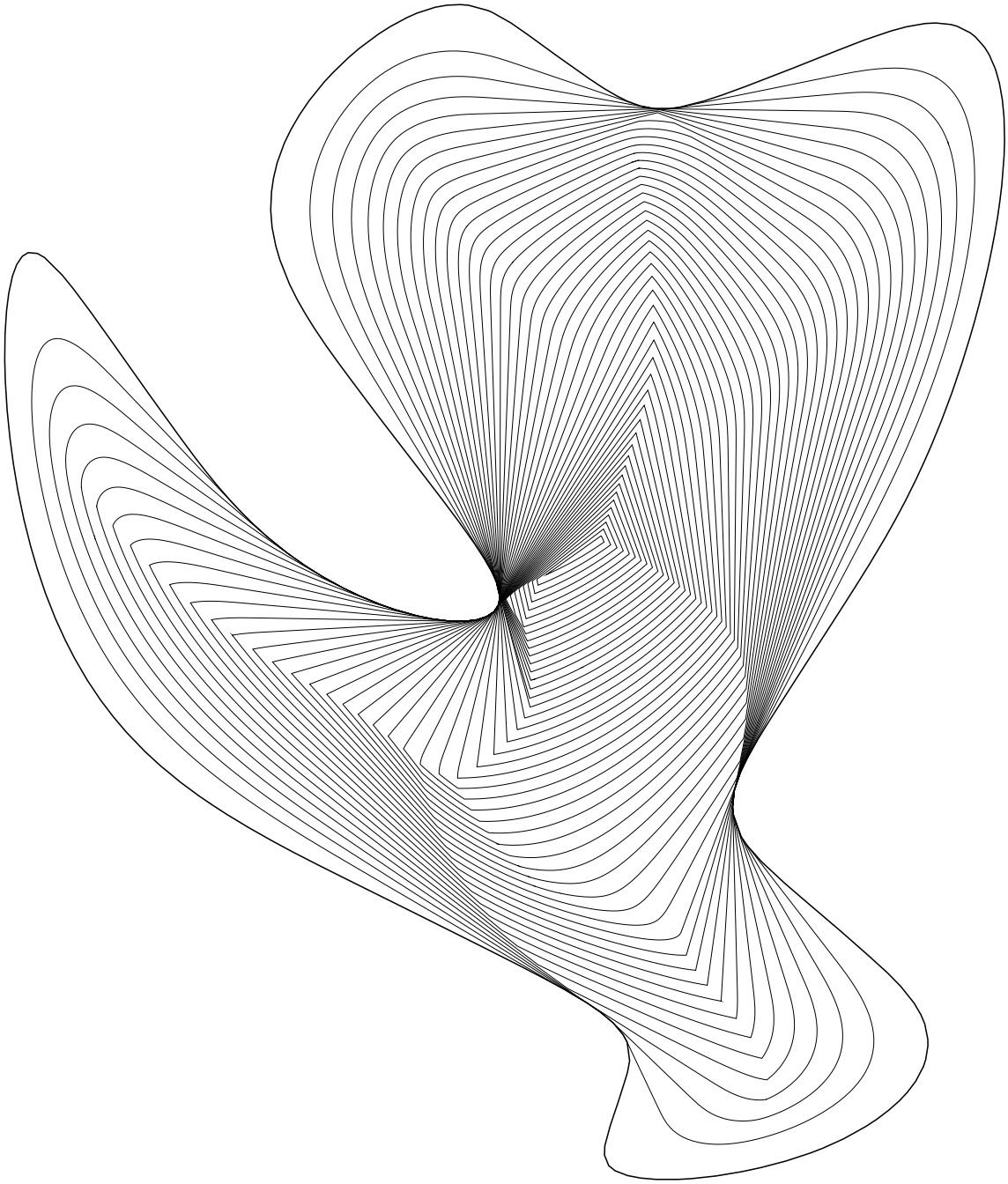

Figure 7.6: Affine erosions (regular curve)

7.1.1 Discretization

The next experiments (Figures 7.7 to 7.9) highlight the affine invariance property of the discretization process we described in the previous chapter. The affine erosion of some of the previous curves is computed for increasing values of the area parameter, and with a rather large sub-sampling area step in order the discretization to be easily seen. Notice how the sampling adapts to the resulting curve.

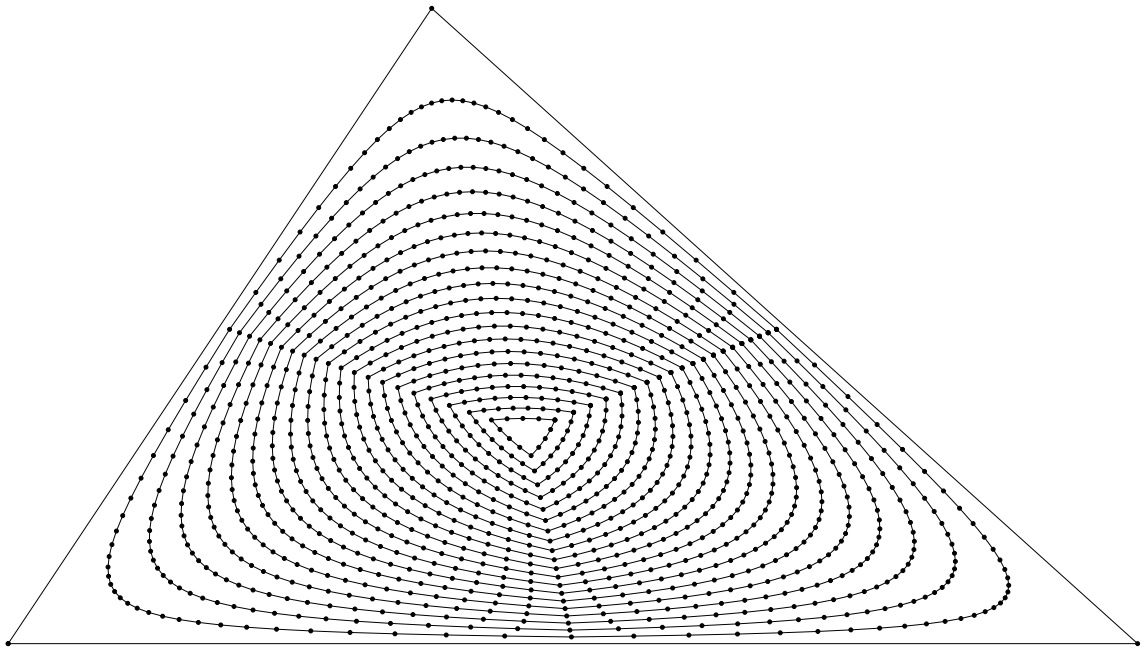

Figure 7.7: Discretized affine erosions (triangle)

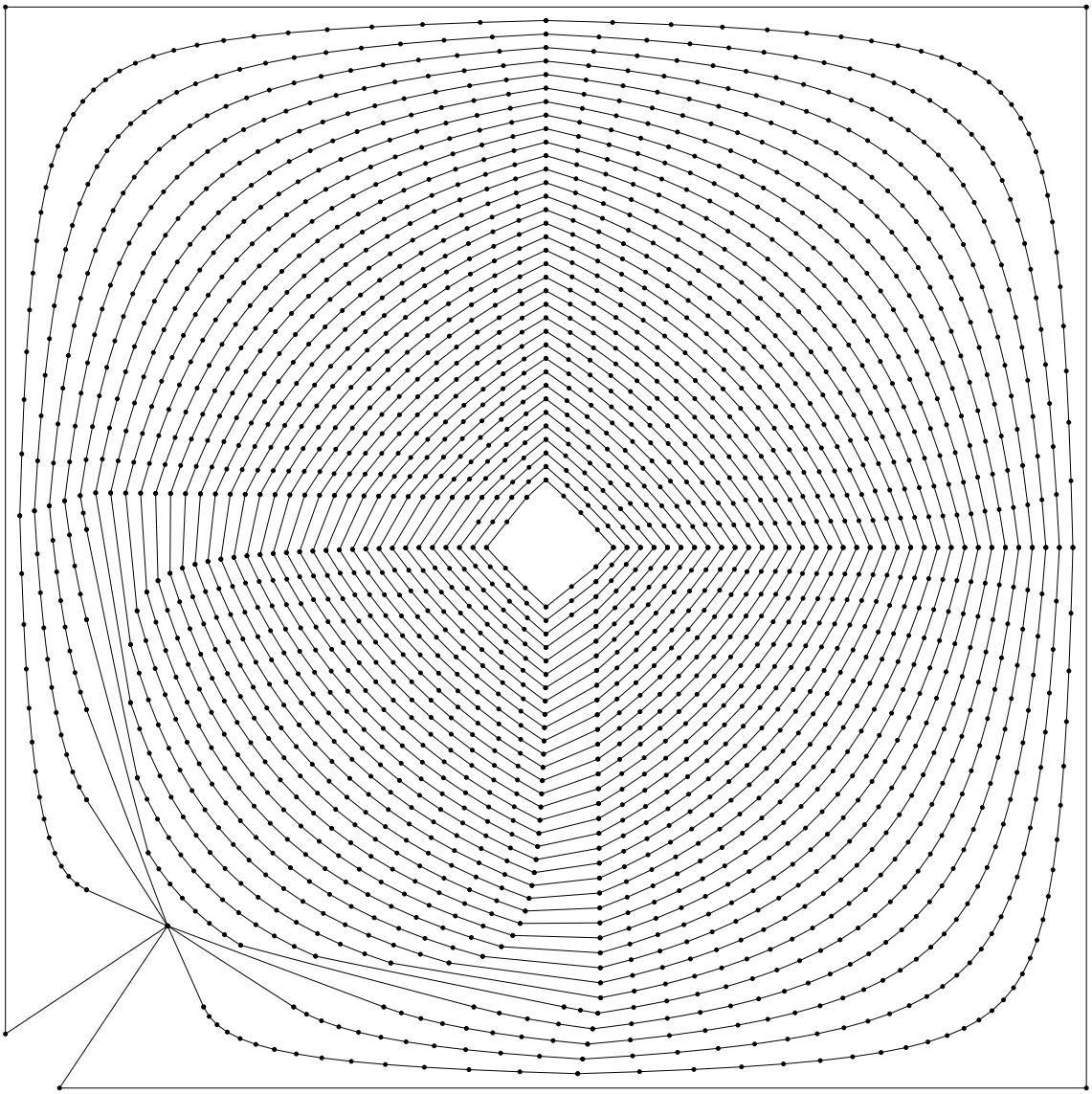

Figure 7.8: Discretized affine erosions (modified square)

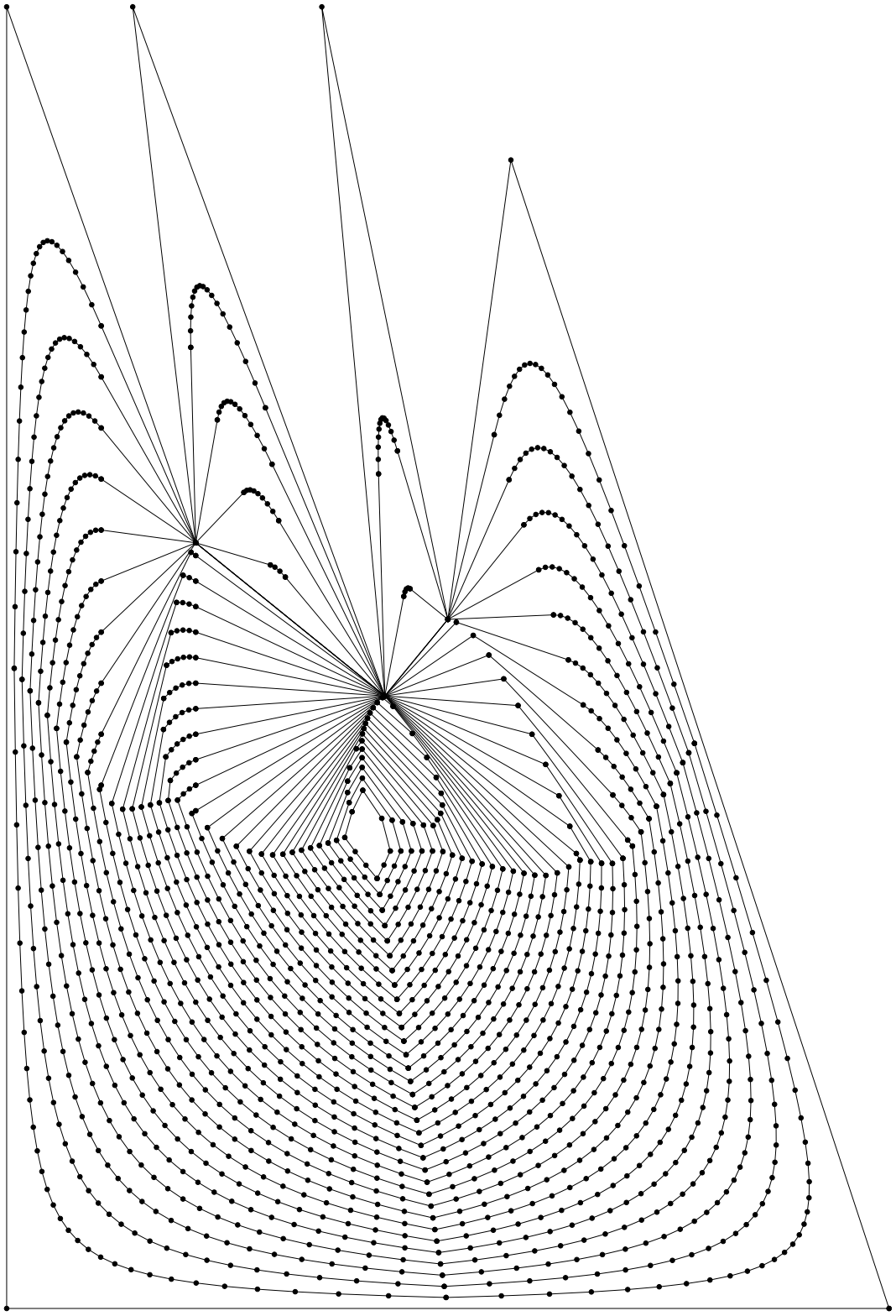

Figure 7.9: Discretized affine erosions (teeth polygon)

7.1.2 Affine Invariance

We now check the affine invariance of the exact algorithm described in the previous chapter. We apply an affine transformation to the initial curve of Figure 7.2 and then compute the affine erosion for the same values of the area parameter (Figure 7.10). The inverse affine transformation being applied (Figure 7.11), we check that we obtain the same result as Figure 7.2.

We use the same method to check that the discretization is affine invariant too (Figure 7.13 to be compared to Figure 7.9).

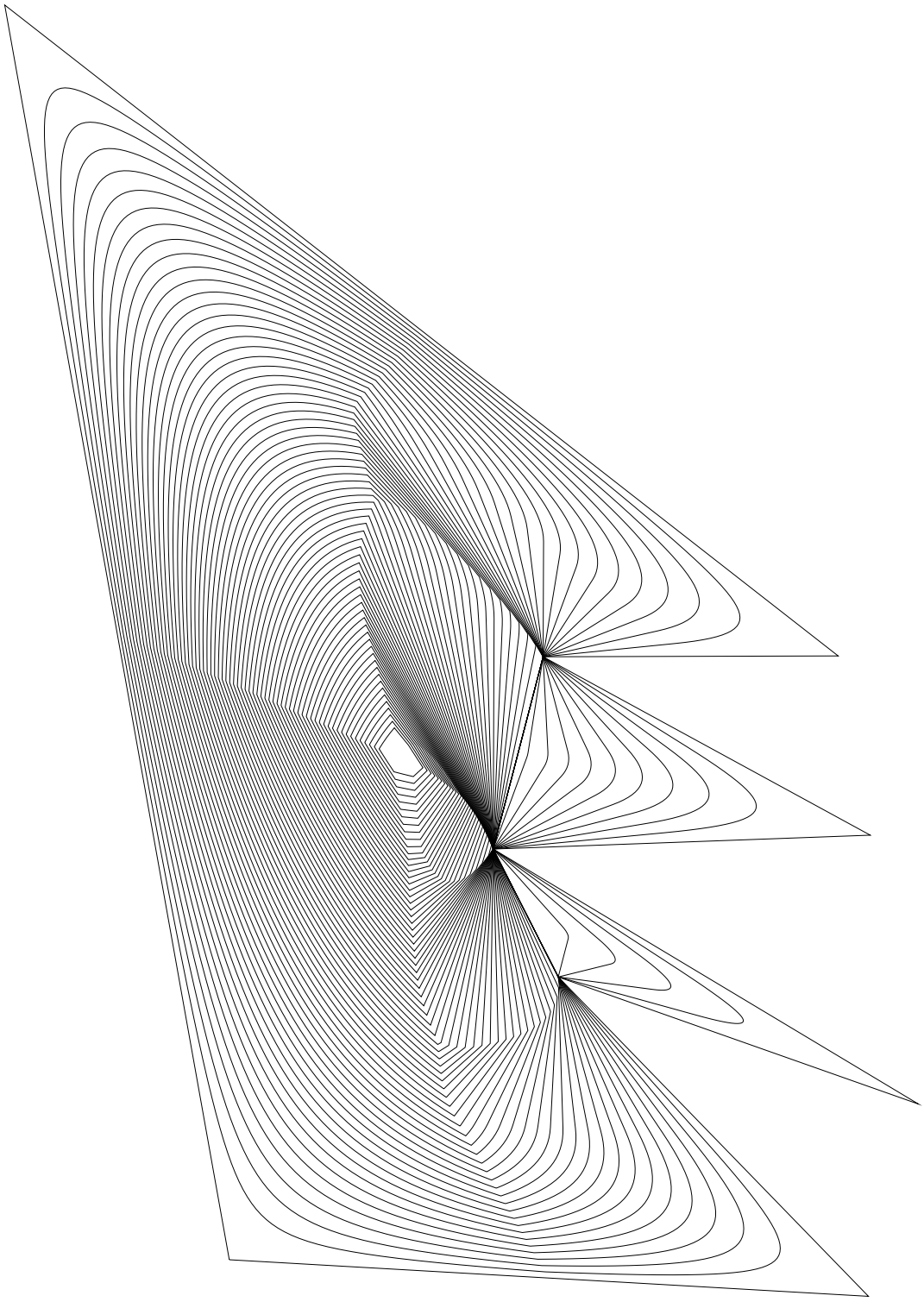

Figure 7.10: Affine erosions (distorted teeth polygon)

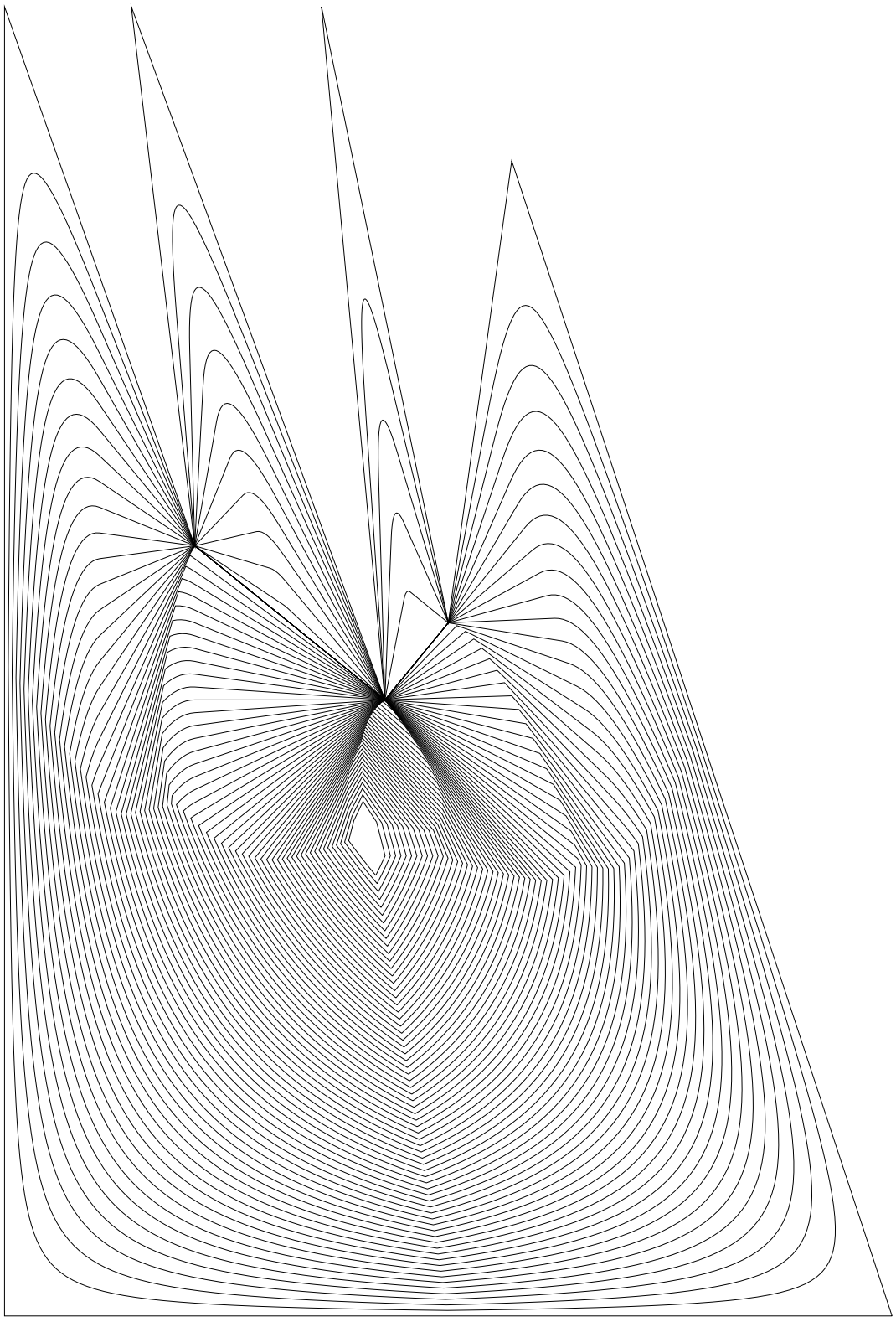

Figure 7.11: Inverse affine transformation of the previous figure
According to the theory, we obtain the same result as on Figure 7.2.

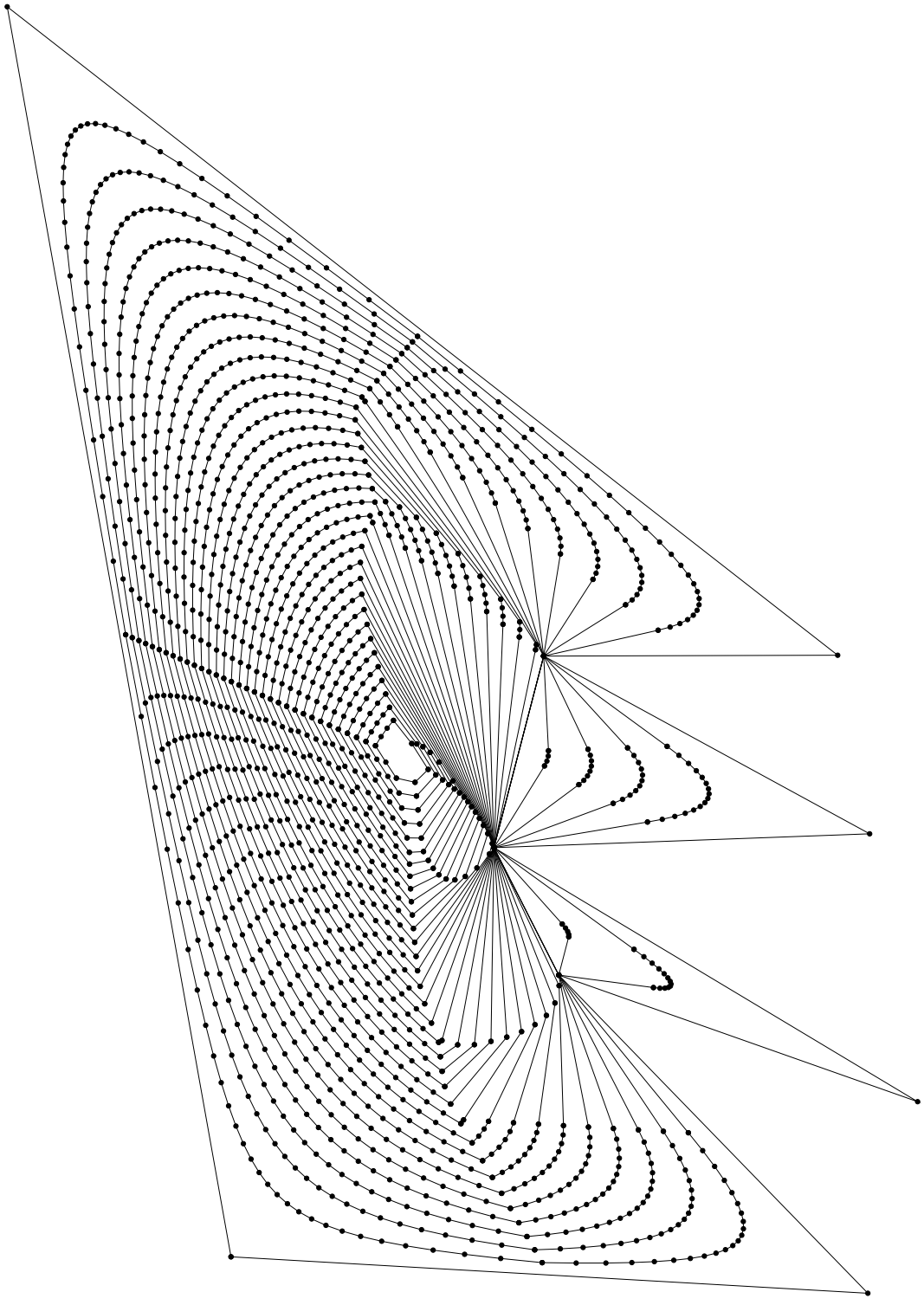

Figure 7.12: Discretized affine erosions (distorted teeth polygon)

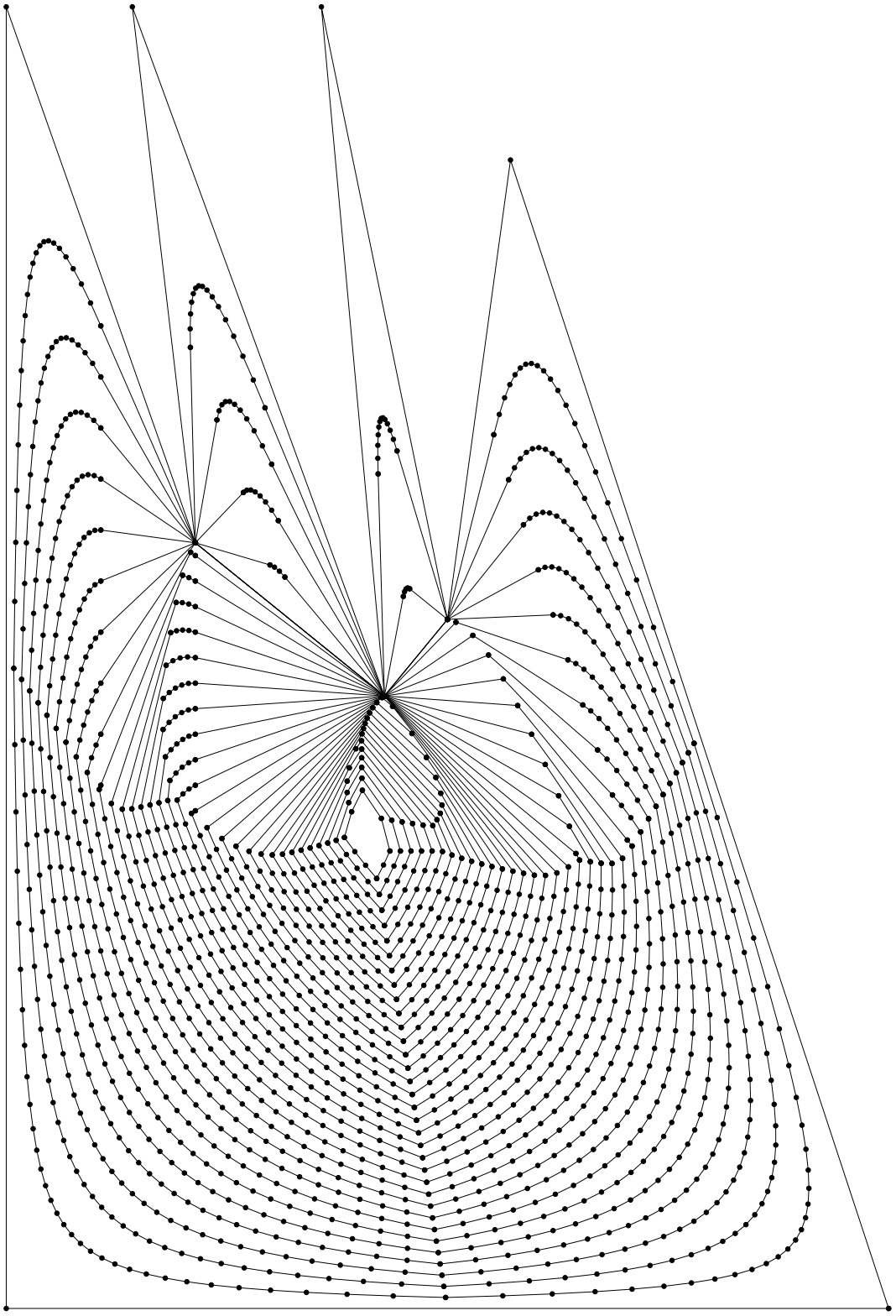

Figure 7.13: Inverse affine transformation of the previous figure

7.2 Affine scale spaces

7.2.1 Exact algorithm

The following experiments simulate the affine scale space on non-convex polygonal curves, as obtained by iterating the exact algorithm . Each curve corresponds to one iteration of the affine erosion plus dilation, computed using the exact algorithm described in the previous section. As predicted by the theory, the curves collapse in a "elliptically shaped" point (see [67]).

Computing the 29 iterations of Figure 7.18 takes 6 minutes (CPU time) on a HP 735/125 station. The number of sampled points reaches 700 for some iterations and the number of computed curves (hyperbolae and segments) attains 1600.

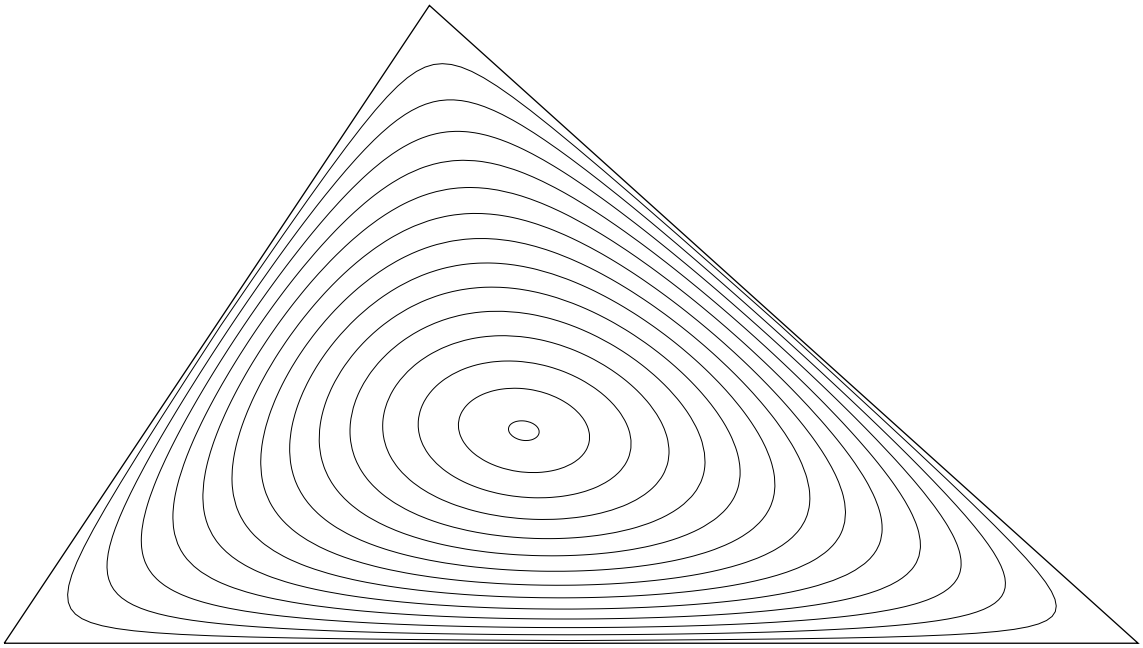

Figure 7.14: Affine scale space (triangle)

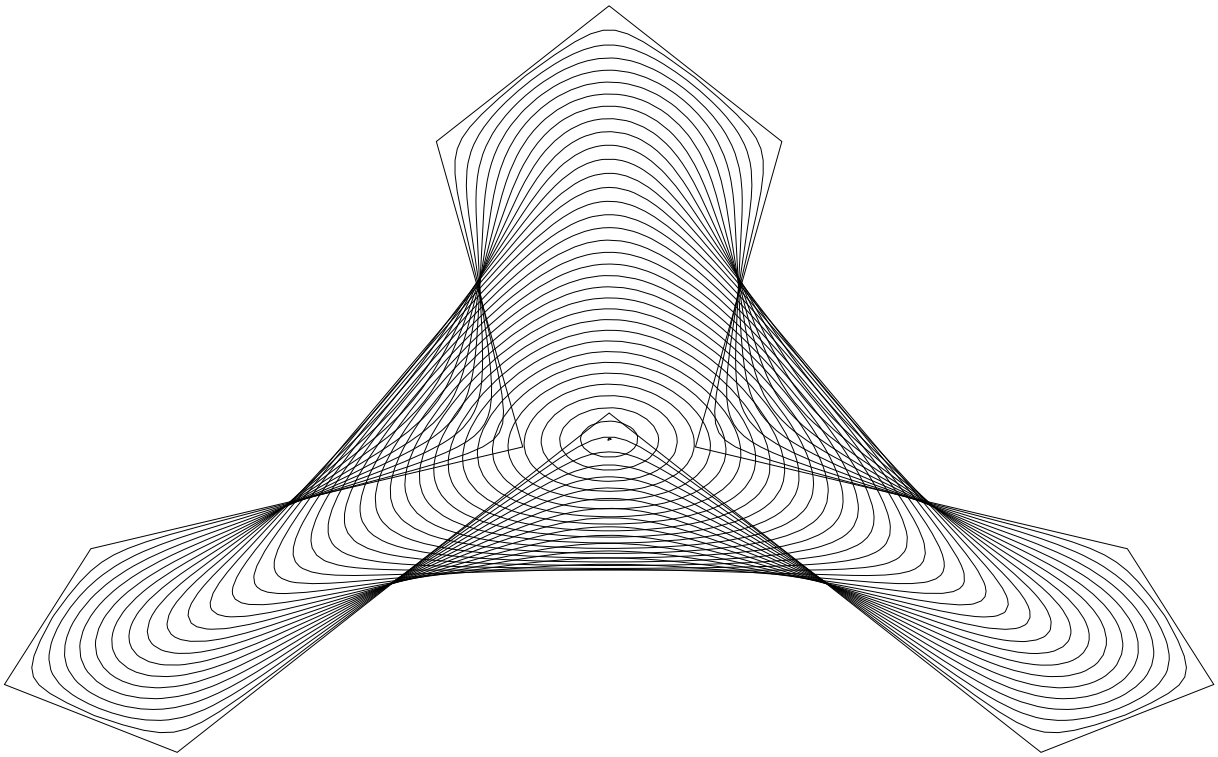

Figure 7.15: Affine scale space (clover polygon)

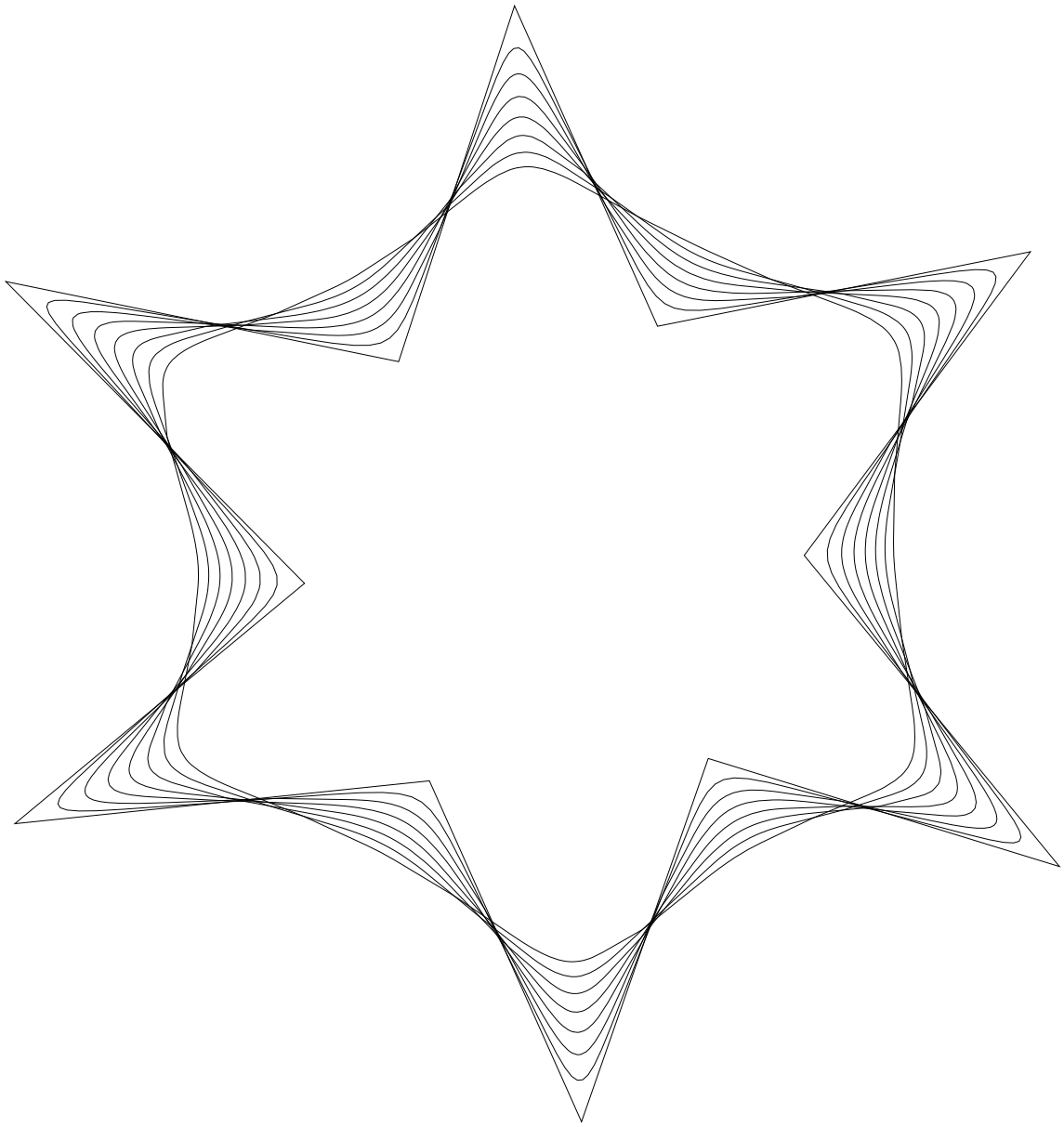

Figure 7.16: Affine scale space (non-symmetric star)

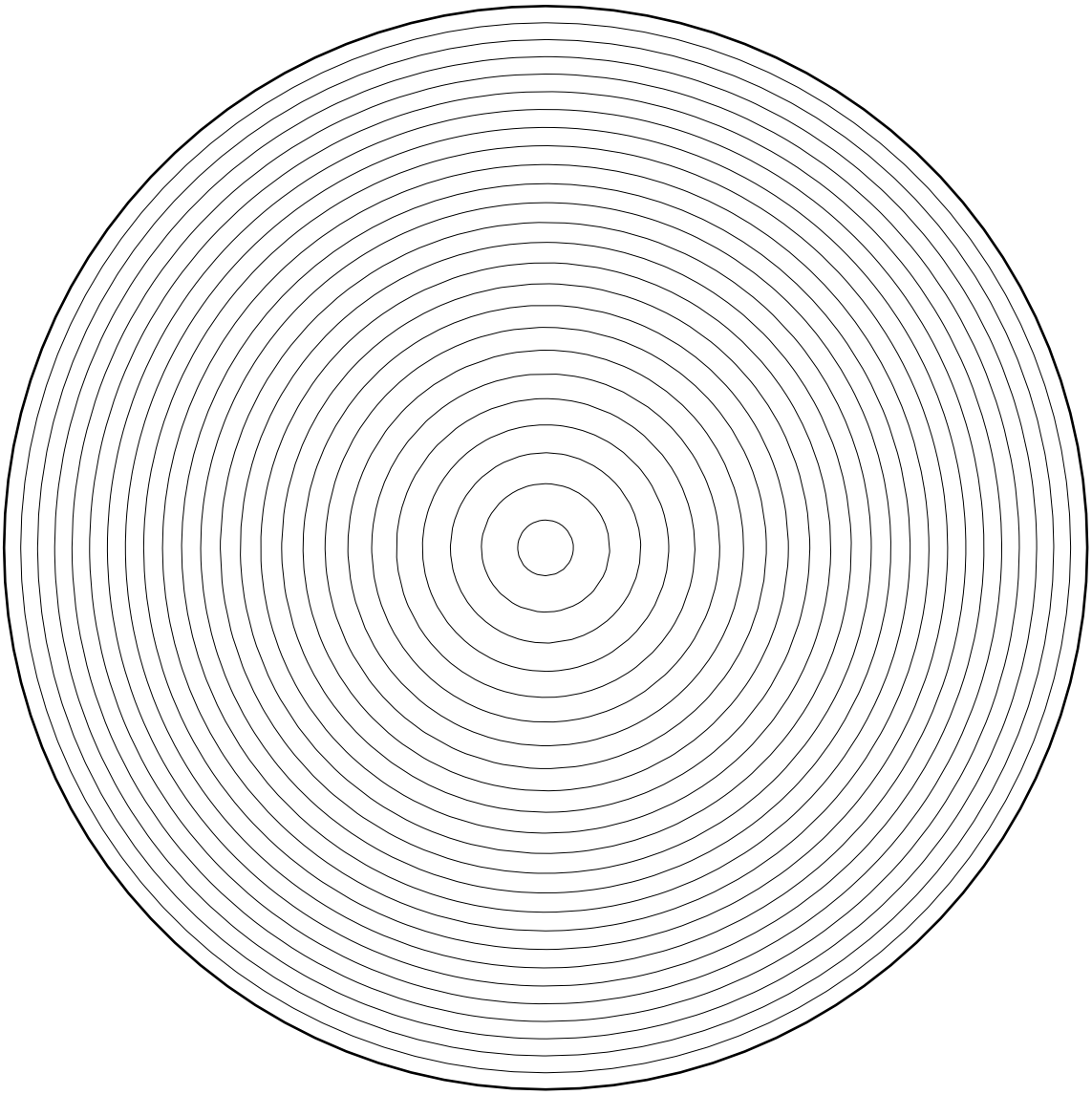

Figure 7.17: Affine scale space (exact circle)

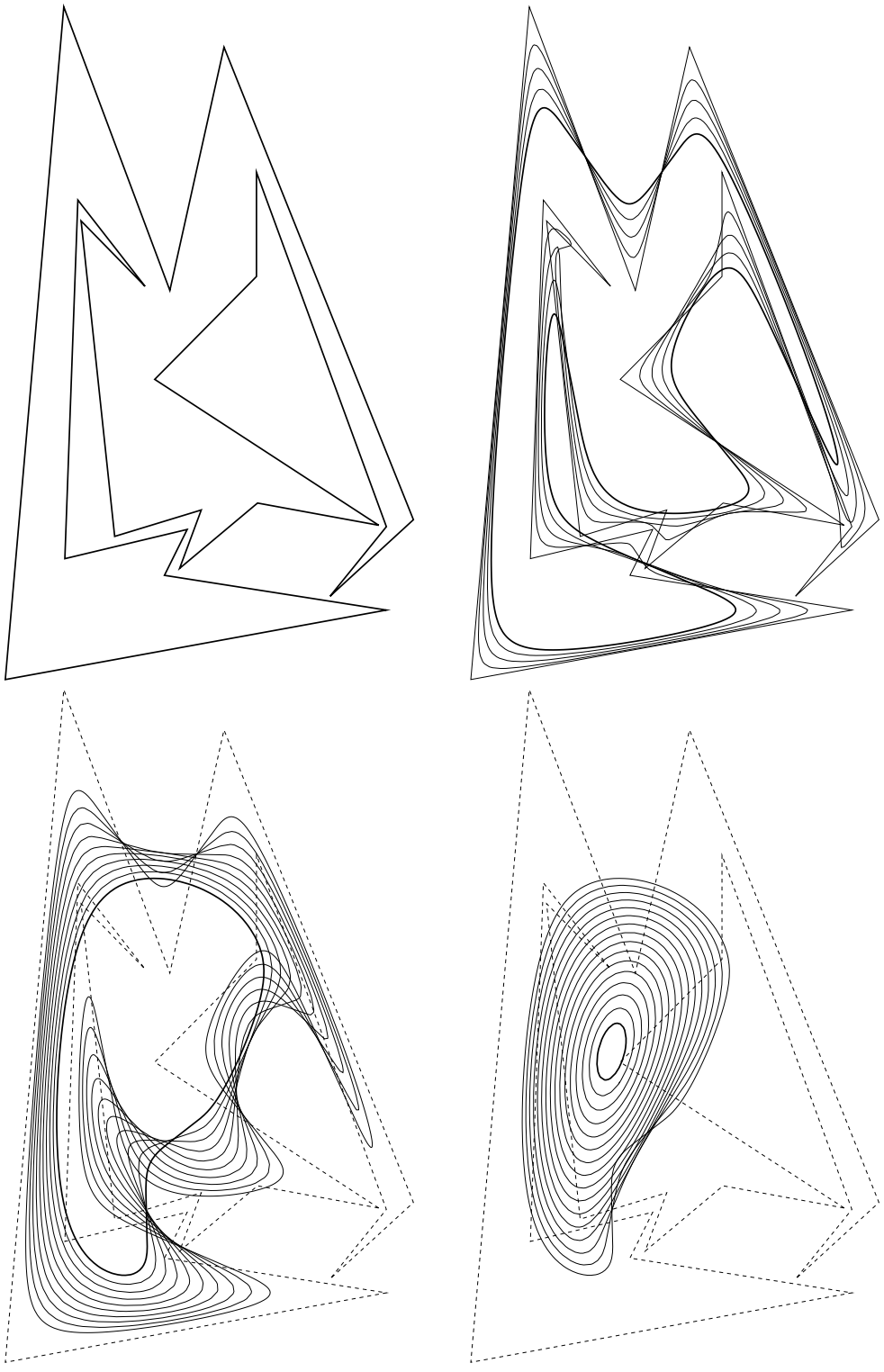

Figure 7.18: Affine scale space (weird polygon) — computation time : 6 minutes

7.2.2 Simplified algorithm

First, we check that the simplified algorithm give similar results to the exact one for the previous "weird" polygon : Figure 7.19 is quite similar to Figure 7.18, while the computation time is reduced to 7 seconds (instead of 6 minutes for the exact algorithm).

Then, we compute the affine scale space of large curves (about 4000 vertices and 1800 convex components for the initial curve represented on Figure 7.27). Notice the fine precision of Figure 7.28, which is impossible to attain with Sethian's algorithm for a reasonable amount of time and memory. For the "whale" polygon (Figures 7.23 to 7.26), the almost auto-intersections of the initial curve would probably cause any finite difference algorithm to fail, because the topological structure of the initial curve is very instable under a pixel discretization.

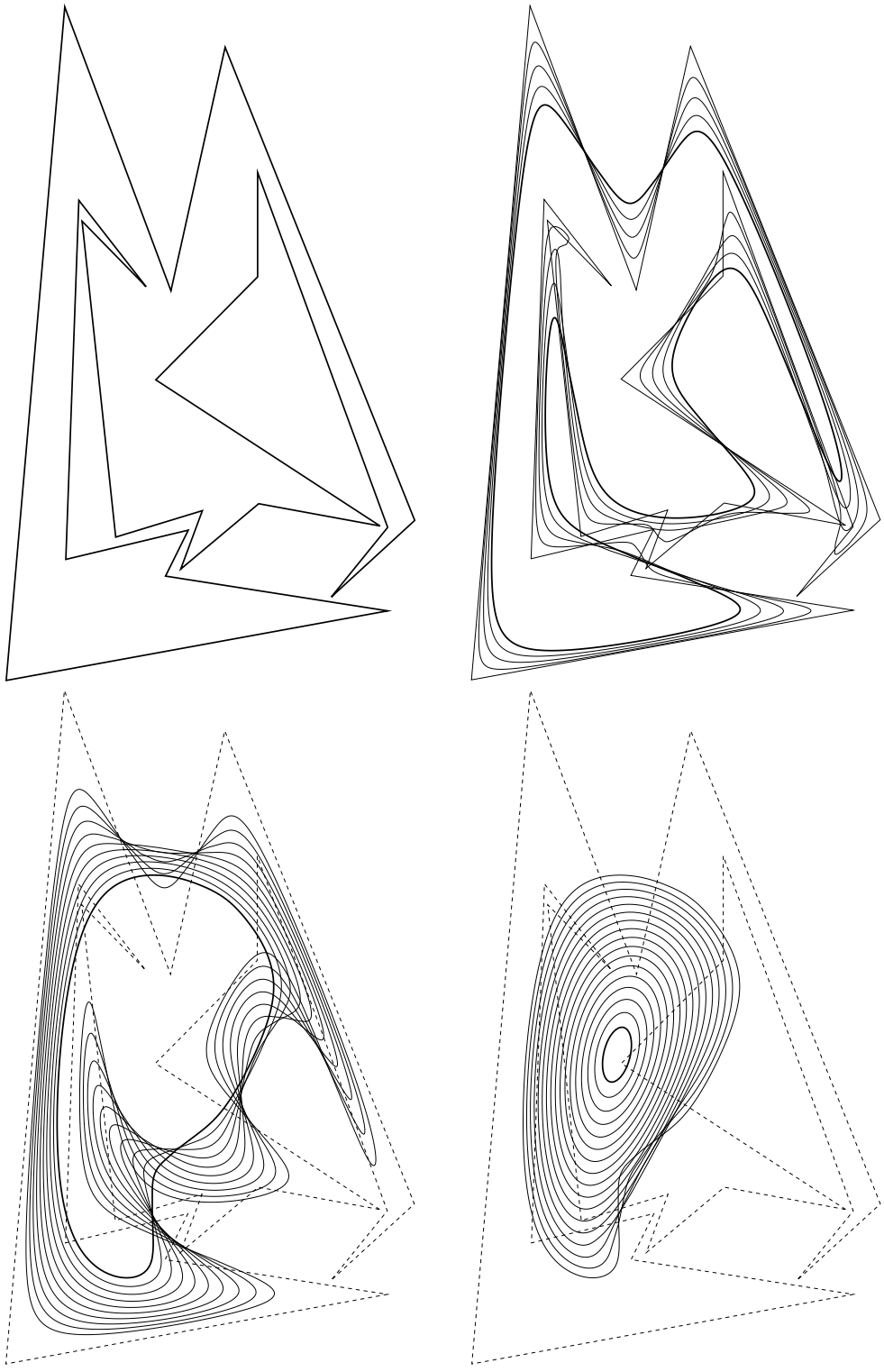

Figure 7.19: Affine scale space using the simplified algorithm (weird polygon) — computation time : 7 seconds

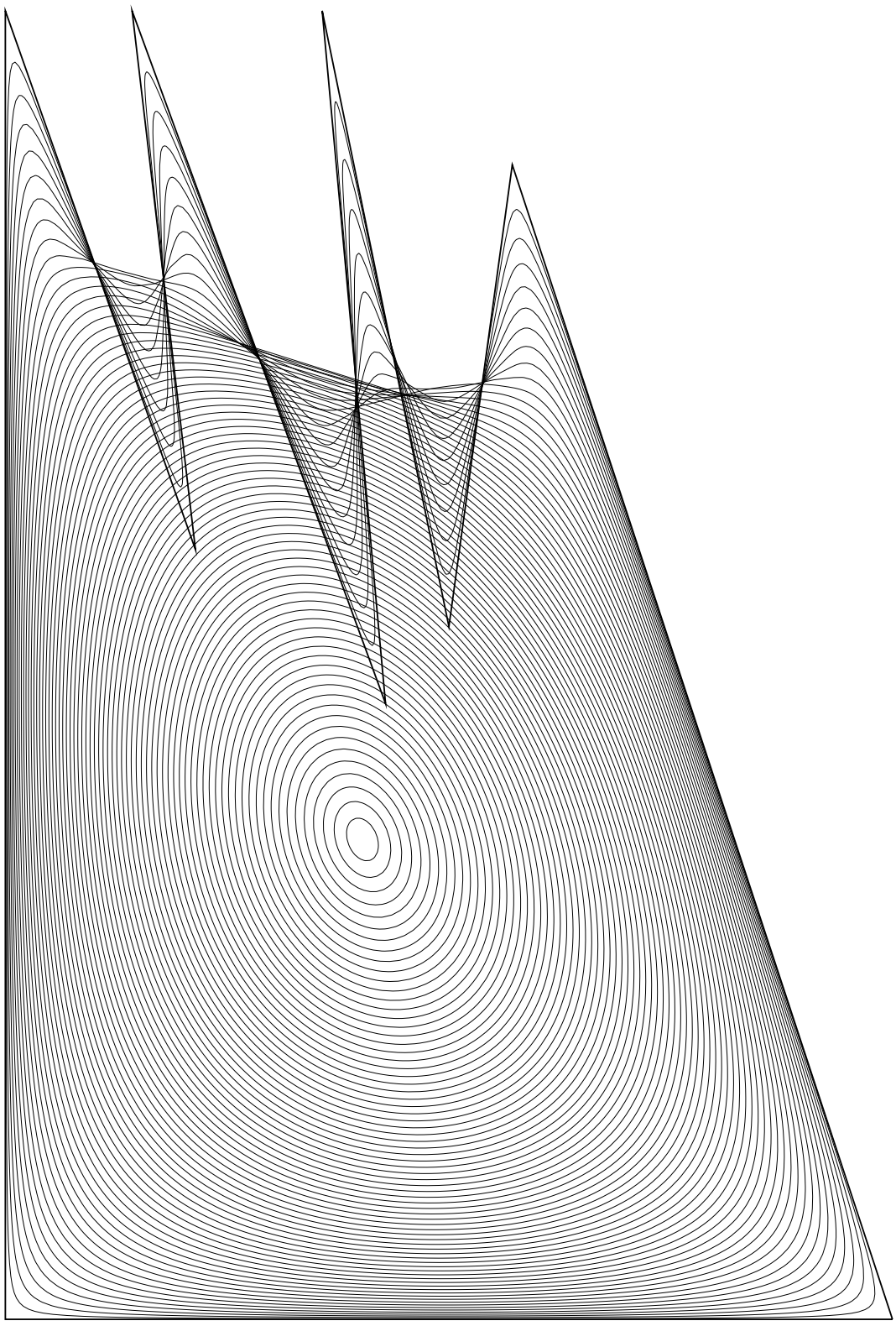

Figure 7.20: Affine scale space using the simplified algorithm (teeth polygon)

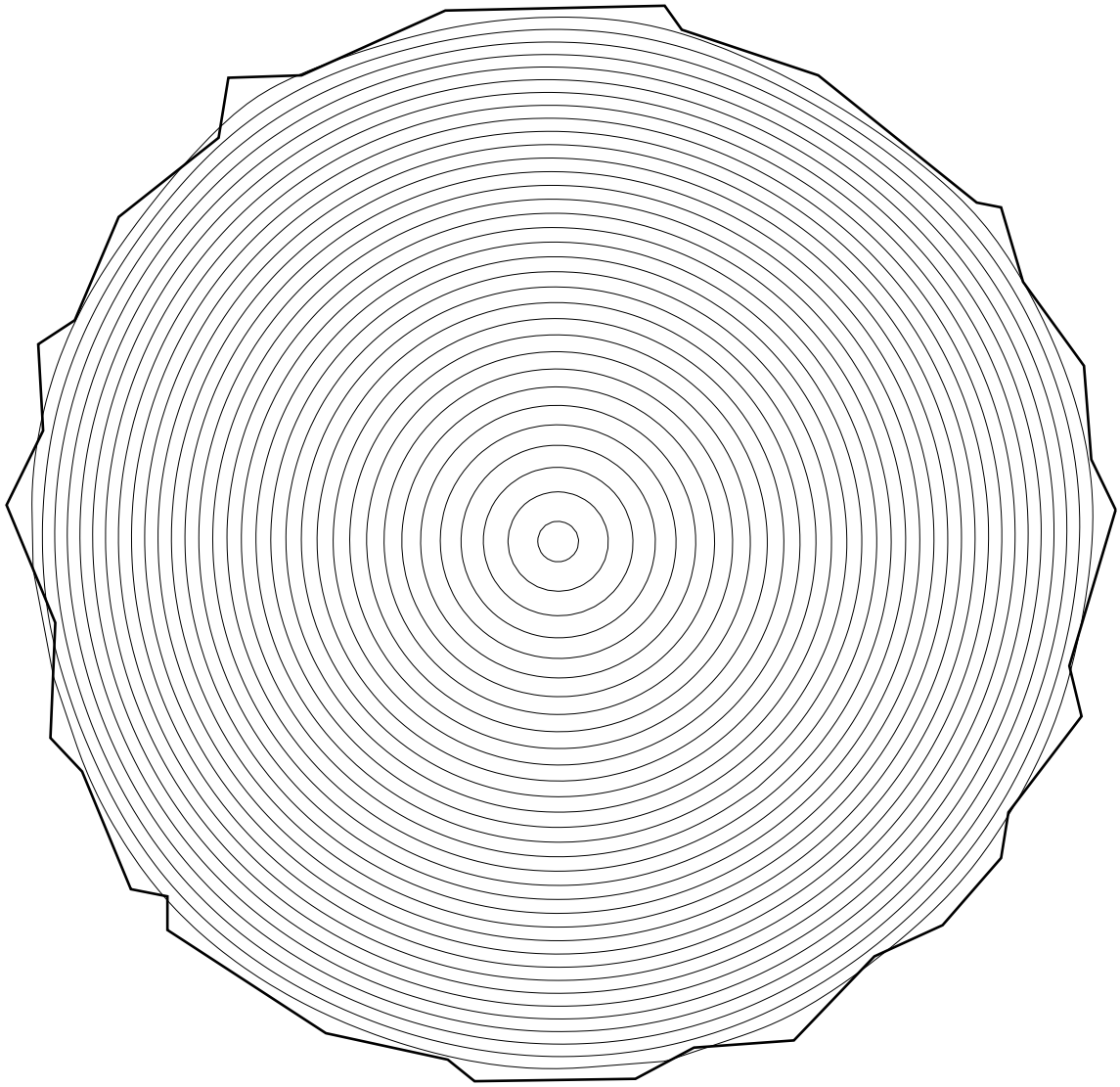

Figure 7.21: Affine scale space (rough circle)

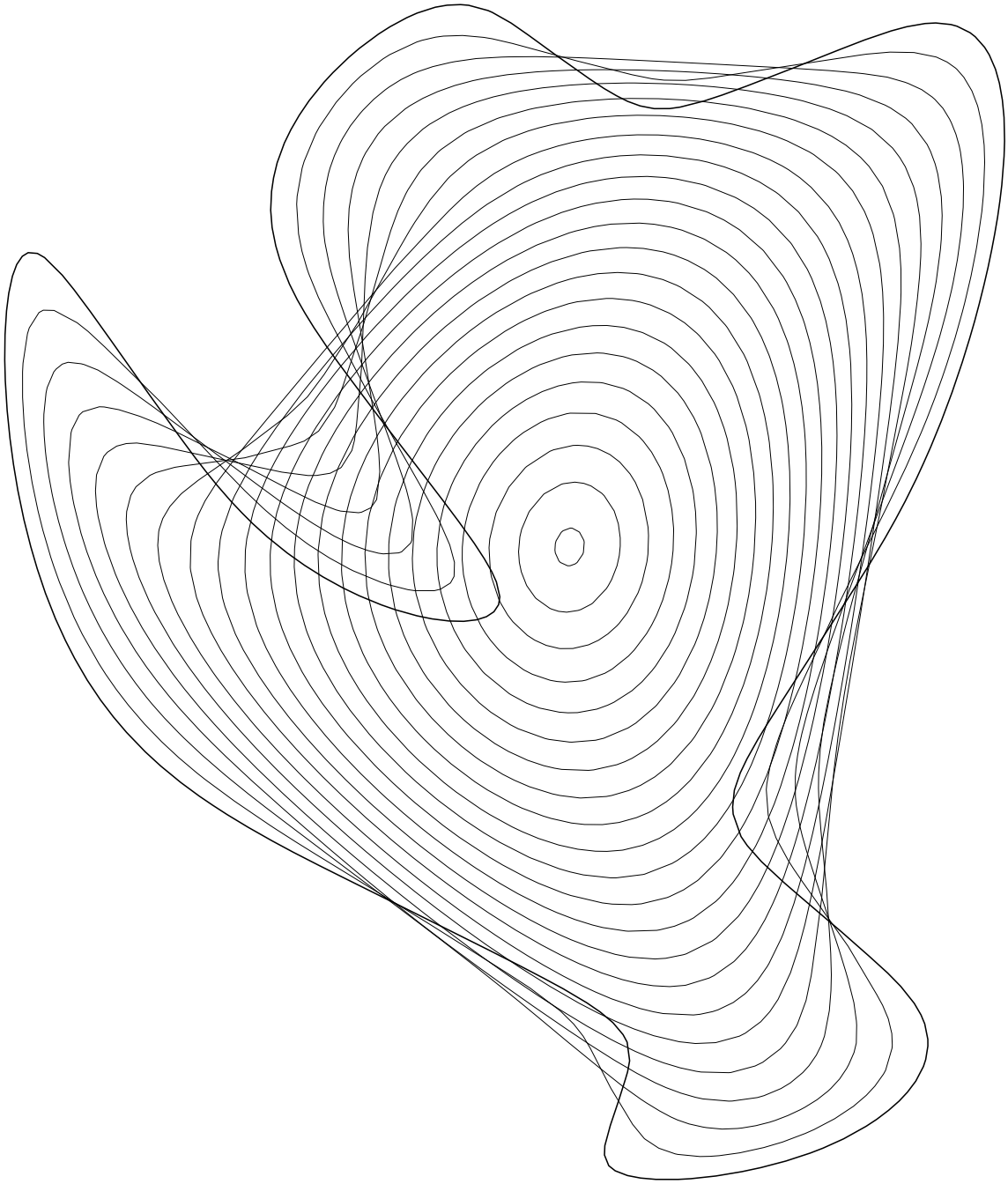

Figure 7.22: Affine scale space using the simplified algorithm (regular curve). The computation time is only 0.9 second, and the algorithm is stable despite the coarse quantization of curves we used here.

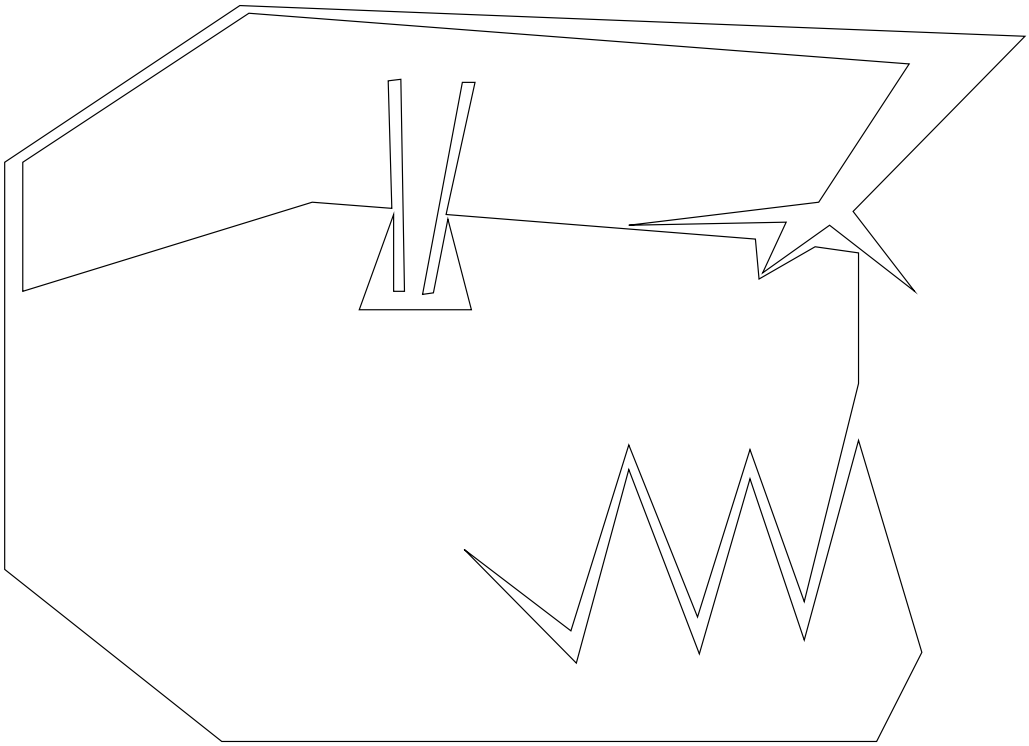

Figure 7.23: whale : initial curve (t=0)

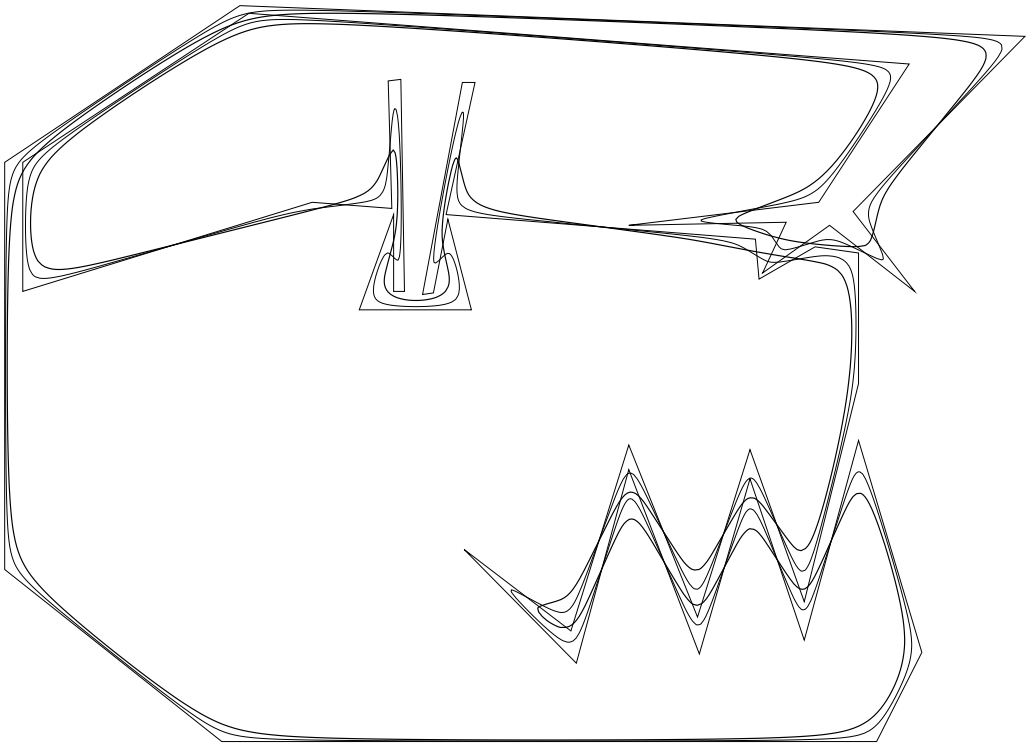

Figure 7.24: whale : filtered curve (t=100, 200)

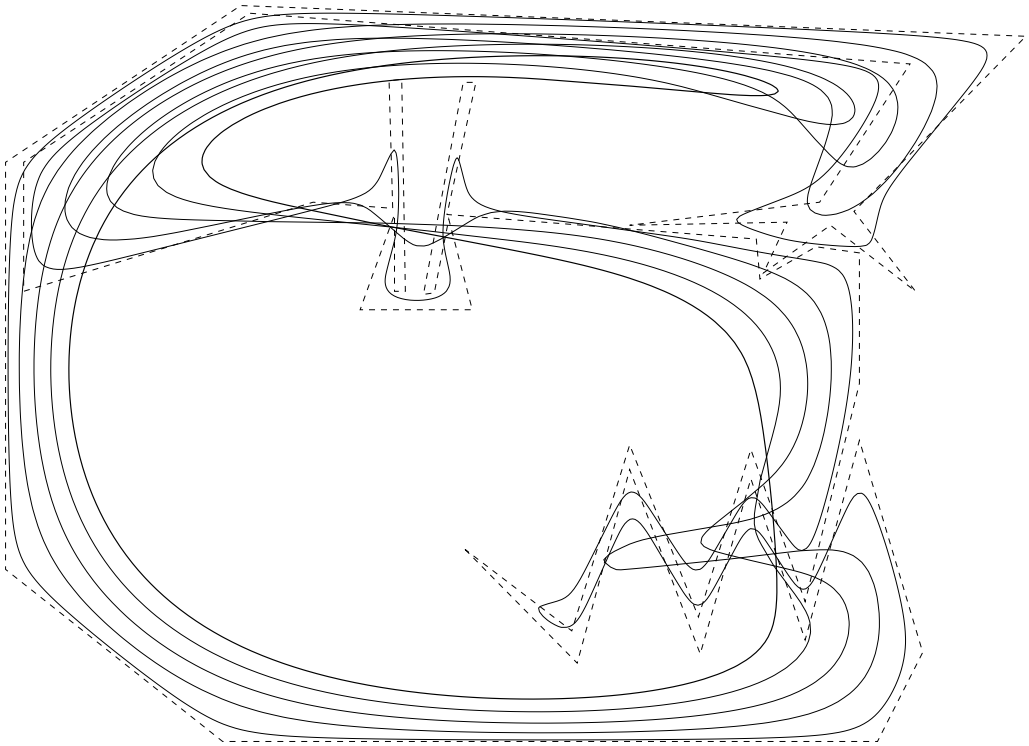

Figure 7.25: whale : filtered curve (t=1200, 2200, 3200, 4200)

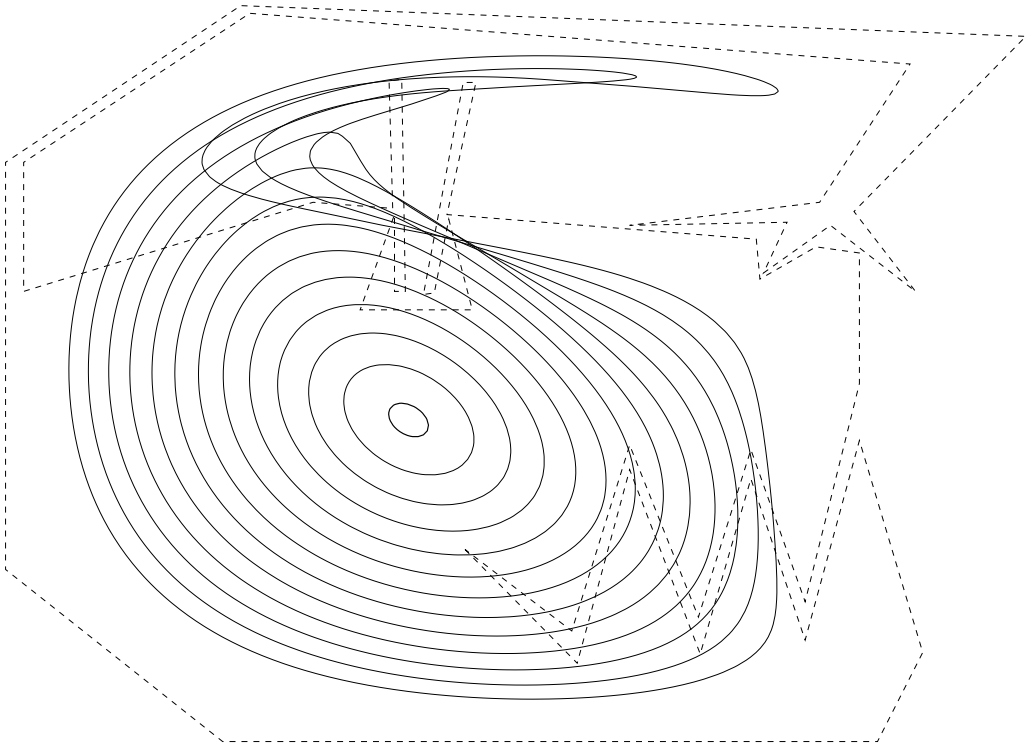

Figure 7.26: whale : filtered curve (t=5200, 6200, ..., 16200)

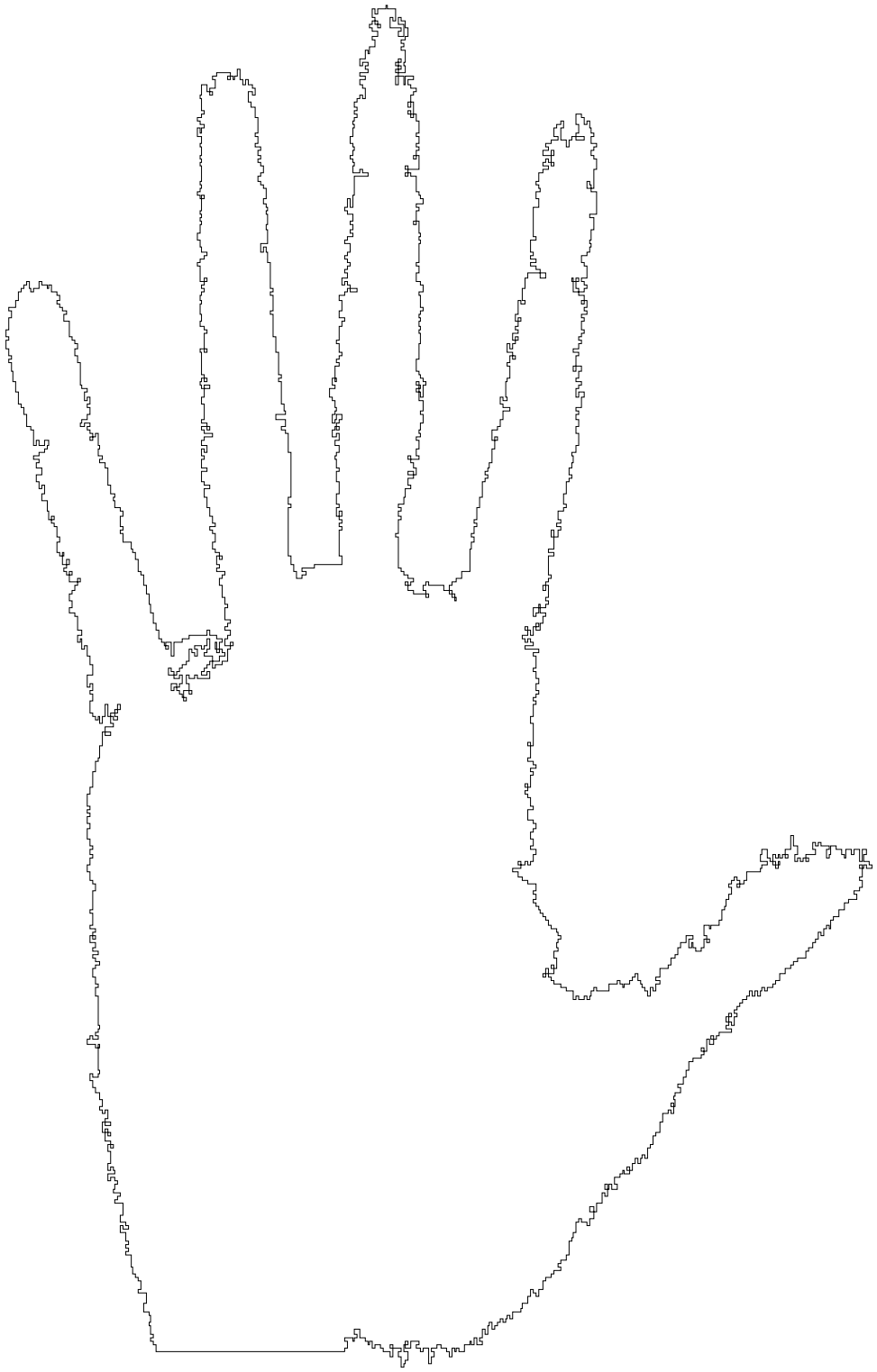

Figure 7.27: hand : initial curve (t=0)

Figure 7.28: hand : filtered curve (t=1)

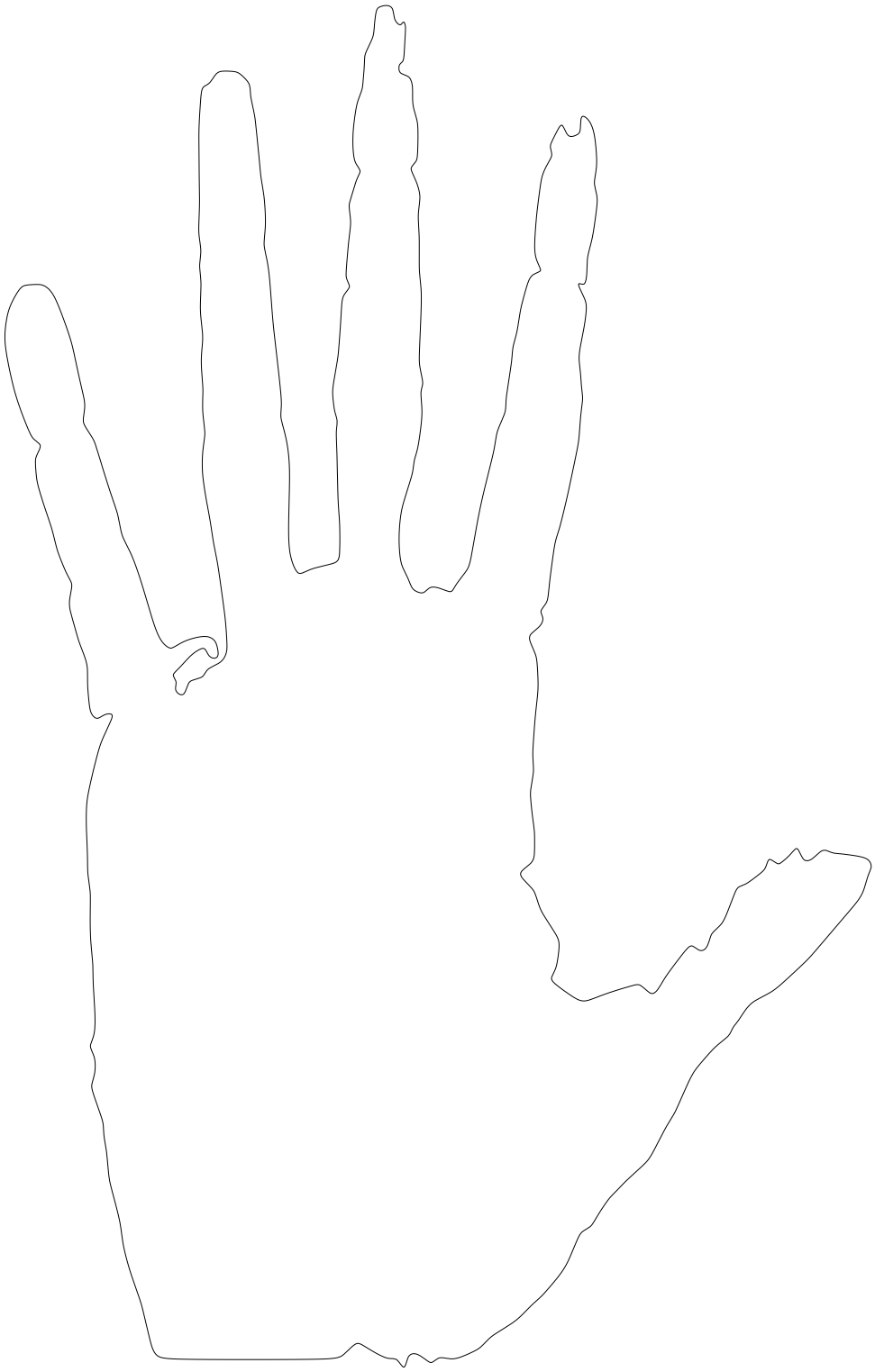

Figure 7.29: hand : filtered curve (t=8)

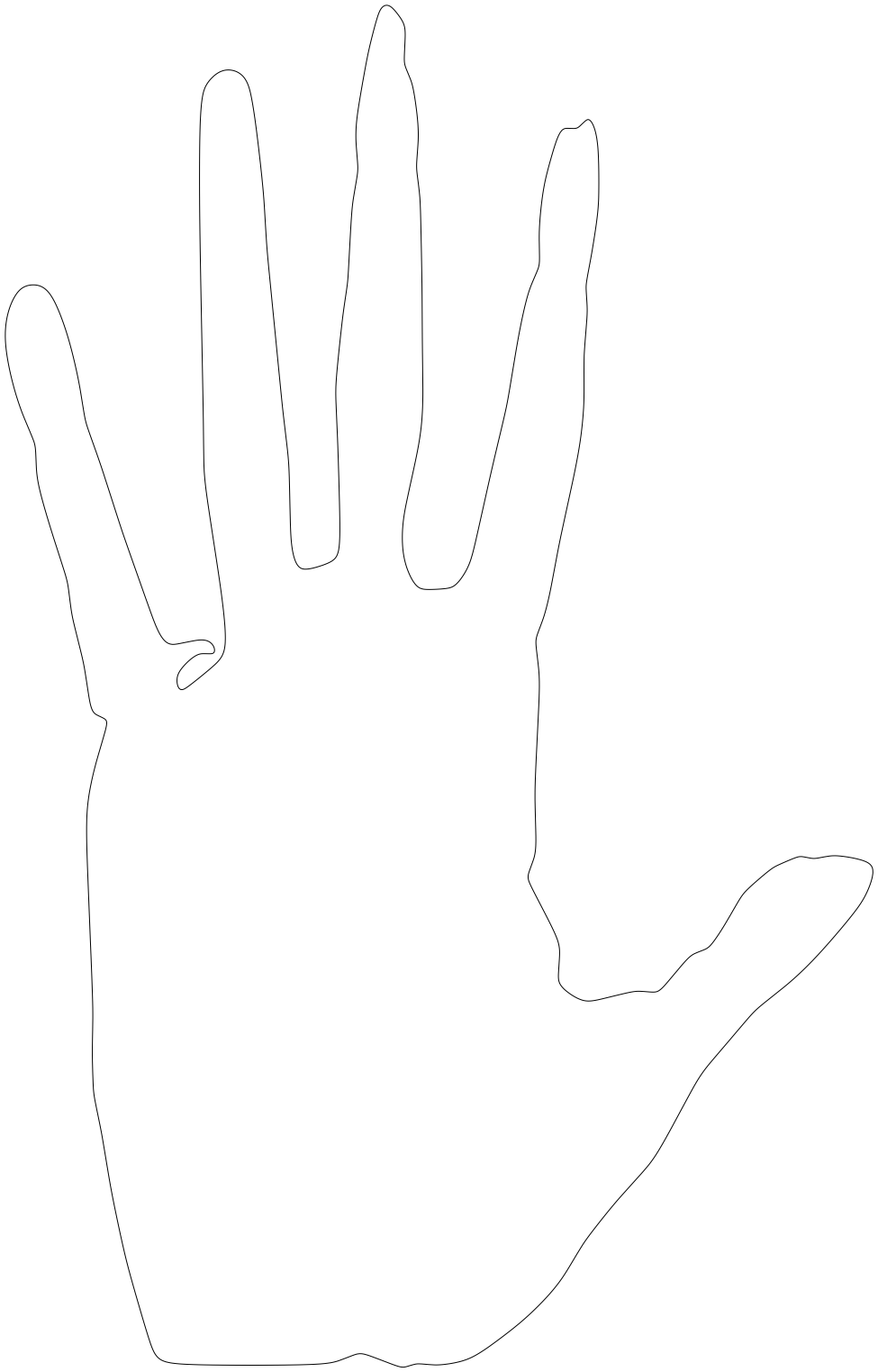

Figure 7.30: hand : filtered curve (t=20)

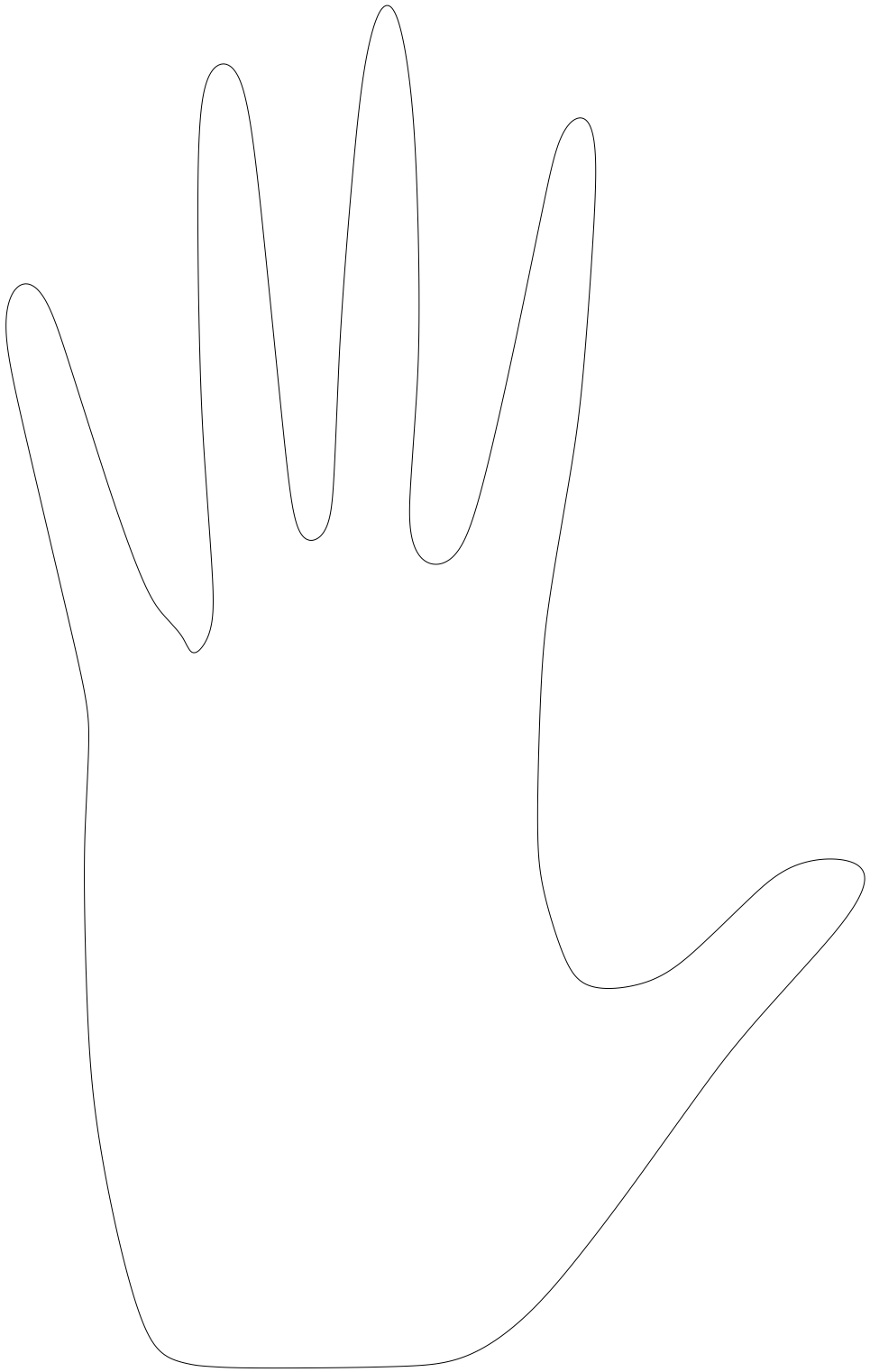

Figure 7.31: hand : filtered curve (t=200)

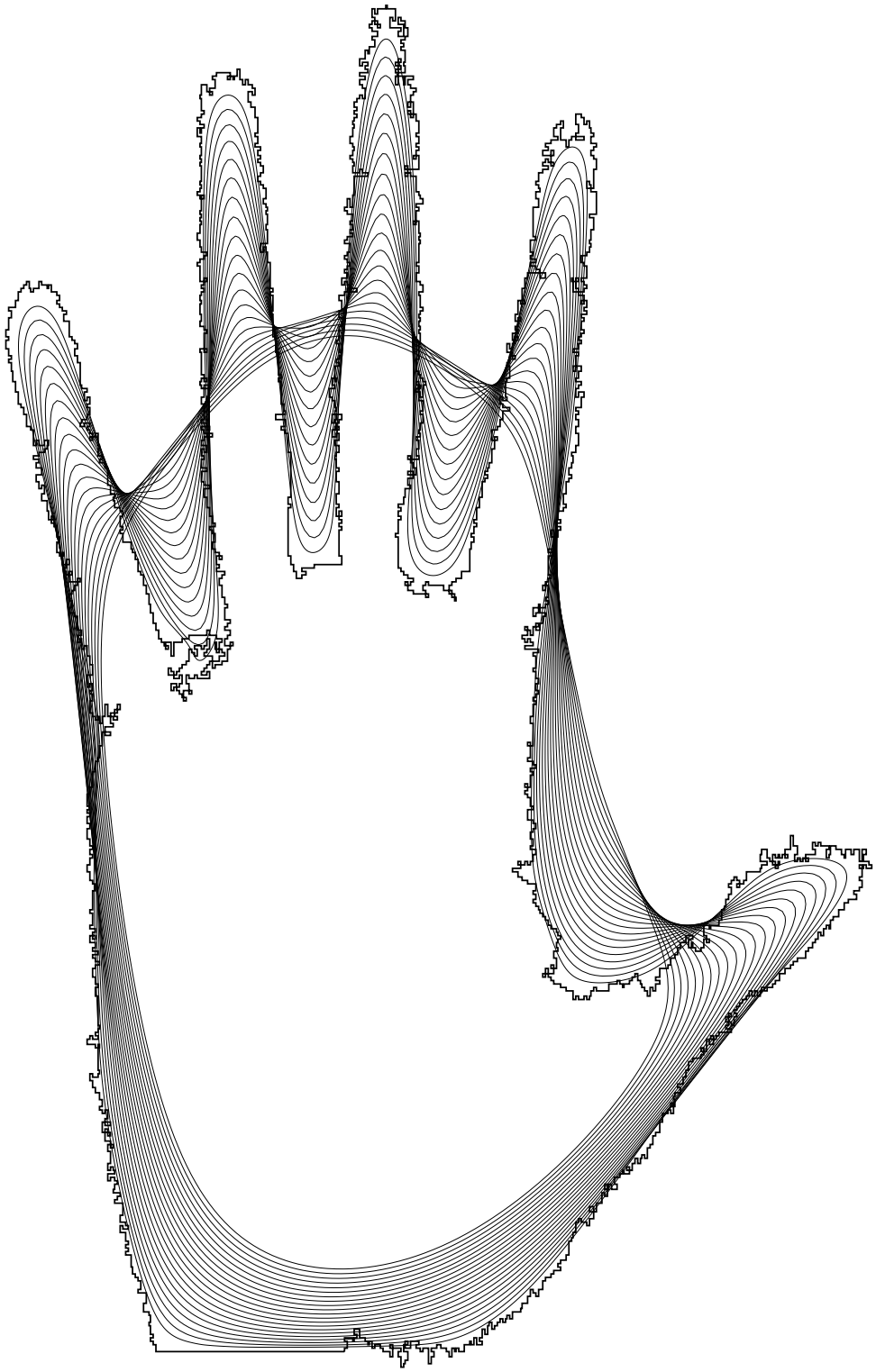

Figure 7.32: hand : filtered curve (t=300, 400, ..., 1300)

Figure 7.33: dog : initial curve (t=0)

Figure 7.34: dog : filtered curve (t=1)

Figure 7.35: dog : filtered curve (t=10)

Figure 7.36: dog : filtered curve (t=100)

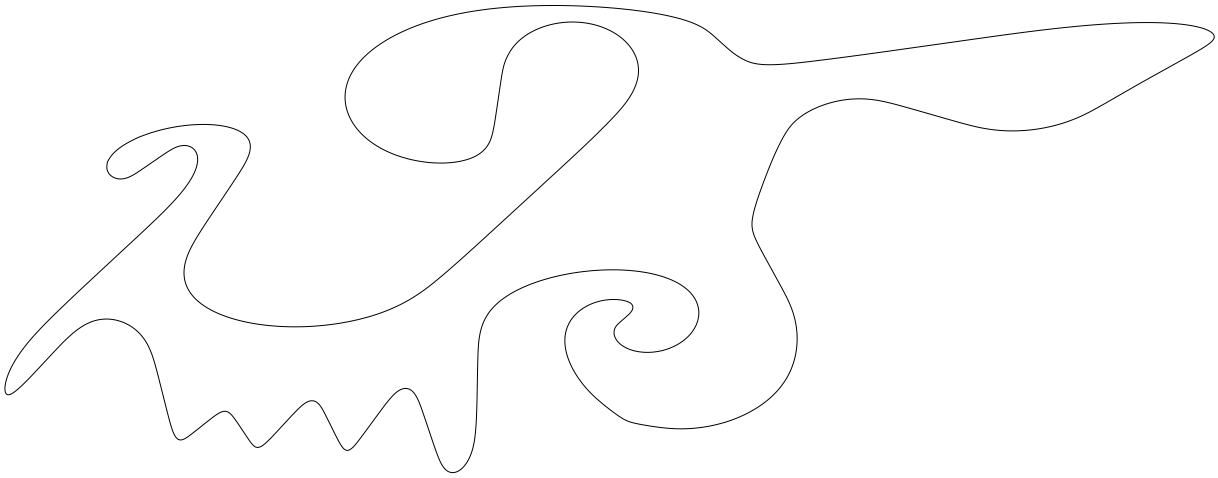

Figure 7.37: dog : filtered curve (t=1000)

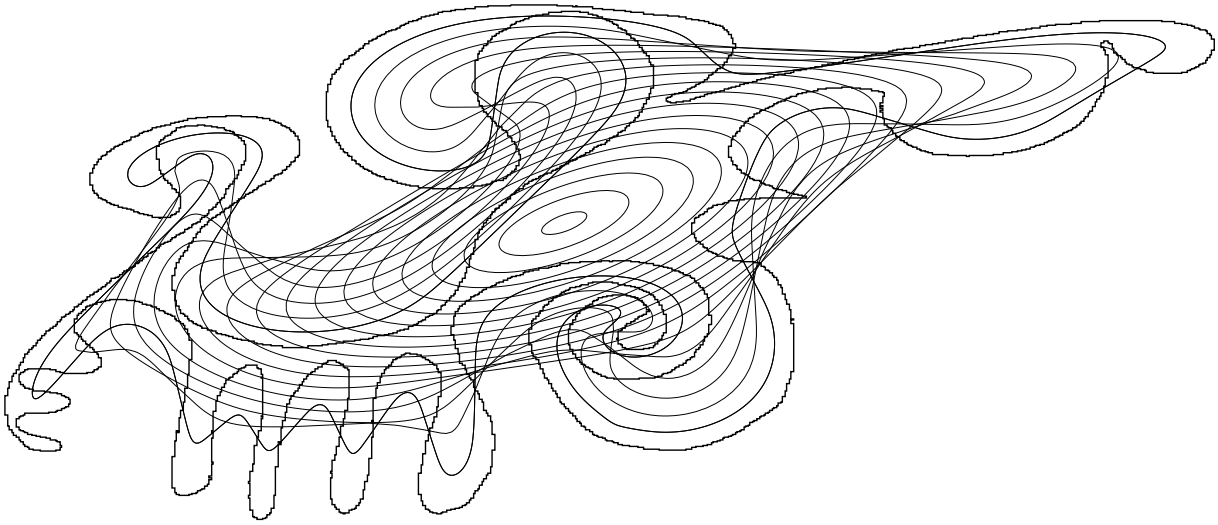

Figure 7.38: dog : filtered curve (t=1000, 2000, ..., 18000) — computation time : 2.5 seconds

7.3 Affine scale space of non-closed curves

Since the simplified algorithm allows to compute affine erosions of non-closed curves, it is possible to compute the affine scale space of a non-closed curve by iterating this operator. The need to consider the affine scale space for non-closed curves is explained in [21] : the affine scale space of non-closed curve can be defined thanks to a symmetrization-periodization process (Neumann condition) which makes the extremities fixed. If the two extremities are distinct, the asymptotic state is a segment. When they are not, a singularity may appear (see Figure 7.40).

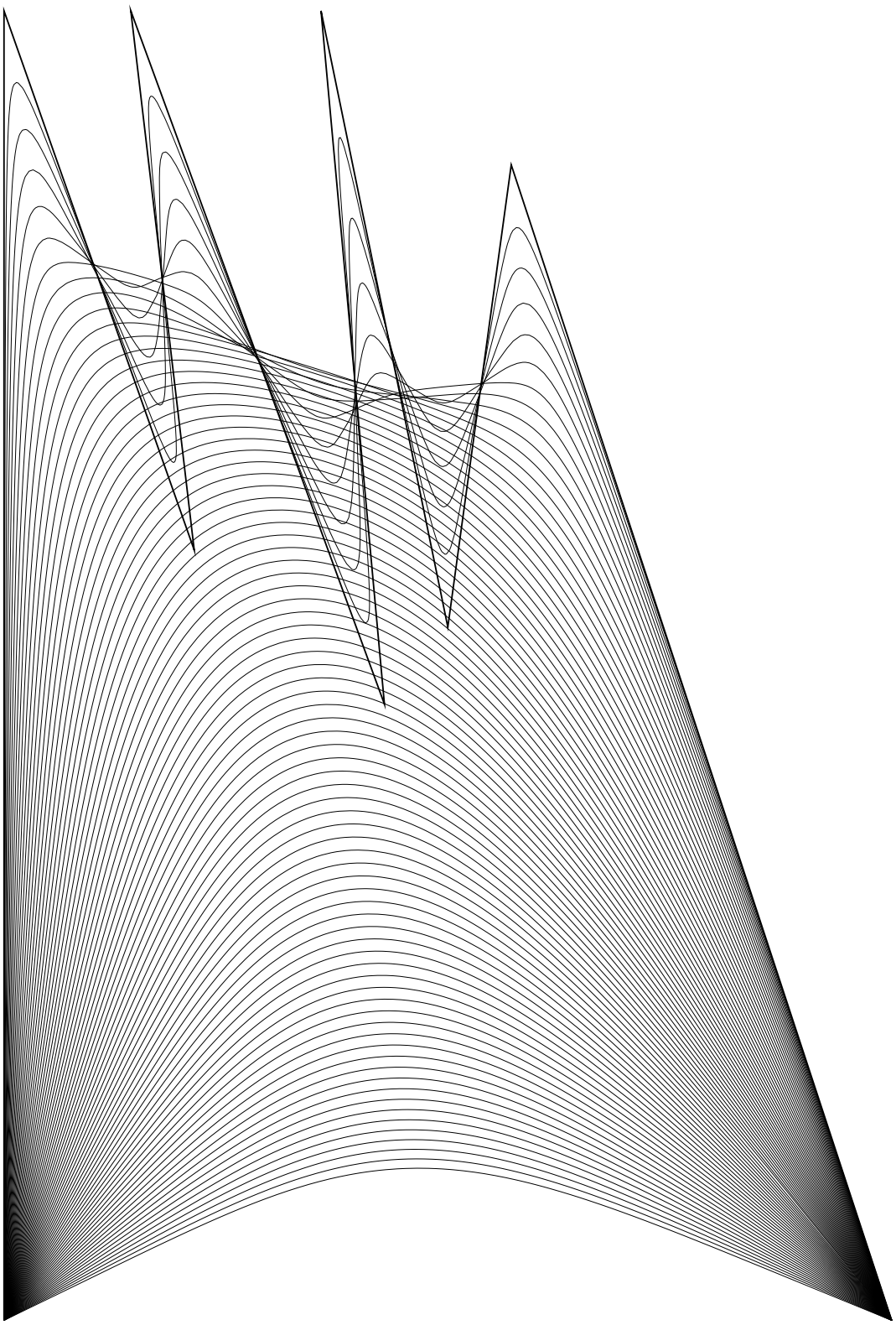

Figure 7.39: Affine scale space a a non-closed curve (modified teeth polygon)

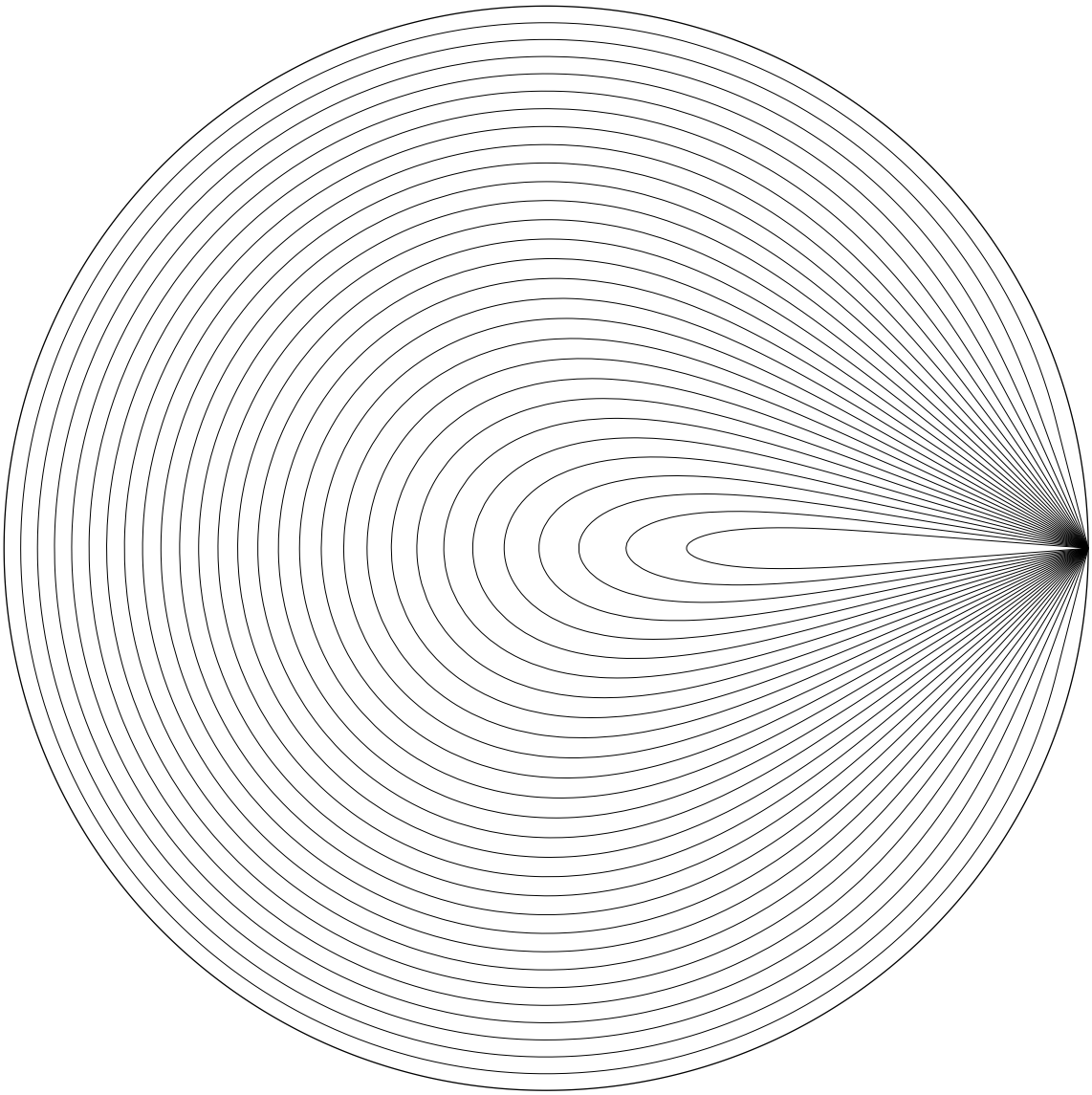

Figure 7.40: Affine scale space of a circle with a fixed point

Chapter 8

Conclusion

In this study, we presented a geometrical algorithm that can compute the affine scale space of a curve. Compared to Sethian's approach based on an image formulation, it is a faster[1] and more accurate method that allows complicated curve evolutions. Unlike classical geometrical schemes that rely on the computation of finite differences to perform point evolutions (see [65]), our scheme satisfies a natural property (the inclusion principle) that guarantees its numerical stability. It is also fully affine invariant, even in its numerical implementation (up to the computer precision). Thanks to these properties, the algorithm we proposed should be an interesting alternative to Sethian's approach, especially for shape recognition tasks (see [26]). We based our method on the iteration of a *non-local* operator which can be exactly computed on polygons. This property allows to separate the two approximation steps required in curve-evolution algorithms : the scale step, directly related to the number of iterations required, and the space step, i.e. the precision used in the discrete representation of curves. In our algorithm, the curve evolution between two iterations can be much larger than the quantization step used to represent the curves, while such a possibility is excluded for classical schemes in order to ensure their stability. The consequence is that our algorithm can accurately compute the evolution of a curve at a large scale in only a few iterations.

8.1 Applications

As we just explained, the main practical application of this study should concern Thierry Cohignac's method for local affine shape recognition (see [26]). Indeed, we can hope that his algorithm would gain computation time, robustness and accuracy by using our geometrical scheme to compute the affine scale space.

From a theoretical point of view, it would also be interesting to know what happens to the characteristic points of a curve when the evolution step t tends to zero. Our study states that

[1]Since the geometrical algorithm is much more precise than the scalar one, it is difficult to compare precisely their computation costs, but a proportion of 1 for 1000 gives a rough idea of it.

the characteristic area is asymptotically equal to $c \cdot t^{\alpha}$, c and α being universal constants, but it is likely that the second term of this expansion depends on the affine curvature[2], which would prove that the characteristic points of a curve tend to the extrema of a function of the affine curvature when t tends towards 0. Be that as it may, we now have an efficient way to compute the affine curvature on a curve, by considering the affine curvature of the pieces of hyperbolae which compose its affine erosion (for a small value of the area parameter of course). Hence, the shape recognition process can be realized by identifying new "characteristic" points defined as points where the affine curvature reaches an extremum.

Due to the duality of the image and curve formulation for the affine scale space, the iterated geometrical affine erosion also allows to compute the affine scale space of an image accurately. The computational cost is rather heavy since the geometrical scheme must be applied to every level curve of the initial image. However, we think that this way of representing an image without an inherent grid could be useful for some image processing tasks (zooming for example). Notice incidentally that this defines the first purely morphological numerical implementation of the AMSS which does not get "stuck" (see Chapter 2).

Last, the properties of the affine erosion we investigated in Chapter 3 might be useful in order to prove the existence of solutions for the geometrical affine scale space (which has not been done yet, as we explained in Chapter 2).

8.2 Further work

In Chapter 6, we defined two algorithms that compute the affine scale space of a curve : an exact algorithm, based on the iteration of the affine erosion, and a simplified algorithm, where the convex components of the evolving curve are processed separately at each iteration. We noticed that this simplified algorithm performs similar evolutions for a much lower computational cost. In fact, the computation cost of the simplified algorithm is proportional to the size of the input curve (that is, its complexity is linear), whereas in general this cost is approximately multiplied by the number of the convex components for the exact algorithm. For non-convex polygonal curves with more than 100 vertices (which correspond to a rather low precision for a complicated curve), the difference can become important. As it computes almost no intersection, the simplified algorithm is also more robust and easier to implement ("only" 900 lines of C source code). Hence, we think that it would be interesting to study more precisely the corresponding operator (the pseudo affine erosion) that we briefly introduced in Chapter 6. In particular, it should be possible to adjust the area step for each iteration automatically in order to obtain the best compromise between precision and computation time.

[2] we are sure that this is true for *one* term of the expansion at least, because the affine erosion would be the affine scale space otherwise.

We also think that it would be worthwhile investigating the case of non semi-closed curves further in relation with the work of V.Caselles, B.Coll and J.-M.Morel (see [21]). According to this paper, T-junctions should be kept fixed in order to perform an image evolution that preserves occlusions : from a geometrical point of view, this involves the evolution of non semi-closed curves.

Extending the affine erosion to higher dimensions seems difficult to achieve, above all in its numerical implementation. However, we think that the general idea we developed could be applied to several other planar curve evolutions. In particular, it is likely that several other geometrical curvature-driven evolution equations of the kind

$$\frac{\partial \boldsymbol{C}}{\partial t} = F(\gamma)\boldsymbol{N},$$

could be numerically simulated using the same method. The main point is to find a non-local operator satisfying three fundamental properties :

1. it is tangent to the evolution semigroup (i.e. consistent with the evolution equation),
2. it satisfies the inclusion principle,
3. it can be explicitly computed on a dense set of curves (polygons for example).

Condition 1 is obviously required. Condition 2 guarantees the numerical stability of the algorithm —which is fundamental for a curve evolution scheme— and allows large scale steps (and consequently a fast algorithm). Condition 3, which may be weakened, enables to process each iteration without depending on the quantization of the curve.

To give an example, let us investigate the case of Mean Curvature Motion (case $F(\gamma) = \gamma$), which is the Euclidean analog of the affine scale space. The affine erosion is based on an area criterion, since it removes from a set any of its chord set having area less than σ. Coming to Euclidean geometry, we can define a chord length-based erosion operator which removes from a set any of its chord set whose chord segment has length lower than a given δ (see Figure 8.1). Such an operator is consistent with the Mean Curvature Motion, and we think that it can be used to compute efficiently the Euclidean shortening of a curve.

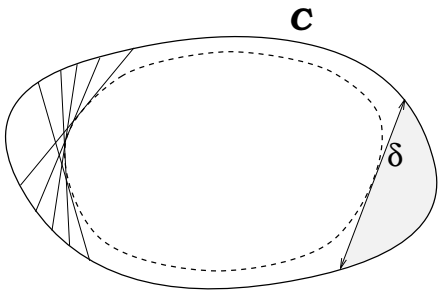

Figure 8.1: Euclidean analog of the affine erosion of a convex curve

The dashed curve is obtained by removing from the inside part of $\mathcal{C}$ any chord set whose chord has length δ. We conjecture that iterating such an operator leads to a good approximation of the Euclidean shortening flow associated to the Mean Curvature Motion.

Part II

Multiscale Analysis of Movies for Depth Recovery

Chapter 9

Introduction

9.1 The depth recovery problem

How can one establish a tridimensional map of a land area ? How can the tridimensional structure of a given object be measured ? How can one make a mobile robot perceive the geometry of an unknown environment ? All these problems are in fact the same : recovering the 3D-structure of a scene (land, object, environment) that can be observed. This problem of structure recovery has motivated many researches for the last twenty years, and multi-image analysis has been quickly identified as the most promising technique. Special devices like laser telemeters have sometimes been used, but for the time being their efficiency seems limited to very particular applications. As regards multi-image analysis, it is based on a simple geometric observation that everybody made once when looking through the side window of a car or a train : when one observes the landscape, the nearest objects "move" quicker than the farthest ones as the vehicle goes forward. Human stereo-vision is based on the same principle : between two observations from slightly different points of view (the two eyes), the relative positions of objects change according to their distance to the observer.

Inspired by human vision, researchers have studied in detail the technique of stereo vision analysis in the last two decades, in particular in association with edge-matching techniques. The principle is simple : the computer gets two pictures of the same scene from two cameras, then it detects on both images some features, for example, edges given by brisk contrast changes along straight lines. Last, it tries to match these edges (that is to say, it tries to associate each edge of the first image to its corresponding edge in the second image), and finally it recovers their depth by analyzing their relative position between the two images. This technique, after a certain success in the beginnings, finally appeared as insufficient for several reasons.

First, a simple analysis proves that the precision obtained in the determination of the depth is better when the cameras are far from each other, whereas the matching process is easier when they are close to each other. This incompatibility forced people to find a compromise between precision and robustness.

Another problem with edge-matching techniques is that they are more or less limited to artificial environments, because they require scenes with strongly-determined edges. In the case of natural textured scenes (e.g. a grass field), they are inefficient, and it can be a real problem to find alternative features to match.

Although edge-matching techniques were still receiving a lot of attention, some researchers tried to overcome the incompatibility between robustness and accuracy by considering whole sequences of images instead of only two images : the question of "depth from motion" was born. Even if the key to depth recovery is the same as to stereovision (analysis of the relative position of scene objects), using a large number of images appeared to bring great improvements. Of course, such a point of view was possible thanks to the increasing power of computers, both in storage capacity and in computation speed. Indeed, it is important to notice that a reasonable sequence of images (say 100 images of size 512x512 in 256 colors) represents 25 Mo of memory, which can be analyzed in a few minutes by a good workstation (for a simple algorithm). With 50 frames per second, this means that real-time movie analysis cannot be performed by now unless massive parallel machines are used.

The "depth from motion" problem (also called "structure from motion") was investigated mainly in two different ways. The first and probably most natural way is a generalization of stereovision techniques : the idea is to track robust features (edges, corners, ...) in the successive images and to deduce their depth from their velocity. This kind of method (see [35] for example) is only efficient for a certain kind of scene (typically, a high-contrasted artificial scene), due to the necessary use of edge-detection (or more generally, feature-detection) techniques.

The second approach for "structure from motion" was inspired by the classical Lagrangian formulation of the problem. It is based on the following Lambertian assumption : the color of a physical point does not depend on the point of view it is observed from. This assumption implies the famous "Motion Constraint Equation", which determines on the image sequence what is called the optical flow : this is simply the apparent velocity flow induced in the sequence of images by the apparent movement of the scene (induced itself by the camera movement). Numerous techniques have been developed in order to determine optical flow, but their efficiency is still debatable because of the stringent hypotheses they rely on (see [11] or [62] for detailed studies). In fact, the main difficulty of the general "structure from motion" problem in its Lambertian approach is that the system produced by the Motion Constraint Equation is under-determined : there are more unknowns than scalar equations. Even worse, the optical flow is not sufficient to recover the depth of objects for a general camera movement. Researchers tried to overcome the difficulty by writing regularity constraints, but this only brought partial solutions (or partial failures, depending on the point of view). In this context, the concept of active vision emerged (see [1]) : *"Most classical ill-posed problems of image sequence processing become well-posed and robust when the processing system controls the motion of the camera"*. Of

course, such an assumption is not always relevant, for most image sequence analyzers are not real-time processes. However, the weakened and less restrictive assumption of a known camera movement (pre-determined or not) seems to be a good compromise : this will be our point of view.

During this study, we shall consider image sequences produced by a moving camera looking at a *fixed* scene (i.e. with no moving objects[1]). In addition, we shall make the assumption that the camera horizontal plane is fixed. This means that the optical axis of the camera and the horizontal axis of the image plane[2] remain in a fixed plane. In order to check that this condition is not too restrictive, we give some examples of camera movements which satisfy this assumption.

1. **Pure translation motion with transversal observation.**
   The camera path is a straight line parallel to the horizontal axis of the camera, and the optical axis remains orthogonal to this line (see Figure 9.1). This situation happens with a camera looking through the side window of a moving vehicle, to go back to our first example. This motion also occurs when an observation plane flies over a region at constant altitude with the camera optical axis pointing downwards[3]. Solving the depth recovery problem in this case enables to establish a 3D-map of the region which has been flown over. This camera movement will be our reference framework in the following.

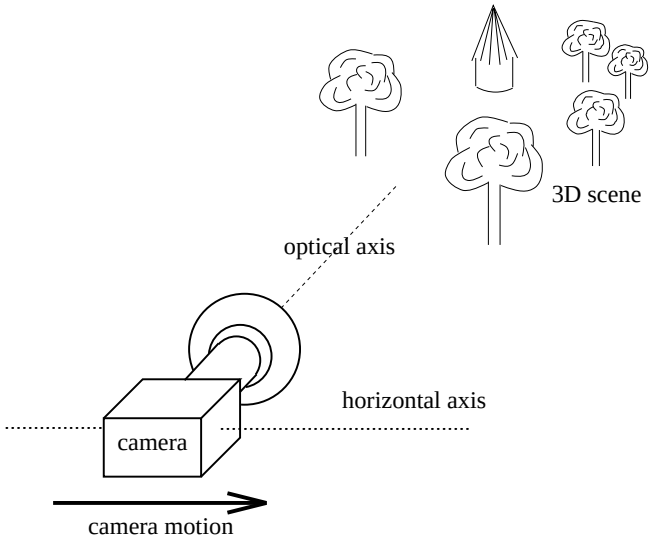

Figure 9.1: Pure translation motion.

2. **Circular motion.**

[1] Notice that it is equivalent to suppose that the camera is fixed and the whole scene has a rigid motion.

[2] The image plane, also called retinal plane or focal plane, is the plane where the physical image is produced by the optical lens system of the camera.

[3] However, we shall see later that our study can be adapted when the altitude of the plane varies with time or when the camera is not exactly pointing downwards.

This kind of motion is more adapted to the determination of the 3D-structure of a given object. The camera path is a circle, and the camera optical axis is constrained to point towards the center of this circle (see Figure 9.2). This motion also naturally occurs for non-geostationary satellites.

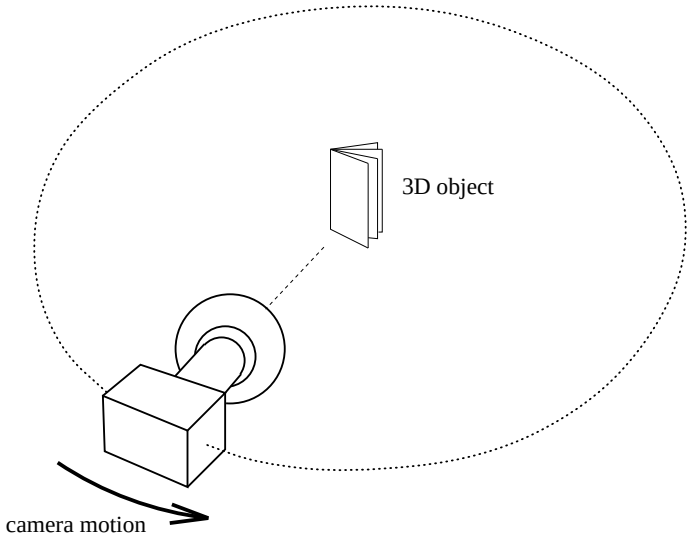

Figure 9.2: Circular motion.

3. **"Radar" motion**
   The camera has a pure rotational motion, and the optical axis remains orthogonal to the rotation axis (see Figure 9.3).

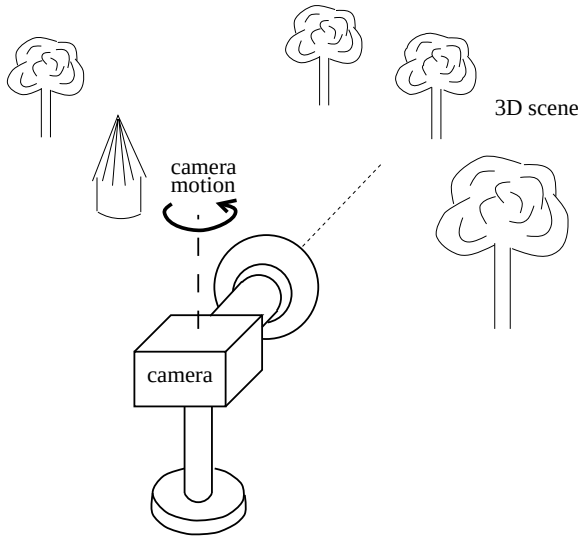

Figure 9.3: "Radar" motion.

The important aspect of the assumption we make on the camera movement is that it constrains the apparent movement of objects to be horizontal in the image plane. The three exam-

ples we gave prove that it is not too restrictive when the camera motion can be controlled. It has often been used in previous works (see [13] and [57] for example).

9.2 Geometric framework

We now come to more precise definitions and notations.

Consider a surface Σ of $\mathbb{R}^3$ represented by the graph of the depth function $Z(X,Y)$. Suppose that Σ is observed under a perspective projection[4] by a camera centered in $(C,0,0)$, with focal length a and an optical axis directed by the Z axis (see Figure 9.4). Each point $M = (X,Y,Z(X,Y))$ of Σ is projected on the image plane $\Pi : Z = a$ into $P = (x,y) = \pi(M)$ defined by

$$\begin{cases} x = a\dfrac{X-C}{Z(X,Y)} \\ \\ y = a\dfrac{Y}{Z(X,Y)} \end{cases} \tag{9.1}$$

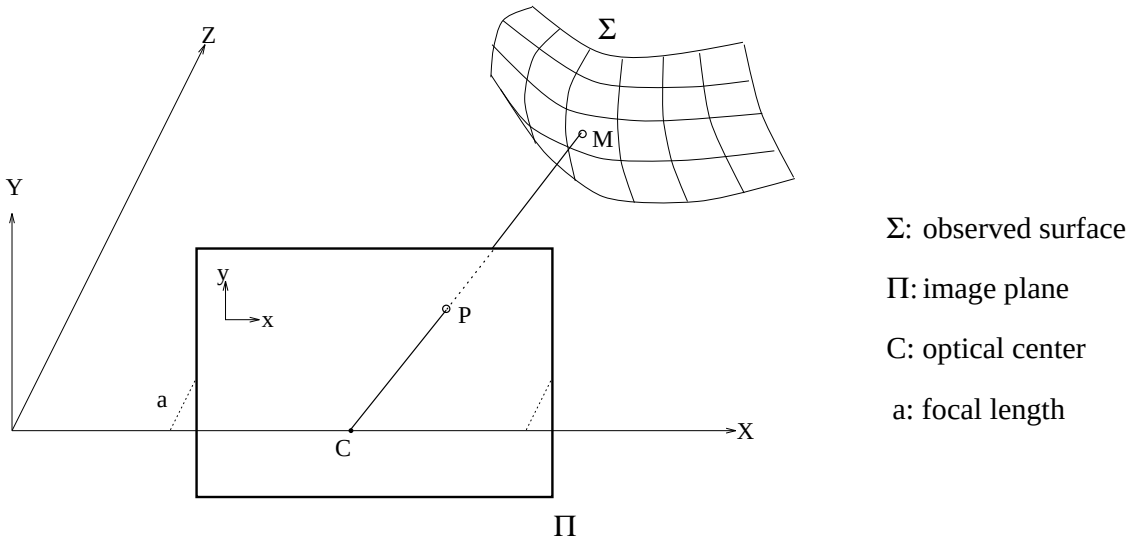

Figure 9.4: Scene geometry

Conversely, given a point P of the image plane, we can define $\mu(P) \in \Sigma$ as the closest point to P on the half line $[CP)$, when it exists. Thus, μ is a right inverse of π since $\pi \circ \mu$ is the identity map of $\pi(\Sigma)$.

Now, if Σ is a Lambertian surface characterized by its luminance $U(M)$, the camera produces the intensity image $u : P \mapsto U(\mu(P))$, up to an increasing rescaling depending on the intensity calibration of the camera. Notice that when the half line $[CP)$ intersects Σ more than once, an **occlusion** arises, and only the nearest point (i.e. $\mu(P)$) is observed, the other ones being masked by it.

[4] This model of projection holds for classical "pinhole" cameras.

We extend this to the case when the camera is moving along the X axis, the optical center following the path $(C(\theta), 0, 0)$, where θ is the time variable. This way, we define the maps $\pi_\theta : \Sigma \mapsto \Pi$ and $\mu_\theta : \Pi \mapsto \Sigma$, and the image $u : P \mapsto u(P)$ becomes a **movie** $u(P, \theta) = U(\mu_\theta(P))$, that is to say a continuous sequence of images regarded as a scalar map defined on a subset of $\mathbb{R}^3$.

The aim of our study is to compute the geometry of Σ — its observed part actually — from the redundant information contained in the movie $(x, y, \theta) \mapsto u(x, y, \theta)$, knowing that it should satisfy the fundamental equation

$$u\left(a\frac{X - C(\theta)}{Z(X,Y)}, a\frac{Y}{Z(X,Y)}, \theta\right) = U(X, Y). \tag{9.2}$$

9.3 Velocity field

To simplify the problem, we shall now suppose that no occlusion appears (we shall discuss the general case later). Then, the relation $M \mapsto P$ is bijective, that is to say we have $\mu = \pi^{-1}$ on $\pi(\Sigma)$. This induces a bijective relation between the scalar **image maps** $f : \Pi \times \mathbb{R} \to \mathbb{R}$ and their corresponding **scene maps** $F : \Sigma \times \mathbb{R} \to \mathbb{R}$ defined by

$$F(M, \theta) = f(\pi_\theta(M), \theta) = f(P(\theta), \theta).$$

Consider now a point M of Σ. Projected on the movie, this point describes the movement $P(\theta) = \pi_\theta(M)$, whose velocity can be determined from Equation 9.1 :

$$\frac{dP}{d\theta} = (\frac{dx}{d\theta}, \frac{dy}{d\theta}) \quad \text{with} \quad \frac{dx}{d\theta} = -\frac{aC'(\theta)}{Z(X,Y)} \quad \text{and} \quad \frac{dy}{d\theta} = 0,$$

C' meaning the derivative of C. Following this idea, we can define the derivative of an image map f along the real movement by

$$\frac{\partial F}{\partial \theta} = \frac{d}{d\theta} f(P(\theta), \theta) = \prec Df, \frac{dP}{d\theta} \succ + \frac{\partial f}{\partial \theta} = \frac{dx}{d\theta} \cdot \frac{\partial f}{\partial x} + \frac{\partial f}{\partial \theta}.$$

In particular, if Equation 9.2 is satisfied, the derivative of u along the movement must be zero, because the corresponding scene function $U(M)$ does not depend on θ. This implies a specific formulation of the Motion Constraint Equation,

$$\frac{dx}{d\theta} \cdot \frac{\partial u}{\partial x} + \frac{\partial u}{\partial \theta} = 0. \tag{9.3}$$

From this equation, it is natural to define the apparent velocity field of the movie by

$$v := -\frac{\frac{\partial u}{\partial \theta}}{\frac{\partial u}{\partial x}}, \tag{9.4}$$

when $\frac{\partial u}{\partial x} \neq 0$, remembering that if a scene interpretation exists (i.e. if Equation 9.2 is satisfied), we have

$$v(x, y, \theta) = -\frac{aC'(\theta)}{Z(X,Y)} \tag{9.5}$$

everywhere v is defined (i.e everywhere $\frac{\partial u}{\partial x} \neq 0$).

Following this idea, we define the **total derivative** of a scalar image map $f : \Pi \times \mathbb{R} \to \mathbb{R}$ as

$$\frac{\mathrm{D}f}{\mathrm{D}\theta} = v\frac{\partial f}{\partial x} + \frac{\partial f}{\partial \theta}.$$

This is exactly the Lie derivative of f along the apparent movement vector $\xi = (v, 0, 1)$. When a scene interpretation is known, it can be identified as the time derivative of the scene map associated to f. The importance of this total derivative operator will appear later.

9.4 Depth recovery

Theoretically, it is possible to estimate the apparent velocity field v using Equation 9.4, and then to recover the depth Z by identifying v with the real velocity in Equation 9.5. This way, choosing a fixed value of θ, we can hope to associate to any point $P = (x, y, \theta)$ of the image plane where the apparent velocity is defined and nonzero, the point $M = \mu_\theta(P)$ of Σ defined by

$$M = \left(C(\theta) - \frac{C'(\theta)x}{va}, -\frac{C'(\theta)y}{va}, -\frac{C'(\theta)}{v}\right).$$

If $C(\theta)$, $C'(\theta)$ and a are not known, the structure of Σ is recovered up to a linear transformation of the kind

$$(X, Y, Z) \mapsto (\alpha X + \beta, \alpha Y, \gamma Z).$$

In practice, several difficulties appear when one tries to recover the geometry of Σ directly. The first one occurs in the computation of v from Equation 9.4. Indeed, it is impossible to obtain good estimations of the time derivative $\frac{\partial u}{\partial \theta}$ using finite difference methods. The reason is that most digital movies have a too large time sampling step, inasmuch as the number of images per second produced in the sampling process is too small compared to the quick change of scene details. In other words, the Nyquist limit is generally exceeded during the sampling process, simply because most acquisition systems (cameras, camescopes, ...) sample each image independently without first processing a time frequency cutoff[5]. Hence, Shannon's Theorem does not apply any more and common approximations cannot be used to estimate time derivatives. As concerns the spatial derivative $\frac{\partial u}{\partial x}$, its estimation hardly makes sense for textured areas, because of the quick changes in the intensity. For areas where the intensity takes a constant (or quasi-constant) value, the estimation of v becomes very sensitive to noise and quantization, since the almost-zero quantity $\frac{\partial u}{\partial x}$ appears in the denominator of v.

The "classical" method to overcome this kinds of problem is to apply a linear spatio-temporal smoothing filter to the movie (see [13] for example), which can be seen as a (post-sampling) low-pass filter. Such a kind of isotropic diffusion has disastrous effects on non-smooth details like

[5]In fact, this is not really a bad thing since the non-continuous structure of images due to the presence of occlusions makes the classical sampling theory inadapted.

edges or textured areas. Like all linear filters, it is not adapted to the structure of images which result more from the superimposition of occluding objects than from the addition of weighted harmonics (see [21]).

Another problem appearing in the naive reconstruction process we just described is that two determinations of Σ made from derivative estimations at different times θ_1 and θ_2 may produce slightly different results in practice, because real movies are not exactly time-coherent. This is a very important problem since, as we saw in the introduction, the large number of images is supposed to guarantee robustness and accuracy in the depth recovery.

All these remarks lead to think that the depth recovery must be achieved on a sort of ideal movie, for which the computation of v can be made accurately and for which the depth interpretation of the scene remains the same at any time. One can reasonably hope to obtain such an ideal movie from a raw one thanks to the redundancy of the information spread among all images. In the following study, we shall see that such a transformation is possible, and that it can be obtained systematically by using an axiomatic formulation of the problem (Chapter 10). This transformation can be formalized by a non-linear diffusion equation along the movement field, which appears to have interesting properties (Chapter 11, 12). In Chapter 13, we provide a numerical algorithm, easily implementable —even on parallel machines—, as well as conclusive experiments on two classical natural movies. To conclude in Chapter 14, we generalize our study to more general camera motions and highlight further axes of extension.

Chapter 10

Axiomatic formulation

In this chapter, we devise a multiscale analysis of movies devoted to the depth recovery by using an axiomatic formulation. Such a methodology is not new : it has been successfully applied in [4] and in [26] to find the Affine Scale Space as the optimal way (in a certain sense) to simplify images and shapes. After making clear requirements, we establish a uniqueness result for our model : there is only one analysis of movies compatible with the depth recovery.

Let us first define some notations. Given an open or closed subset Ω of $\mathbb{R}^n$, $C^n(\Omega)$ means the space of continuous maps $u : \overline{\Omega} \to \mathbb{R}$ of class C^n on Ω. As usual, $\overline{\Omega}$ means the topological closure of Ω in $\mathbb{R}^n$. We shall also write $\mathcal{S}(\mathbb{R}^3)$ to denote the set of real symmetric 3x3 matrices.

As we saw previously, a movie is a real-valued map u defined on a subset of $\mathbb{R}^3$, the value $u(x, y, \theta)$ representing the light intensity at a point (x, y) of the plane at time θ. The natural domain for a digital movie is $[x_1, x_2] \times [y_1, y_2] \times [\theta_1, \theta_2]$, but we shall see that it is simpler and more logical to suppose that a movie is defined on $\mathbb{R}^2 \times \overline{I}$, with either $I =]\theta_1, \theta_2[$ or $I = S^1$ (case of a time-periodic movie).

We recall that a multiscale analysis is a family of operators $(T_t : \mathcal{M} \to \mathcal{M})_{t \geqslant 0}$, t representing the scale of analysis. Here, $\mathcal{M}$ is a movie space, that is to say a space of continuous real-valued maps defined on $\mathbb{R}^2 \times \overline{I}$. The choice of $\mathcal{M}$ will become natural later, but is not necessary for the time being since we only want to find constraints on (T_t). However, because of the singularity which appears in the computation of the velocity field when the partial derivative u_x vanishes (u_x is a short notation for $\frac{\partial u}{\partial x}$), we shall suppose in the following that for any $n \geqslant 1$, the space

$$\mathcal{M}^n = \{u \in \mathcal{M} \cap C^n(\mathbb{R}^2 \times \overline{I}, \mathbb{R});\ \forall \boldsymbol{z} \in \mathbb{R}^3, u_x(\boldsymbol{z}) \neq 0\}$$

is nonempty, and that given $(\lambda, \boldsymbol{p}, A) \in \mathbb{R} \times \mathbb{R}^3 \times \mathcal{S}(\mathbb{R}^3)$, it is possible to find $u \in \mathcal{M}^2$ such that

$$u(\boldsymbol{0}) = \lambda, \quad Du(\boldsymbol{0}) = \boldsymbol{p} \quad \text{and} \quad D^2u(\boldsymbol{0}) = A.$$

10.1 Architectural axioms

In the spirit of [4], we first constrain our multiscale analysis to satisfy some architectural axioms :

• **[Recursivity]** : $T_0 = Id$ and $\forall t, t' > 0, \quad T_{t+t'} = T_{t'} \circ T_t$.

• **[Local Comparison Principle]** : if $u < \tilde{u}$ on $B(\boldsymbol{z}, r)$, then $T_t u(\boldsymbol{z}) \leqslant T_t \tilde{u}(\boldsymbol{z})$ for $t > 0$ small enough.

• **[Regularity]** : if u is a quadratic form (that is, $u(\boldsymbol{z}) = [A](\boldsymbol{z}, \boldsymbol{z}) + \prec \boldsymbol{p}, \boldsymbol{z} \succ + \lambda$ where A is a symmetric 3x3 matrix ($[A]$ being the associated bilinear map), $\boldsymbol{p}$ a 3-dimensional vector and λ a given constant), then

$$\lim_{t \to 0} \frac{T_t u - u}{t}(\boldsymbol{z}) = F(A, \boldsymbol{p}, \lambda)$$

and F depends continuously on A when $p_1 \neq 0$ (p_1 being the component of $\boldsymbol{p}$ along the x coordinate).

The **[Recursivity]** axiom constrains the multiscale analysis to have a semi-group structure. If the scale t is discretized, this means that the analysis is obtained at scale n by iterating n times a fixed filter. This axiom can be weakened in

[Pyramidal Architecture] : $\forall t, h, \exists\, T_{t+h,t}, \quad T_{t+h} = T_{t+h,t} \circ T_t$.

However, we checked that under this hypothesis the final classification remains the same up to a rescaling (as it has been proved in [4] for the affine scale space). This is the reason why we directly assume that (T_t) is a semi-group.

The **[Local Comparison Principle]** axiom is very important : it prevents the multiscale analysis from creating new details in the analyzed movie as the scale increases. It also guarantees the stability of associated numerical algorithms.

The **[Regularity]** axiom also contains the classical **[Translation Invariance]** axiom, which states that the multiscale analysis does not depend on the origin of space and time coordinates. When $I =]\theta_1, \theta_2[$, the classical formulation of **[Translation Invariance]** is not possible any longer because the domain is not translation-invariant.

These axioms can be found in the axiomatic characterization of the affine morphological scale space for example ; only the **[Regularity]** axiom has been adapted to the depth recovery problem. Please refer to [40] for complete discussion.

The classification starts with the following theorem.

Theorem 8 *A multiscale analysis $T_t : u_0(\cdot) \mapsto u(\cdot, t)$ satisfying **[Recursivity]**, **[Local Comparison Principle]** and **[Regularity]** can be described by a partial differential equation of the kind*

$$\frac{\partial u}{\partial t} = F(D^2 u, Du, u) \tag{10.1}$$

submitted to initial condition $u(\cdot,0)=u_0$. Moreover, F is elliptic (that is to say nondecreasing with respect to its first argument for the usual order on 3x3 symmetric matrices), and continuous with respect with its first argument at any point where $u_x \neq 0$.

The proof of an equivalent theorem can be found in [40] for example. The existence of F is a direct consequence of the **[Regularity]** axiom. The fact that the evolution is given by a PDE of order two (and not more) results from the **[Local Comparison Principle]** axiom, as well as the ellipticity of F.

Notice that Equation 10.1 makes sense (in terms of existence and unicity of solutions) according to the theory of viscosity solutions (see [27]), provided that the singularity $u_x = 0$ is not involved. This point will become clearer in the next chapter. By now, the only important point is that Equation 10.1 is satisfied in the classical sense by u at any point where u is C^2 and $u_x \neq 0$.

10.2 Specific axioms

We now come to specific axioms with respect to the depth recovery problem. First, remember that when $u \in \mathcal{M}^n$ $(n \geqslant 1)$, the apparent velocity field operator is well defined by

$$v[u] = -\frac{u_\theta}{u_x}.$$

Since we are interested in the apparent velocity field, it seems natural that our analysis focuses mainly on this datum. In that sense, it is rather natural to constrain the analysis to commute with operators that preserve the apparent velocity field. This justifies the following axiom.

- **[v-Compatibility]**: For any $h : \mathbb{R}^4 \mapsto \mathbb{R}$, if

$$\forall u \in \mathcal{M}^1,\ R_h u \in \mathcal{M}^1 \quad \text{and} \quad v[R_h u] = v[u], \quad \text{with} \quad R_h u(x,y,\theta) = h\left(u(x,y,\theta), x, y, \theta\right),$$

then

$$\forall t,\ T_t \circ R_h = R_h \circ T_t.$$

This axiom implies two weaker axioms, obtained for specific choices of h.

◇ **[Strong Morphological Invariance]**: For any monotone scalar map g,

$$\forall u \in \mathcal{M}, \forall t,\ T_t g(u) = g(T_t u).$$

◇ **[Transversal Invariance]**: For any nonvanishing map g,

$$\forall u \in \mathcal{M}, \forall t,\ T_t(g(y) \cdot u) = g(y) \cdot (T_t u).$$

The first one is obtained by choosing $h(u,x,y,\theta) = g(u)$. It is a strong formulation of the morphological invariance, because g can be decreasing as well as increasing. In fact, this axiom is

equivalent to the classical **[Morphological Invariance]** axiom plus the **[Contrast reversal]** axiom. The second one, obtained with $h(u,x,y,\theta) = g(y) \cdot u$, is a kind of morphological invariance in the direction transversal to the movement. Notice that we supposed implicitely that $\mathcal{M}$ is stable under the operations $u \mapsto g \circ u$ and $u \mapsto g(y) \cdot u$. Following [40], we also constrain the analysis to commute with the superimposition of any uniform movement of the camera.

- **[Galilean Invariance]**:

$$\forall \alpha \in \mathbb{R},\ \forall u \in \mathcal{M},\ \forall t,\ T_t(u \circ B_\alpha) = (T_t u) \circ B_\alpha, \quad \text{with} \quad B_\alpha(x,y,\theta) = (x - \alpha\theta, y, \theta).$$

Last, we would like the analysis not to depend on the focal length of the camera (the a variable in the previous chapter). This can be translated into a commutation with spatial homothetic transformations.

- **[Zoom Invariance]**:

$$\forall \lambda \neq 0,\ \forall u \in \mathcal{M}, \forall t,\ T_t(u \circ H_\lambda) = (T_t u) \circ H_\lambda, \quad \text{with} \quad H_\lambda(x,y,\theta) = (\lambda x, \lambda y, \theta).$$

10.3 Fundamental equation

We now prove that the set of axioms we constrained the multiscale analysis to satisfy is sufficient to restrain the possible analyses to one candidate only[1]. We shall prove later that this candidate is actually a solution.

Theorem 9 *There exists at most one multiscale analysis of movies defined on $\mathcal{M}^2$ satisfying the architectural axioms plus **[v-Compatibility]**, **[Galilean Invariance]** and **[Zoom Invariance]**. It must be described by the partial differential equation*

$$u_t = u_{\theta\theta} - 2\frac{u_\theta}{u_x} u_{\theta x} + (\frac{u_\theta}{u_x})^2 u_{xx}. \tag{10.2}$$

Remark 1 : For the time being, Equation 10.2 is defined in the classical sense for $u(\cdot,t) \in \mathcal{M}^2$. In fact, we shall see in the next chapter how we can define weak solutions of Equation 10.2 that are not in $\mathcal{M}^2$ but only continuous.

Remark 2 : Equation 10.2 can be rewritten into

$$u_t = u_{\xi\xi} \quad \text{with} \quad \xi = (-\frac{u_\theta}{u_x}, 0, 1) \quad \text{and} \quad u_{\xi\xi} = [D^2 u](\xi, \xi),$$

[1] Of course, the identity operator is irrelevant here.

which means an anisotropic diffusion of u along the movement direction. The apparent acceleration in the movie can be defined by

$$? = \frac{\mathrm{D}v}{\mathrm{D}\theta} = v_\theta + v v_x,$$

which can be expanded in

$$? = -\frac{1}{u_x}\left(u_{\theta\theta} - 2\frac{u_\theta}{u_x}u_{\theta x} + (\frac{u_\theta}{u_x})^2 u_{xx}\right) = -\frac{u_{\xi\xi}}{u_x}.$$

Hence, Equation 10.2 can also be rewritten into

$$u_t = -? \, u_x.$$

Lemma 17 *For any multiscale analysis satisfying the architectural axioms and [v-Compatibility], there exists a map $F : \mathbb{R}^2 \mapsto \mathbb{R}$ such that*

$$u_t = u_x F(?, v). \tag{10.3}$$

Proof :

Let us first make clear that the map F we write here is not the map F of Equation 10.1 : we simply use the same notation to avoid introducing too many symbols.

We are going to use the fact that the **[v-Compatibility]** axiom implies the simpler axioms **[Strong Morphological Invariance]** and **[Transversal Invariance]**, as we noticed before.

Applying **[Strong Morphological Invariance]** for $g(u) = u + \lambda$ (λ being an arbitrary constant) proves that F cannot depend on u in Equation 10.1, so that we have

$$\frac{\partial u}{\partial t} = G(D^2 u, Du) \tag{10.4}$$

Now, the **[Transversal Invariance]** axiom states that for any nonvanishing function g of class C^2,

$$\forall u \in \mathcal{M}^2, \forall y, \quad G(D^2(g(y)\cdot u), D(g(y)\cdot u)) = G(D^2 u, Du). \tag{10.5}$$

Let $A = [a_{ij}] \in \mathcal{S}(\mathbb{R}^3)$, $\lambda \in \mathbb{R}$ and $\boldsymbol{p} = (p_i) \in \mathbb{R}^3$ such that $p_1 \neq 0$ (the coordinates x, y, θ will be indexed by $1, 2, 3$ in the following). By hypothesis on $\mathcal{M}^2$, we can build a movie $u \in \mathcal{M}^2$ such that

$$u(0,0,0) = \lambda, \qquad Du(0,0,0) = \boldsymbol{p}, \qquad \text{and} \qquad D^2 u(0,0,0) = A.$$

Now, consider the vector $\boldsymbol{y} = \begin{pmatrix} 0 \\ 1 \\ 0 \end{pmatrix}$, the projection matrix on the (x, θ) plane

$$Q_{y^\perp} = \begin{pmatrix} 1 & 0 & 0 \\ 0 & 0 & 0 \\ 0 & 0 & 1 \end{pmatrix},$$

and the projection matrix on the line $\mathbb{R}\boldsymbol{y}$

$$Q_y = \boldsymbol{y} \otimes \boldsymbol{y} = I - Q_{y^\perp} = \begin{pmatrix} 0 & 0 & 0 \\ 0 & 1 & 0 \\ 0 & 0 & 0 \end{pmatrix},$$

I being the identity matrix of $\mathcal{S}(\mathbb{R}^3)$. Applying Equation 10.5 to u in $(0,0,0)$, we obtain

$$G(g(0)A + g'(0)\,\boldsymbol{y} \otimes \boldsymbol{p} + g''(0)\lambda Q_y, g(0)\,\boldsymbol{p} + g'(0)\,\boldsymbol{y}) = G(A, \boldsymbol{p}).$$

If we choose $g(y) = 1 + y^2/2$, we get

$$\forall A, p, \lambda, \quad G(A + \lambda Q_y, \boldsymbol{p}) = G(A, \boldsymbol{p}), \tag{10.6}$$

and taking $\lambda = -a_{22}$ yields

$$\forall A, \boldsymbol{p}, \quad G(..., a_{22}, ...) = G(..., 0, ...),$$

where the two terms only differ in the a_{22} variable. Hence, G does no depend on a_{22}.

Now we are going to show that G does not depend on a_{12} and a_{23} either, by using the **[Causality]** axiom, using a technique from Giga et Goto [37][2]. Let us define $A' = A - a_{22}Qy$ and for $\varepsilon > 0$,

$$I_\varepsilon = \varepsilon Q_{y^\perp} + \frac{a_{21}^2 + a_{23}^2}{\varepsilon} Q_y = \begin{pmatrix} \varepsilon & 0 & 0 \\ 0 & \dfrac{a_{21}^2 + a_{23}^2}{\varepsilon} & 0 \\ 0 & 0 & \varepsilon \end{pmatrix}.$$

The characteristic polynom of the matrix

$$A_\varepsilon = Q_{y^\perp} A' Q_{y^\perp} - A' + I_\varepsilon = \begin{pmatrix} \varepsilon & -a_{21} & 0 \\ -a_{21} & \dfrac{a_{21}^2 + a_{23}^2}{\varepsilon} & -a_{23} \\ 0 & -a_{23} & \varepsilon \end{pmatrix}$$

is

$$\det(xI - A_\varepsilon) = x(x - \varepsilon)\left(x - (\varepsilon + \frac{a_{21}^2 + a_{23}^2}{\varepsilon})\right).$$

As the eigenvalues of A_ε are nonnegative, A_ε is positive (for the usual order in $\mathcal{S}(\mathbb{R}^3)$), and symmetrically $A_{-\varepsilon}$ is negative, which yields

$$A' - I_\varepsilon \leqslant Q_{y^\perp} A' Q_{y^\perp} \leqslant A' + I_\varepsilon$$

But the **[Causality]** axiom implies (see [37])

$$\forall A, B, \boldsymbol{p}, \quad A \geqslant B \;\Rightarrow\; G(A, p) \geqslant G(B, \boldsymbol{p}),$$

[2] If we suppose that G is differentiable, then this property follows immediatly. Indeed, the **[Causality]** axiom implies

$$\forall i, j, \;\; \det_{i,j}[D^2 G] = \frac{\partial G}{\partial a_{ii}} \frac{\partial G}{\partial a_{jj}} - \left(\frac{\partial G}{\partial a_{ij}}\right)^2 \geqslant 0$$

and since $\frac{\partial G}{\partial a_{22}} = 0$, we get $\frac{\partial G}{\partial a_{21}} = \frac{\partial G}{\partial a_{23}} = 0$

so that

$$\forall A, \boldsymbol{p}, \quad G(A' - I_\varepsilon, \boldsymbol{p}) \leqslant G(Q_{y^\perp} A' Q_{y^\perp}, \boldsymbol{p}) \leqslant G(A' + I_\varepsilon, \boldsymbol{p}).$$

Then, using Equation 10.6, we get

$$\forall A, \boldsymbol{p}, \quad G(A + \varepsilon I, \boldsymbol{p}) \leqslant G(Q_{y^\perp} A Q_{y^\perp}, \boldsymbol{p}) \leqslant G(A + \varepsilon I, \boldsymbol{p})$$

and taking the limit when $\varepsilon \to 0$, the continuity of G implies

$$\forall A, \boldsymbol{p}, \quad G(A, \boldsymbol{p}) = G(Q_{y^\perp} A Q_{y^\perp}, \boldsymbol{p}),$$

which means that we can write

$$\forall A, \boldsymbol{p}, \quad G(a_{11}, a_{12}, a_{13}, a_{22}, a_{23}, a_{33}, p_1, p_2, p_3) = H(a_{11}, a_{13}, a_{33}, p_1, p_2, p_3).$$

Now, applying again the **[Transversal Invariance]** axiom to H, we obtain

$$\forall A, \boldsymbol{p}, g, y \quad H(a_{11}, a_{13}, a_{33}, p_1, p_2, p_3) = H(a_{11}, a_{13}, a_{33}, p_1, g'(y)p_2, p_3) \tag{10.7}$$

Choosing $p_2 = 1$ and $g(y) = 1 + y^2/2$ as before, Equation 10.7 yields

$$\forall A, p_1, p_3, y \quad H(a_{11}, a_{13}, a_{33}, p_1, 1, p_3) = H(a_{11}, a_{13}, a_{33}, p_1, y, p_3),$$

which proves that H does not depend on its fifth argument p_2.

Now we use the **[Strong Morphological Invariance]** axiom. It has been proven (see [4] for example) that this axiom, in combination with the **[Causality]** axiom, forces the second order terms of the evolution to be of the kind $[D^2u](\boldsymbol{a}, \boldsymbol{b})$, where $\boldsymbol{a}$ and $\boldsymbol{b}$ belong to the plane orthogonal to Du, written $(Du)^-$. Now, as we just saw, the **[Transversal Invariance]** axiom forbids any dependency on y, so that $\boldsymbol{a}$ and $\boldsymbol{b}$ must also belong to the $(\boldsymbol{y})^- = (x, \theta)$ plane. Finally, $\boldsymbol{a}$ and $\boldsymbol{b}$ must belong to the line $(Du)^- \cap (\boldsymbol{y})^- = (\xi)^-$, so that the only admissible second order term is $? = -\frac{1}{u_x}[D^2u](\xi, \xi)$, up to a multiplicative first order term. Notice that $?$ is a morphological operator.

As regards the first order terms, the **[Transversal Invariance]** axiom forbids any dependency on u_y. Hence, as $?$ does not contain the u_y term, u must satisfy an evolution equation of the kind

$$u_t = F(?, u_x, u_\theta).$$

We rewrite this equation into

$$u_t = u_x G(?, v, u_x)$$

and apply the **[Strong Morphological Invariance]** axiom. Since $?$ and v are morphological operators, it yields

$$\forall u, \ \forall \lambda \neq 0, \quad G(?, v, u_x) = G(?, v, \lambda u_x). \tag{10.8}$$

For any $(\alpha,\beta)\in\mathbb{R}^2$, we consider a movie $u\in\mathcal{M}^2$ such that

$$u(x,y,\theta)=\frac{\alpha}{2}\theta^2+x-\beta\theta$$

in a vicinity of $(x,y,\theta)=\mathbf{0}$. We have $u_x(\mathbf{0})=1$, $v(\mathbf{0})=\beta$ and $?(\mathbf{0})=\alpha$ so that Equation 10.8 can be rewritten into

$$\forall\alpha,\beta,\ \forall\lambda\neq 0,\ \ G(\alpha,\beta,1)=G(\alpha,\beta,\lambda),$$

which means that G does not depend on its third argument (notice that G does not need to be defined when $u_x=0$). As a consequence, we can write

$$u_x=u_x\,F(?,v)$$

as announced. □

Remark : We proved that the **[v-Compatibility]** axiom, in association with the architectural axioms, forbids any dependency of the evolution on y. In other words, the sliced images $(x,\theta)\mapsto u(x,y,\theta)$ (with y fixed) are processed independently. In the following, we shall often ignore the y coordinate and we shall write $u(x,\theta)$ instead of $u(x,y,\theta)$, the y variable being supposed fixed.

Lemma 18 *A multiscale analysis satisfying the architectural axioms plus **[v-Compatibility]** and **[Galilean Invariance]** can be written*

$$u_t=u_xF(?) \tag{10.9}$$

Proof :

Since the multiscale analysis commutes with the operator

$$B_\alpha:(x,y,\theta)\mapsto(x-\alpha\theta,y,\theta),$$

we have

$$\frac{\partial}{\partial t}(u\circ B_\alpha)=\frac{\partial u}{\partial t}\circ B_\alpha.$$

Writing $\tilde{u}=u\circ B_\alpha$ yields

$$\begin{aligned}
\tilde{u}_x &= \frac{\partial}{\partial x}u(x-\alpha\theta,\theta)=u_x\circ B_\alpha\\
\tilde{u}_\theta &= \frac{\partial}{\partial\theta}u(x-\alpha\theta,\theta)=(u_\theta-\alpha u_x)\circ B_\alpha\\
\tilde{v} &= -\frac{\tilde{u}_\theta}{\tilde{u}_x}=v\circ B_\alpha+\alpha\\
\tilde{?} &= \frac{\mathrm{D}\tilde{v}}{\mathrm{D}\theta}=\tilde{v}_\theta+\tilde{v}\tilde{v}_x=(v_\theta-\alpha v_x+(v+\alpha)v_x)\circ B_\alpha=?\circ B_\alpha.
\end{aligned}$$

From Lemma 17 we know that $u_t = u_x F(?\,, v)$. Hence,

$$\forall u, \alpha, \quad u_x F(?\,, v+\alpha) = u_x F(?\,, v),$$

so that F does not depend on its second argument. □

Lemma 19 *A multiscale analysis satisfying the architectural axioms plus* ***[v-Compatibility]*** *and* ***[Zoom Invariance]*** *can be written*

$$u_t = \begin{cases} u_\theta F(\dfrac{?}{v}) \ \text{ if } \ u_\theta \neq 0, \\ \\ a\,u_x \ \text{ if } \ u_\theta = 0. \end{cases} \tag{10.10}$$

Proof :

We proceed as for Lemma 18 : writing $\tilde{u} = u \circ H_\lambda$ with $H_\lambda : (x, y, \theta) \mapsto (\lambda x, \lambda y, \theta)$, we get

$$\begin{aligned} \tilde{v} &= -\frac{\tilde{u}_\theta}{\tilde{u}_x} = -\frac{u_\theta}{\lambda u_x} \circ H_\lambda = \frac{v}{\lambda} \circ H_\lambda \\ \tilde{?} &= \tilde{v}_\theta + \tilde{v}\tilde{v}_x = (\frac{v_\theta}{\lambda} + \frac{v}{\lambda}\frac{\lambda v_x}{\lambda}) \circ H_\lambda = \frac{?}{\lambda} \circ H_\lambda \end{aligned}$$

We can write Equation 10.3 as

$$u_t = u_x F(?\,, v) = u_\theta G(\frac{?}{v}, v)$$

everywhere $u_\theta \neq 0$, and since the evolution commutes with H_λ, we have

$$\forall u, \lambda, \quad u_\theta G(\frac{?}{v}, v) = u_\theta G(\frac{?}{v}, \frac{v}{\lambda}).$$

Taking the limit $\lambda \to \infty$ proves that G cannot depend on its second argument. Besides, everywhere $u_\theta = 0$ we have

$$\forall u, \lambda, \quad u_x F(?\,, 0) = u_x F(\frac{?}{\lambda}, 0),$$

so that $F(?\,, 0) = F(0, 0)$. □

Proof of Theorem 9 :

If a multiscale analysis satisfies the axioms of Theorem 9, the corresponding evolution equation can be written in both forms given in Equation 10.9 and Equation 10.10. But the only common case is

$$u_t = -u_x ? = u_\theta \frac{?}{v} = u_{\xi\xi},$$

which is the announced equation. □

Conversely, we have to check that it is possible to define from Equation 10.2 a multiscale analysis of movies satisfying the previous axioms. This is the aim of the next chapter.

Chapter 11

The Depth-Compatible Multiscale Analysis

In this chapter, we give a rigorous definition for the DCMA Equation[1]

$$u_t = u_{\theta\theta} - 2\frac{u_\theta}{u_x}u_{\theta x} + (\frac{u_\theta}{u_x})^2 u_{xx}. \qquad (DCMA)$$

We define classical and weak solutions, and we establish uniqueness and existence theorems in both cases. We also establish the link with the theory of viscosity solutions of second order partial differential equations.

11.1 Classical solutions of the DCMA

For the reason we explained before, we forget the y variable in the following, and a movie is defined on $\mathbb{R} \times \overline{I}$, with either $I =]\theta_1, \theta_2[$ or $I = S^1$. In the space variable, a periodization has no meaning in terms of scene interpretation, so that we shall rather suppose that u tends towards some constant when x grows to infinity. Notice that such a condition is classical, even in a more restrictive formulation (e.g. u *equals* a constant outside a compact set, see [31] for example).

Definition 20 *For $c = (c^-, c^+) \in I\!R^2$ and $n \geqslant 0$, $\mathcal{C}_c^n$ is the space of movies $u \in C^n(I\!R \times I)$ such that*

$$\sup_{\theta \in \overline{I}} |u(-x, \theta) - c^-| + |u(x, \theta) - c^+| \to 0 \quad \text{as} \quad x \to +\infty. \qquad (11.1)$$

In all the following, we write $\Omega = \mathbb{R} \times I \times]0, +\infty[$ ($\overline{\Omega}$ is the domain of movie analyses).

Definition 21 *For $c \in I\!R^2$ and $n, p \geqslant 0$, $\mathcal{C}_c^{n,p}$ is the space of movie analyses $u \in C^0(\overline{\Omega})$ such that*

[1] The reason why we call this evolution equation DCMA (for Depth-Compatible Multiscale Analysis) will become clear in the next chapter.

1. $\sup_{\theta\in\overline{I},t\leqslant R} |u(-x,\theta,t)-c^-|+|u(x,\theta,t)-c^+|\to 0 \quad \text{as} \quad x\to+\infty,$

2. *on* Ω, $(x,\theta,t)\mapsto u(x,\theta,t)$ *is of class* C^n *with respect to* (x,θ) *and* C^p *with respect to* t.

When $c^-=c^+=0$, we shall say that u is "null at infinity".

Let us come back to our problem. We want to define classical solutions of Equation (DCMA). However, the space $\mathcal{M}^2$ we introduced in the axiomatic formulation is too restrictive, because of the condition $u_x\neq 0$. Indeed, this condition forces the partial maps $x\mapsto u(x,y,\theta)$ to be increasing or decreasing, which is not satisfactory, and prevents u from satisfying Equation 11.1 with $c^+=c^-$ (this is the reason why we did not constrain $c^+=c^-$ in the previous definitions : since we want the axiomatic formulation to be relevant, the space $\mathcal{M}^2$ must be nonempty). For those reasons, we forget the condition $u_x\neq 0$ and write a degenerate formulation of Equation (DCMA) when u_x vanishes.

Example : Consider $g\in C^2(\mathbb{R})$ such that $g(x)\to 0$ as $|x|\to+\infty$. We define the movie analysis $u:\mathbb{R}\times S^1\times[0,+\infty[\to\mathbb{R}$ by

$$u(x,\theta,t)=g(x-\theta^2-2t),$$

the representant of θ being taken in $[-\pi,\pi[$. Then, Equation (DCMA) is satisfied by u at any point where $u_x\neq 0$, and when $u_x=0$ we have also $u_t=0$. This suggests a simple degenerate formulation of Equation (DCMA) when u_x vanishes.

Incidentally, notice that $u\in\mathcal{C}_0^{2,2}$, but the condition

$$\sup_{\theta\in\overline{I},t\geqslant 0} |u(x,\theta,t)|\to 0 \quad \text{as} \quad |x|\to+\infty$$

is not satisfied unless $g\equiv 0$. This is the reason why it is logical to consider the sup on $\{\theta\in\overline{I},t\leqslant R\}$ in Condition 1 of Definition 21.

Definition 22 *Given* $u_0\in\mathcal{C}_c^0$, *we say that* u *is a classical solution of the DCMA associated to the initial datum* u_0 *if*

(i) $u\in\mathcal{C}_c^{2,1}$,

(ii) *on* $\Omega=\mathbb{R}\times I\times]0,+\infty[$,

$$\begin{cases} u_t=u_{\theta\theta}-2\dfrac{u_\theta}{u_x}u_{\theta x}+(\dfrac{u_\theta}{u_x})^2u_{xx} & \text{when} \quad u_x\neq 0,\\ \\ u_t=0 & \text{when} \quad u_x=0. \end{cases}$$

(iii) $\forall(x,\theta,t)\in\partial\Omega,\ \ u(x,\theta,t)=u_0(x,\theta)$.

Remark : If $I = S^1$, $\partial I = \emptyset$ and the boundary condition (iii) means

$$\forall (x,\theta) \in \mathbb{R} \times \overline{I}, \;\; u(x,\theta,0) = u_0(x,\theta).$$

If we choose to fix a time-boundary condition (i.e. $I =]\theta_1, \theta_2[$) instead of a time-periodicity condition, (iii) also constrains

$$\forall (x,t) \in \mathbb{R} \times [0,+\infty[, \;\; u(x,\theta_i,t) = u_0(x,\theta_i) \;\text{ for }\; i = 1,2$$

In order to state the uniqueness of solutions, we first establish a comparison principle.

Lemma 20 (comparison principle) *Suppose that u and $\tilde{u}$ are two classical solutions of the DCMA associated to initial data u_0 and $\tilde{u}_0$ respectively. If $u_0 \leqslant \tilde{u}_0$, then $u \leqslant \tilde{u}$ on Ω.*

Proof :

For $R > 0$, let us write

$$\varepsilon(R) = \sup_{|x| \geqslant R, \theta \in \overline{I}, t \leqslant R} u(x,\theta,t) - \tilde{u}(x,\theta,t).$$

Since u and $\tilde{u}$ belong to $\mathcal{C}^{2,1}_c$ and $\mathcal{C}^{2,1}_{\tilde{c}}$, we have

$$\varepsilon(R) \to \max(c^- - \tilde{c}^-, c^+ - \tilde{c}^+) \quad \text{as} \quad R \to +\infty,$$

with $c - \tilde{c} \leqslant 0$ because $u_0 \leqslant \tilde{u}_0$. For $\alpha > 0$, we consider

$$\Lambda(x,\theta,t) = u(x,\theta,t) - \tilde{u}(x,\theta,t) - \alpha t.$$

On the compact set $K_R = [-R,R] \times \overline{I} \times [0,R]$, the continuous map Λ attains its maximum value at a point $\boldsymbol{z}_0 = (x_0, \theta_0, t_0)$.

1. Suppose that

$$|x_0| < R, \quad \theta_0 \in I \quad \text{and} \quad t_0 \in]0,R]. \tag{11.2}$$

In $\boldsymbol{z}_0$ we have

$$\Lambda_x = \Lambda_\theta = 0, \quad \Lambda_t \geqslant 0 \quad \text{and} \quad D^2\Lambda \leqslant 0.$$

This yields

$$Du(\boldsymbol{z}_0) = D\tilde{u}(\boldsymbol{z}_0), \tag{11.3}$$

$$u_t(\boldsymbol{z}_0) - \tilde{u}_t(\boldsymbol{z}_0) \geqslant \alpha, \tag{11.4}$$

$$\text{and} \quad D^2u(\boldsymbol{z}_0) \leqslant D^2\tilde{u}(\boldsymbol{z}_0), \tag{11.5}$$

the last inequality being meant for the usual order on symmetric 2x2 matrices.

1.a. If $u_x(\boldsymbol{z}_0) \neq 0$, then $\tilde{u}_x(\boldsymbol{z}_0) = u_x(\boldsymbol{z}_0) \neq 0$. Now recall that

$$u_t = u_{\theta\theta} - 2\frac{u_\theta}{u_x}u_{\theta x} + (\frac{u_\theta}{u_x})^2 u_{xx} = F(D^2u, Du),$$

where F is an elliptic operator, that is to say nondecreasing with respect to its first argument. Hence, Equations 11.3 and 11.5 imply $u_t(\boldsymbol{z}_0) \leqslant \tilde{u}_t(\boldsymbol{z}_0)$, which is in contradiction with Equation 11.4.

1.b. If $u_x(\boldsymbol{z}_0) = 0$, then $\tilde{u}_x(\boldsymbol{z}_0) = 0$, and since u and $\tilde{u}$ are solutions of the DCMA, we have $u_t(z_0) = \tilde{u}_t(z_0) = 0$, which is a contradiction with Equation 11.4.

2. As a consequence of 1.a and 1.b, Assumption 11.2 is false and necessarily we have either $|x_0| = R$ or $\theta_0 \in \partial I$ or $t_0 = 0$. If $|x_0| = R$, then $\Lambda(x_0, \theta_0, t_0) \leqslant \varepsilon(R) + \alpha R$, while $\Lambda(x_0, \theta_0, t_0) \leqslant \alpha R$ when $\theta_0 \in \partial I$ or $t_0 = 0$. Consequently, we have

$$\max_{K_R} \Lambda \leqslant \max(0, \varepsilon(R)) + \alpha R,$$

and making $\alpha \to 0$ proves that

$$u \leqslant \tilde{u} + \max(0, \varepsilon(R)) \qquad \text{on} \quad \mathbb{R} \times \overline{I} \times [0, R].$$

Last, sending R to infinity forces $\max(0, \varepsilon(R))$ to vanish and the proof is complete. □

Corollary 9 (contraction property) *If u and $\tilde{u}$ are two classical solutions of the DCMA associated to the initial data u_0 and $\tilde{u}_0$, then*

$$\|u - \tilde{u}\|_\infty \leqslant \|u_0 - \tilde{u}_0\|_\infty.$$

Proof :

We simply need to notice that

$$u_0 - \|u_0 - \tilde{u}_0\|_\infty \leqslant \tilde{u}_0 \leqslant u_0 + \|u_0 - \tilde{u}_0\|_\infty,$$

and apply the comparison principle, remarking that if u is a classical solution of the DCMA, so is $u + \lambda$ for any $\lambda \in \mathbb{R}$. □

Corollary 10 (uniqueness) *A classical solution of the DCMA associated to a given initial datum $u_0 \in \mathcal{C}_c^2$ is unique.*

The proof follows immediatly from Corollary 9.

In order to ensure the existence of classical solutions of the DCMA, we now restrain the space of initial data.

Definition 23 *For $n \geqslant 1$, we write $\mathcal{V}_c^n$ the space of movies $u \in \mathcal{C}_c^n$ for which there exists a movie $v \in \mathcal{C}_0^{n-1}$ such that*

$$u_\theta + v u_x = 0 \quad \text{on} \quad I\!R \times \overline{I}. \tag{11.6}$$

v is called a velocity map of u.

The space $\mathcal{V}_c^{n,p}$ is defined as elements of $\mathcal{C}_c^{n,p}$ admitting a velocity map $v \in \mathcal{C}_0^{n-1,p}$.

Remark : Consider a movie $u \in \mathcal{V}_c^n$. If $u_x(x,\theta) \neq 0$, $v(x,\theta)$ is uniquely determined because Equation 11.6 forces

$$v(x,\theta) = -\frac{u_\theta}{u_x}(x,\theta).$$

But as we noticed previously, $u_x(x,\theta)$ is forced to vanish at least once for any value of θ, because

$$\lim_{|x| \to +\infty} u(x,\theta) = c.$$

When $u_x(x,\theta) = 0$, Equation 11.6 implies $u_\theta(x,\theta) = 0$, and if $n \geqslant 2$, differentiating Equation 11.6 with respect to θ and x yields

$$u_{\theta\theta}(x,\theta) + v(x,\theta) u_{x\theta}(x,\theta) = 0 \tag{11.7}$$

and

$$u_{\theta x}(x,\theta) + v(x,\theta) u_{xx}(x,\theta) = 0. \tag{11.8}$$

We deduce from Equation 11.7 and 11.8 that $u_{\theta\theta} + 2v u_{\theta x} + v^2 u_{xx} = 0$ as soon as $u_x = 0$.

A consequence is that if $u \in \mathcal{V}_c^{2,1}$ is a classical solution of the DCMA, then any velocity map v of u satisfies on Ω

$$\begin{cases} u_\theta + v u_x = 0 \\ \\ u_t = u_{\theta\theta} + v u_{\theta x} + v^2 u_{xx}. \end{cases} \tag{11.9}$$

□

Proposition 27 (existence) *Given an initial datum $u_0 \in \mathcal{V}_c^n$ ($n \geqslant 2$), there exists a unique classical solution of the DCMA, and it belongs to $\mathcal{V}_c^{n,n}$.*

Proof :

The existence will be a consequence of Lemma 22 (which follows), and the uniqueness follows from Corollary 10. □

We are going to build explicit solutions of the DCMA. The idea is to notice that the trajectories (i.e. the curves $x(\theta)$ along which u is constant) are smoothed by the linear heat equation. For that purpose, we need to introduce the natural domain $I^\star$ for such trajectories. If $I =]\theta_1, \theta_2[$ then $I^\star = I$, and if $I = S^1$, then $I^\star = I\!R$ (the natural injection $S^1 \hookrightarrow [0, 2\pi[\subset I\!R$ being implicit). To simplify the notations, we suppose in the following that $0 \in \overline{I}$.

Definition 24 *A map $\varphi \in C^n(\mathbb{R} \times I^\star)$ $(n \geqslant 0)$ is a* **θ-graph** *of $u \in \mathcal{C}_c^n$ if*

1. *for any $\theta \in \overline{I^\star}$, the map $x \mapsto \varphi(x,\theta)$ is increasing and bijective*
2. *for any $(x,\theta) \in \mathbb{R} \times \overline{I^\star}$,*
$$u(\varphi(x,\theta),\theta) = u(x,0), \tag{11.10}$$
3. *for any $x \in \mathbb{R}$, $\varphi(x,0) = x$, and if $I = S^1$, then for any $(x,\theta) \in \mathbb{R} \times \overline{I^\star}$,*
$$\varphi(x,\theta+2\pi) = \varphi(\varphi(x,2\pi),\theta), \tag{11.11}$$
4. $\sup_{|x| \geqslant R, \theta \in \overline{I}} |\varphi_\theta(x,\theta)| \to 0$ as $R \to +\infty$ *(in a generalized sense if $n = 0$).*

Remark : Notice that in Condition 4, the sup is taken for $\theta \in \overline{I}$ and not for $\theta \in \overline{I^\star}$. If $n = 0$, the term $|\varphi_\theta(x,\theta)|$ must be replaced by
$$\limsup_{h \to 0} |\frac{\varphi(x,\theta+h) - \varphi(x,\theta)}{h}|.$$
A simple proof by induction establishes that when $I = S^1$, Equation 11.11 implies
$$\varphi(x,\theta+2\pi n) = \varphi(\varphi(x,2\pi n),\theta)$$
for any $(x,\theta,n) \in \mathbb{R} \times \overline{I^\star} \times \mathbb{N}$.

Lemma 21 *A movie $u \in \mathcal{C}_c^n$ $(n \geqslant 2)$ belongs to $\mathcal{V}_c^n$ if and only if it admits a θ-graph of class C^n.*

Proof :

1. Suppose that u admits a θ-graph of class C^n. Then, Condition 1 implies that the relation
$$v(\varphi(x,\theta),\theta) = \varphi_\theta(x,\theta) \tag{11.12}$$
defines a unique continuous map v on $\mathbb{R} \times \overline{I}$ (if $I = S^1$, Equation 11.11 ensures the periodicity of v in the θ variable). We can write
$$\forall (x,\theta) \in \mathbb{R} \times I,\ \forall h \in \mathbb{R},\ \ v(\varphi(x,\theta) + h\varphi_x(x,\theta) + o(h),\theta) = \varphi_\theta(x,\theta) + h\varphi_{\theta x}(x,\theta) + o(h).$$
Since $\varphi_x(x,\theta) > 0$ a.e. due to Condition 1, we deduce that v is derivable with respect to x and
$$\varphi_x(x,\theta) v_x(\varphi(x,\theta),\theta) = \varphi_{\theta x}(x,\theta).$$
A similar reasoning proves that v is of class C^{n-1}. Differentiating Equation 11.10 with respect to θ yields
$$\forall (x,\theta) \in \mathbb{R} \times \overline{I},\quad \varphi_\theta(x,\theta) u_x(\varphi(x,\theta),\theta) + u_\theta(\varphi(x,\theta),\theta) = 0,$$

so that v is a velocity map of u thanks to Equation 11.12.

Now let us write diam (I) the diameter of I. Given $\varepsilon > 0$, Condition 4 ensures the existence of a $R > 0$ such that

$$\forall (x,\theta) \in \mathbb{R} \times \overline{I}, \qquad |x| \geqslant R \;\Rightarrow\; |\varphi_\theta(x,\theta)| \leqslant \varepsilon.$$

Hence, if $|x| \geqslant R' = R + \varepsilon \cdot \text{diam}\,(I)$ we have

$$\varphi(x,\theta) = \varphi(x,0) + \int_0^\theta \varphi_\theta(x,\tau)d\tau \geqslant x - \varepsilon|\theta| \geqslant R$$

and consequently

$$\sup_{|x|\geqslant R',\theta\in\overline{I}} |v(x,\theta)| \leqslant \varepsilon.$$

It follows that $v \in \mathcal{C}_0^{n-1}$ and the same reasoning proves that u is constant at infinity, so that $u \in \mathcal{V}_c^n$.

2. Conversely, if $u \in \mathcal{V}_c^n$, consider a velocity movie v of u. Given $(x_0,\theta_0) \in \mathbb{R} \times \overline{I}$, there exists a unique solution $X \in C^n(\overline{I^\star})$ of the ordinary differential equation

$$\frac{dX}{d\theta}(\theta) = v(X(\theta),\theta) \tag{11.13}$$

submitted to the condition $X(\theta_0) = x_0$. Since $v \in \mathcal{C}_0^{n-1}$, v is bounded, so that X is defined on the whole interval $\overline{I^\star}$. Call $\varphi(x_0,\theta)$ the solution X associated to $\theta_0 = 0$, and let $k = \text{diam}\,(I) \cdot \|v\|_\infty$. Then

$$\sup_{|x|\geqslant R,\theta\in\overline{I}} |\varphi_\theta(x,\theta)| \leqslant \sup_{|x|\geqslant R-k,\theta\in\overline{I}} |v(x,\theta)| \to 0 \quad \text{as} \quad R \to +\infty,$$

so that Condition 4 is satisfied for φ.

In addition, the uniqueness of the solutions constrains the relation

$$\text{if} \quad \theta = 0, \qquad x < x' \;\Rightarrow\; \varphi(x,\theta) < \varphi(x',\theta)$$

to extend to any value of θ, so that the map $x \mapsto \varphi(x,\theta)$ is increasing. Now, suppose that the value x_0 is not attained by the map $x \mapsto \varphi(x,\theta_0)$ for a given value θ_0. By considering the ODE 11.13 submitted to initial condition $X(\theta_0) = x_0$, we obtain the existence of a value $X(0)$ such that $\varphi(X(0),\theta_0) = x_0$, which is a contradiction. Hence, the map $x \mapsto \varphi(x,\theta_0)$ is surjective and Condition 1 is satisfied. If $I = S^1$, Equation 11.11 is satisfied by φ simply because v is 2π-periodic in the θ variable.

Last, a classical theorem (dependency with initial conditions, see [7] for example) states that φ is C^n and we can write

$$\frac{d}{d\theta}\left(u(\varphi(x,\theta),\theta)\right) = \varphi_\theta(x,\theta)u_x(\varphi(x,\theta),\theta) + u_\theta(\varphi(x,\theta),\theta) = \left(vu_x + u_\theta\right)(\varphi(x,\theta),\theta) = 0. \tag{11.14}$$

Then, integrating Equation 11.14 yields for any $(x,\theta) \in \mathbb{R} \times \overline{I}$,

$$u(\varphi(x,\theta),\theta) = u(\varphi(x,0),0) = u(x,0),$$

so that Condition 2 is satisfied and φ is a θ-graph of u of class C^n. □

Lemma 22 *Let $u_0 \in \mathcal{V}_c^n$ $(n \geqslant 2)$, and φ_0 be a θ-graph of u_0 of class C^n. Define $(x,\theta,t) \mapsto \varphi(x,\theta,t)$ as the unique solution of the monodimensional heat equation*

$$\frac{\partial \varphi}{\partial t} = \frac{\partial^2 \varphi}{\partial \theta^2} \tag{11.15}$$

on $\Omega^\star = I\!R \times I^\star \times]0,+\infty[$ submitted to the boundary condition

$$\forall (x,\theta,t) \in \partial\Omega^\star, \;\; \varphi(x,\theta,t) = \varphi_0(x,\theta). \tag{11.16}$$

Then, the unique map $u : \overline{\Omega} \to I\!R$ defined by

$$\forall (x,\theta,t) \in \overline{\Omega}, \;\; u(\varphi(x,\theta,t),\theta,t) = u_0(x,0) \tag{11.17}$$

belongs to $\mathcal{V}_c^{n,n}$ and is a classical solution of the DCMA associated to the initial datum u_0.

Proof :

1. Since the heat equation satisfies the comparison principle, the condition

$$x < x' \;\Rightarrow\; \varphi_0(x,\cdot) < \varphi_0(x',\cdot)$$

is preserved along evolution so that

$$x < x' \;\Rightarrow\; \forall \theta, t, \quad \varphi(x,\theta,t) < \varphi(x',\theta,t).$$

and $x \mapsto \varphi(x,\theta,t)$ is increasing as expected.

2. Now we prove that $x \mapsto \varphi(x,\theta,t)$ is surjective. Condition 4 of Definition 24 shows that we can find two constants A and B (with $B = 0$ if $I^\star$ is bounded) such that

$$|\varphi_0(x,\theta) - x| \leqslant A + B|\theta|$$

on $\mathbb{R} \times \overline{I}$. If $I = S^1$, Equation 11.11 extends this property to $\mathbb{R} \times \overline{I^\star}$. A simple result about the heat Equation (see appendix to follow) states that

$$\forall (x,\theta,t) \in \overline{\Omega^\star}, \quad |\varphi(x,\theta,t) - x| \leqslant A + B|\theta| + B\sqrt{\frac{4t}{\pi}}. \tag{11.18}$$

As a consequence, for any $(\theta,t) \in \overline{I} \times]0,+\infty[$, $x \mapsto \varphi(x,\theta,t)$ is surjective.

3. Hence, Equation 11.17 defines a unique map $u : \overline{\Omega} \to \mathbb{R}$ and a proof similar to the one of Lemma 21 shows that $u \in \mathcal{V}_c^{n,n}$ thanks to Equation 11.18.

4. We check the boundary condition. For any $(x,\theta,t) \in \partial\Omega$, due to Equation 11.16 we have

$$\varphi(x,\theta,t) = \varphi_0(x,\theta),$$

while the definition of u (Equation 11.17) implies

$$u(\varphi(x,\theta,t),\theta,t) = u_0(x,0) = u_0(\varphi_0(x,\theta),\theta),$$

and consequently

$$u(\varphi_0(x,\theta),\theta,t) = u_0(\varphi_0(x,\theta),\theta).$$

Hence, the boundary condition (iii) of Definition 22 is satisfied since the map

$$\begin{array}{ccc} \partial\Omega & \rightarrow & \partial\Omega \\ (x,\theta,t) & \mapsto & (\varphi_0(x,\theta),\theta,t) \end{array}$$

is bijective.

5. Let us note $\boldsymbol{z}_1 = (\varphi(\boldsymbol{z}),\theta,t)$ for a given $\boldsymbol{z} \in \Omega$. If $u_x(\boldsymbol{z}_1) = 0$, differentiating Equation 11.17 with respect to t yields

$$\varphi_t(\boldsymbol{z})u_x(\boldsymbol{z}_1) + u_t(\boldsymbol{z}_1) = u_t(\boldsymbol{z}_1) = 0$$

as expected. If $u_x(\boldsymbol{z}_1) \neq 0$, we obtain

$$u_t(\boldsymbol{z}_1) = -\varphi_t(\boldsymbol{z})u_x(\boldsymbol{z}_1),$$

$$\text{and} \qquad \frac{d}{d\theta}(u_0(x,0)) = 0 = \varphi_\theta(\boldsymbol{z})u_x(\varphi(\boldsymbol{z}),\theta,t) + u_\theta(\varphi(\boldsymbol{z}),\theta,t),$$

as well as

$$\begin{aligned} 0 &= \frac{d^2}{d\theta^2}(u_0(x,0)) \\ &= \frac{d}{d\theta}\left(\varphi_\theta(\boldsymbol{z})u_x(\varphi(\boldsymbol{z}),\theta,t) + u_\theta(\varphi(\boldsymbol{z}),\theta,t)\right) \\ &= \varphi_{\theta\theta}(\boldsymbol{z})u_x(\varphi(\boldsymbol{z}),\theta,t) + \varphi_\theta^2(\boldsymbol{z})u_{xx}(\varphi(\boldsymbol{z}),\theta,t) + 2\varphi_\theta(\boldsymbol{z})u_{x\theta}(\varphi(\boldsymbol{z}),\theta,t) + u_{\theta\theta}(\varphi(\boldsymbol{z}),\theta,t) \\ &= \varphi_t(\boldsymbol{z})u_x(\boldsymbol{z}_1) + \varphi_\theta^2(\boldsymbol{z})u_{xx}(\boldsymbol{z}_1) + 2\varphi_\theta(\boldsymbol{z})u_{x\theta}(\boldsymbol{z}_1) + u_{\theta\theta}(\boldsymbol{z}_1) \\ &= \left(-u_t + u_{\theta\theta} - 2\frac{u_\theta}{u_x}u_{\theta x} + (\frac{u_\theta}{u_x})^2 u_{xx}\right)(\boldsymbol{z}_1), \end{aligned}$$

so that condition (ii) of Definition 22 is satisfied. Hence, u is a classical solution of the DCMA associated to the initial datum u_0. □

Lemma 22 proves that the DCMA Equation is a scalar formulation of the monodimensional heat equation (11.15), like two other important equations of image processing : the Mean Curvature Motion and the Affine Morphological Scale Space. The difference between them only comes from the intrinsic parameter of the level lines : the Euclidean abscissa for the Mean Curvature Motion, the affine abscissa for the Affine Scale space. For the DCMA, the natural parameter is the time θ, which means that level lines are not considered as curves but as **graphs**. This remark will permit to prove the existence of weak solutions for the DCMA, but in certain cases only, namely, when the level lines of the initial datum can be described by graphs.

11.2 Weak solutions of the DCMA

We define weak (only continuous) solutions of the DCMA as uniform limits of classical solutions.

Definition 25 *Given a movie $u_0 \in \mathcal{C}_c^0$, we say that a map $u \in \mathcal{C}_c^{0,0}$ is a weak solution of the DCMA associated to the initial datum u_0 if*

$$\forall (x,\theta,t) \in \partial\Omega, \quad u(x,\theta,t) = u_0(x,\theta)$$

and if there exists a sequence $(u^\varepsilon)_{\varepsilon>0}$ of classical solutions of the DCMA such that $u^\varepsilon \to u$ uniformly on $\overline{\Omega}$ when $\varepsilon \to 0$.

Lemma 23 (uniqueness) *A weak solution of the DCMA associated to a given initial datum is unique.*

Proof :

We simply prove that the contraction property (Corollary 9) is still satisfied. Let u and $\tilde{u}$ be two weak solutions of the DCMA associated to the initial data u_0 and $\tilde{u}_0$. Then, we can find two sequences u^ε and $\tilde{u}^\varepsilon$ which converge uniformly towards u and $\tilde{u}$. Writing $u_0^\varepsilon = u^\varepsilon(\cdot,\cdot,0)$ and $\tilde{u}_0^\varepsilon = \tilde{u}^\varepsilon(\cdot,\cdot,0)$, Corollary 9 ensures that

$$\|u^\varepsilon - \tilde{u}^\varepsilon\|_\infty \leqslant \|u_0^\varepsilon - \tilde{u}_0^\varepsilon\|,$$

and taking the (uniform) limits when $\varepsilon \to 0$ yields

$$\|u - \tilde{u}\|_\infty \leqslant \|u_0 - \tilde{u}_0\|$$

as expected. □

Proposition 28 (existence) *Call $\overline{\mathcal{V}_c}$ the topological closure of $\mathcal{V}_c^2$ with respect to the $\|\cdot\|_\infty$ norm. Then, given $u_0 \in \overline{\mathcal{V}_c}$, there exists a unique weak solution u of the DCMA associated to the initial datum u_0.*

Proof :

According to the hypothesis on u_0, we can find a sequence $u_0^\varepsilon \in \mathcal{V}_c^2$ which converges uniformly towards u_0. Then, call u^ε the classical solution of the DCMA associated to the initial datum u_0^ε (Proposition 27 ensures the existence of u^ε). Lemma 20 forces u^ε to converge uniformly towards a limit $u \in \mathcal{C}_c^{0,0}$, which is by construction a weak solution of the DCMA. □

To make more precise this existence property, we now build explicit weak solutions. The construction is similar to the one used for classical solutions in the proof of Lemma 22.

Definition 26 *We write $\mathcal{V}_c^0$ the space of movies $u \in \mathcal{C}_c^0$ which admit a continuous θ-graph.*

This generalizes Definition 23 thanks to Lemma 21.

Proposition 29 *Let $u_0 \in \mathcal{V}_c^0$, and φ_0 be a θ-graph of u_0. Define $(x,\theta,t) \mapsto \varphi(x,\theta,t)$ as the unique solution of the monodimensional heat equation 11.15 submitted to the boundary condition 11.16. Then, the unique map u defined from φ by Equation 11.17 is a weak solution of the DCMA.*

Proof :

1. As for the definition of u and its belonging to $\mathcal{C}_c^{0,0}$, the proof is already contained in Lemma 22.

2. Since $\mathcal{V}_c^0 \subset \overline{\mathcal{V}_c}$, we can consider $\tilde{u}$ the weak solution of the DCMA associated to the initial datum u_0, and (u^ε) a sequence of classical solutions which converges uniformly towards $\tilde{u}$. Now we want to prove that $u = \tilde{u}$, or, equivalently, that

$$\forall (x,\theta,t) \in \overline{\Omega},\ \ \tilde{u}(\varphi(x,\theta,t),\theta,t) = u_0(x,0).$$

Given $x_0 \in \mathbb{R}$, $\varepsilon > 0$, $\alpha > 0$ and $T > 0$, define

$$\Lambda(\theta,t) = u^\varepsilon(\varphi(x_0,\theta,t),\theta,t) - u_0(x_0,0) - \alpha t.$$

Since Λ is continuous on the compact set $K_T = \overline{I} \times [0,T]$, there exists $(\theta_0,t_0) \in K_T$ such that

$$\max_{K_T} \Lambda = \Lambda(\theta_0,t_0).$$

2.a. Suppose that

$$\theta_0 \in I \quad \text{and} \quad t_0 > 0. \tag{11.19}$$

Then, in (θ_0,t_0) we have

$$\Lambda_t \geqslant 0, \quad \Lambda_\theta = 0 \quad \text{and} \quad \Lambda_{\theta\theta} \leqslant 0.$$

This yields

$$\varphi_t u_x^\varepsilon + u_t^\varepsilon \geqslant \alpha, \tag{11.20}$$

$$\varphi_\theta u_x^\varepsilon + u_\theta^\varepsilon = 0, \tag{11.21}$$

$$\text{and} \quad \varphi_\theta^2 u_{xx}^\varepsilon + 2\varphi_\theta u_{\theta x}^\varepsilon + u_{\theta\theta}^\varepsilon + \varphi_{\theta\theta} u_x^\varepsilon \leqslant 0. \tag{11.22}$$

If $u_x^\varepsilon = 0$, then $u_t^\varepsilon = 0$, which is in contradiction with Equation 11.20. If $u_x^\varepsilon \neq 0$, since $\varphi_t = \varphi_{\theta\theta}$ and u^ε is a classical solution of the DCMA, Equation 11.21 and 11.22 imply

$$u_t^\varepsilon + \varphi_t u_x^\varepsilon \leqslant 0,$$

which contradicts Equation 11.20 as well.

2.b. Hence, Assumption 11.19 is false and we have either $\theta_0 \in \partial I$ or $t_0 = 0$, so that $\varphi(x_0, \theta_0, t_0) = \varphi_0(x_0, \theta_0)$. Writing $u_0^\varepsilon = u^\varepsilon(\cdot, \cdot, 0)$, we get

$$\begin{aligned} u^\varepsilon(\varphi(x_0, \theta_0, t_0), \theta_0, t_0) &= u_0^\varepsilon(\varphi_0(x_0, \theta_0), \theta_0) \\ &\leqslant u_0(\varphi_0(x_0, \theta_0), \theta_0) + \|u_0^\varepsilon - u_0\|_\infty \\ &\leqslant u_0(x_0, 0) + \|u_0^\varepsilon - u_0\|_\infty, \end{aligned}$$

so that

$$\forall (x, \theta, t) \in \mathbb{R} \times K_T, \qquad u^\varepsilon(\varphi(x, \theta, t), \theta, t) \leqslant u_0(x, 0) + \alpha T + \|u_0^\varepsilon - u_0\|_\infty.$$

Then, sending α to zero and T to infinity yields

$$\forall (x, \theta, t) \in \overline{\Omega}, \qquad u^\varepsilon(\varphi(x, \theta, t), \theta, t) \leqslant u_0(x, 0) + \|u_0^\varepsilon - u_0\|_\infty,$$

and passing to the limit when $\varepsilon \to 0$ establishes

$$\forall (x, \theta, t) \in \overline{\Omega}, \qquad \tilde{u}(\varphi(x, \theta, t), \theta, t) \leqslant u_0(x, 0).$$

A symmetrical reasoning proves that $\tilde{u}(\varphi(x, \theta, t), \theta, t) \geqslant u_0(x, 0)$ as well, so that $u = \tilde{u}$ as announced. □

A consequence of this characterization of weak solutions is that a weak solution of the DCMA associated to an initial datum $u_0 \in \mathcal{V}_c^n$ admits a kind of velocity movie as soon as u_0 is locally Lipschitz in the x variable. To simplify the proof, we directly assume that the whole analysis u is locally Lipschitz in the x variable, although it is not difficult to see that u inherits this property from the initial datum u_0.

Corollary 11 *Let u be the weak solution of the DCMA associated to an initial datum $u_0 \in \mathcal{V}_c^0$. If u is locally Lipschitz in the x variable, then there exists a continuous map v defined on $\Omega = \mathbb{R} \times I \times]0, +\infty[$ such that on Ω,*

$$u(x + \tau v(x, \theta, t), \theta + \tau, t) = u(x, \theta, t) + o(\tau) \tag{11.23}$$

$$\text{and} \quad u(x + \tau v(x, \theta, t), \theta + \tau, t - \frac{\tau^2}{2}) = u(x, \theta, t) + o(\tau^2). \tag{11.24}$$

Proof :

We associate φ to u_0 as in Proposition 29, and define v by Equation 11.12. Then,

$$\begin{aligned} u_0(x, 0) &= u\left(\varphi(x, \theta + \tau, t), \theta + \tau, t\right) \\ &= u\left(\varphi(x, \theta, t) + \tau \varphi_\theta(x, \theta, t) + o(\tau), \theta + \tau, t\right) \\ &= u\left(\varphi(x, \theta, t) + \tau v(\varphi(x, \theta, t), \theta, t), \theta + \tau, t\right) + o(\tau), \end{aligned}$$

which establishes the first equality. For the second one, we write

$$\begin{aligned} u_0(x,0) &= u\left(\varphi(x,\theta+\tau,t-\frac{\tau^2}{2}),\theta+\tau,t-\frac{\tau^2}{2}\right) \\ &= u\left(\varphi(x,\theta,t)+\tau\varphi_\theta(x,\theta,t)+o(\tau^2),\theta+\tau,t-\frac{\tau^2}{2}\right) \\ &= u\left(\varphi(x,\theta,t)+\tau v(\varphi(x,\theta,t),\theta,t),\theta+\tau,t-\frac{\tau^2}{2}\right)+o(\tau^2) \end{aligned}$$

and the proof is complete. □

Remark : Defining the Lie derivative of a map f along the vector $\xi=(v,1)$ by

$$f_\xi(x,\theta,t)=\left(\frac{d}{d\tau}f(x+\tau v(x,\theta,t),\theta+\tau,t)\right)_{\tau=0},$$

Equation 11.24 is equivalent to $u_\xi=0$. As concerns Equation 11.24, it implies

$$\left(\frac{d^{[2]}}{d\tau^2}u(x+\tau v(x,\theta,t),\theta+\tau,t-\frac{\tau^2}{2})\right)_{\tau=0}=0,$$

where the notation $d^{[2]}f/d\tau^2$ means the pseudo-second derivative of f, defined in x by

$$\frac{d^{[2]}f}{dx^2}(x)=\lim_{h\to 0}\frac{f(x+h)+f(x-h)-2f(x)}{h^2}.$$

Notice that this property is a generalization of Equation 11.9.

11.3 A viscosity formulation

We now establish the link between our definition of weak solutions and the theory of viscosity solutions (see [27] for further details on viscosity solutions). For the DCMA, defining viscosity solutions is not necessary because smooth movies remain smooth, which permits the previous construction of weak solutions as uniform limits of smooth solutions. However, this is not generally the case with non-linear parabolic PDE of the kind

$$\frac{\partial u}{\partial t}=F(D^2u,Du,u)$$

defined from an elliptic operator F (consider the Mean Curvature Motion or the Affine Morphological Scale Space for example). Moreover, it is convenient to define weak solutions intrinsically, without using limits of regular solutions. In the following, we give a reasonable definition of a viscosity solution of the DCMA, and prove that a weak solution is a viscosity solution.

Definition 27 *A bounded continuous map $u:\overline{\Omega}\to\mathbb{R}$ is a viscosity subsolution of the DCMA if for any $\phi\in C^\infty(\overline{\Omega})$, at any point $z_0\in\Omega$ where $u-\phi$ attains a local maximum, we have*

(i) If $\phi_x \neq 0$, *then* $\phi_t \leqslant \phi_{\theta\theta} - 2\frac{\phi_\theta}{\phi_x}\phi_{\theta x} + (\frac{\phi_\theta}{\phi_x})^2\phi_{xx}$,

(ii) If $\phi_x = 0$, *then* $\phi_\theta = \phi_t = 0$ *and* $\exists\lambda \in \mathbb{R}$ *such that* $0 \leqslant \phi_{\theta\theta} + 2\lambda\phi_{\theta x} + \lambda^2\phi_{xx}$.

Condition (i) is the classical formulation of viscosity subsolutions, whereas (ii) is a degenerate condition particular to the DCMA (see [31], [9] for examples of degenerate viscosity solutions in the case of the Mean Curvature Motion).

The definition of a supersolution is symmetrical :

Definition 28 *A bounded continuous map* $u : \overline{\Omega} \to \mathbb{R}$ *is a viscosity supersolution of the DCMA if for any* $\phi \in C^\infty(\overline{\Omega})$, *at any point* $\boldsymbol{z}_0 \in \Omega$ *where* $u - \phi$ *attains a local minimum, we have*

(i') If $\phi_x \neq 0$, *then* $\phi_t \geqslant \phi_{\theta\theta} - 2\frac{\phi_\theta}{\phi_x}\phi_{\theta x} + (\frac{\phi_\theta}{\phi_x})^2\phi_{xx}$,

(ii') If $\phi_x = 0$, *then* $\phi_\theta = \phi_t = 0$ *and* $\exists\lambda \in \mathbb{R}$ *such that* $0 \geqslant \phi_{\theta\theta} + 2\lambda\phi_{\theta x} + \lambda^2\phi_{xx}$.

We give the following equivalent definition of a subsolution for completeness.

Proposition 30 *A bounded continuous map* $u : \overline{\Omega} \to \mathbb{R}$ *is a viscosity subsolution of the DCMA if for any* $(\boldsymbol{p}, A) \in \mathbb{R}^3 \times S_3$ *and* $\boldsymbol{z}_0 \in \Omega$ *such that*

$$u(\boldsymbol{z}) \leqslant u(\boldsymbol{z}_0) + \boldsymbol{p}\cdot(\boldsymbol{z}_0 - \boldsymbol{z}) + [A](\boldsymbol{z}_0 - \boldsymbol{z}, \boldsymbol{z}_0 - \boldsymbol{z}) + o(|\boldsymbol{z}_0 - \boldsymbol{z}|^2) \quad \text{as} \quad \boldsymbol{z} \to \boldsymbol{z}_0,$$

we have, writing $\boldsymbol{p} = (p_i)$ *and* $A = [a_{ij}]$,

(i) If $p_1 \neq 0$, *then* $p_3 \leqslant a_{22} - 2\frac{p_2}{p_1}a_{21} + (\frac{p_2}{p_1})^2 a_{11}$,

(ii) If $p_1 = 0$, *then* $p_2 = p_3 = 0$ *and* $\exists\lambda \in \mathbb{R}$ *such that* $0 \leqslant a_{22} + 2\lambda a_{21} + \lambda^2 a_{11}$.

The equivalent definition for supersolutions is straightforward.

Definition 29 *A bounded continuous map* $u : \overline{\Omega} \to \mathbb{R}$ *is a viscosity solution of the DCMA if it is both a viscosity super-solution and a viscosity sub-solution.*

Proposition 31 *Given an initial datum* $u_0 \in \mathcal{V}_c^0$, *the unique weak solution of the DCMA is a viscosity solution.*

Proof :

Let u be the weak solution of the DCMA associated to the initial datum u_0. We prove that u is a viscosity subsolution of the DCMA. Consider $\phi \in C^\infty(\overline{\Omega})$, and suppose that $u - \phi$ attains a local maximum in $\boldsymbol{z}_0 = (x_0, \theta_0, t_0) \in \Omega$. Let φ be the map defined from u_0 as in Proposition

29, and define $\boldsymbol{z}_1 = (x_1, \theta_0, t_0)$ by $\varphi(\boldsymbol{z}_1) = x_0$. Then, for b and c in a vicinity of 0 (actually such that $\theta_0 + b \in I$ and $t_0 + c > 0$),

$$u(\varphi(x_1, \theta_0 + b, t_0 + c), \theta_0 + b, t_0 + c) = u_0(x_1, 0) = u(\varphi(x_1, \theta_0, t_0), \theta_0, t_0) = u(\boldsymbol{z}_0).$$

We can estimate

$$\begin{aligned} a(b,c) &:= \varphi(x_1, \theta_0 + b, t_0 + c) - x_0 \\ &= \varphi(x_1, \theta_0 + b, t_0 + c) - \varphi(x_1, \theta_0, t_0) \\ &= b\varphi_\theta(\boldsymbol{z}_1) + \frac{b^2}{2}\varphi_{\theta\theta}(\boldsymbol{z}_1) + c\varphi_t(\boldsymbol{z}_1) + o(b^2 + c) \end{aligned}$$

as $b, c \to 0$. Now, since $u - \phi$ attains a local maximum in $\boldsymbol{z}_0$ and

$$u(x_0 + a(b,c), \theta_0 + b, t_0 + c) - u(x_0, \theta_0, t_0) = 0,$$

we have

$$\begin{aligned} 0 &\leqslant \phi(x_0 + a(b,c), \theta_0 + b, t_0 + c) - \phi(x_0, \theta_0, t_0) \\ &\leqslant a(b,c)\phi_x(\boldsymbol{z}_0) + b\phi_\theta(\boldsymbol{z}_0) + c\phi_t(\boldsymbol{z}_0) + \frac{a^2(b,c)}{2}\phi_{xx}(\boldsymbol{z}_0) + ba(b,c)\phi_\theta(\boldsymbol{z}_0) + \frac{b^2}{2}\phi_{\theta\theta}(\boldsymbol{z}_0) + o(b^2 + c) \\ &\leqslant \left(b\varphi_\theta(\boldsymbol{z}_1) + \frac{b^2}{2}\varphi_{\theta\theta}(\boldsymbol{z}_1) + c\varphi_t(\boldsymbol{z}_1)\right)\phi_x(\boldsymbol{z}_0) + b\phi_\theta(\boldsymbol{z}_0) + c\phi_t(\boldsymbol{z}_0) + \frac{b^2}{2}\varphi_\theta^2(\boldsymbol{z}_1)\phi_{xx}(\boldsymbol{z}_0) \\ &\quad + b^2\varphi_\theta(\boldsymbol{z}_1)\phi_{\theta x}(\boldsymbol{z}_0) + \frac{b^2}{2}\phi_{\theta\theta}(\boldsymbol{z}_0) + o(b^2 + c). \end{aligned}$$

Necessarily, both factors of b and c must be zero and the factor of b^2 must be nonnegative. This yields

$$\varphi_\theta(\boldsymbol{z}_1)\phi_x(\boldsymbol{z}_0) + \phi_\theta(\boldsymbol{z}_0) = 0, \tag{11.25}$$

$$\varphi_t(\boldsymbol{z}_1)\phi_x(\boldsymbol{z}_0) + \phi_t(\boldsymbol{z}_0) = 0, \tag{11.26}$$

$$\text{and} \quad \varphi_{\theta\theta}(\boldsymbol{z}_1)\phi_x(\boldsymbol{z}_0) + \varphi_\theta^2(\boldsymbol{z}_1)\phi_{xx}(\boldsymbol{z}_0) + 2\varphi_\theta(\boldsymbol{z}_1)\phi_{\theta x}(\boldsymbol{z}_0) + \phi_{\theta\theta}(\boldsymbol{z}_0) \geqslant 0, \tag{11.27}$$

but as $\varphi_t(\boldsymbol{z}_1) = \varphi_{\theta\theta}(\boldsymbol{z}_1)$, Equation 11.26 and 11.27 imply

$$\phi_t(\boldsymbol{z}_0) \leqslant \varphi_\theta^2(\boldsymbol{z}_1)\phi_{xx}(\boldsymbol{z}_0) + 2\varphi_\theta(\boldsymbol{z}_1)\phi_{\theta x}(\boldsymbol{z}_0) + \phi_{\theta\theta}(\boldsymbol{z}_0). \tag{11.28}$$

1. If $\phi_x(\boldsymbol{z}_0) \neq 0$, Equation 11.25 gives

$$\varphi_\theta(\boldsymbol{z}_1) = -\frac{\phi_\theta}{\phi_x}(\boldsymbol{z}_0)$$

and Equation 11.28 leads to the desired condition (i).

2. If $\phi_x(\boldsymbol{z}_0) = 0$, then $\phi_\theta = \phi_t(\boldsymbol{z}_0) = 0$ is a consequence of Equation 11.25 and 11.26, while Equation 11.28 implies that the polynomial

$$X \mapsto X^2\phi_{xx}(\boldsymbol{z}_0) + 2X\phi_{\theta x}(\boldsymbol{z}_0) + \phi_{\theta\theta}(\boldsymbol{z}_0)$$

takes at least one nonnegative value, which is the desired condition (ii).

Consequently, u is a viscosity subsolution of the DCMA. A symmetrical reasoning shows that it is a viscosity supersolution as well. □

We conjecture that a viscosity solution associated to a given initial datum is unique. In particular, this would imply that the viscosity and the weak solutions of the DCMA are the same, provided that the initial datum u_0 lies in $\mathcal{V}_c^0$.

11.4 Appendix on the heat equation

In the previous section, we used several results about the monodimensional heat equation. For completeness, we briefly recall them. In all the following, either $J =]\theta_1, \theta_2[$ or $J = \mathbb{R}$, and $\Omega = J \times]0, +\infty[$.

Proposition 32 *Given a continuous map $f : \overline{J} \to I\!R$ such that*

$$\exists A, B,\ \forall \theta \in \overline{J}, \quad |f(\theta)| \leqslant A + B|\theta|, \tag{11.29}$$

there exists a unique continuous map $\varphi : \overline{\Omega} \to I\!R$ such that

(i) on Ω, $(\theta, t) \mapsto \varphi(\theta, t)$ is C^2 with respect to θ and C^1 with respect to t,

(ii) on Ω, $\dfrac{\partial \varphi}{\partial t} = \dfrac{\partial^2 \varphi}{\partial \theta^2}$,

(iii) for any $(\theta, t) \in \partial\Omega$, $\varphi(\theta, t) = f(\theta)$

(iv) $\forall T > 0$, $\exists A, B$, $\forall (\theta, t) \in \overline{J} \times [0, T]$, $\quad |\varphi(\theta, t)| \leqslant A + B|\theta|$.

Remark : If J is bounded, then Equation 11.29 simply means that f is bounded, and Condition (iv) means that φ is bounded too. If $J = \mathbb{R}$, f and φ are constrained to be "sub-linear" in the θ variable.

We give a quick justification of Proposition 32 since the heat equation is generally considered for bounded maps in the literature. (see [16] for example). As for the uniqueness, it results from the following comparison principle.

Proposition 33 (comparison principle) *Consider φ a solution of the heat equation (in the sense of Proposition 32) associated to the initial datum $f \leqslant 0$. Then, $\varphi \leqslant 0$.*

Proof :

Suppose first that $J = \mathbb{R}$. Given $T > 0$, there exists A, B such that

$$\forall (\theta, t) \in \overline{J} \times [0, T], \quad \varphi(\theta, t) - A - B|\theta| \leqslant 0. \tag{11.30}$$

For $R > 0$ fixed, we consider the map

$$\Lambda(\theta, t) = \varphi(\theta, t) - (\frac{A}{R^2} + \frac{B}{R})(\theta^2 + 2t).$$

Λ satisfies the heat equation, and the maximum principle (see [16] for example) tells that

$$\max_{[-R,R]\times[0,T]} \Lambda = \max_{[-R,R]\times\{0\}\cup\{-R,R\}\times[0,T]} \Lambda.$$

On $[-R, R] \times \{0\}$, $\Lambda \leqslant 0$ because $f \leqslant 0$, while Equation 11.30 yields $\Lambda \leqslant 0$ on $\{-R, R\} \times [0, T]$. Hence, we have

$$\forall (\theta, t) \in [-R, R] \times [0, T], \quad \varphi(\theta, t) \leqslant (\frac{A}{R^2} + \frac{B}{R})(\theta^2 + 2t).$$

Sending R to infinity yields

$$\forall (\theta, t) \in \overline{J} \times [0, T], \quad \varphi(\theta, t) \leqslant 0, \tag{11.31}$$

so that $\varphi \leqslant 0$ on $\overline{J} \times [0, +\infty[$. If J is bounded, Equation 11.31 is a direct consequence of the maximum principle applied to φ, and the conclusion still holds. □

Now we give an explicit construction of solutions. If $J = \mathbb{R}$, the solution is given by the convolution with the Gaussian kernel :

$$\varphi(\theta, t) = \int_{-\infty}^{+\infty} f(\theta - \alpha) \frac{1}{\sqrt{4\pi t}} e^{-\alpha^2/4t} d\alpha.$$

If $J =]\theta_1, \theta_2[$, we write $\tilde{f}(\theta) = f(\theta) - l(\theta)$, where l is the unique affine map which forces $\tilde{f}(\theta_1) = \tilde{f}(\theta_2) = 0$. Then, we extend $\tilde{f}$ to an odd and $2(\theta_2 - \theta_1)$-periodic map and apply the previous convolution formula. This way, we obtain a map $\tilde{\varphi}$ which satisfies conditions (i), (ii) and (iv) as well as $\tilde{\varphi}(\theta_1, t) = \tilde{\varphi}(\theta_2, t) = 0$ for any $t \geqslant 0$. Last, the map

$$\begin{aligned} \varphi \quad : \quad & \overline{J} \times [0, +\infty[\to \mathbb{R} \\ & (\theta, t) \mapsto \tilde{\varphi}(\theta, t) + l(\theta) \end{aligned}$$

satisfies the desired conditions (i), (ii), (iii) and (iv).

Proposition 34 *Here we suppose $J = \mathbb{R}$. If f satisfies*

$$\forall \theta \in \mathbb{R}, \quad |f(\theta)| \leqslant A + B|\theta|,$$

then the solution φ of the heat equation with initial datum f satisfies

$$\forall (\theta, t) \in \mathbb{R} \times [0, +\infty[, \quad |\varphi(\theta, t)| \leqslant A + B|\theta| + B\sqrt{\frac{4t}{\pi}}.$$

Proof :

Calling G_t the Gaussian kernel, we have

$$|\varphi(\theta,t)| \leqslant \int_{-\infty}^{+\infty} |f(\theta-\alpha)| G_t(\alpha) d\alpha \leqslant \int_{-\infty}^{+\infty} (A + B|\theta| + B|\alpha|) G_t(\alpha) d\alpha,$$

and the announced result is a consequence of the equalities

$$\int_{-\infty}^{+\infty} G_t(\alpha) d\alpha = 1 \quad \text{and} \quad \int_{-\infty}^{+\infty} |\alpha| G_t(\alpha) d\alpha = \sqrt{\frac{4t}{\pi}}.$$

□

11.5 Further existence properties

In the previous sections, we did not prove the existence of (weak or classical) solutions of the DCMA in the general case, that is to say when the initial datum admits no θ-graph. In fact, we do not believe that the DCMA admits a solution in general, at least a solution in the sense we defined.

When the initial datum u_0 admits a θ-graph, the DCMA is obtained by applying the linear monodimensional heat equation to the level lines of u_0. For an ordinary continuous map u_0, the level lines have no reason to be graphs in the θ variable, since to a given value of θ, several values of x will correspond in general. Hence, defining general solutions of the DCMA is somewhat equivalent to defining solutions of the heat equation for multi-valued data. It is in that spirit that L.C.Evans studied independently Equation 10.2 in his article "A geometric Interpretation of the Heat Equation with Multivalued Initial Data" (see [32]). He regards the DCMA Equation as the limit when $\varepsilon \to 0$ of the more regular equation

$$u_t = \frac{u_x^2 u_{\theta\theta} - 2u_x u_\theta u_{x\theta} + u_\theta^2 u_{xx}}{u_x^2 + \varepsilon^2 u_\theta^2}. \tag{11.32}$$

Equation 11.32 admits viscosity solutions because it is more or less the Mean Curvature Motion (actually, the case $\varepsilon = 1$ is exactly the Mean Curvature Motion). He noticed that in the general case (that is, when the level lines of the initial datum are not graphs), the regularizing effects of the heat equation are so strong that the limit of approximate solutions is not continuous at scale $t = 0$, because the level lines are constrained to become graphs instantaneously. It seems difficult to overcome this difficulty unless we allow solutions of the DCMA not to be continuous at scale $t = 0$. In fact, it might be possible to define a kind of projection operator which makes the level lines of a movie unfold and become graphs. We shall come back to this when studying a numerical scheme in Chapter 13.

Chapter 12

Properties of the DCMA

In this chapter, we investigate several properties of the DCMA. We first check the ones that are constrained by the axiomatic formulation, and then we prove that the DCMA acts as a strong smoothing process along the movement. We also establish integral estimations and try to associate the DCMA to a variational principle. Coming back to the original context of depth interpretation, we finally highlight geometrical properties and find a new characterization of the DCMA.

12.1 Checking the axioms

In order to be sure that our axiomatic formulation is consistent, we have to check that the axioms we introduced are satisfied by the DCMA. As regards the three architectural axioms ([**Recursivity**], [**Local Comparison Principle**] and [**Regularity**]), they are direct consequences of the fact that the DCMA is given by an evolution equation

$$u_t = F(D^2u, Du),$$

where F is an elliptic operator. Now we prove that the DCMA satisfies the [**Strong Morphological Invariance**] property.

Proposition 35 *Let u be a weak solution of the DCMA and $g : \mathbb{R} \mapsto \mathbb{R}$ a continuous map. Then, $g \circ u$ is a weak solution of the DCMA.*

Proof :

Notice that this proposition makes sense because if $u \in \mathcal{C}_c^0$, then $g \circ u \in \mathcal{C}_{\tilde{c}}^0$ with

$$\tilde{c} = (g(c^-), g(c^+)).$$

1. First, suppose that u is a classical solution of the DCMA and that g is of class C^2. Writing $\tilde{u} = g \circ u$, a simple computation gives

$$\tilde{u}_x = (g' \circ u) \cdot u_x, \quad \tilde{u}_t = (g' \circ u) \cdot u_t,$$

and

$$\begin{aligned}\tilde{u}_{\xi\xi} &= \tilde{u}_{\theta\theta} - \frac{\tilde{u}_\theta}{\tilde{u}_x}\tilde{u}_{\theta x} + (\frac{\tilde{u}_\theta}{\tilde{u}_x})^2\tilde{u}_{xx} \\ &= g''\circ u\cdot(u_\theta^2 - 2u_\theta^2 + u_\theta^2) + g'(u)\left(u_{\theta\theta} - 2\frac{u_\theta}{u_x}u_{\theta x} + (\frac{u_\theta}{u_x})^2 u_{xx}\right) \\ &= g'(u)\cdot u_{\xi\xi}\end{aligned}$$

whenever $\tilde{u}_x \neq 0$. Hence, we have $\tilde{u}_t = 0$ if $\tilde{u}_x = 0$, and $\tilde{u}_t = \tilde{u}_{\xi\xi}$ if $\tilde{u}_x \neq 0$, so that $\tilde{u}$ is a classical solution of the DCMA.

2. Now let us come back to the general case when g is only continuous. Given $\varepsilon > 0$, there exists a map $g^\varepsilon \in C^2(\mathbb{R})$ such that $\|g - g^\varepsilon\|_\infty \leqslant \varepsilon$. Since the set

$$K = [-\|u\|_\infty - \varepsilon, \|u\|_\infty + \varepsilon]$$

is compact, g is uniformly continuous on K thanks to Heine's Theorem : in other words there exists a positive number $\alpha \leqslant \varepsilon$ such that $|g(x) - g(y)| \leqslant \varepsilon$ as soon as $|x - y| \leqslant \alpha$. Besides, we can find a classical solution u^ε of the DCMA such that $\|u - u^\varepsilon\|_\infty \leqslant \alpha$. Then, we have

$$\|g\circ u - g^\varepsilon \circ u^\varepsilon\|_\infty \leqslant \|g\circ u - g\circ u^\varepsilon\|_\infty + \|g\circ u^\varepsilon - g^\varepsilon\circ u^\varepsilon\|_\infty \leqslant 2\varepsilon,$$

and $g^\varepsilon \circ u^\varepsilon$ is a classical solution of the DCMA. □

As for the [**Transversal Invariance**] property, it is clearly satisfied by the DCMA since the y coordinate does not even appear in its definition.

Now we can check the [**v-Compatibility**] property. Consider a map $h : \mathbb{R}^4 \mapsto \mathbb{R}$ such that

$$\forall u \in \mathcal{M}^1,\ R_h u \in \mathcal{M}^1 \quad \text{and} \quad v[R_h u] = v[u],$$

with $R_h u(x,y,\theta) = h\left(u(x,y,\theta), x, y, \theta\right)$. Choosing $u(x,y,\theta) = \lambda \tanh x$ (tanh meaning the hyperbolic tangent) proves that h is C^1. In addition, for any $u \in \mathcal{M}^1$ we must have

$$u_x h_\theta = u_\theta h_x$$

in order that the condition $v[R_h u] = v[u]$ is satisfied. If we now choose $u(x,y,\theta) = \tanh x + b\theta$, we obtain $h_\theta = 0$ with $b = 0$ and then $h_x = 0$ with $b = 1$, so that we finally have

$$h(\lambda, x, y, \theta) = f(\lambda, y).$$

Then, the relation $T_t \circ R_h = R_h \circ T_t$ is a direct consequence of Proposition 35, the y coordinate being fixed. □

The last two axioms, [**Galilean Invariance**] and [**Zoom Invariance**], are clearly satisfied by the DCMA thanks to Lemma 18 and Lemma 19.

12.2 Asymptotics of the DCMA

Given an evolution equation like the DCMA, a natural question arises : is there an asymptotic state ? In other words, we would like to know whether the movie $u(\cdot,t)$ tends towards a limit movie u_∞ as $t \to +\infty$.

Proposition 36 *If $u \in \mathcal{V}_c^0$ is a weak solution of the DCMA, then the limit*

$$u_\infty = \lim_{t\to+\infty} u(\cdot,t)$$

exists and satisfies

- *if $I = S^1$, $u_\infty(x,y,\theta) = u_\infty(x,y,0)$,*
- *if $I =]\theta_1,\theta_2[$, there exists $v \in C^0(\mathbb{R}^2)$ such that*

$$u_\infty(x - v(x,y)\theta, y, \theta) = u_\infty(x,y,0).$$

Proof :

We proved in Proposition 29 that u satisfies

$$u(\varphi(x,y,\theta,t),y,\theta,t) = u(x,y,0,0).$$

Since φ is a solution of the heat equation, there exists two maps a and b such that

$$\varphi(x,y,\theta,t) \to a(x,y)\theta + b(x,y) \quad \text{as} \quad t \to +\infty,$$

and if $I = S^1$ the condition

$$\varphi_\theta(x,y,\theta,0) \to 0 \quad \text{as} \quad |x| \to +\infty$$

forces $a(x,y) = 0$. □

Remark : The stronger condition in the case $I = S^1$ is only a consequence of the space of solutions we choose. The main idea that must emerge from this proposition is that the trajectories of the initial movie eventually become straight lines as t reaches infinity.

12.3 Diffusion of the movement

In the following, v is a map of class C^2 defined on a subset Ω' of $\Omega = \mathbb{R} \times I \times]0,+\infty[$, and on Ω' v satisfies

$$u_\theta + v u_x = 0. \tag{12.1}$$

This defines on Ω' the operator

$$\frac{\mathrm{D}}{\mathrm{D}\theta} = \frac{\partial}{\partial\theta} + v\frac{\partial}{\partial x},$$

as well as the notation

$$f_{\xi\xi} = [D^2 f](\xi,\xi) \quad \text{with} \quad \xi = (v,1).$$

Proposition 37 *Let $u \in \mathcal{C}_c^{n+3,1}$ be a classical solution of the DCMA, with $n \geqslant 0$. Then the movement derivatives (velocity $v = -\dfrac{u_\theta}{u_x}$, acceleration $? = \dfrac{\mathrm{D}v}{\mathrm{D}\theta}$, $\ldots \dfrac{\mathrm{D}^n v}{\mathrm{D}\theta^n}$, $\ldots$) are diffused in the same direction as u, that is*

$$\forall k \in \{0,\ldots n\}, \qquad \left(\frac{\mathrm{D}^k v}{\mathrm{D}\theta^k}\right)_t = \left(\frac{\mathrm{D}^k v}{\mathrm{D}\theta^k}\right)_{\xi\xi} \quad \text{whenever} \quad u_x \neq 0.$$

In particular, the apparent velocity v follows the polynomial and causal diffusion equation

$$v_t = v_{\theta\theta} + 2vv_{\theta x} + v^2 v_{xx} \quad \text{whenever} \quad u_x \neq 0.$$

To establish this property, it is interesting to introduce the formalism of the Lie brackets associated to the partial derivatives $\frac{\partial}{\partial x}$, $\frac{\partial}{\partial\theta}$, $\frac{\partial}{\partial t}$, which commute together, and to the total derivative $\frac{\mathrm{D}}{\mathrm{D}\theta} = \frac{\partial}{\partial\theta} + v\frac{\partial}{\partial x}$.

We compute

$$[\frac{\partial}{\partial x}, \frac{\mathrm{D}}{\mathrm{D}\theta}] = \frac{\partial}{\partial x}\frac{\mathrm{D}}{\mathrm{D}\theta} - \frac{\mathrm{D}}{\mathrm{D}\theta}\frac{\partial}{\partial x} = \frac{\partial}{\partial x}(\frac{\partial}{\partial\theta} + v\frac{\partial}{\partial x}) - (\frac{\partial}{\partial\theta} + v\frac{\partial}{\partial x})\frac{\partial}{\partial x} = v_x\frac{\partial}{\partial x}.$$

One easily checks as well that

$$[\frac{\partial}{\partial\theta}, \frac{\mathrm{D}}{\mathrm{D}\theta}] = v_\theta\frac{\partial}{\partial x} \quad \text{and} \quad [\frac{\partial}{\partial t}, \frac{\mathrm{D}}{\mathrm{D}\theta}] = v_t\frac{\partial}{\partial x}.$$

This way, we can expand the $f_{\xi\xi} = [D^2 f](\xi,\xi)$ notation into

$$\begin{aligned}
(\quad)_{\xi\xi} &= \frac{\partial^2}{\partial\theta^2} + 2v\frac{\partial^2}{\partial\theta\partial x} + v^2\frac{\partial^2}{\partial x^2} \\
&= (\frac{\partial}{\partial\theta} + v\frac{\partial}{\partial x})\frac{\partial}{\partial\theta} + v(\frac{\partial}{\partial\theta} + v\frac{\partial}{\partial x})\frac{\partial}{\partial x} \\
&= \frac{\mathrm{D}}{\mathrm{D}\theta}\frac{\partial}{\partial\theta} + v\frac{\mathrm{D}}{\mathrm{D}\theta}\frac{\partial}{\partial x} \\
&= \frac{\mathrm{D}}{\mathrm{D}\theta}(\frac{\partial}{\partial\theta} + v\frac{\partial}{\partial x}) - \frac{\mathrm{D}v}{\mathrm{D}\theta}\frac{\partial}{\partial x}
\end{aligned}$$

and finally we get, writing $? = \dfrac{\mathrm{D}v}{\mathrm{D}\theta}$,

$$(\quad)_{\xi\xi} = \frac{\mathrm{D}^2}{\mathrm{D}\theta^2} - ?\,\frac{\partial}{\partial x}.$$

In particular, if we write $\psi = \dfrac{\mathrm{D}?}{\mathrm{D}\theta}$ the total derivative of $?$, we have

$$v_{\xi\xi} = \psi - ?\,v_x.$$

Lemma 24 *Independently of any evolution equation, on Ω' we have*

$$[\frac{\partial}{\partial t} - (\ )_{\xi\xi}, \frac{\mathrm{D}}{\mathrm{D}\theta}] = (v_t - v_{\xi\xi})\frac{\partial}{\partial x}. \tag{12.2}$$

Proof :

We compute the Lie bracket

$$\begin{aligned}
[()_{\xi\xi}, \frac{\mathrm{D}}{\mathrm{D}\theta}] &= [\frac{\mathrm{D}^2}{\mathrm{D}\theta^2} - ?\,\frac{\partial}{\partial x}, \frac{\mathrm{D}}{\mathrm{D}\theta}] \\
&= [\frac{\mathrm{D}^2}{\mathrm{D}\theta^2}, \frac{\mathrm{D}}{\mathrm{D}\theta}] - [?\,\frac{\partial}{\partial x}, \frac{\mathrm{D}}{\mathrm{D}\theta}] \\
&= 0 + \frac{\mathrm{D}?}{\mathrm{D}\theta}\frac{\partial}{\partial x} - ?\,[\frac{\partial}{\partial x}, \frac{\mathrm{D}}{\mathrm{D}\theta}] \\
&= (\psi - ?\,v_x)\frac{\partial}{\partial x} \\
&= v_{\xi\xi}\frac{\partial}{\partial x}.
\end{aligned}$$

Now, by linearity, we get as announced

$$[\frac{\partial}{\partial t} - ()_{\xi\xi}, \frac{\mathrm{D}}{\mathrm{D}\theta}] = [\frac{\partial}{\partial t}, \frac{\mathrm{D}}{\mathrm{D}\theta}] - [()_{\xi\xi}, \frac{\mathrm{D}}{\mathrm{D}\theta}] = (v_t - v_{\xi\xi})\frac{\partial}{\partial x}.$$

□

Proof of Proposition 37 :

We take $\Omega' = \{\boldsymbol{z} \in \Omega,\ u_x(\boldsymbol{z}) \neq 0\}$, so that v is uniquely defined by Equation 12.1 on Ω'. Applying Equation 12.2 to u yields

$$\left(\frac{\partial}{\partial t} - (\ )_{\xi\xi}\right)\frac{\mathrm{D}u}{\mathrm{D}\theta} + \frac{\mathrm{D}}{\mathrm{D}\theta}(u_t - u_{\xi\xi}) = (v_t - v_{\xi\xi})u_x. \tag{12.3}$$

As u satisfies $\frac{\mathrm{D}u}{\mathrm{D}\theta} = 0$ as well as $u_t = u_{\xi\xi}$ on Ω' (u is solution of the DCMA), the left term of Equation 12.3 is zero. Hence, on Ω' we have $v_t = v_{\xi\xi}$ as announced in Proposition 37.

This proves that the right term of Equation 12.2 is zero on Ω', so that

$$[\frac{\partial}{\partial t} - (\ )_{\xi\xi}, \frac{\mathrm{D}}{\mathrm{D}\theta}] = 0 \quad \text{whenever} \quad u_x \neq 0.$$

Consequently, for any $q : \Omega' \to \mathbb{R}$ of class C^3 satisfying

$$q_t = q_{\xi\xi},$$

we have

$$\left(\frac{\mathrm{D}q}{\mathrm{D}\theta}\right)_t = \left(\frac{\mathrm{D}q}{\mathrm{D}\theta}\right)_{\xi\xi} \quad \text{whenever} \quad u_x \neq 0.$$

Thus, a simple induction proves that the diffusion equation $q_t = q_{\xi\xi}$ is satisfied by all successive total derivatives of v of class C^2, that is, $\frac{\mathrm{D}v}{\mathrm{D}\theta}, \ldots, \frac{\mathrm{D}^n v}{\mathrm{D}\theta^n}$. □

Now we would like to generalize Proposition 37 to the whole Ω, i.e. even at points where u_x vanishes.

Proposition 38 *If $u \in \mathcal{V}_c^{n+3,1}$, then there exists a velocity map v associated to u which satisfies,* ***on the whole*** *Ω,*

$$\forall k \in \{0, \dots n\}, \qquad \left(\frac{\mathrm{D}^k v}{\mathrm{D}\theta^k}\right)_t = \left(\frac{\mathrm{D}^k v}{\mathrm{D}\theta^k}\right)_{\xi\xi}. \tag{12.4}$$

Moreover, if $I =]\theta_1, \theta_2[$, then

$$\forall (x, i, t) \in I\!R \times \{1, 2\} \times]0, +\infty[\qquad ?\,(x, \theta_i, t) = 0. \tag{12.5}$$

Proof :

Define φ as in Lemma 22, and consider the velocity map v defined by

$$v(\varphi(x, \theta, t), \theta, t) = \varphi_\theta(x, \theta, t). \tag{12.6}$$

1. We get, writing $\boldsymbol{z}_0 = (x, \theta, t)$ and $\boldsymbol{z}_1 = (\varphi(x, \theta, t), \theta, t)$,

$$\begin{aligned} v_t(\boldsymbol{z}_1) &= \varphi_{\theta t}(\boldsymbol{z}_0) - \varphi_t(\boldsymbol{z}_0) v_x(\boldsymbol{z}_1) \\ &= \varphi_{\theta\theta\theta}(\boldsymbol{z}_0) - \varphi_{\theta\theta}(\boldsymbol{z}_0) v_x(\boldsymbol{z}_1), \end{aligned}$$

while

$$\varphi_{\theta\theta}(\boldsymbol{z}_0) = v_\theta(\boldsymbol{z}_1) + \varphi_\theta(\boldsymbol{z}_0) v_x(\boldsymbol{z}_1)$$

and

$$\varphi_{\theta\theta\theta}(\boldsymbol{z}_0) = v_{\theta\theta}(\boldsymbol{z}_1) + 2\varphi_\theta(\boldsymbol{z}_0) v_{\theta x}(\boldsymbol{z}_1) + \varphi_\theta^2(\boldsymbol{z}_0) v_{xx}(\boldsymbol{z}_1) + \varphi_{\theta\theta}(\boldsymbol{z}_0) v_x(\boldsymbol{z}_1).$$

Hence, we have

$$\begin{aligned} v_t(\boldsymbol{z}_1) &= v_{\theta\theta}(\boldsymbol{z}_1) + 2\varphi_\theta(\boldsymbol{z}_0) v_{\theta x}(\boldsymbol{z}_1) + \varphi_\theta^2(\boldsymbol{z}_0) v_{xx}(\boldsymbol{z}_1) \\ &= \left(v_{\theta\theta} + 2v v_{\theta x} + v^2 v_{xx}\right)(\boldsymbol{z}_1) \\ &= v_{\xi\xi}(\boldsymbol{z}_1) \end{aligned}$$

as expected. This proves that the right term of Equation 12.2 is identically zero on the whole Ω, so that this diffusion property extends to the successive total derivatives of v as we noticed in the proof of Proposition 37.

2. Differentiating Equation 12.6 with respect with θ, we get

$$?\,(\varphi(x, \theta, t), \theta, t) = \varphi_{\theta\theta}(x, \theta, t),$$

so that for any (x, i, t) in $\mathbb{R} \times \{1, 2\} \times]0, +\infty[$ we have

$$?\,(\varphi(x, \theta_i, t), \theta_i, t) = \varphi_t(x, \theta_i, t) = \frac{\partial}{\partial t}\varphi(x, \theta_i, t) = \frac{\partial}{\partial t}\varphi(x, \theta_i, 0) = 0.$$

□

Remark : If $u \in \mathcal{C}_c^{0,0}$ is a weak solution of the DCMA, locally Lipschitz in the x variable, it is possible to establish an equivalent result in the continuation of Corollary 11, provided that we substitute the total derivative $\frac{\mathrm{D}}{\mathrm{D}\theta}$ by the Lie derivative

$$f_\xi(x,\theta,t) := \left(\frac{d}{d\tau} f(x+\tau v(x,\theta,t),\theta+\tau,t)\right)_{\tau=0}.$$

From Corollary 11 we know that there exists a velocity map v (i.e. such that $u_\xi = 0$), defined on Ω, which also constrains

$$u(x+\tau v(x,\theta,t),\theta+\tau,t-\frac{\tau^2}{2}) = u(x,\theta,t) + o(\tau^2).$$

Then, it is not difficult to show that

$$v(x+\tau v(x,\theta,t),\theta+\tau,t-\frac{\tau^2}{2}) = v(x,\theta,t) + \tau v_\xi(x,\theta,t) + o(\tau^2).$$

More generally, the successive Lie derivatives of v along the movement are well defined ($? = v_\xi$, $\psi = ?_\xi, \ldots, v^{[n+1]} = (v^{[n]})_\xi, \ldots$) and satisfy

$$v^{[n]}(x+\tau v(x,\theta,t),\theta+\tau,t-\frac{\tau^2}{2}) = v^{[n]}(x,\theta,t) + \tau v^{[n+1]}(x,\theta,t) + o(\tau^2).$$

This highlights an interesting property of the DCMA : the velocity field is smoothed indirectly through the anisotropic diffusion of u. Notice that the diffusion Equation

$$v_t = v_{\theta\theta} + 2vv_{\theta x} + v^2 v_{xx}$$

presents no singularity and is of the kind

$$v_t = F(D^2 v, Dv, v),$$

where F is a continuous elliptic operator. This means in particular that the classical theory of viscosity solutions (see [27]) applies. Our study goes a little further as v does not necessarily exist at $t = 0$, but we saw that it can be defined for any $t > 0$ as soon as $u_0 \in \mathcal{V}_c^0$. This is a direct consequence of the strong regularization effects of the heat equation.

As regards boundary conditions for v when u_0 is regular enough, we have

$$\forall (x,\theta) \in \mathbb{R} \times \overline{I}, \qquad v(x,\theta,0) = v_0(x,\theta)$$

and if $I =]\theta_1,\theta_2[$, then

$$\forall (x,i,t) \in \mathbb{R} \times \{1,2\} \times]0,+\infty[, \qquad (v_\theta + vv_x)(x,\theta_i,t) = 0$$

according to Proposition 38.

12.4 A conservation law

12.4.1 Compactly supported movies

We would like to consider integrals like

$$\int_I \int_{-\infty}^{+\infty} u(x,\theta)\, dx d\theta.$$

To simplify the results, we are going to work on compactly supported movies, which is not very restrictive physically speaking. We first recall the classical

Definition 30 *A movie $u : \mathbb{R} \times \overline{I} \to \mathbb{R}$ is **compactly supported** if it is zero outside a compact set of $\mathbb{R} \times \overline{I}$.*

Practically, it is equivalent to say that there exists $R > 0$ such that $u(x,\theta) = 0$ as soon as $|x| \geqslant R$.

Lemma 25 *A compactly supported movie $u \in \mathcal{V}_0^n$ $(n \geqslant 1)$ admits a compactly supported velocity map.*

Proof :

Suppose that $u(x,\theta) = 0$ when $|x| \geqslant R$ and let v be a velocity map of u. There exists a map $\phi \in C^\infty(\mathbb{R})$ such that $\phi(x) = 0$ if $|x| \geqslant R+1$ and $\phi(x) = 1$ if $|x| \leqslant R$. Thus, the map

$$\tilde{v} : (x,\theta) \mapsto \phi(x) \cdot v(x,\theta)$$

is a velocity map of u because $u_\theta = u_x = 0$ when $|x| > R$. Last, it is clear that $\tilde{v}$, as well as v, is bounded and of class C^{n-1}. □

Proposition 39 *Let u be the (weak or classical) solution of the DCMA associated to a compactly supported initial datum $u_0 \in \mathcal{V}_0^n$. Then,*

$$\exists R > 0,\ \forall (x,\theta,t) \in \mathbb{R} \times \overline{I} \times [0,+\infty[, \qquad |x| \geqslant R + t \ \Rightarrow\ u(x,\theta,t) = 0. \tag{12.7}$$

and if $n \geqslant 1$, u admits a velocity map which satisfies the same conclusion.

Proof :

This is a simple consequence of Equation 11.18. Recall that the solution u of the DCMA can be defined by

$$\forall (x,\theta,t) \in \overline{\Omega},\ \ u(\varphi(x,\theta,t),\theta,t) = u_0(x,0),$$

where φ satisfies

$$\exists C,\ \forall (x,\theta,t) \in \overline{\Omega}, \quad |\varphi(x,\theta,t)| \geqslant |x| - C - t$$

thanks to Equation 11.18. But since u_0 is compactly supported, there exists $R > 0$ such that $u_0(x,\theta) = 0$ as soon as $|x| \geqslant R - C$. Then, we have $u(x,\theta,t) = 0$ as soon as $|x| \geqslant t + R$. □

12.4.2 Light Energy conservation

Proposition 40 *Let $u \in \mathcal{V}_0^{2,1}$ be the classical solution of the DCMA associated to a compactly supported initial datum. Suppose that*

(a) either $I = S^1$,

(b) or $I \neq S^1$ and $\forall (x,i) \in I\!R \times \{1,2\}, \quad u(x,\theta_i,0) = 0$.

Then, the light energy at scale t, defined by

$$I(t) = \frac{1}{2} \iint u^2(x,\theta,t)\, dx d\theta,$$

is independent of t.

Proof :

We take the convention $(\theta_1,\theta_2) = (0,2\pi)$ if $I = S^1$, and remark that if $I =]\theta_1,\theta_2[$, then the boundary condition on u implies

$$\forall (x,i,t) \in \mathbb{R} \times \{1,2\} \times [0,+\infty[\quad u(x,\theta_i,t) = u(x,\theta_i,0) = 0$$

thanks to Condition (b), so that

$$\forall (x,i,t) \in \mathbb{R} \times \{1,2\} \times [0,+\infty[\quad u_x(x,\theta_i,t) = \frac{\partial}{\partial x} u(x,\theta_i,t) = 0.$$

In the following, v is a velocity map associated to u. Since $u(\cdot,\cdot,t)$ is compactly supported thanks to Proposition 39, the integral

$$I(t) = \frac{1}{2} \iint u^2 dx d\theta$$

is taken on a compact set. Consequently, as $u \in \mathcal{C}_0^{2,1}$, I is derivable and we can derive under the integral symbol to obtain

$$\begin{aligned} I'(t) &= \iint u u_t \, dx d\theta \\ &= \iint u u_{\xi\xi} \, dx d\theta \\ &= -\iint u u_x ? \, dx d\theta \\ &= -\iint u u_x (v_\theta + v v_x) \, dx d\theta \\ &= -\iint u u_x v_\theta - u u_\theta v_x \, dx d\theta. \end{aligned}$$

By integrating by parts, we get

$$I'(t) = -\int [u u_x v]_{\theta_1}^{\theta_2} \, dx + \int [u u_\theta v]_{-\infty}^{+\infty} \, d\theta + \iint (u u_x)_\theta v - (u u_\theta)_x v \, dx d\theta.$$

The first term is zero thanks to (a) or (b), the second one is zero because $u(\cdot,\cdot,t)$ is compactly supported and v is bounded, and the third one is evidently zero. Hence, $I(t)$ does not depend on t. □

12.5 A variational principle

12.5.1 A minimization law

Proposition 41 *Let $u \in \mathcal{V}_0^{4,1}$ be the classical solution of the DCMA associated to a compactly supported initial datum. Then the quantity*

$$E(t) = \frac{1}{2} \iint ?^2(x,\theta,t)\, dx d\theta$$

decreases with scale and we have

$$\frac{dE}{dt}(t) = -\iint (\frac{\mathrm{D}?}{\mathrm{D}\theta})^2\, dx d\theta. \tag{12.8}$$

Proof :

In all the following, v is a velocity field of u satisfying Equation 12.7. First notice that

$$?_{\xi\xi} = \frac{\mathrm{D}^2?}{\mathrm{D}\theta^2} - ?\,?_x = \frac{\mathrm{D}\Psi}{\mathrm{D}\theta} - ?\,?_x$$

as soon as

$$\Psi = \frac{\mathrm{D}?}{\mathrm{D}\theta} = ?_\theta + v?_x.$$

We compute the derivative of $E(t)$,

$$\begin{aligned} E'(t) &= \iint ?\,?_{\xi\xi}\, dx d\theta \\ &= \iint ?\,(\Psi_\theta + v\Psi_x - ?\,?_x)\, dx d\theta \\ &= \iint ?\,\Psi_\theta + (v?)\Psi_x - ?^2?_x\, dx d\theta. \end{aligned}$$

Integrating by parts the first two terms yields

$$E'(t) = \int [?\,\psi]_{\theta_1}^{\theta_2}\, dx + \int [v?\,\psi]_{-\infty}^{+\infty}\, d\theta - \iint ?_\theta\Psi + (v?)_x\Psi + ?^2?_x\, dx d\theta.$$

The first bracket is zero thanks to Equation 12.5 (or thanks to the periodicity of $?\,\Psi$ if $I = S^1$), and the second one is zero because $v?\,\Psi$ is compactly supported at any scale t. Hence, we have

$$\begin{aligned} E'(t) &= -\iint ?_\theta\Psi + (v?)_x\Psi + ?^2?_x\, dx d\theta \\ &= -\iint \Psi(?_\theta + v?_x + v_x?) + ?^2?_x\, dx d\theta \\ &= -\iint \Psi^2 dx d\theta - \iint v_x?\,\Psi\, dx d\theta + \iint ?^2?_x\, dx d\theta. \end{aligned} \tag{12.9}$$

But as

$$\iint ?^2?_x\, dx d\theta = \frac{1}{3} \iint \frac{\partial}{\partial x}(?^3)\, dx d\theta = 0$$

(because ? is compactly supported at any scale t), the second term of Equation 12.9 can be rewritten

$$\begin{aligned} B(t) = \iint v_x ? \Psi \, dx d\theta &= \iint v_x ? \Psi - ?^2 ?_x \, dx d\theta \\ &= \iint ? \left(?_\theta v_x + v v_x ?_x - ?_x v_\theta - v v_x ?_x \right) dx d\theta \\ &= \frac{1}{2} \iint (2? ?_\theta) v_x - (2? ?_x) v_\theta \, dx d\theta. \end{aligned}$$

then, another integration by parts yields

$$2B(t) = \int \left[?^2 v_x \right]_{\theta_1}^{\theta_2} dx + \int \left[?^2 v_\theta \right]_{-\infty}^{+\infty} d\theta - \iint ?^2 (v_{x\theta} - v_{\theta x}) \, dx d\theta = 0.$$

Finally, coming back to Equation 12.9, we obtain

$$E'(t) = - \iint \Psi^2 dx d\theta \leqslant 0$$

as announced. □

Remark : Since $E(t)$ is positive and decreases with scale, it converges to a minimum value as $t \to +\infty$, and $E'(t) \to 0$ as $t \to +\infty$. Now, what are the movies u for which $\Psi = 0$? Coming back to the construction of the solutions of the DCMA, one easily checks that the condition $\Psi = 0$ is equivalent to the condition

$$\forall (x, \theta) \in \mathbb{R} \times I, \quad \varphi_{\theta\theta\theta}(x, \theta) = 0, \tag{12.10}$$

the map φ being defined as usual by

$$u(\varphi(x, \theta), \theta) = u(x, 0).$$

Equation 12.10 implies the existence of three maps A, B, C such that

$$\forall (x, \theta) \in \mathbb{R} \times I, \quad \varphi(x, \theta) = A(x)\theta^2 + B(x)\theta + C(x).$$

and since $\varphi(x, 0) = x$, necessarily $C(x) = x$. Hence, the level lines of a movie u satisfying $\Psi = 0$ are parabolae.

12.5.2 A variational interpretation

At this point, it is natural to wonder whether Equation 12.8 results from a variational principle. Let us consider the functional

$$\mathcal{E}(v) = \frac{1}{2} \iint (v_\theta + v v_x)^2 \, dx d\theta,$$

defined on compactly supported movies of class C^2. Then, we can differentiate $\mathcal{E}$ to obtain

$$\begin{aligned} D_v\mathcal{E}(h) &= \iint (v_\theta + vv_x)(h_\theta + (vh)_x)\,dxd\theta \\ &= \iint ?\,h_\theta + (?\,v)h_x + ?\,v_x h\,dxd\theta. \end{aligned}$$

By integrating by parts the first two terms, we get, assuming that Equation 12.5 is satisfied by $?$ if $I \neq S^1$,

$$D_v\mathcal{E}(h) = \iint -?_\theta h - ?_x vh\,dxd\theta = -\iint \frac{\mathrm{D}?}{\mathrm{D}\theta} h\,dxd\theta,$$

that is to say

$$D_v\mathcal{E}(h) = -\iint \frac{\mathrm{D}^2 v}{\mathrm{D}\theta^2}\cdot h\,dxd\theta.$$

Hence, the canonical evolution equation associated to the variational problem of minimizing $\mathcal{E}$ would be

$$\frac{\partial v}{\partial t} = \frac{\mathrm{D}^2 v}{\mathrm{D}\theta^2} = v_{\xi\xi} + ?\,v_x.$$

Because of the last term $?\,v_x$, we can see that the equation $v_t = v_{\xi\xi}$ induced by the DCMA is not exactly the evolution equation associated to the minimization of $\mathcal{E}$. However, Proposition 41 showed that for the DCMA evolution,

$$D_v\mathcal{E}(\frac{\partial v}{\partial t}) = \frac{d}{dt}E(t) = -\iint \left(\frac{\mathrm{D}^2 v}{\mathrm{D}\theta}\right)^2 dxd\theta$$

as if it was the case[1]. Hence, the DCMA is somewhat related to the problem of minimizing $\mathcal{E}$.

12.6 Interpretation for the observed scene

In this section, we do not omit the y variable any longer.

12.6.1 Ideal movies

Definition 31 *A movie $u : \mathbb{R}^2 \times \overline{I} \to \mathbb{R}$ is **ideal** if one can find three maps $(C, Z, U) \in C^0(I^\star) \times C^0(\mathbb{R}^2) \times C^0(\mathbb{R}^2)$ such that*

$$\begin{array}{rccl} \Pi & : & \mathbb{R}^2 \times \overline{I^\star} & \to & \mathbb{R}^2 \times \overline{I} \\ & & (X, Y, \theta) & \mapsto & \left(\dfrac{X - C(\theta)}{Z(X,Y)}, \dfrac{Y}{Z(X,Y)}, \theta\right) \end{array}$$

is bijective and

$$\forall (X, Y, \theta) \in \mathbb{R}^2 \times \overline{I^\star}, \qquad u \circ \Pi(X, Y, \theta) = U(X, Y). \tag{12.11}$$

[1]The reason is simply that

$$\iint \frac{\mathrm{D}^2 v}{\mathrm{D}\theta^2} \Gamma v_x\,dxd\theta = 0$$

as we noticed previously.

In other terms, a movie is ideal if it can be interpreted as the perfect observation of a scene $Z(X,Y), U(X,Y)$ (depth and Lambertian luminance) by a unit focal length camera submitted to the movement $X = C(\theta)$. In this definition, occlusions are forbidden because Π is constrained to be bijective. If $I = S^1$, the natural injection $\mathbb{R} \hookrightarrow S^1$ is implicit in the definition.

It is important to notice that the interpretation of a movie is never unique. Indeed, if (C, Z, U) is an interpretation of u, then $(\lambda C, \lambda Z \circ D_\lambda, U \circ D_\lambda)$ with $D_\lambda : (X,Y) \mapsto (X/\lambda, Y/\lambda)$ is another interpretation of u. This ambiguity is called the aperture problem : if one do not know the focal length of a camera, the depth on the movie it produces can at most be recovered up to a multiplicative factor . Moreover, it is clear that the depth cannot be recovered in regions $(X, Y, Z(X,Y))$ where U is constant. Ambiguities in the depth recovery can also appear in case of special relations between the depth (or luminance) and the camera movement, which are actually not likely to occur in practice (see [44]).

12.6.2 Differential characterization of ideal movies

Proposition 42 *If a movie is ideal and allows a derivable movement interpretation, then it admits a velocity map v, and in any point where v is C^2 we have*

$$v \cdot \nabla ? \; - \; ? \cdot \nabla v = \mathbf{0}. \tag{12.12}$$

In Equation 12.12 the symbol ∇ means the spatial gradient operator

$$\nabla = (\frac{\partial}{\partial x}, \frac{\partial}{\partial y}),$$

and as usual

$$? = \frac{\mathrm{D}v}{\mathrm{D}\theta} = v_\theta + v v_x.$$

Hence, Equation 12.12 can also be rewritten

$$\begin{cases} v v_{\theta x} + v^2 v_{xx} - v_\theta v_x = 0 \\ v v_{\theta y} + v^2 v_{xy} - v_\theta v_y = 0 \end{cases}$$

Proof :

Let (C, Z, U) be an interpretation of u such that C is of class C^1. We define a unique movie $v : \mathbb{R}^2 \times \overline{I} \to \mathbb{R}$ by

$$v \circ \Pi(X, Y, \theta) = \frac{-C'(\theta)}{Z(X,Y)}. \tag{12.13}$$

Then, differentiating Equation 12.11 with respect to θ yields

$$(v u_x + u_\theta) \circ \Pi = 0,$$

so that v is a velocity map of u as announced. Now, anywhere v is C^2 we have

$$(v v_x + v_\theta) \circ \Pi(X, Y, \theta) = \frac{-C''(\theta)}{Z(X,Y)},$$

which can be combined with Equation 12.13 to yield

$$C'(\theta) \cdot ? \circ \Pi(X, Y, \theta) = C''(\theta) \cdot v \circ \Pi(X, Y, \theta)$$

because Z does not vanish. Now, if $C'(\theta) \neq 0$, then $v \neq 0$ and $?/v$ does not depend on x, so that

$$0 = \nabla \frac{?}{v} = \frac{v \nabla ? \, - ? \, \nabla v}{v^2}$$

as announced. If $C'(\theta) = 0$ and $C''(\theta) \neq 0$, the same reasoning applies to the map $v/?$. Last, if $C'(\theta) = 0$ and $C''(\theta) = 0$, Equation 12.12 is clearly satisfied because $v = ? = 0$. □

A natural question arises : does an ideal movie remain ideal when it evolves according to the DCMA ? To prove that the answer is yes, we could show that the differential invariant of Equation 12.12 remains null if it is null at initial scale. In fact, we state a better property by interpreting the evolution of an ideal movie.

12.6.3 Evolution of ideal movies

Theorem 10 *Let $u_0 \in \mathcal{C}_c^2$ be an ideal movie associated with an interpretation $(Z_0(\cdot), U_0(\cdot), C_0(\cdot))$ such that*

$$\exists A, B, \ \forall \theta \in I^\star, \quad |C_0(\theta)| \leqslant A + B|\theta|.$$

Then the classical solution u of the DCMA defined from the initial datum u_0 is a multi-scale collection of ideal movies $((u(\cdot, t))_{t \geqslant 0}$. Moreover, these movies can be interpreted as $(Z_0(\cdot), U_0(\cdot), C(\cdot, t))$, where $C(\cdot, \cdot)$ is defined by

$$C_t = C_{\theta\theta} \quad \text{on} \quad \Omega = I^\star \times]0, +\infty[$$

with the boundary condition

$$\forall (\theta, t) \in \partial\Omega, \qquad C(\theta, t) = C_0(\theta).$$

Proof :

1. The movie u_0 being ideal, we have

$$\forall (X, Y, \theta) \in \mathbb{R}^2 \times \overline{I}, \quad u_0 \left(\frac{X - C_0(\theta)}{Z_0(X, Y)}, \frac{Y}{Z_0(X, Y)}, \theta \right) = U_0(X, Y).$$

Let C be the solution of the heat equation as specified in the theorem. The map

$$\begin{array}{rccl} \Pi & : & \mathbb{R}^2 \times \overline{I^\star} & \to & \mathbb{R}^2 \times \overline{I} \times [0, +\infty[\\ & & (X, Y, \theta, t) & \mapsto & \left(\dfrac{X - C(\theta, t)}{Z_0(X, Y)}, \dfrac{Y}{Z_0(X, Y)}, \theta, t \right) \end{array}$$

is bijective because the heat equation satisfies the comparison principle. Hence, we can define a collection of ideal movies $\tilde{u}(\cdot,t)$ from

$$\tilde{u}\circ\Pi(X,Y,\theta)=U_0(X,Y), \tag{12.14}$$

2. First we check that $\tilde{u}$ is C^2. Choose $(X_0,Y_0,\theta_0,t_0)\in\mathbb{R}^2\times\overline{I^\star}\times]0,+\infty[$, and write $(X(h),Y(h))$ the unique element of $\mathbb{R}^2$ such that

$$\Pi(X(h),Y(h),\theta_0,t_0)=\Pi(X_0,Y_0,\theta_0,t_0)+(h,0,0)=(x_0+h,y_0,\theta_0,t_0).$$

We have, for any θ and h,

$$\tilde{u}(x_0+h,y_0,\theta_0,t_0)=U_0(X(h),Y(h))=u_0(x_0+h+\frac{C(\theta_0,t_0)-C_0(\theta)}{Z_0(X(h),Y(h))},y_0,\theta).$$

Now, there exists a unique θ_1 such that

$$C_0(\theta_1)=C(\theta_0,t_0),$$

so that we finally get

$$\tilde{u}(x_0+h,y_0,\theta_0,t_0)=u_0(x_0+h,y_0,\theta_1).$$

This proves that $\tilde{u}$ is, like u_0, derivable with respect to x. A similar reasoning establishes that $u\in\mathcal{C}_c^{2,1}$.

3. Now we prove that $u=\tilde{u}$. If we compute the derivatives of Equation 12.14 with respect to θ and t, we obtain

$$-\frac{C'(\theta,t)}{Z_0(X,Y)}\tilde{u}_x\circ\Pi+\tilde{u}_\theta\circ\Pi=0\quad\text{and}\quad-\frac{C''(\theta,t)}{Z_0(X,Y)}\tilde{u}_x\circ\Pi+\tilde{u}_t\circ\Pi=0.$$

If $\tilde{u}_x\circ\Pi=0$, then $\tilde{u}_t\circ\Pi=0$, and if $\tilde{u}_x\circ\Pi\neq0$, eliminating C yields

$$\tilde{u}_t\circ\Pi=\frac{\tilde{u}_x\circ\Pi}{Z_0(X,Y)}\frac{\partial}{\partial\theta}\left(Z_0(X,Y)\frac{\tilde{u}_\theta}{\tilde{u}_x}\circ\Pi\right)=\left[\tilde{u}_x\frac{\mathrm{D}}{\mathrm{D}\theta}(\frac{\tilde{u}_\theta}{\tilde{u}_x})\right]\circ\Pi=\tilde{u}_{\xi\xi}\circ\Pi.$$

Hence, $\tilde{u}$ is a classical solution of the DCMA submitted to the same boundary constraint as u. Since these conditions define a unique solution, we can deduce that $u=\tilde{u}$, which proves that each movie $u(\cdot,\cdot,\cdot,t)$ is ideal and that we can choose the interpretation announced in the theorem. □

The signification of Theorem 10 is simple : when analyzed by the DCMA, an ideal movie remains ideal and its interpretation is preserved up to a smoothing process on the camera movement.

12.6.4 Characterization of the DCMA

We now give another justification for the DCMA equation obtained in Theorem 9.

Theorem 11 *The DCMA is, up to a rescaling, the only*[2] *multiscale analysis satisfying the architectural axioms, the [v-compatibility] axiom, and such that an ideal movie* (C_0, Z, U) *is transformed into a sequence of ideal movies* $(C(t), Z, U)$ *such that* $C(t)$ *depends linearly on* C_0.

Proof :

1. Let us start by writing the relations between the scene referential (X, Y, Θ, T) and the image referential (x, y, θ, t) :

$$\begin{aligned} X &\leftrightarrow x = \frac{X - C(\theta, t)}{Z(X, Y, T)} \\ Y &\leftrightarrow y = \frac{Y}{Z(X, Y, T)} \\ \Theta &\leftrightarrow \theta \\ T &\leftrightarrow t \end{aligned}$$

From this, we compute the differentials

$$\begin{aligned} dx &= \frac{1 - xZ_X}{Z} dX - \frac{xZ_Y}{Z} dY - \frac{V}{Z} d\Theta - \frac{1}{Z}(C_t + xZ_T) dT \\ dy &= -\frac{yZ_X}{Z} dX - \frac{1 - yZ_Y}{Z} dY - \frac{y}{Z} Z_T dT \end{aligned}$$

Now, given a map F defined on both referentials, we have

$$dF = F_X dX + F_Y dY + F_\Theta d\Theta + F_T dT = F_x dx + F_y dy + F_\theta d\theta + F_t dt,$$

so that

$$F_X = F_x\left(\frac{1 - xZ_X}{Z}\right) + F_y\left(\frac{-yZ_X}{Z}\right) \tag{12.15}$$

$$F_Y = F_x\left(\frac{-xZ_Y}{Z}\right) + F_y\left(\frac{1 - yZ_Y}{Z}\right) \tag{12.16}$$

$$F_\Theta = F_x\left(\frac{-V}{Z}\right) + F_\theta \tag{12.17}$$

$$F_T = F_x\left(-\frac{C_t}{Z}\right) - \frac{Z_T}{Z}(xF_x + yF_y) + F_t. \tag{12.18}$$

Notice that Equation 12.17 simply gives the total derivative of F,

$$\frac{\mathrm{D}F}{\mathrm{D}\theta} = F_\Theta = F_\theta + vF_x.$$

Now, applying Equation 12.15 and 12.16 to $F = Z$, we get

$$\begin{cases} ZZ_X = Z_x(1 - xZ_X) + Z_y(-yZ_X) \\ ZZ_Y = Z_x(-xZ_Y) + Z_y(1 - yZ_Y) \end{cases}$$

[2] Once again, the identity operator is naturally irrelevant here.

which yields, when the denominators do not vanish,

$$Z_X = \frac{Z_x}{Z + xZ_x + yZ_y} \quad \text{and} \quad Z_Y = \frac{Z_y}{Z + xZ_x + yZ_y}.$$

Using Equation 12.18 applied to Z, we finally obtain

$$Z_T = \frac{-Z_x C_t + ZZ_t}{Z + xZ_x + yZ_y} = Z_X \left(\frac{ZZ_t}{Z_x} - C_t \right).$$

2. Consider a multiscale analysis satisfying the hypotheses of Theorem 11. Then, from Lemma 17 we know that it can be described by an evolution equation of the kind

$$u_t = u_\theta F(\frac{?}{v}, v), \tag{12.19}$$

provided that we suppose that v does not vanish. If u is an ideal movie, we have $v = -V/Z$ if we note $V = C_\theta$, and Equation 12.19 can be rewritten

$$\frac{\partial u}{\partial t} = u_\theta F(\frac{V_\theta}{V}, -\frac{V}{Z}).$$

Then we can compute

$$v_t = -\frac{1}{u_x}\frac{\mathrm{D}u_t}{\mathrm{D}\theta} = v_\theta F + v\frac{VV_{\theta\theta} - V_\theta^2}{V^2}F_1 - v\frac{V_\theta}{Z}F_2, \tag{12.20}$$

F_1 and F_2 meaning the partial derivatives of F with respect to arguments 1 and 2. Now, as

$$\frac{v_\theta}{v} = \frac{V_\theta}{V} - \frac{Z_\theta}{Z} = \frac{V_\theta}{V} - \frac{VZ_x}{Z^2}$$

and

$$\frac{v_t}{v} = \frac{V_t}{V} - \frac{Z_T}{Z},$$

Equation 12.20 yields

$$\frac{V_t}{V} - \frac{Z_T}{Z} = (\frac{V_\theta}{V} - \frac{VZ_x}{Z^2})F + \frac{VV_{\theta\theta} - V_\theta^2}{V^2}F_1 - \frac{V_\theta}{Z}F_2$$

Since the multiscale analysis must preserve the depth interpretation of the scene, we must have $Z_T = 0$, that is to say

$$\frac{Z}{Z_x}Z_t = C_t \quad \text{whenever} \quad Z_X \neq 0,$$

from what we deduce

$$\frac{V_t}{V} - \frac{V_\theta}{V}F - \frac{VV_{\theta\theta} - V_\theta^2}{V^2}F_1 - \frac{V_\theta}{Z}F_2 = \frac{Z_x}{Z^2}(C_t - VF). \tag{12.21}$$

The left term of Equation 12.21 only depends on Z, θ, and t. Therefore, by formal independency of Z_x we necessarily have $C_t = VF$ and F only depends on θ and t, that is to say $F_2 = 0$. Then, Equation 12.21 is equivalent to

$$V_t = (V_{\theta\theta} - \frac{V_\theta^2}{V})F_1 + V_\theta F,$$

and the only possibility for V to evolve linearly is

$$V_t = \lambda V_\theta,$$

which yields a trivial evolution equation on u, and $V_t = \lambda V_{\theta\theta}$, that is to say

$$F(a,b) = \lambda a.$$

This corresponds to the announced evolution Equation $u_t = u_{\xi\xi}$, up to the rescaling $t \mapsto \lambda t$. $\square$

Chapter 13

Numerical scheme and experiments

In this chapter, we propose a simple morphological scheme to implement the DCMA numerically. We prove its consistency in the "regular case", and investigate its behaviour when singularities appear. We link these observations with the difficulty encountered when trying to obtain theoretical existence properties for general initial data. Last, we present experiments on two classical movies of outdoor scenes, and we highlight both time regularization effects of the DCMA and its usefulness for depth recovery.

13.1 Definition

In order to apply the DCMA evolution to real movies, we need to devise a numerical scheme. A "naive" discretization of the partial derivatives of u cannot be used, because in practice it is well known that the time discretization is not thin enough. Moreover, such a discretization is not likely to satisfy the axioms that we imposed to the DCMA. This is the reason why we focus our attention on an inf-sup scheme. To this end, given a movie $u : \mathbb{R}^2 \times \overline{I} \to \mathbb{R}$, we define

$$\begin{aligned} IS_h u(x_0, y_0, \theta_0) &= \inf_{v \in \mathbb{R}} \sup_{-h \leqslant \theta \leqslant h} u(x_0 + v\theta, y_0, \theta_0 + \theta), \\ SI_h u(x_0, y_0, \theta_0) &= \sup_{v \in \mathbb{R}} \inf_{-h \leqslant \theta \leqslant h} u(x_0 + v\theta, y_0, \theta_0 + \theta), \\ \text{and} \quad T_h u &= \frac{1}{2} \left(IS_h u + SI_h u \right). \end{aligned}$$

If $I = S^1$, all the quantities above are well defined. If $I =]\theta_1, \theta_2[$, we take the convention that

$$u(x, y, \theta) = \begin{cases} u(x, y, \theta_1) & \text{for} \quad x < \theta_1, \\ u(x, y, \theta_2) & \text{for} \quad x > \theta_2. \end{cases}$$

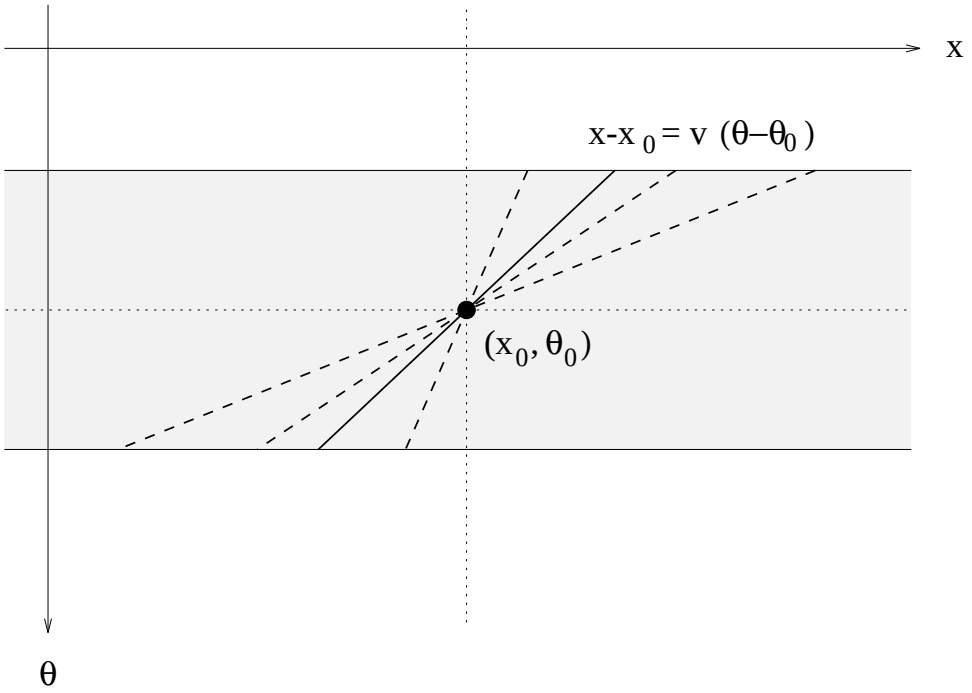

Figure 13.1: Inf-sup scheme used to implement the DCMA.

13.2 Consistency (regular case)

First, we establish a consistency result at points where u_x does not vanish.

Theorem 12 *If u is a bounded movie locally C^3 near $\boldsymbol{z}_0$, with $u_x(\boldsymbol{z}_0) \neq 0$, then*

$$\begin{aligned} IS_h u(\boldsymbol{z}_0) &= u(\boldsymbol{z}_0) + h^2 u^+_{\xi\xi}(\boldsymbol{z}_0) + O(h^3), \\ SI_h u(\boldsymbol{z}_0) &= u(\boldsymbol{z}_0) + h^2 u^-_{\xi\xi}(\boldsymbol{z}_0) + O(h^3), \\ T_h u(\boldsymbol{z}_0) &= u(\boldsymbol{z}_0) + \frac{1}{2} h^2 u_{\xi\xi}(\boldsymbol{z}_0) + O(h^3). \end{aligned}$$

and the $O(h^3)$ is uniform in a neighborhood of $\boldsymbol{z}_0$.

From now on, we shall omit the y variable in the movies we consider. Since most of the quantities involved in the following are continuous with respect to the y variable, the corresponding estimations are easily proved to be locally uniform in the y coordinate.

Lemma 26 *Consider a bounded movie u locally C^2 near $\boldsymbol{z}_0$ and such that $u_x(\boldsymbol{z}_0) \neq 0$. Then, in a neighborhood of $\boldsymbol{z}_0$ we have, for h small enough,*

$$IS_h u = I\tilde{S}_h u,$$

$$\text{with} \qquad I\tilde{S}_h u : (x_1, \theta_1) \mapsto \inf_{|v| \leqslant \frac{1}{\sqrt{h}}} \sup_{|\theta| \leqslant h} u(x_1 + v\theta, \theta_1 + \theta).$$

Proof :

1. Let K be a compact neighborhood of $\boldsymbol{z}_0$ on which u is C^2 and u_x does not vanish. We consider the compact set $K' = K + [-1,1] \times [-1,1]$, and write

$$A = \inf_K |u_x| \quad \text{and} \quad B = \sup_{K'} |u_x| + |u_\theta|.$$

From Taylor's Theorem, the map

$$C(x) = \sup_{(x_1,\theta_1)\in K} \frac{|u(x_1+x,\theta_1) - u(x_1,\theta_1) - x\,u_x(x_1,\theta_1)|}{x^2}$$

is upper-bounded on $[-1,1]$ by

$$\frac{1}{2} \sup_{K'} |u_{xx}|,$$

while on $[-\infty,-1] \cup [1,+\infty]$ we have

$$C(x) \leqslant \sup_{|x|\geqslant 1} \frac{2\|u\|_\infty + B|x|}{x^2} < \infty.$$

Therefore, writing $C = \|C\|_\infty$ yields

$$\forall (x_1,\theta_1) \in K,\ \forall x \in \mathbb{R}, \quad u(x_1+x,\theta_1) \geqslant u(x_1,\theta_1) + x\,u_x(x_1,\theta_1) - Cx^2.$$

For $h \leqslant 1$, let us take

$$x_2(x_1,\theta_1,h) = \frac{\operatorname{sgn}\left(u_x(x_1,\theta_1)\right)}{1+\frac{2C}{A}}\sqrt{h},$$

with the classical convention that

$$\operatorname{sgn}(x) = \begin{cases} 1 & \text{if} \quad x > 0, \\ 0 & \text{if} \quad x = 0, \\ -1 & \text{if} \quad x < 0. \end{cases}$$

We obtain

$$\begin{aligned} u(x_1+x_2,\theta_1) &\geqslant u(x_1,\theta_1) + \frac{\sqrt{h}}{1+\frac{2C}{A}}\left(|u_x(x_1,\theta_1)| - \frac{C\sqrt{h}}{1+\frac{2C}{A}}\right) \\ &\geqslant u(x_1,\theta_1) + \frac{\sqrt{h}}{1+\frac{2C}{A}}(A - \frac{A}{2}) \\ &\geqslant u(x_1,\theta_1) + D\sqrt{h} \quad \text{with} \quad D = \frac{A^2}{2A+4C} > 0. \end{aligned}$$

Moreover, as $|x_2| \leqslant \sqrt{h}$, we have

$$|v| \geqslant \frac{1}{\sqrt{h}} \quad \Rightarrow \quad \theta_2(x_1,\theta_1,h,v) := \frac{x_2}{vh} \in [-1,1] \quad \text{and} \quad (x_1+v\theta_2 h, \theta_1+\theta_2 h) \in K'.$$

Hence,

$$u(x_1+v\theta_2 h, \theta_1+\theta_2 h) \geqslant u(x_1+v\theta_2 h,\theta_1) - B|\theta_2|h \geqslant u(x_1,\theta_1) + D\sqrt{h} - Bh,$$

and taking $h_1 = \inf\left(1, \left(\frac{D}{2B}\right)^2\right)$ yields for any $(x_1, \theta_1) \in K$,

$$h \leqslant h_1, |v| \geqslant \frac{1}{\sqrt{h}} \quad \Rightarrow \quad s_h(v)(x_1,\theta_1) := \sup_{|\theta|\leqslant 1} u(x_1 + v\theta h, \theta_1 + \theta h) \geqslant u(x_1,\theta_1) + \frac{D}{2}\sqrt{h}. \quad (13.1)$$

2. For $(x_1, \theta_1) \in K$, we write

$$v_c(x_1,\theta_1) = \frac{-u_\theta}{u_x}(x_1,\theta_1) \quad \text{and} \quad f_{x_1,\theta_1}(x) = u(v_c x, x).$$

A second-order expansion of f_{x_1,θ_1} yields

$$\forall h \leqslant h_1,\ \forall (x_1,\theta_1) \in K,\ \forall (v,\theta) \in \mathbb{R} \times [-1,1], \quad u(x_1 + v\theta h, \theta_1 + \theta h) \leqslant u(x_1,\theta_1) + \frac{\theta^2 h^2}{2} E,$$

where

$$E = \sup_{(x_1,\theta_1)\in K, |x|\leqslant h_1} f''_{x_1,\theta_1}(x).$$

Thus, for $h \leqslant h_0 := \inf\left(h_1, \left(\frac{D}{E}\right)^{\frac{2}{3}}\right)$, Equation 13.1 yields

$$IS_h u(x_1,\theta_1) \leqslant u(x_1,\theta_1) + \frac{D}{2}\sqrt{h} \leqslant \inf_{|v|\geqslant \frac{1}{\sqrt{h}}} s_h(x_1,\theta_1),$$

which proves that

$$\forall h \leqslant h_0,\ \forall (x_1,\theta_1) \in K, \quad IS_h u(x_1,\theta_1) = \inf_{|v|\leqslant \frac{1}{\sqrt{h}}} s_h(v)(x_1,\theta_1) = I\tilde{S}_h u(x_1,\theta_1)$$

as expected. □

In the following Lemma, we equip the space $\mathbb{R}[X,\Theta]$ of 2-variables real polynomials with the norm given by the maximum of the absolute values of the coefficients, that is

$$\|\sum_{i,j} a_{ij} X^i \Theta^j\| = \max_{i,j} |a_{ij}|.$$

Lemma 27 *Let $P(x,\theta)$ be a polynomial whose degree is at most two. If $P_x(0,0) \neq 0$, then*

$$\forall h \leqslant \frac{\inf(1, P_x(0,0)^2)}{16\|P\|^2 + 1}, \quad I\tilde{S}_h P(0,0) = P(0,0) + h^2 P^+_{\xi\xi}(0,0).$$

Proof :

1. Since the degree of P is at most two, the second-order expansion of P is exact :

$$P(v\theta,\theta) = P(0,0) + \theta(av+b) + \theta^2 (v,1)^T [D^2 P](v,1) \quad \text{with} \quad (a,b) = (P_x, P_\theta)(0,0).$$

Let us consider the new coordinate system $(av+b,\theta)$ instead of (v,θ) (this is valid because $a \neq 0$). Writing

$$Q(\delta) = (\frac{\delta - b}{a}, 1)^T [D^2 P](\frac{\delta - b}{a}, 1),$$

we get

$$\begin{aligned}
I\tilde{S}_h P(0,0) &= \inf_{|v| \leqslant \frac{1}{\sqrt{h}}} \sup_{-h \leqslant \theta \leqslant h} P(v\theta, \theta) \\
&= P(0,0) + \inf_{|v| \leqslant \frac{1}{\sqrt{h}}} \sup_{-h \leqslant \theta \leqslant h} \theta(av+b) + \theta^2 (v,1)^T [D^2 P](v,1) \\
&= P(0,0) + \inf_{|\frac{\delta \perp b}{a}| \leqslant \frac{1}{\sqrt{h}}} \sup_{-h \leqslant \theta \leqslant h} \theta\delta + \theta^2 Q(\delta) \\
&= P(0,0) + \inf_{|\frac{\delta \perp b}{a}| \leqslant \frac{1}{\sqrt{h}}} \sup_{0 \leqslant \theta \leqslant 1} \theta|\delta|h + \theta^2 h^2 Q(\delta).
\end{aligned}$$

Now, let us define

$$u_h(\delta,\theta) = \theta h|\delta| + \theta^2 h^2 Q(\delta), \quad s_h(\delta) = \sup_{0 \leqslant \theta \leqslant 1} u_h(\delta,\theta) \quad \text{and} \quad A_h = \inf_{|\frac{\delta \perp b}{a}| \leqslant \frac{1}{\sqrt{h}}} s_h(\delta).$$

We want to show that $A_h = h^2 Q(0)^+$ for h small enough.

2. For $h \leqslant \frac{a^2}{b^2}$, we have $|\frac{0-b}{a}| \leqslant \frac{1}{\sqrt{h}}$, so that

$$A_h = \inf_{|\frac{\delta \perp b}{a}| \leqslant \frac{1}{\sqrt{h}}} s_h(\delta) \leqslant s_h(0) = \sup_{0 \leqslant \theta \leqslant 1} \theta^2 h^2 Q(0) = h^2 Q(0)^+.$$

Besides, as $s_h(\delta) = \sup_{0 \leqslant \theta \leqslant 1} u_h(\delta,\theta) \geqslant u_h(\delta,0) = 0$, we know that

$$A_h = \inf_{\delta \in \mathbb{R}} s_h(\delta) \geqslant 0.$$

In particular, this proves that if $Q(0) \leqslant 0$, then $A_h = 0 = h^2 Q(0)^+$.

3. Let us study the case $Q(0) > 0$. One easily checks that $Q(\delta)$ is a polynomial with degree at most two, and that

$$\sup_{|\frac{\delta \perp b}{a}| \leqslant \frac{1}{\sqrt{h}}} |Q'(\delta)| \leqslant 2\|P\| \left(\frac{1}{\sqrt{h}} + \frac{1}{|a|} \right).$$

As a consequence, for $h \leqslant a^2$ we have

$$\begin{aligned}
\forall \delta, \quad |\frac{\delta - b}{a}| \leqslant \frac{1}{\sqrt{h}} \quad &\Rightarrow \quad Q(\delta) \geqslant Q(0) - 4\frac{\|P\|}{\sqrt{h}}|\delta| \\
&\Rightarrow \quad \forall \theta \in [0,1], \quad \theta h|\delta| + \theta^2 h^2 Q(\delta) \geqslant \theta h|\delta| + h^2\theta^2 (Q(0) - 4\frac{\|P\|}{\sqrt{h}}|\delta|) \\
&\Rightarrow \quad \forall \theta \in [0,1], \quad u_h(\delta,\theta) \geqslant \theta h|\delta|(1 - 4\|P\|\sqrt{h}\theta) + h^2\theta^2 Q(0) \\
&\Rightarrow \quad \sup_{\theta \in [0,1]} u_h(\delta,\theta) \geqslant \Big(\theta h|\delta|(1 - 4\|P\|\sqrt{h}\theta) + h^2\theta^2 Q(0) \Big)_{\theta=1} \\
&\Rightarrow \quad s_h(\delta) \geqslant h|\delta|(1 - 4\|P\|\sqrt{h}) + h^2 Q(0),
\end{aligned}$$

and taking the inf on δ yields

$$\forall h \leqslant h_1 := \frac{1}{16\|P\|^2}, \qquad A_h = \inf_{|\frac{\delta \perp b}{a}| \leqslant \frac{1}{\sqrt{h}}} s_h(\delta) \geqslant h^2 Q(0).$$

4. We showed in 2 and 3 that $A_h = h^2 Q(0)^+$ as soon as $h \leqslant h_0$, with

$$h_0 := \frac{\inf(1, a^2)}{16\|P\|^2 + 1} \leqslant \inf\left(a^2, \frac{a^2}{b^2}, \frac{1}{16\|P\|^2}\right).$$

This achieves the proof since

$$\begin{aligned} \forall h \leqslant h_0, \quad I\tilde{S}_h P(0,0) &= P(0,0) + h^2 Q(0)^+ \\ &= P(0,0) + h^2 \left[(\frac{-b}{a}, 1)^T [D^2 P] (\frac{-b}{a}, 1) \right]^+ \\ &= P(0,0) + h^2 P^+_{\xi\xi}(0,0). \end{aligned}$$

□

Proof of Theorem 12 :

Let K be a compact neighborhood of $\boldsymbol{z}_0 = (x_0, \theta_0)$ on which u is C^3 and u_x does not vanish. For $(x_1, \theta_1) \in K$, we write P_{x_1,θ_1} the second-order expansion of u near (x_1, θ_1). The regularity of u ensures the existence of a constant $C > 0$ such that

$$\forall (x_1, \theta_1) \in K,\ \forall (x, \theta) \in [-1, 1]^2, \quad |u(x_1 + x, \theta_1 + \theta) - P_{x_1,\theta_1}(x, \theta)| \leqslant C\sqrt{x^2 + \theta^2}^3.$$

This implies, for $h \in [0, 1]$,

$$\forall |\theta| \leqslant 1,\ \forall |v| \leqslant \frac{1}{\sqrt{h}}, \quad |u(x_1 + v\theta h, \theta_1 + \theta h) - P_{x_1,\theta_1}(v\theta h, \theta h)| \leqslant C\sqrt{2}h^3. \tag{13.2}$$

From now on, we fix $(x_1, \theta_1) \in K$ and write P for P_{x_1,θ_1}. If we apply the nondecreasing operator $I\tilde{S}_h$ to Equation 13.2, we get

$$\forall h \in [0, 1], \quad I\tilde{S}_h P(x_1, \theta_1) - C\sqrt{2}h^3 \leqslant I\tilde{S}_h u(x_1, \theta_1) \leqslant I\tilde{S}_h P(x_1, \theta_1) + C\sqrt{2}h^3.$$

Notice that the regularity of u implies that the map

$$(x_1, \theta_1) \mapsto P_{x_1,\theta_1}$$

is continuous, as well as the map

$$P \mapsto \frac{\inf(1, P_x(0,0)^2)}{16\|P\|^2 + 1}.$$

Hence, Lemma 27 ensures the existence of a constant $h_1 > 0$ *independent of* (x_1, θ_1) such that

$$\forall h \in [0, 1], \quad I\tilde{S}_h P(0,0) = P(0,0) + h^2 P^+_{\xi\xi}(0,0) = u(x_1, \theta_1) + h^2 u^+_{\xi\xi}(x_1, \theta_1).$$

In addition, from Lemma 26 we know that there exists h_2, independent of (x_1, θ_1), such that

$$\forall h \leqslant h_2, \quad IS_h u(x_1, \theta_1) = I\tilde{S}_h u(x_1, \theta_1).$$

Therefore, for any $h \leqslant h_0 := \inf(h_1, h_2)$ we have

$$IS_h(u) = u + h^2 u^+_{\xi\xi} + O(h^3)$$

uniformly on K. The symmetric estimation on SI_h arises from

$$SI_h(u) = -IS_h(-u) = u - h^2(-u_{\xi\xi})^+ + O(h^3) = u + h^2 u^-_{\xi\xi} + O(h^3),$$

and summing up these two estimations establishes the desired consistency property

$$T_h(u) = u + h^2 u_{\xi\xi} + O(h^3)$$

uniformly on K. □

Theorem 12 proves the consistency of the numerical scheme given by the iteration of T_h with respect to the DCMA evolution. Due to the h^2 coefficient in the expansion of T_h, it is natural to consider the numerical scheme which associates, to a given movie u_0 and a scale $t \geqslant 0$, the sequence of movies $(u_{n,t})_{n \geqslant 1}$ given by

$$u_n = T^n_{h_n} u_0, \quad \text{with} \quad h_n = \sqrt{2t/n},$$

and satisfying the boundary constraint

$$\forall (x, y, \theta) \in \partial(\mathbb{R}^2 \times I), \qquad u_n(x, y, \theta) = u_0(x, y, \theta).$$

For an operator T, the notation T^n means $T \circ T \circ \ldots \circ T$ n times.

Thanks to Theorem 12, we know that such a scheme is consistent. As for the convergence, we could hope to prove that u_n converges towards the DCMA of u_0 when the partial derivative of u_0 with respect to x never vanishes (but this would no be very useful). Unfortunately, we do not think that this numerical scheme (or any other) converges towards a solution of the DCMA in the general case. Indeed, as we explained in Chapter 11, we believe that such a solution does not exist in general. We try to make clearer that point by investigating what happens near singular points, i.e. points where $u_x = 0$. Although the non-existence of general solutions for the DCMA is a real theoretical problem, in practice the convergence of the numerical scheme is assured due to the discrete nature of computer data (of course, the question of the interpretation of the limit then becomes more tricky).

13.3 Singular points

We first establish a preliminary lemma.

Lemma 28 *If $(a,b) \in \mathbb{R} \times [0,+\infty[$, then*

$$F(a,b) := \sup_{0 \leqslant \theta \leqslant 1} \frac{a}{2}\theta^2 + b\theta = \begin{cases} \dfrac{a}{2} + b & \text{if} \quad a \geqslant -b, \\ -\dfrac{b^2}{2a} & \text{if} \quad a < -b. \end{cases}$$

Proof :

The map

$$\varphi(\theta) = \theta \mapsto \frac{a}{2}\theta^2 + b\theta$$

is C^1 on the compact set $K = [0,1]$, so that it attains its maximum value on K either on ∂K or in a critical point. That is,

$$\sup_{0 \leqslant \theta \leqslant 1} \varphi(\theta) = \max(\varphi(0), \varphi(1), \varphi(-\frac{b}{a})) = \max(0, \frac{a}{2} + b, -\frac{b^2}{2a}),$$

with the convention $-b/a = -b^2/(2a) = -\infty$ if $a = 0$. □

Proposition 43 *Let P be a polynomial with degree at most two such that $P_x(x_0,\theta_0) = 0$. Then, in (x_0,θ_0) we have, as $h \to 0$,*

$$T_h P = P + \frac{h}{2}\,|P_\theta|\,\mathrm{sgn}(P_{xx}) + O(h^2)$$

Proof :

Without loss of generality, we can suppose that $(x_0,\theta_0) = (0,0)$. Since the degree of P is at most two, we have

$$P(v\theta h, \theta h) = P(0,0) + b \cdot \theta h + \frac{h^2\theta^2}{2} Q(v),$$

where

$$b = P_\theta(0,0) \quad \text{and} \quad Q(v) = P_{\theta\theta}(0,0) + 2vP_{\theta x}(0,0) + v^2 P_{xx}(0,0).$$

Therefore,

$$\begin{aligned} (IS_hP - P)(0,0) &= \inf_v \sup_{|\theta| \leqslant 1} \left(b \cdot \theta h + \frac{h^2\theta^2}{2} Q(v) \right) \\ &= h \cdot \inf_v \sup_{0 \leqslant \theta \leqslant 1} \left(|b| \cdot \theta + \frac{h\theta^2}{2} Q(v) \right) \\ &= h \inf_v F(hQ(v), |b|) \\ &= hF(h \cdot \inf Q, |b|) \end{aligned}$$

because the map $a \mapsto F(a,b)$ is increasing.

- if $|b| = 0$ or $\inf Q = -\infty$, then

$$(IS_h P - P)(0,0) = \frac{h^2}{2} [\inf Q]^+ .$$

- if $|b| \neq 0$ and $\inf Q > -\infty$, then $h \cdot \inf Q \geqslant -|b|$ for h small enough, so that

$$(IS_h P - P)(0,0) = h \cdot |b| + \frac{h^2}{2} \inf Q + o(h^2).$$

Now, one can see easily that

(i) if $P_{xx}(0,0) > 0$, then $\inf Q = \left(P_{\theta\theta} - \dfrac{P_{\theta x}^2}{P_{xx}} \right)(0,0)$.

(ii) if $P_{xx}(0,0) = P_{\theta x}(0,0) = 0$, then $\inf Q = P_{\theta\theta}(0,0)$.

(iii) if $P_{xx}(0,0) < 0$ or ($P_{xx}(0,0) = 0$ and $P_{\theta x}(0,0) \neq 0$), then $\inf Q = -\infty$.

Hence, in $(0,0)$ we have

$$IS_h P = P + O(h^2) + \begin{cases} h|P_\theta| & \text{if} \quad P_{xx} > 0 \ \text{ or } \ P_{xx} = P_{\theta x} = 0, \\ 0 & \text{else.} \end{cases}$$

Recalling that $SI_h P = -(IS_h(-P))$, we obtain

$$SI_h P = P + O(h^2) + \begin{cases} -h|P_\theta| & \text{if} \quad P_{xx} < 0 \ \text{ or } \ P_{xx} = P_{\theta x} = 0, \\ 0 & \text{else.} \end{cases}$$

and finally

$$T_h P = P + O(h^2) + \frac{1}{2} \cdot \begin{cases} h|P_\theta| & \text{if} \quad P_{xx} > 0, \\ -h|P_\theta| & \text{if} \quad P_{xx} < 0, \\ 0 & \text{else} \end{cases}$$

as expected. □

The following table gives the values of IS_h, SI_h and T_h up to order 2 in h according to conditions on P_θ, P_{xx} and $P_{\theta x}$. All these equalities hold for h small enough, and we took the convention that

$$P_{\xi\xi} := \begin{cases} P_{\theta\theta} & \text{if} \quad P_{xx} = P_{\theta x} = 0, \\ P_{\theta\theta} - \dfrac{P_{\theta x}^2}{P_{xx}} & \text{if} \quad P_{xx} \neq 0. \end{cases}$$

P_θ	P_{xx}	$P_{\theta x}$	$IS_h P - P$	$SI_h P - P$	$T_h P - P$
$= 0$	$= 0$	$= 0$	$\frac{h^2}{2} P_{\xi\xi}^+$	$\frac{h^2}{2} P_{\xi\xi}^-$	$\frac{h^2}{4} P_{\xi\xi}$
$= 0$	> 0		$\frac{h^2}{2} P_{\xi\xi}^+$	0	$\frac{h^2}{4} P_{\xi\xi}^+$
$= 0$	< 0		0	$\frac{h^2}{2} P_{\xi\xi}^-$	$\frac{h^2}{4} P_{\xi\xi}^-$
$\neq 0$	> 0		$h\|P_\theta\| + \frac{h^2}{2} P_{\xi\xi}$	0	$\frac{h}{2}\|P_\theta\| + \frac{h^2}{4} P_{\xi\xi}$
$\neq 0$	< 0		0	$-h\|P_\theta\| + \frac{h^2}{2} P_{\xi\xi}$	$-\frac{h}{2}\|P_\theta\| + \frac{h^2}{4} P_{\xi\xi}$
$\neq 0$	$= 0$	$= 0$	$h\|P_\theta\| + \frac{h^2}{2} P_{\xi\xi}$	$-h\|P_\theta\| + \frac{h^2}{2} P_{\xi\xi}$	$\frac{h^2}{4} P_{\xi\xi}$
	$= 0$	$\neq 0$	0	0	0

□

Proposition 43 shows that if u_x happens to vanish when u_θ does not, then we can expect the numerical scheme to blow up because of the non-zero coefficient of h. In fact, in case the limit of $u_n(x,\theta,t)$ exists as $n \to +\infty$, it is not likely that it will be continuous in $t = 0$. The best we can expect is that

$$u_0 \mapsto \lim_{t\to 0} \lim_{n\to+\infty} u_n(t)$$

defines a kind of projection from $\mathcal{C}_c^0$ to $\mathcal{V}_c^0$. According to Proposition 43, this projection might be obtained by the asymptotic state as $t \to +\infty$ of the solution of the PDE

$$u_t = \begin{cases} |u_\theta|\mathrm{sgn}(u_{xx}) & \text{if} \quad u_x = 0, \\ 0 & \text{else.} \end{cases}$$

Of course, all of this is purely intuitive. Evans also predicted a projection property (see [32]) by considering the DCMA Equation as the limit when $\varepsilon \to 0$ of the more regular equation

$$u_t = \frac{u_x^2 u_{\theta\theta} - 2u_x u_\theta u_{x\theta} + u_\theta^2 u_{xx}}{u_x^2 + \varepsilon^2 u_\theta^2}. \tag{13.3}$$

In particular, Equation 13.3 admits viscosity solutions as a slightly modified version of the mean curvature motion. The difference is that Evans proved that when u is the characteristic function of an S-shaped curve, his construction leads to a different projection operator, based on a Maxwell area construction (see Figure 13.2).

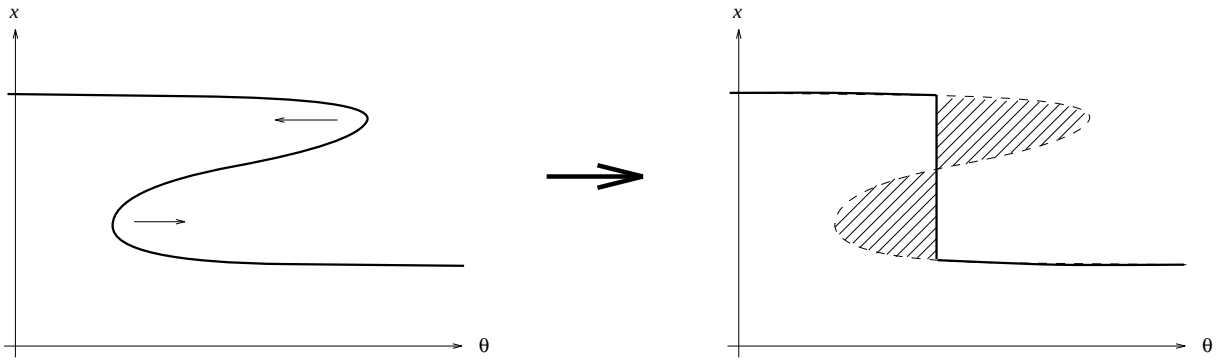

Figure 13.2: An S-shaped curve is immediatly transformed into a graph, the two dashed zones being of equal area (Maxwell equi-area construction). "The smoothing effects of the heat equation are so pronounced that a multi-valued data instantaneously unfolds into a graph" (Evans). The consequence for the DCMA is that solutions are not likely to exist for an initial datum whose level curves are not graphs. Indeed, such solutions could not be continuous at scale $t = 0$.

13.4 Algorithms

In this section, we describe the algorithms we used to experiment our analysis on numerical movies. These algorithms (and many others) will be available in the next public version of the MegaWave2 software, which can be freely[1] downloaded by anonymous ftp to the address ceremade.dauphine.fr or on the web server http://www.ceremade.dauphine.fr.

13.4.1 Data preparation

Even if a movie is realized in the conditions we described in introduction (that is to say, a straight translation of the camera parallel to its horizontal axis), in practice it is impossible to ensure that the camera movement has no vertical component at all. Hence, it is generally necessary to apply little vertical translations to the images of a real movie in order to compensate for the small vertical moves of the camera. Such an operation had already been performed (as explained in [13]) on the "TREES" movie we got from the SRI International Center. We needed to perform this operation on the "GARDEN" movie ourself (both these movies are presented later). The determination of these little vertical translations is not difficult since they affect all points of each image equally. In practice, it can be done by using a simple correlation measure. Such a simple algorithm is quite precise enough for our aim : in fact, we discovered later that an error of one pixel in a vertical movement compensation is immediatly overcome by the DCMA filtering.

13.4.2 Filtering with the DCMA

In order to experiment the effects of the DCMA, we need to discretize the numerical inf-sup scheme we described in the beginning of this chapter. The natural discrete choice for h is $h = one\ image$, and in order to take into account the discrete nature of velocities it is also natural to consider discrete 3-points segments of the kind

$$\{(x - v, y, \theta - 1), (x, y, \theta), (x + v + \varepsilon, y, \theta + 1)\},$$

where all quantities are integer and $\varepsilon \in \{-1, 0, 1\}$. Hence, the discrete inf-sup operator is

$$ISu(x, y, \theta) = \min_{\substack{v \in \{-v_{max}, ..., -1, 0\} \\ \varepsilon \in \{-1, 0, 1\}}} \max\{u(x - v, y, \theta - 1), u(x, y, \theta), u(x + v + \varepsilon, y, \theta + 1)\}.$$

The parameter v_{max} must not be smaller than the largest velocity on the processed movie, which can easily be estimated. More important is the non-symmetric choice we made on v by allowing only nonpositive velocities. There are several reasons for this choice : first, if the camera always goes forwards and never stops and goes back, then all velocities on the movie

[1] for non commercial use only, see the MegaWave2 documentation.

must be theoritically nonpositive. In addition, since the velocity field follows a causal evolution equation, it satisfies the maximum principle and is then forced to remain nonpositive at any scale of analysis. This proves the consistency of our non-symmetric choice of allowed velocities. Another reason that justifies this choice and that we shall discuss later is related to the filtering of occlusions.

The SI and IS operator being defined, we still have an alternative : either we iterate the mean operator $\frac{1}{2}(IS+SI)$ as we explained in the numerical scheme, or we iterate the alternated operator[2] $IS \circ SI$. No computational cost seems relevant to choose between the two possibilities, because it is roughly equivalent to compute IS or simultaneously IS and SI on a movie, and one easily checks that one iteration of the alternated operator is also roughly equivalent, in terms of scale of analysis, to two iterations of the mean operator. In fact, when we tried both solutions, the advantage came to the alternated scheme, for two reasons.

The first reason is that it is purely morphological (and hence more consistent with our axiomatic formulation), with the consequence that no new grey-level is created when a movie is processed. This overcomes a purely numerical constraint : since the grey levels of a movie are practically discretized (typically, in {0,1,...255} when represented by a 8-bit unsigned character), the division by two is not symmetrical and the result often has to be truncated, which has undesirable consequences after several iterations (notice that this cannot be avoided in practice by considering float values because of the huge amount of memory involved). Of course, the choice of an alternated operator is not symmetrical either (you can choose $IS \circ SI$ or $SI \circ IS$), but there are many less consequences.

The second reason is that a pure morphological scheme was more adapted to the algorithm we chose in order to compute the velocity field on the movie. This will become clear in the next section.

It is important to notice the extreme simplicity of the algorithm we presented : in particular, it can be implemented very easily on a massive parallel machine. Our optimized code in C language for one iteration consists of only 23 instructions.

13.4.3 Computing velocities

Of course, since the DCMA is devoted to the depth recovery — or, equivalently, to the computation of the velocity field —, it would not be enough to show filtered movies without checking the consequences of the DCMA on their inherent velocity fields. For that reason, we need to devise an algorithm to compute such velocity fields. Now comes the great interest of the DCMA : since the multiscale analysis theoretically produces a perfect time-coherent movie, we can use a naive algorithm to compute the velocity field.

[2]Though we did not prove explicitely the consistency of the alternated operator, it seems rather clear if we compare it to classical related schemes.

Our algorithm is global and takes only one parameter : the number n of matching images we require to decide that a velocity is reliable. Given a point (x_0, y_0, θ_0), we look for the maximum value of k for which there exist two real numbers v_1 and v_2 satisfying

$$-v_{max} \leqslant v_1 \leqslant v_2 \leqslant 0$$

and such that[3]

$$\forall \theta \in \{\theta_0, \ldots, \theta_0 + k\}, \forall x \in \{E(x_0 - v_1\theta), \ldots, E(x_0 - v_2\theta)\}, \qquad u(x, y_0, \theta) = u(x_0, y_0, \theta_0).$$

Then, we decide that the velocity field in (x_0, y_0, θ_0) is non-computable if $k < n$, and equal to v_1 if $k \geqslant n$ (of course, the interval $[v_1, v_2]$ is supposed to have a maximal length). The choice of v_1 (instead of $\frac{1}{2}(v_1 + v_2)$ for example) is logical but not very important since in practice we almost always have $v_1 \simeq v_2$ For symmetry, we also look for matchings in "past" times $\{\theta_0 - k, \ldots, \theta_0\}$.

[3]here, the function $E()$ means the rounded integer part, that is to say $E(x) = n \in \mathbb{N} \Leftrightarrow n - \frac{1}{2} < x \leqslant n + \frac{1}{2}$.

13.5 Experiments

13.5.1 TREES movie (natural)

We picked up the "TREES" movie used by the SRI center (see [13]) by anonymous ftp to the adress periscope.cs.umass.edu. We obtained 64 images of size 256x233, which represent an amount of data of 3.8 Mo. According to [13], this movie is supposed to contain 128 images, but we could not find the remaining images ; however, 64 images were quite enough to test our algorithm.

Since the images were very dark, we first applied an optimal contrast change[4] to the movie : this process has only visual consequences thanks to the pure morphological invariance of our algorithms.

As we said before, this movie did not require a compensation for small vertical movements of the camera (it had been already done according to [13]).

Each iteration of the DCMA filter took 24 seconds. This represents a processing speed of about 0.16 Mo/s.

This movie is not the best choice to highlight the good properties of the DCMA, because of the strong occlusion caused by the foreground tree (we remind that our theory does not handle with occlusions). This occlusion caused smudging effects on the right side of this tree (and not on the left side thanks to the nonpositiveness of allowed velocities). However, these bad effects excepted, the algorithm proved to behave very well. The first striking visual effect of the algorithm on this movie is the strong time-coherence induced on the movie : it looks like all images become exactly equivalent except that the relative velocities of objects differ. In particular, there were important global intensity fluctuations between images on the initial movie : such a defect was completely removed by the DCMA. One could object that this regularization is paid by a visual loss of details on the ground texture. This is true and very logical since all non-time-coherent details cannot be preserved by the analysis. Although the DCMA has theoretically no spatial regularizing effects, such a spatial regularization actually occurs as a consequence of the time regularization.

[4] Applying a contrast change consists of modifying an initial movie u into the movie $g \circ u$, where g is an increasing grey-level correspondance map. It is said to be optimal if the histogram of the resulting movie is as flat as possible (which means that the grey levels are "used" in the best possible manner).

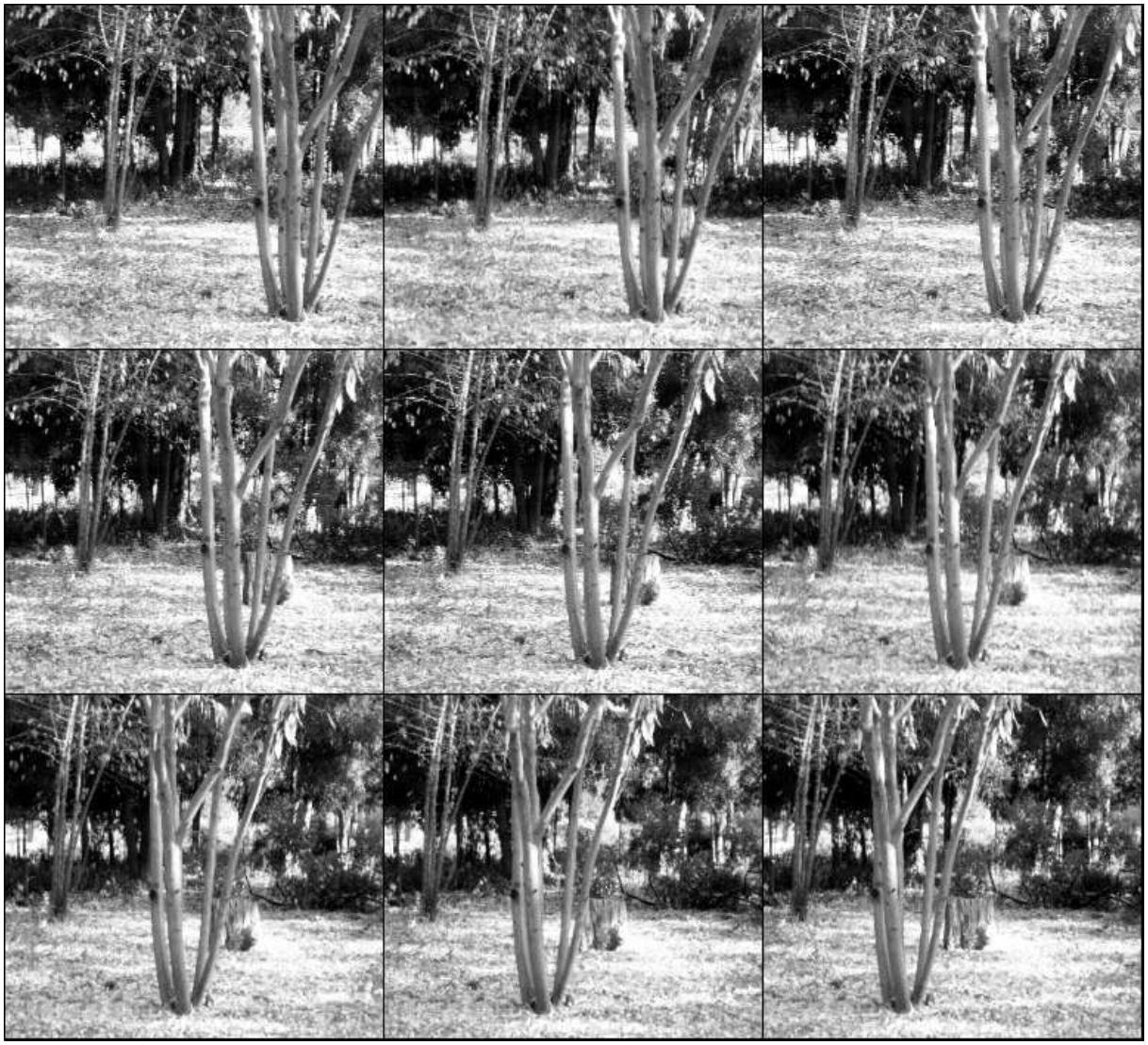

Figure 13.3: Original "TREES" movie.

From left to right and then top to bottom : images number 1, 9, 17, 25, 32, 40, 48, 56 and 64 of the "TREES" movie (made of 64 image). The camera has a straight translation movement parallel to the horizontal axis of the image plane, and moving to the right. The relative positions of objects vary due to their different distances from the image plane (the closer they are, the quicker they "move" on the image).

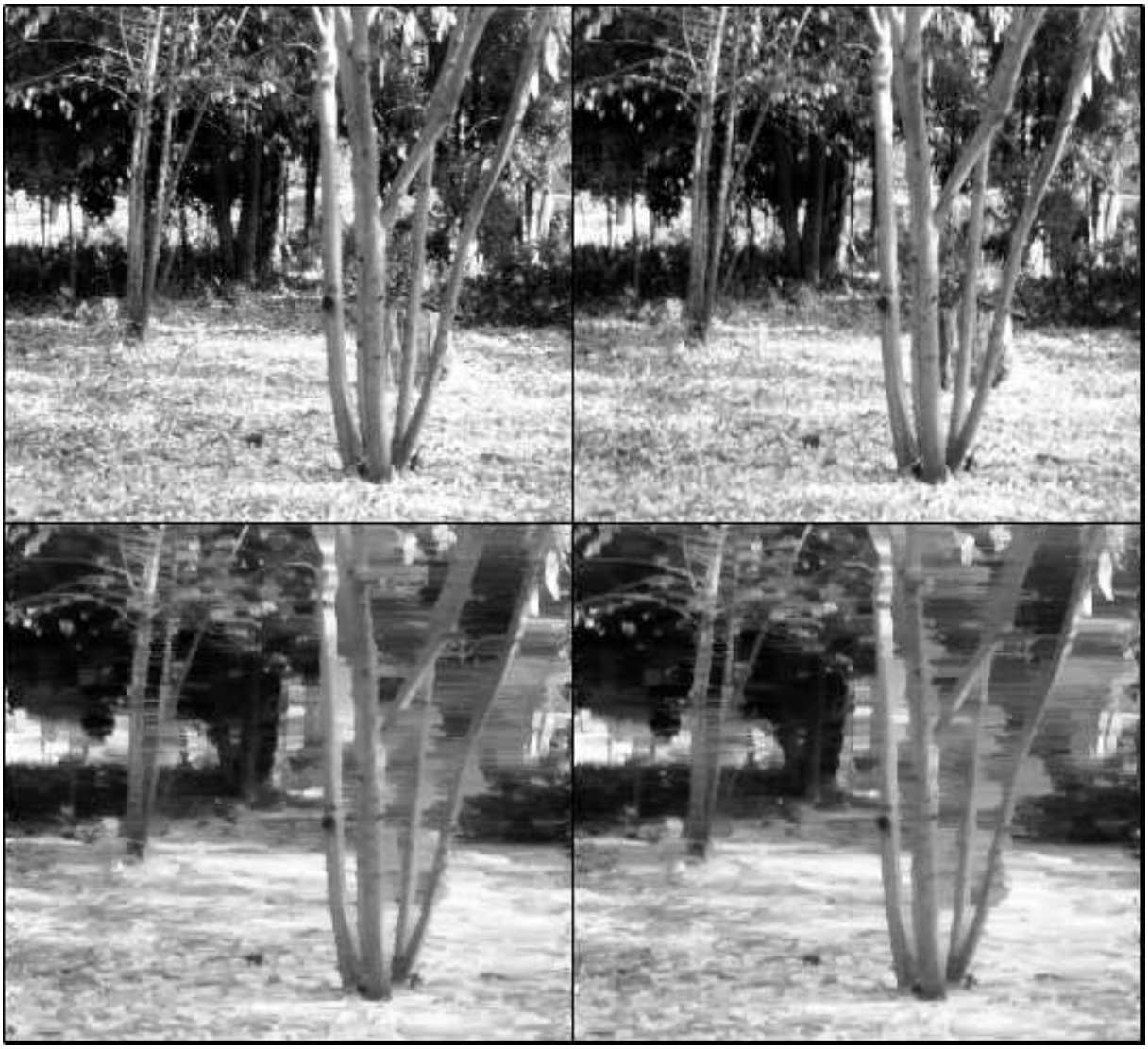

Figure 13.4: Filtering of the "TREES" movie.

Top row : *images 18 (left) and 22 (right) of the original "TREES" movie*
Bottom row : *images 18 and 22 of the "TREES" movie processed with 31 iterations.*

The original movie has small details which cannot be tracked between successive images (they are not time-coherent), because the Nyquist limit for the time frequencies has been exceeded during the sampling process. The strong smoothing effects of the analysis (on the ground for example) are necessary to ensure the time coherence of the movie. The smudging effects near the branches of the foreground tree, however, are undesired and due to the incapacity of the DCMA to handle occlusions.

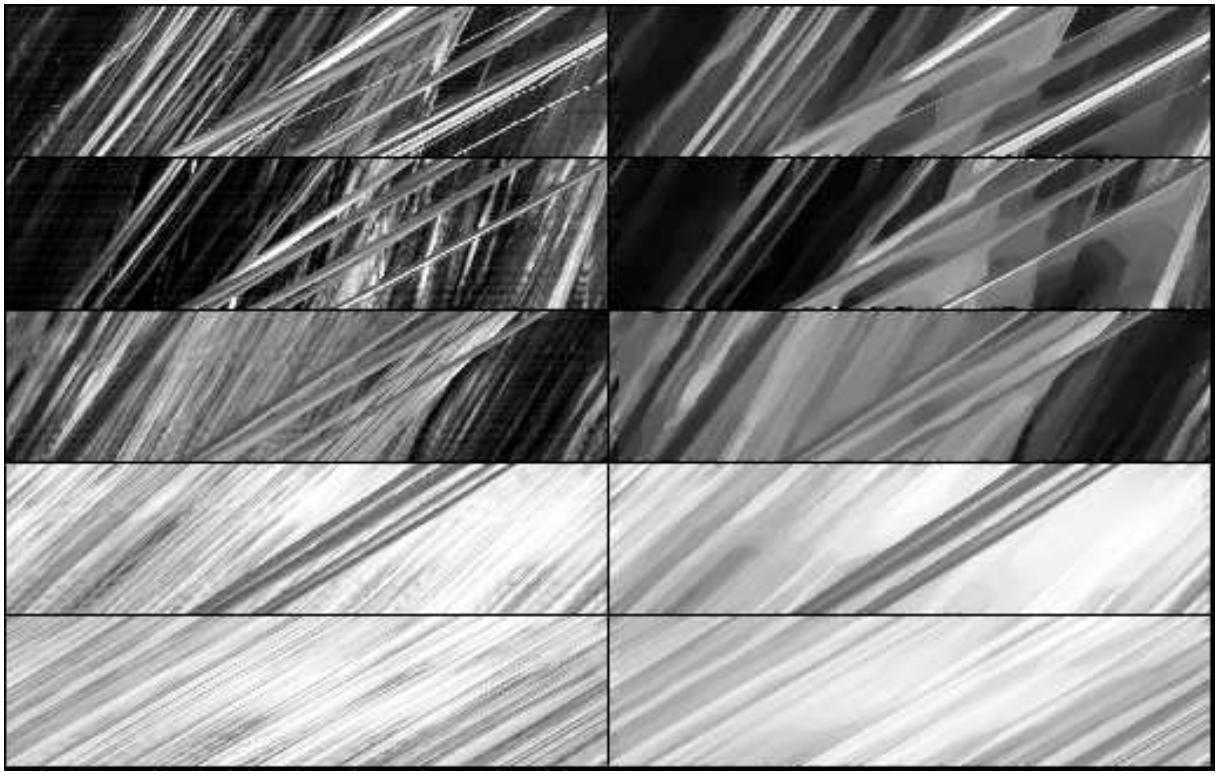

Figure 13.5: Analysis of the epipolar images.

The epipolar images are obtained by slicing the movie $u(x, y, \theta)$ along (x, θ) planes for fixed values of y. The resulting images $(x, \theta) \mapsto u(x, y, \theta)$ are represented as follows : the x axis is taken horizontal and the time axis θ is taken vertical pointing downwards. The epipolar images on colum 1 are taken from the original "TREES" movie (the values of y are 20, 60, 140, 180, 220 respectively for rows 1, 2, 3, 4, 5). Those on column 2 are obtained after processing the original ones with 31 iterations.

Remember that the DCMA operates independently on all these epipolar images. The level lines of these images tend to become straight lines when analyzed by the DCMA ; a consequence is that the time-coherence of the analyzed movie increases with scale. On the original epipolar images, occlusions appear when two lines intersect : only the one with the smallest slope (i.e. representing the object closest to the camera) remains during the occlusion, the other one being occluded. Notice that occluded objects are often destroyed by the DCMA (see row 2 for example), because the DCMA cannot handle occlusions.

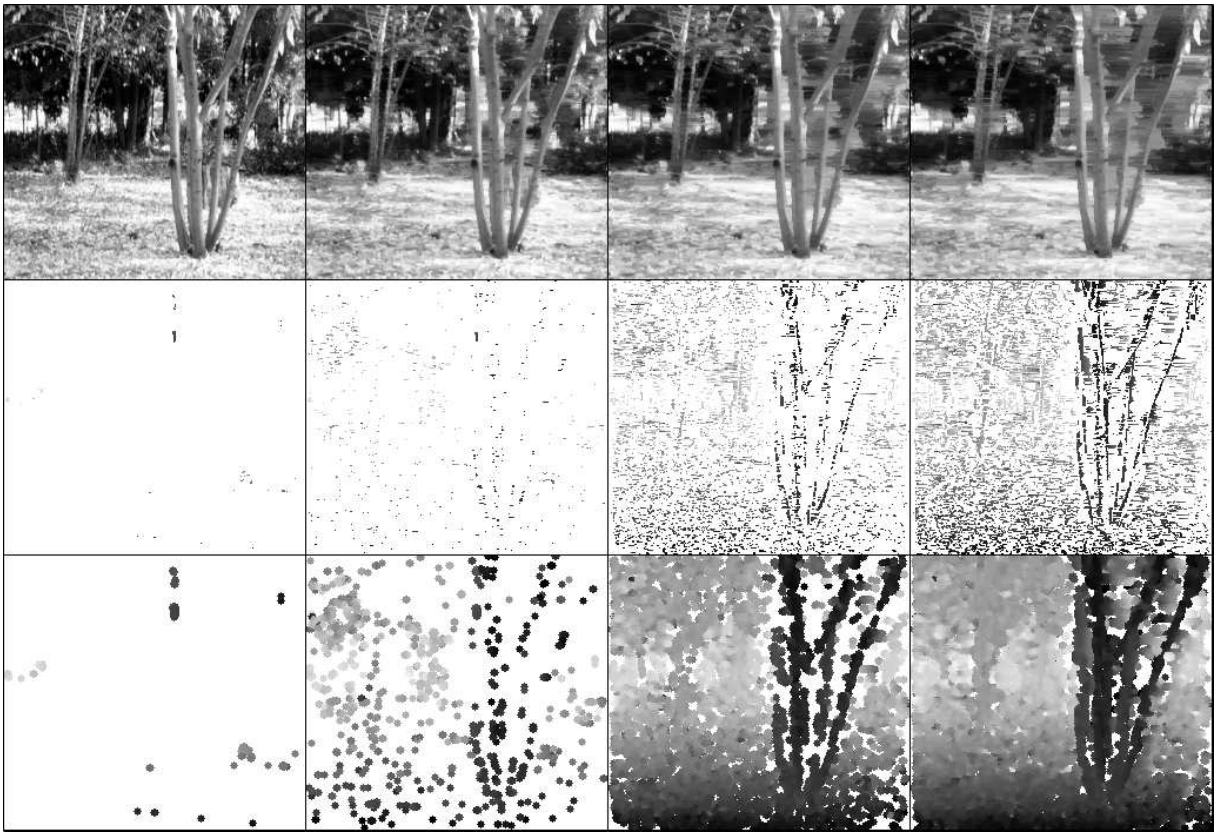

Figure 13.6: Computation of the velocity field (minimum of 15 matchings).

The four images on the first row are taken from four different movies : each image is the 20th image (over 64) of the movie it belongs to. These movies result from the DCMA at different scales :

column 1: original "TREES" movie
column 2: processed movie (5 iterations)
column 3: processed movie (15 iterations)
column 4: processed movie (31 iterations)

Then, the velocity field of each movie was computed on the 20th image using the algorithm we described previously, with a matching constraint of 15 images. These velocities are represented on row 2 : the white color means points where no matching was found with respect to the constraint, and the grey scale (from light grey to black) measures the velocity from 0.0 to 2.0 pixels per image. On the third row, the velocity images of row 2 were "dilated" to produce more readable results. Notice how the velocity information, which is almost inexistant on the original movie (for the matching constraint we imposed), progressively appears on the DCMA as the scale increases. Since the distance of objects to the image plane is inversely proportional to their velocity, closest points appear in black and farthest ones in light grey. On the last image of row 3, we distinguish the foreground tree in black, the ground from black to middle grey, the background tree in middle grey, and the far background in light grey.

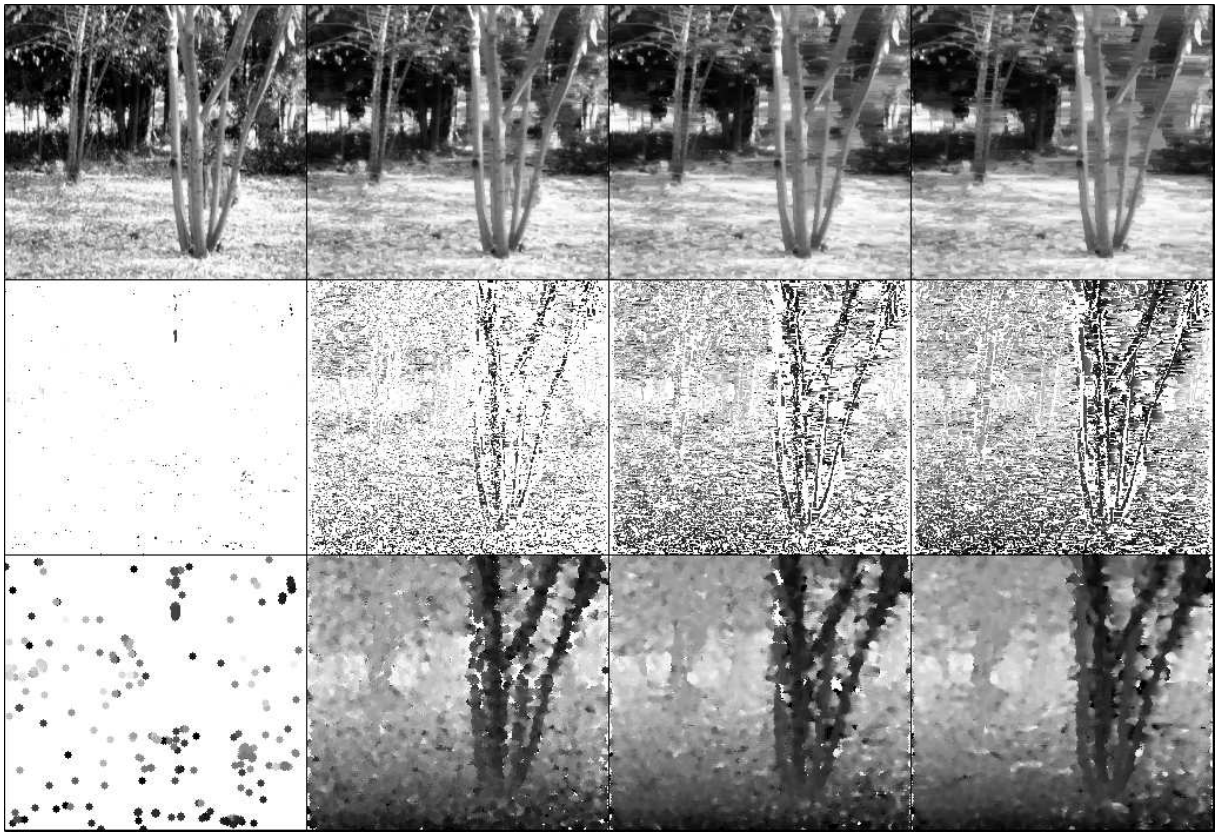

Figure 13.7: Computation of the velocity field (minimum of 5 matchings).

The representation is the same as for Figure 13.6, but this time, the velocities were computed with a less restrictive matching constraint of 5 images (instead of 15 for Figure 13.6).

The velocity images we obtain (row 2) are more dense because new computable velocities appear. However, these new obtained velocities are less reliable due to the less restrictive matching constraint. This explains the noisy appearence of the images on row 3 compared to those of Figure 13.6. Notice that this noise decreases as the scale of analysis increases : this is coherent with the theory which predicts that the velocity field is progressively smoothed as the scale of analysis increases (see Proposition 37).

13.5.2 GARDEN movie (natural)

We found this movie on the web site http://www.image.cityu.edu.hk:80. It was originally composed of 50 interlaced frames of size 720x486.

It needed a little movement compensation along the y coordinate. This was performed using the correlation method we mentioned previously.

We extracted 50 sub-images of size 400x338. Each iteration of the DCMA took approximately 50 seconds.

Once again we observed the good effects of the DCMA. This time, no undesirable effects were caused by occluding objects like for the "TREES" movie. In fact, the "GARDEN" movie contains several occluding objects (in front of the background houses), but they did not seem to cause much trouble to the algorithm, maybe thanks to the reasonable depth gap occuring at the boundary of these occlusions.

Figure 13.8: Original "GARDEN" movie.

From left to right and then top to bottom : images number 1, 7, 13, 16, 26, 31, 37, 43, 50 of the "GARDEN" movie (made of 50 images). The camera goes to the right.

Figure 13.9: Filtering of the "GARDEN" movie.

Top : *image 25 of the original "GARDEN" movie*
Bottom : *image 25 of the "GARDEN" movie processed with 24 iterations.*

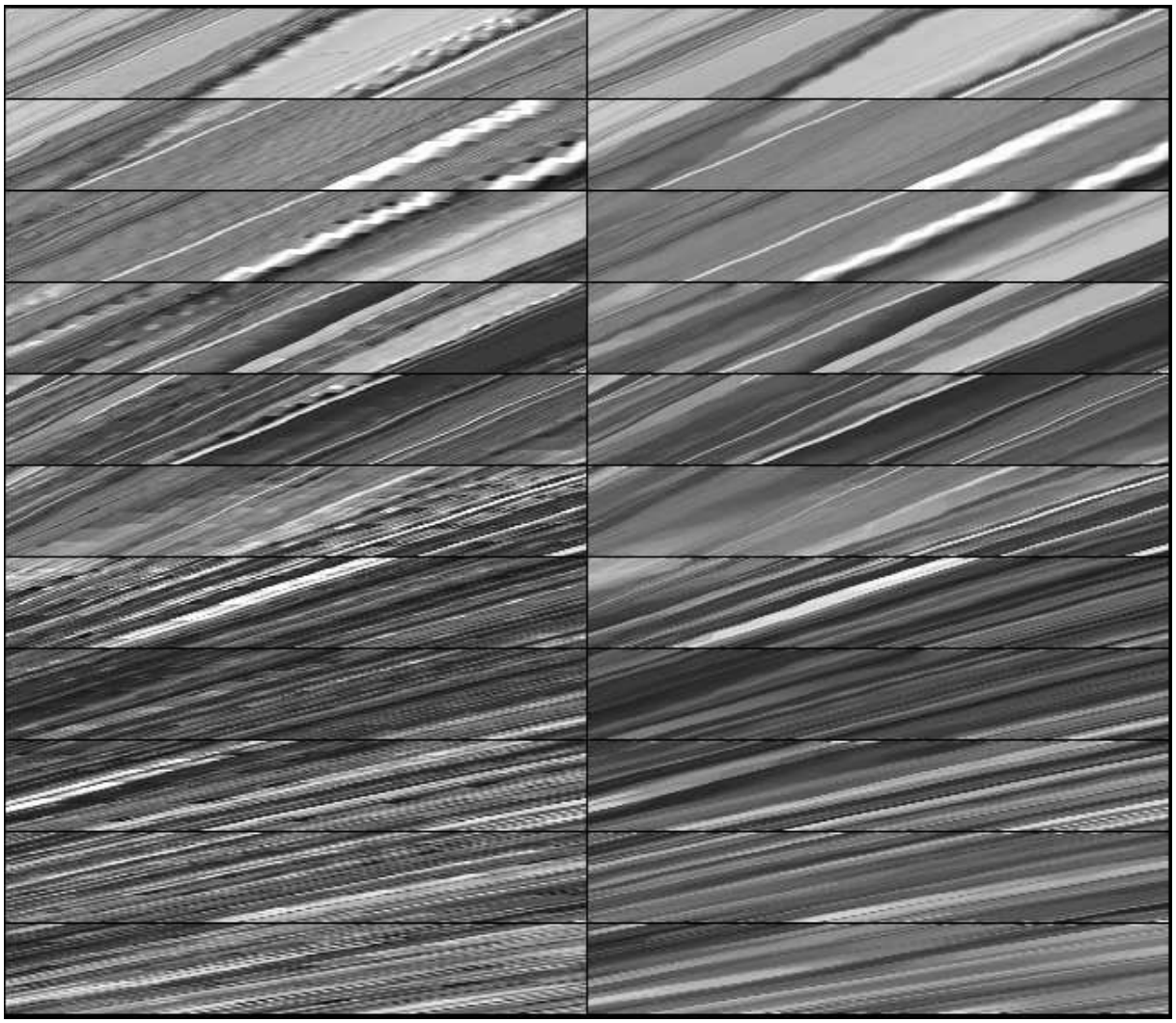

Figure 13.10: Evolution of the epipolar images.

Epipolar images are represented, taken from the original movie (column 1) and from the processed movie after 24 iterations (column 2). The values of y are 30, 60, 90, ... 300, 330 respectively for rows 1, 2, 3, ..., 10, 11.

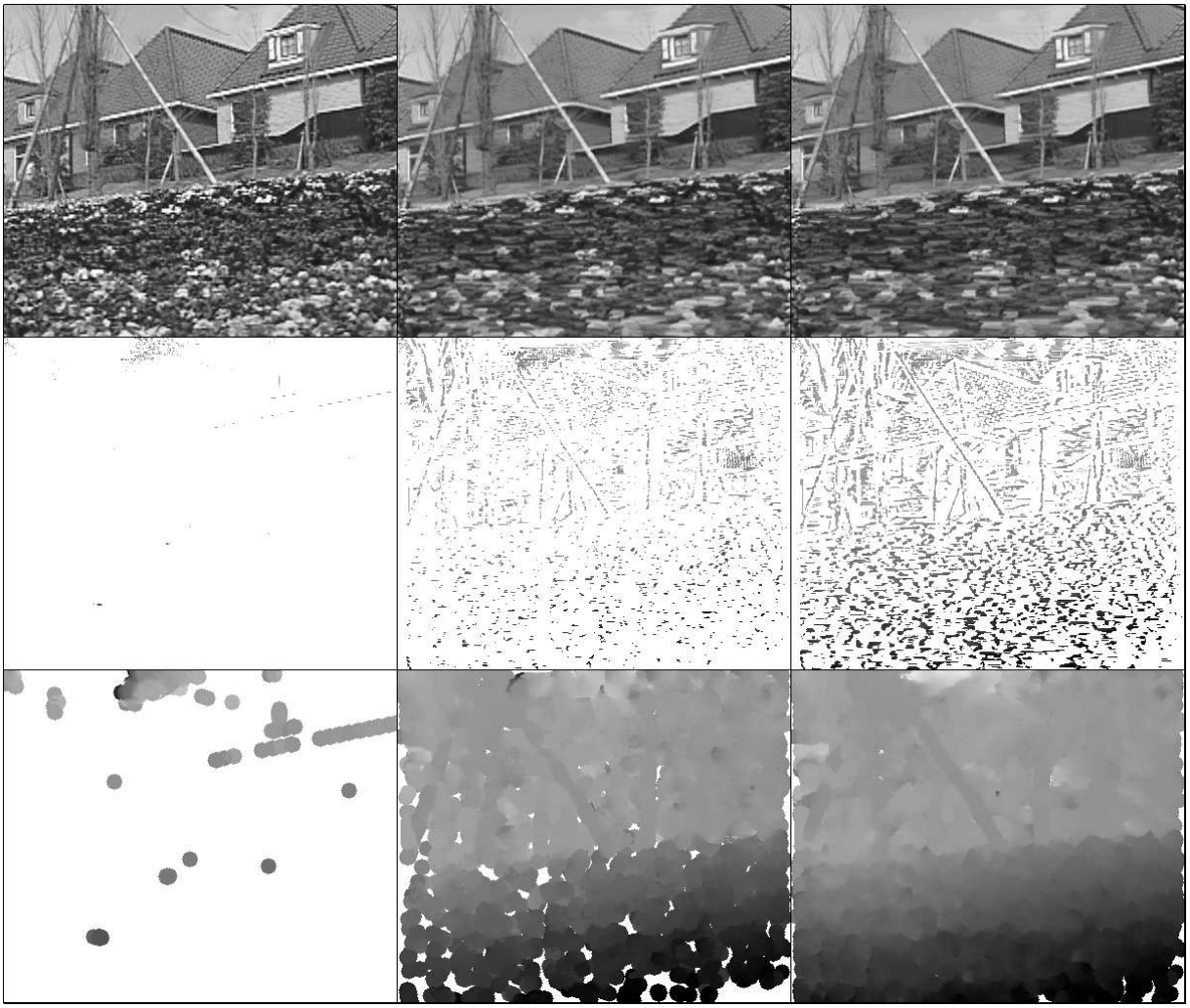

Figure 13.11: Computation of the velocity field (minimum of 12 matchings).

The three images on the first row are taken from three different movies :

column 1: original movie
column 2: processed movie (5 iterations)
column 3: processed movie (24 iterations).

Each image is the 25th image (over 50) of the movie it belongs to. On row 2, the velocity field of each movie is represented, as computed on the 25th image with a matching constraint of 12 images. The white color means points where no matching was found with respect to the constraint, and the grey scale (from light grey to black) measures the velocity from 0.0 to 6.0 pixels per image. On the third row, the velocity images of row 2 were "dilated" to produce more readable results. On the bottom-right image, we recognize the oblique plane made by the rocks of the foreground : the regular variation of the grey level indicates a regular variation of the depth. On the background, the houses appear in light grey and we can make out the two oblique poles in front of them.

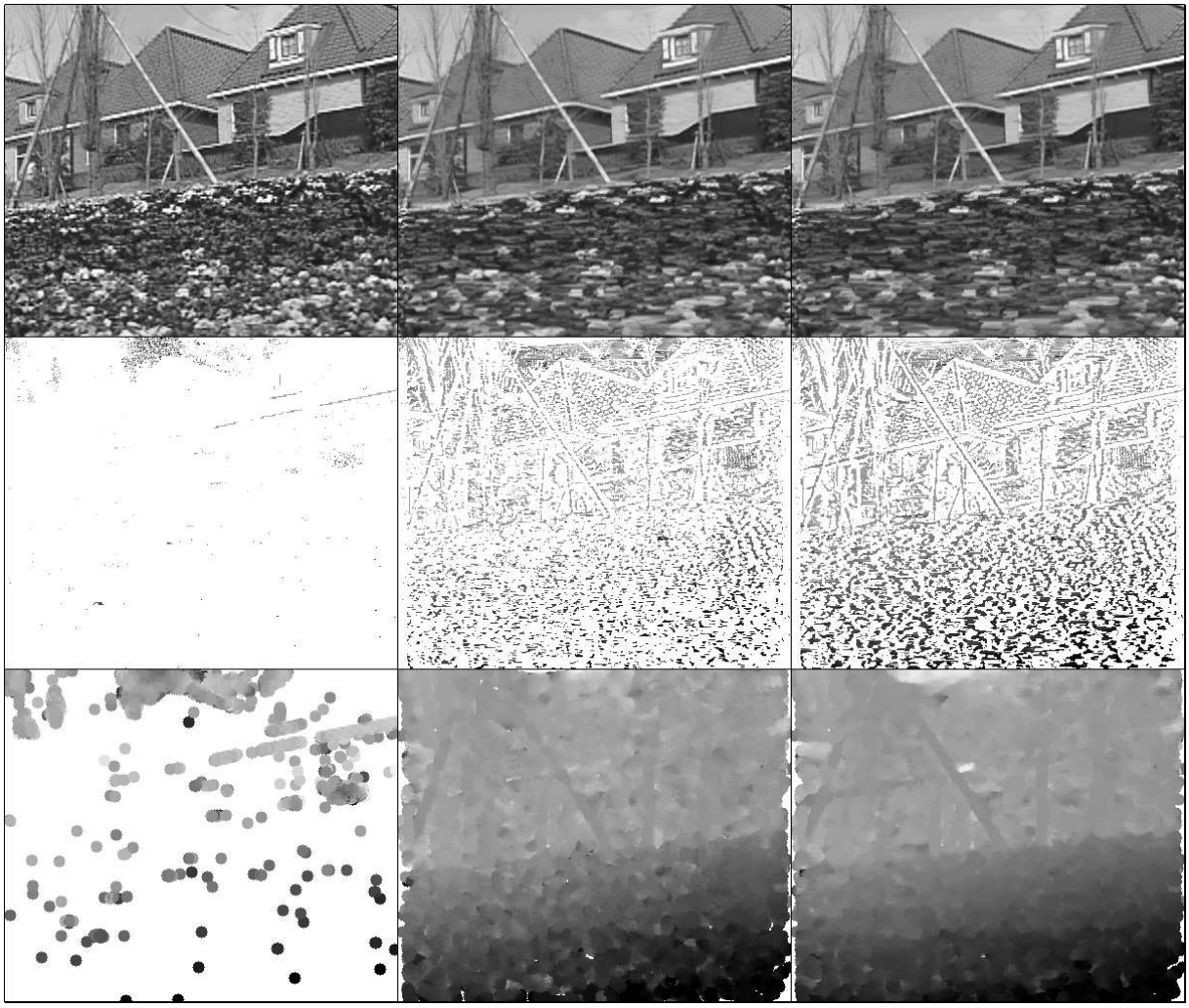

Figure 13.12: Computation of the velocity field (minimum of 5 matchings).

The representation is the same as for Figure 13.11, but this time the velocities were computed with a less restrictive matching constraint of 5 images (instead of 12 for Figure 13.11).

13.5.3 Sensitivity to noise

We now want to test how robust to noise our method is : are the DCMA analysis and the induced velocity estimation still reliable when applied to a noisy data ? In order to check this, we took the previous "TREES" movies and corrupted it strongly by replacing 50% of its grey values $u(i,j,k)$ by totally random, uniformly distributed and uncorrelated values. This kind of noise is called *impulse noise* : it is very destructive and impossible to remove efficiently with linear filters. On this corrupted movie, we applied exactly the same processing as in the original one. The figures to follow (to be compared with the corresponding figures for the original movie) show that both the visual aspect and the velocity field are well recovered by the DCMA although half of the original information was lost and replaced with random values.

Figure 13.13: Filtering of the noisy "TREES" movie.

Row 1 : images 18 and 22 of the noisy "TREES" movie
Row 2 : images 18 and 22 of the noisy "TREES" movie processed with 31 iterations.

The images on row 1 are very noisy : 50% of their pixel values were chosen by a non-correlated, uniformly distributed random generator (and this 50% amount of pixel was chosen itself by a random generator). When playing the movie, one has the impression of looking at a TV-image received in very poor conditions. In particular, it is almost impossible to see any detail of the ground texture. Filtering this movie with the DCMA gives impressive enhancement results : not only the noise impression is removed, but in addition some details appear that were not visible on the first movie (in particular on the ground and on the left tree). This means that the DCMA takes more advantage of the time coherence and redundancy of information contained in a movie than the human visual system does.

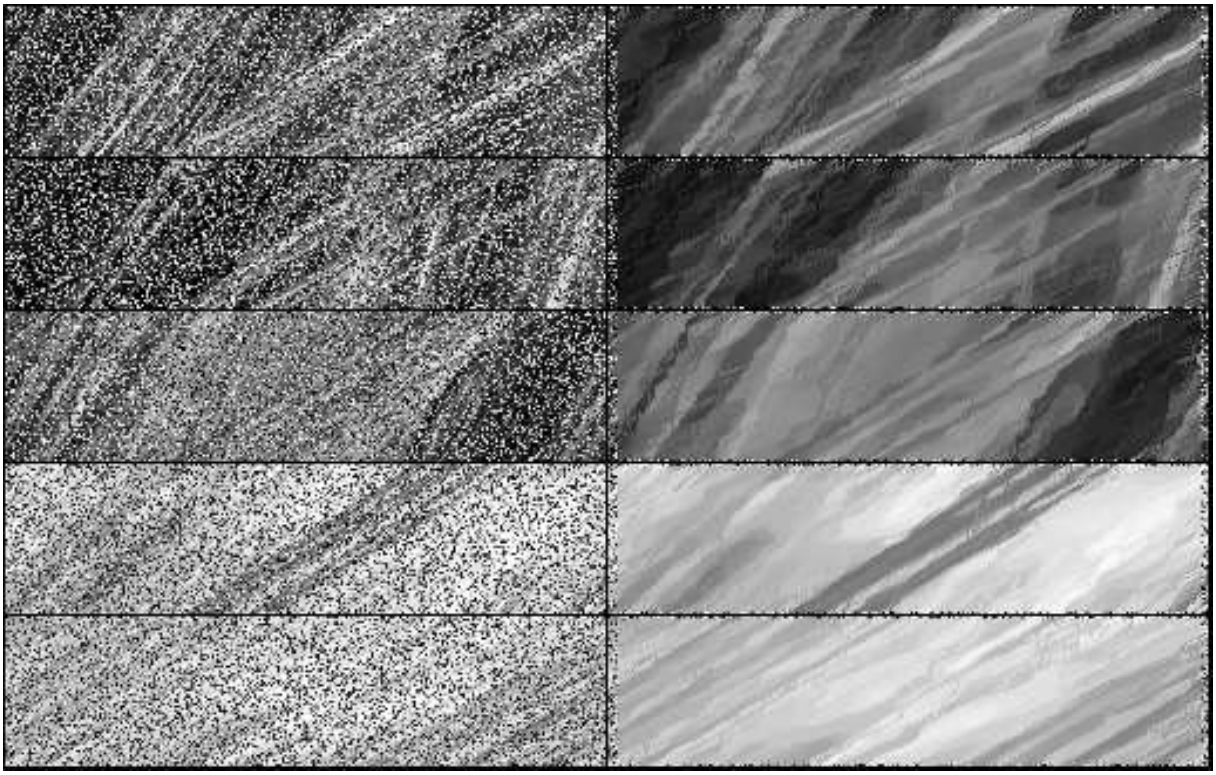

Figure 13.14: Analysis of the epipolar images.

As on Figure 13.5, epipolar images are shown both for the original noisy movie (column 1) and for its processed version after 31 iterations (column 2).

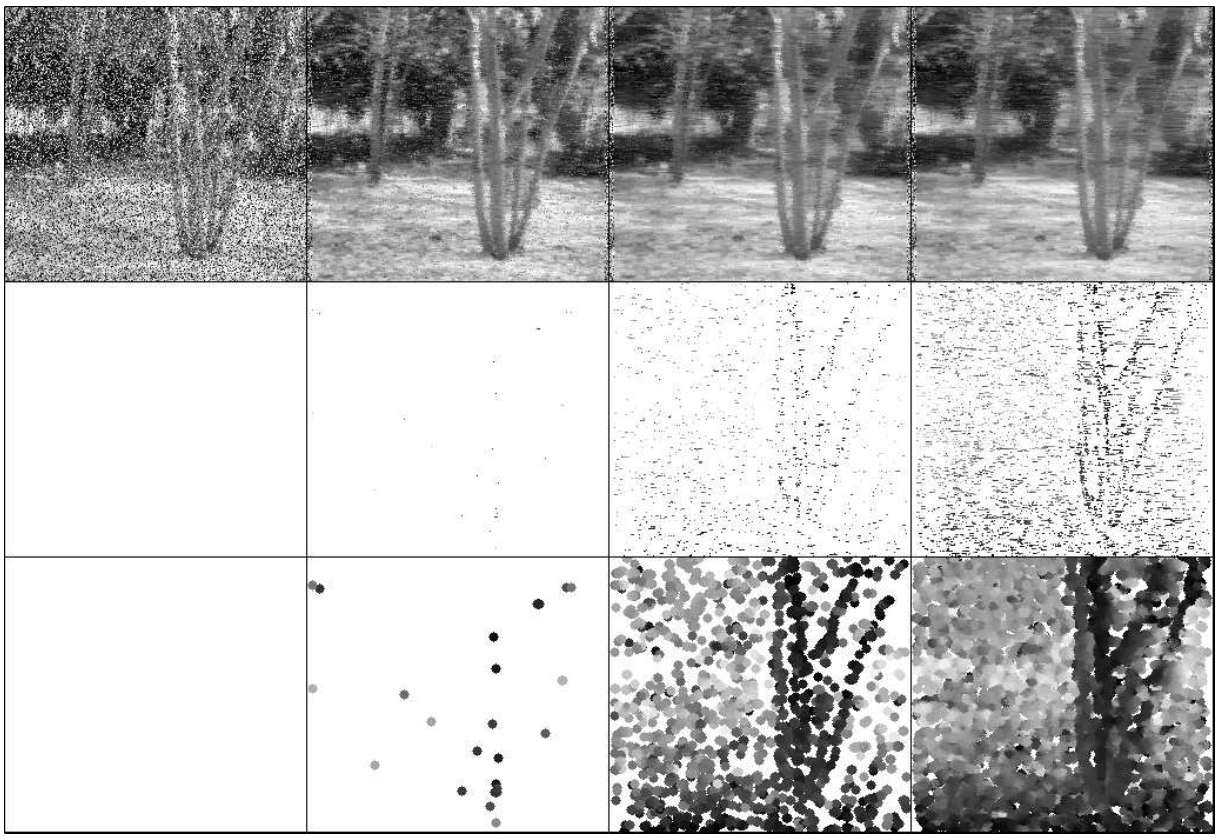

Figure 13.15: Computation of the velocity field (minimum of 15 matchings).

Like on Figure 13.6, the four images on the first row are the 20th image of four different movies :

column 1: *original noisy "TREES" movie*
column 2: *processed movie (5 iterations)*
column 3: *processed movie (15 iterations)*
column 4: *processed movie (31 iterations)*

Row 2 and 3 represent the extracted velocity field (for a minimum of 15 matching images), in the original (row 2) and dilated (row 3) representation. As expected, not only the movie is filtered, but the velocity of objects is recovered despite a lot of destructed clues due to the large amount of noise put on the movie. Of course, the velocity recovery is not as good as if the movie had not been initially corrupted, but the depth structure of the scene still appear on the bottom-right image.

Chapter 14

Extensions and conclusion

14.1 Extension to more general geometric configurations

In this section, we show that the geometric configuration we adopted throughout our study is not really required. In fact, the DCMA can easily be extended to a more general motion, provided that it is known or that it can be recovered (but we shall not properly investigate the problem of motion recovery here).

14.1.1 The camera motion is not horizontal

Practically, it is difficult to ensure that the camera moves exactly along the direction given by the horizontal axis of the image plane. The consequence is that the y-sections $(x, \theta) \mapsto u(x, y, \theta)$ of the movie should not be processed independently, for the epipolar lines are not contained in the (x, θ) plane. However, if the direction of the camera displacement is known, given by the angle ν with the x axis, then it is theoretically possible to bring the problem back to the ideal case ($\nu = 0$) with the simple rotation of the image plane given by

$$P' = \begin{pmatrix} \cos\nu & \sin\nu \\ -\sin\nu & \cos\nu \end{pmatrix} P.$$

The angle ν may be directly measured by an inertial system on the mobile robot. It can also be easily estimated on the resulting movie since it is a very redundant information.

14.1.2 The camera motion does not lie in the image plane

We now suppose that the motion of the camera is not contained in the image plane, that is to say its component along the direction orthogonal to the image plane is non-zero. We define the (OX) axis as the direction given by the motion of the camera, and the (OY) axis as the only direction orthogonal to (OX) and contained in the image plane. Then, the remaining axis (OZ), naturally defined from (OX) and (OY) in order to form an orthogonal system, makes an angle

α with the direction orthogonal to the image plane (see Figure 14.1). The projection from the scene to the image plane is given by

$$\begin{aligned} x &= \frac{X - C - Z\tan\alpha}{Z + (X - C)\tan\alpha} \\ y &= \frac{Y}{Z + (X - C)\tan\alpha}. \end{aligned}$$

Compared to the ideal case $\alpha = 0$, the case $\alpha \neq 0$ induces a deformation of the image plane given by

$$\begin{aligned} x' &= \frac{x\cos\alpha - \sin\alpha}{\cos\alpha + x\sin\alpha} = \frac{x - \tan\alpha}{1 + x\tan\alpha} \\ y' &= \frac{y}{\cos\alpha + x\sin\alpha} \end{aligned}$$

The map $(x, y) \mapsto (x', y')$ is defined on $(\mathbb{R} - \{-\text{cotan}\alpha\}) \times \mathbb{R}$, the singularity $x = -\text{cotan}\alpha$ giving a characterization of α. Thus, all previous results should still apply, provided that we rewrite the DCMA evolution equation according to this deformation map.

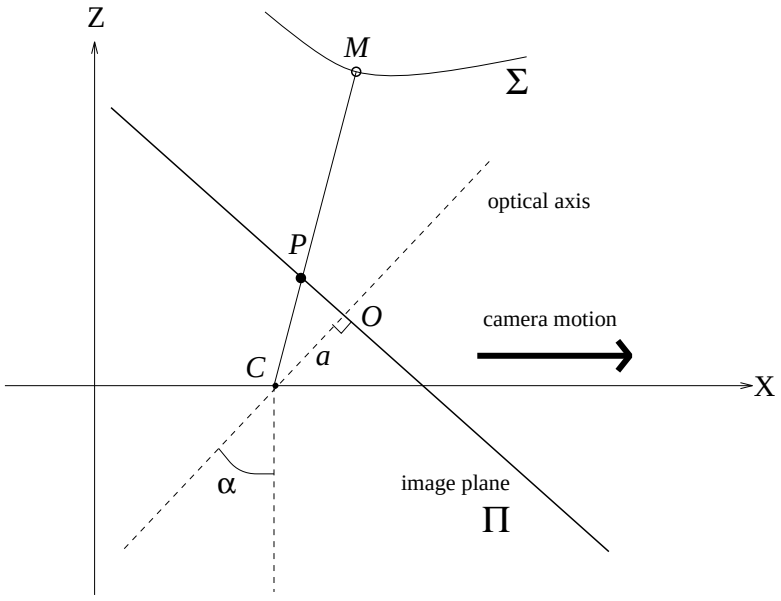

Figure 14.1: Camera motion does not lie in the image plane.

14.1.3 Case of pure zooming

If the camera moves in the direction of the optical axis, which corresponds to a pure "zooming", the movement of a physical point projected in P on the image plane is given by

$$\frac{dP}{d\theta} = \frac{V}{Z}P.$$

Thus, going to polar coordinates, the apparent velocity is

$$v = \frac{r}{Z}V = -\frac{u_\theta}{u_r}$$

everywhere $u_r \neq 0$. This case is formally equivalent to the ideal translation along the X axis as soon as the polar coordinate r is substituted to the x coordinate everywhere. In particular, the apparent acceleration is

$$? = \frac{\mathrm{D}v}{\mathrm{D}\theta} = -\frac{u_{\xi\xi}}{u_r} \quad \text{with} \quad \xi = (-\frac{u_\theta}{u_r}, 0, 1).$$

Rewriting the axiomatic formulation in that special case, we can expect to obtain the evolution equation

$$\frac{\partial u}{\partial t} = u_{\theta\theta} - 2\frac{u_\theta}{u_r}u_{\theta r} + \left(\frac{u_\theta}{u_r}\right)^2 u_{rr},$$

formally equivalent to the DCMA up to a change of coordinates.

14.2 Case of any rigid motion

The two previous cases can be combined to cover all situations of pure translation motion of the camera. The case of pure rotation with a fixed axis ("radar motion") is not very different from the case of pure translation : the filtering is the same and only the depth interpretation deduced from the velocity field changes.

In case of a general camera motion (translation T + rotation R), there are 6 instantaneous motion parameters : 3 for the translation and 3 for the rotation. More precisely, the movement of a physical point $M(X, Y, Z)$ is given in the camera referential by

$$\frac{dM}{d\theta} = -T - R \wedge M,$$

where we wrote $\wedge$ for the usual vector product in $\mathbb{R}^3$. Then, the perspective projection $(x, y) = \frac{1}{Z}(X, Y)$ induces in the image referential the movement

$$\frac{dP}{d\theta} = \frac{1}{Z}\begin{pmatrix} -1 & 0 & x \\ 0 & -1 & y \end{pmatrix} T + \begin{pmatrix} xy & -(1+x^2) & y \\ 1+y^2 & -xy & -x \end{pmatrix} R = \frac{1}{Z}AT + BR. \tag{14.1}$$

while the well-known Motion Constraint Equation is

$$\nabla u.\frac{dP}{d\theta} + u_\theta = 0, \tag{14.2}$$

∇u standing for the spatial gradient of u. Combining Equations 14.1 and 14.2 yields a scalar equation satisfied by the partial derivatives of u, with one unknow (the depth Z) and six motion parameters (T and R). It permits to compute the disparity $d = 1/Z$ by

$$d = -\frac{u_\theta + (BR).\nabla u}{(AT).\nabla u}.$$

Therefore, depth recovery is still theoretically possible as soon as the camera motion is known. We guess that it is possible to rewrite the DCMA in case of such a general camera motion, by introducing the motion parameters in the evolution equation.

14.3 Occlusions

In this study, we made several allusions to the problem of occlusions, which is not solved by the algorithm we presented. We know precise this point, and try to explain why this is the most important improvement to be brought to our method.

Two kinds of occlusions appear on a movie : the **natural occlusions**, occuring when a part of the scene masks another part (see Figure 14.2), and the **boundary occlusions**, which happen on the border of the image. The natural occlusions are consequences of both the scene geometry and the camera parameters, and they can be theoretically avoided by choosing an optical system with a small field width (or equivalently, with a large focal length). Of course, boundary occlusions cannot be avoided. In addition, avoiding natural occlusions forces the relative depth variations to be small, which prevents the depth estimation from being very accurate. Therefore, being able to deal with occlusions is a key point of the movie analysis, and it is not surprising that the human visual system makes a strong use of occlusions phenomena.

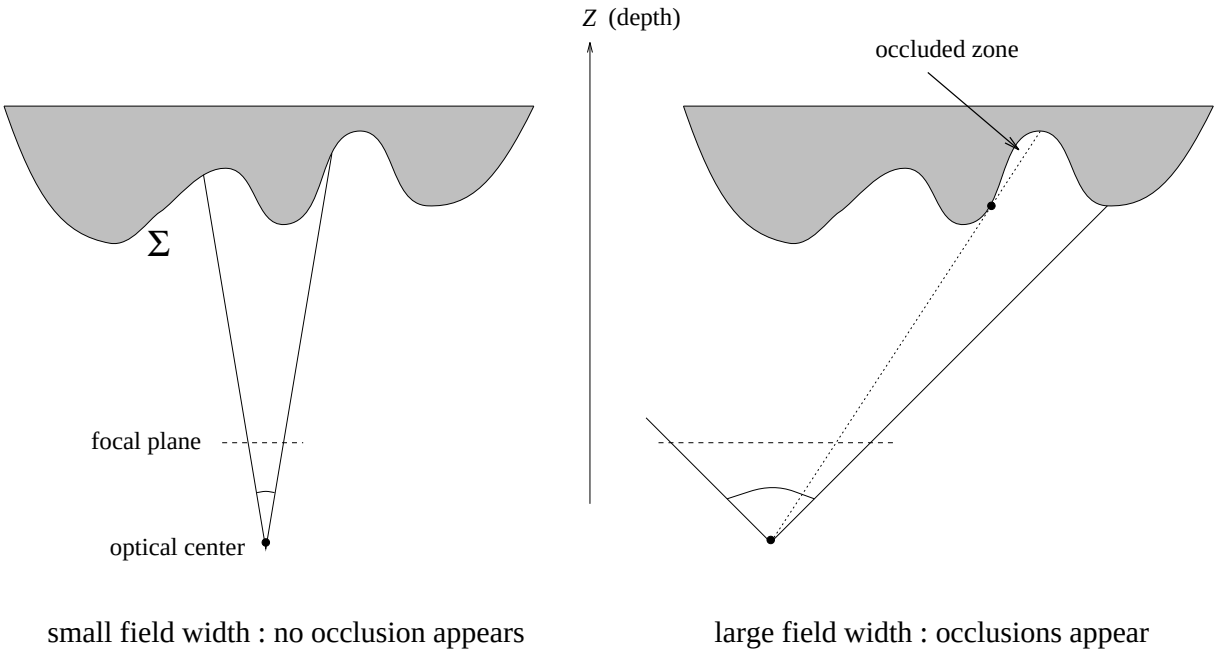

Figure 14.2: Field width and natural occlusions

Figure 14.3 shows what appears in the epipolar plane when occlusions happen : the level lines with the largest velocity (i.e. with the smallest slope on Figure 14.3) occlude the other ones. The reason is simply that when an occlusion arises between two objects, only the nearest one (that is, the one with the largest velocity) remains visible. As in the spatial case (see [21]), the occluding line is characterized by the presence of T-junctions.

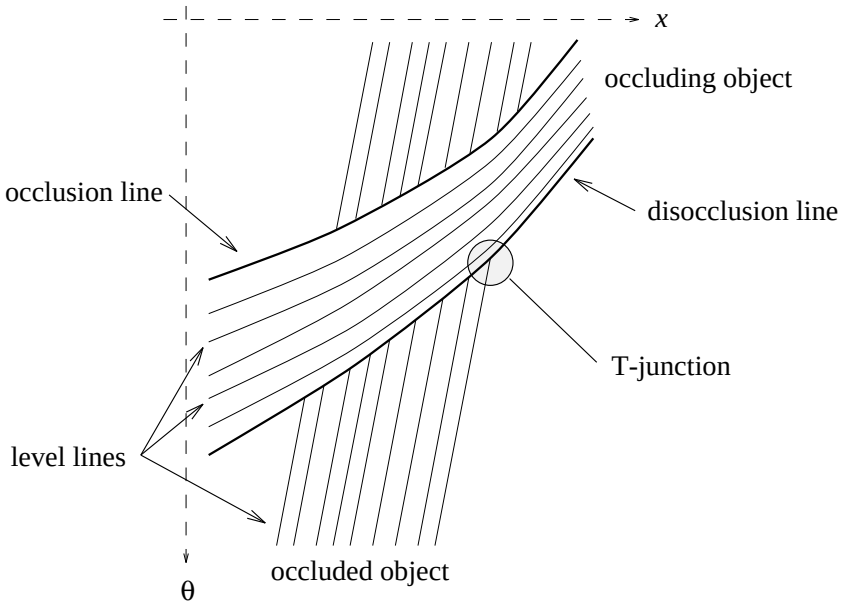

Figure 14.3: Typical occlusions in an epipolar plane

14.4 Conclusion

In this study, we presented a multiscale analysis of movies which is well adapted to the depth recovery. We devised it thanks to an axiomatic formulation in agreement with the depth recovery problem. This multiscale analysis can be viewed as a diffusion process along the movement, with the consequence that it brings time-coherence to movies without performing an undesirable spatial smoothing. In particular, it permits to gather the redundant but incoherent depth information spread among the images of a raw movie into a perfect movie on which the depth can be easily and robustly estimated.

From a theoretical point of view, this multiscale analysis is described by a second order partial differential evolution equation, which presents strong singularities and is not treated by the classical theory of viscosity solutions. We proved uniqueness and existence theorems, although existence is not ensured (at least in a classical sense) in the completely general case. This PDE has interesting properties that can be physically interpreted : in particular, we proved that an ideal movie (that is to say a movie which can be interpreted in terms of a camera movement and a depth map) remains ideal when analyzed by this scale space. We also showed that the corresponding evolution equation is somewhat related to a simple minimization problem.

We provided a very simple numerical scheme which can easily be implemented on parallel machines. By performing numerical experiments on two real movies, we checked the good behaviour of this method, as a movie processing device, and as a depth-recovery preprocessing device.

We think that this study is a good starting point to find robust solutions to the depth recovery

problem. The next step would be to adapt the theory for general movies where occlusions are allowed. Of course, such a generalization should require a non-continuous formulation due to the nature of occlusions. It may also bring new elements to circumvent the strong singularity that appears in the DCMA equation.

Bibliography

[1] J.Aloimonos, A.Bandyopadhyay, "Active Vision", Proceedings IEEE 1987, pp. 35-54.

[2] S.J.Altschuler, M.A.Grayson, "Shortening space curves and flow through singularities", *Journal of Differential Geometry* 35, pp. 283-298, 1992.

[3] L.Alvarez, "Axiomatisation et Nouveaux Opérateurs de la Morphologie Mathématique", Preprint CEREMADE, 1992.

[4] L. Alvarez, F. Guichard, P.L. Lions, J.M. Morel, "Axioms and fundamental equations of image processing", *Archives for Rational Mechanics* 123, pp. 199-257, 1993.

[5] L. Alvarez, F. Morales, "Affine Morphological Multiscale Analysis of Corners and Multiple Junctions", *International Journal of Computer Vision*, 1995.

[6] L. Alvarez, J.-M. Morel, "Formalization and Computational Aspects of Image Analysis", *Acta Numerica*, Cambridge University Press, 1994.

[7] V.Arnold, *Ordinary Differential Equations*, Springer Verlag, 1992.

[8] M.Asada, "Cylindrical Shape from Contour and Shading without knowledge of lighting conditions or surface albedo", Proceedings IEEE 1987, pp. 412-416.

[9] G.Barles, C.Georgelin, "A simple proof for the convergence of an approximate scheme for computing Mean Curvature Motions", *SIAM Journal of Numerical Analysis* 32:2, pp. 484-500, 1995.

[10] G.Barles, *Solutions de viscosité des équations de Hamilton-Jacobi*, Springer Verlag, Berlin, 1994.

[11] J.L.Barron, D.J.Fleet, S.S.Beauchemin "Performance of Optical Flow Techniques", *International Journal of Computer Vision* 12:1, pp. 43-77, 1994.

[12] J.Bence, B.Merriman, S.Osher, "Diffusion generated motion by mean curvature", Preprint, 1992.

[13] R.C.Bolles, H.H.Baker, D.H.Marimont, "Epipolar-Plane Image Analysis : An Approach to Determining Structure from Motion", *International Journal of Computer Vision* 1, pp. 7-55, 1987.

[14] S.Boukir, F.Chaumette "Reconstruction 3D de primitives géométriques par vision active", INRIA report #1722, july 1992.

[15] M.Brady, A.Yuille "An Extremum Principle for Shape from Contours", Proceedings IEEE, pp. 186-199, 1984.

[16] Arne Broman, *Introduction to Partial Differential Equations,* Dover, New-York, 1989.

[17] A.M. Bruckstein, A. Cohen, G. Sapiro, "A Subdivision Scheme for continuous-scale B-splines and affine invariant progressive smoothing", Preprint CEREMADE #9403, 1994.

[18] A.M.Bruckstein, A.Tannenbaum, "Some Mathematical Problems in Computer Vision", Preprint, Israel Institute of Technology, july 1992.

[19] P.Burlina, R.Chellappa, "Spatio-temporal moments and generalized spectral analysis of divergent images for motion estimation". Proceedings IEEE, pp. 328-332, 1994.

[20] F.Cao, "Morphological and Affine Invariant Filters : the N-dimensionnal case of Infsup Operators", to appear.

[21] V.Caselles, B.Coll, J.-M. Morel "Is Scale Space possible ?", to appear in *IEEE Transactions on Image Processing.*

[22] F. Catté, F. Dibos, "A morphological approach of mean curvature motion", Preprint CEREMADE #9310, 1993.

[23] Y.G.Chen, Y.Giga, S.Goto, "Uniqueness and existence of viscosity solutions of generalized Mean Curvature flow Equations", *Journal of Differential Geometry* 33, pp. 749-786, 1991.

[24] D.L.Chopp, "Numerical Computation of Self-Similar Solutions for Mean Curvature Flow", Internal Report, 1993.

[25] R.Cipolla, A.Blake, "Surface Shape from the Deformation of Apparent Contours", *International Journal of Computer Vision* 9:2, pp. 83-112, 1992.

[26] T.Cohignac, "Reconnaissance de formes planes", PhD Dissertation, CEREMADE, 1994.

[27] M.G.Crandall, H.Ishii,P.-L. Lions, "User's guide to viscosity solutions of second order partial differential equations", *Bulletin of American Mathematical Society* 27, pp. 1-67, 1992.

[28] J.-P.d'Alès, "Approximation linéaire et non linéaire de fonctions aléatoires : application à la compression d'images", PhD Dissertation, CEREMADE, 1996.

[29] C.L.Epstein, M.Gage, "The curve shortening flow", *Wave Motion Theory, Modeling and Computation*, A.Chorin and A.Majda Editors, Springer-Verlag, New-York, 1987.

[30] L.C.Evans, "Convergence of an Algorithm for Mean Curvature Motion", Preprint, 1992.

[31] L.C.Evans, J.Spruck, "Motion of Level Sets by Mean Curvature I", *Journal of Differential Geometry* 33, pp. 635-681, 1991.

[32] L.C.Evans, "A geometric Interpretation of the Heat Equation with Multivalued Initial Data", *SIAM Journal of Mathematical Analysis* 27:2, pp. 932-958, 1996.

[33] F.Falzon, G.Giraudon, M.Berthod, "Vers un modèle pour l'analyse multiéchelle de surfaces 3D", INRIA report #1639, march 1992.

[34] O.Faugeras, T.Papadopoulo, "A theory of the motion fields of curves", *International Journal of Computer Vision* 10:2, pp. 125-156, 1993.

[35] O.Faugeras, Lustman, Toscani, "Motion and Structure from Motion from Point and Lines Matches", Proceedings IEEE, pp. 25-34, 1987.

[36] M. Gage and R.S. Hamilton, "The heat equation shrinking convex plane curves", *Journal of Differential Geometry* 23, pp. 69-96, 1986.

[37] Y.Giga, S.Goto, "Motion of hypersurfaces and geometric equations", *Journal of Mathematical Society Japan*, vol. 44, no 1, 1992.

[38] E. Giusti, *Minimal surfaces and functions of bounded variation*, Birkhäuser, 1984.

[39] M.A. Grayson, "The heat equation shrinks embedded plane curves to round points", *Journal of Differential Geometry* 26, pp. 285-314, 1987.

[40] F. Guichard, "Axiomatisation des analyses multi-échelles d'images et de films", PhD Dissertation, CEREMADE, 1994.

[41] F. Guichard and J.-M. Morel, "Partial differential equations and image iterative filtering", Preprint CEREMADE and Tutorial ThP2 of *IEEE International Conference on Image Processing*, 1995.

[42] D.J.Heeger, "Optical Flow using Spatiotemporal filters", *International Journal of Computer Vision*, pp. 279-302, 1988.

[43] B.Horn, B.Shunk, "Determining Optical Flow", *Artificial Intelligence* 17, pp. 185-203, 1981.

[44] B.Horn, "Motion Fields Are Hardly Ever Ambiguous", *International Journal of Computer Vision* 1, pp. 259-274, 1987.

[45] H.Ishii, "A generalization of the Bence, Merriman and Osher algorithm for motion by mean curvature", Preprint.

[46] T.Kanade, "Geometrical Aspects of Interpreting Images as a 3D scene", Proceedings IEEE 1983, pp. 555-568.

[47] G.Kanizsa, *Grammatica del Vedere*, Il Mulino, Bologna, 1980. Traduction : *La grammaire du voir*, Diderot Editeur, Arts et Sciences, 1996.

[48] R.Kimmel, A.M.Bruckstein, "Shape Offsets via Level sets", Preprint, Israel Inst. of Technology, march 1992.

[49] G.Koepfler, C.Lopez, J.-M.Morel, "A Multiscale Algorithm for image segmentation by variational method", *Siam Journal of Numerical Analysis* 31:1, pp. 282-299, 1994.

[50] H.Longuet-Higgins, "A computer algorithm for reconstructing a scene from two projections", *Nature* vol. 293, no. 5828, pp. 133-135, 1981.

[51] C.Lopez, J.-M.Morel, "Axiomatisation of Shape Analysis and Application to Texture Hyperdiscrimination". Preprint CEREMADE, dec. 1992.

[52] L.Marce, P.Bouthemy, "Determination of a depth map from an image sequence", Rapport INRIA #765, dec. 1987.

[53] D.Marr, *Vision*, Freeman and Co., 1982.

[54] G.Matheron, *Random Sets and Integral Geometry,* John Wiley, New York, 1975.

[55] F.Meyer, P.Bouthemy, "Region-Based Tracking in an Image Sequence", INRIA report #1723, july 1992.

[56] Y.Meyer, *Les ondelettes, algorithmes et applications*, Armand Collin, Paris, 1992.

[57] L.Matthies, T.Kanade, R.Szeliski, "Kalman Filter-based Algorithms for Estimating Depth from Image Sequences", *International Journal of Computer Vision* 3, pp. 209-236, 1989.

[58] L.Moisan, "Analyse multiéchelle de films pour la reconstruction du relief", Note au compte rendu de l'Académie des sciences, Paris, tome 320, série I, pp. 279-284, feb. 1995.

[59] L.Moisan, "Perspective invariant movie analysis for depth recovery", Proceedings SPIE, vol. 2567, pp. 84-94, july 1995.

[60] L.Moisan, "Multiscale Analysis of Movies for Depth Recovery", *Proceeding of the International Conference on Image Processing*, vol. 3, pp. 25-28, oct. 1995.

[61] L.Moisan, "Affine plane curve evolution : a fully consistent scheme", Preprint CEREMADE, nov. 1996, to appear in *IEEE Transactions on Image Processing.*

[62] P.Monasse, "A review of Optical Flow Techniques", Personal communication, 1997.

[63] D.Mumford, "The problem of Robust Shape Descriptors", Proceedings IEEE, pp. 602-606, 1987.

[64] A.Naeve, J.-O.Eklundh, "On Projective Geometry and the Recovery of 3D Structure", Proceedings IEEE, pp. 128-135, 1987.

[65] S.Osher and J.A.Sethian, "Fronts Propagating with Curvature-Dependent Speed : Algorithms Based on Hamilton-Jacobi Formulations", *Journal of Computational Physics* 79:1, pp. 12-49, 1988.

[66] A.Rosenfeld, "Image Analysis : Problems, progress and prospects", *Pattern Recognition* 17:1, pp. 3-12, 1984.

[67] G.Sapiro and A.Tannenbaum, "On affine plane curve evolution", *Journal of Functional Analysis* 119, pp. 79-120, 1994.

[68] G.Sapiro and A.Tannenbaum, "Affine Invariant Scale Space", *International Journal of Computer Vision* 11:1, pp. 25-44, 1993.

[69] M.Schmitt, *Morphologie Mathématique*, Masson, 1993.

[70] J.Serra, *Image analysis and mathematical morphology*, vol. 2, Academic Press, 1982.

[71] J.A. Sethian, "Curvature and the Evolution of Fronts", *Communications in Mathematical Physics* 101, pp. 487-499, Springer-Verlag, 1985.

[72] J.A. Sethian, *Level Set Methods*, Cambridge University Press, 1996.

[73] S.Soatto, R.Frezza, "Recursive Motion Estimation on the Essential Manifold", Rapport interne, 1993.

[74] M.Spetsakis, J.Aloimonos, "A multi-frame Approach to Visual Motion Perception", *International Journal of Computer Vision* 6:3, pp. 245-255, 1991.

[75] K.A.Stevens, "The Visual Interpretation of Surfaces Contours", *Artificial Intelligence* 17, pp. 47-73, 1981.

[76] G.Tziritas, "Estimation of motion and structure of 3D objects from a sequence of images", Proceedings IEEE, pp. 693-697, 1987.

[77] E.J.Weldon Jr., H.Liu, "How accurately can direct motion vision determine depth ?", Proceedings IEEE, pp. 613-618, 1991.

[78] J.Weng, "Optimal Motion and Structure Estimation", *Pattern Analysis and Machine Intelligence* 15:9, pp. 864, sept. 1993.

[79] M.Wertheimer, "Untersuchungen zur Lehre der Gestalt", II, Psychologische Forschung, vol. 4, pp. 301-350, 1923.

[80] A.P.Witkin, "Scale-Space filtering", Proceedings of IJCAI, Karlsruhe, pp. 1019-1021, 1983.

[81] G.Xu, S.Tsuji, "Inferring Surfaces from boundaries", Proceedings IEEE, pp. 716-720, 1987.